Elucidating the Skeletal and Non-Skeletal Consequences of Alterations in Vitamin K Produced by Bacteria

A thesis presented to
The faculty of the Gerald J. and Dorothy R. Friedman
School of Nutrition Science and Policy

by

Minying Liu

In partial fulfillment of the requirements for the
Degree of Doctor of Philosophy

Tufts University

November 2025

Acknowledgements

I would like to acknowledge several people who have helped me complete this dissertation. First and foremost, I am deeply grateful to my advisor, Dr. Kyla Shea, for her invaluable guidance, support, and the countless hours she devoted to mentoring me over the past three years. She shaped me into a critical scientist while also supporting me through difficult times, teaching me independence and resilience. Her mentorship combined rigor with care in a way that felt like family, for which I am profoundly grateful.

I would also like to thank the members of my thesis committee. To Dr. Sarah Booth, for her insightful guidance, generous support, and encouragement at every critical step; and to Dr. Chris Hernandez and Dr. Jen Lee, for their essential guidance in study design, analysis, and interpretation. I am also grateful to Dr. Xueyan Fu, for her training in the lab, patience in reviewing data, and inspiration in method development. My thanks also go to Xiaohua Shen, for her kindness and for caring for me.

I am especially grateful to my good friend Wen Zhang, who has been with me through every step of undergraduate and graduate school, offering support, humor, and shared tears along the way. To my boyfriend, Zichao Wei, for his love and encouragement, and to my family, for their unwavering love, support, and belief in me.

Finally, I also would like to dedicate this dissertation to memory of my beloved cat, OJ.

Abstract

Vitamin K has long been associated with bone health due to its role as an enzymatic cofactor required for the post-translational carboxylation of vitamin K-dependent proteins, including osteocalcin, a component of the bone matrix. However, despite this biological role, evidence supporting its direct skeletal benefits remains equivocal. Findings of a comprehensive meta-analysis indicate that supplementation with phylloquinone and menaquinone-4, two forms of vitamin K, does not significantly affect bone mineral density. However, bone tissue quality is a critical aspect of bone not captured by bone mineral density that vitamin K may be involved in but has not been studied extensively.

Vitamin K exists in multiple naturally occurring forms that support carboxylation. Phylloquinone (vitamin $K_{1)}$ is plant-based, whereas menaquinones (collectively referred to as vitamin K_2) are a class of vitamin K compounds, most of which are produced by bacteria. Menaquinones are found in fermented foods, meat and dairy products, and are also abundant in the gut microbiota. Despite their bacterial origin, the contribution of gut bacterially produced menaquinones to the host's overall vitamin K tissue stores is uncertain. Similarly, their specific influence on bone health is unclear. Notably, menaquinone-4 is a unique menaquinone because it is not extensively produced by bacteria. Instead, it is a metabolite derived from all forms of vitamin K and is the predominant vitamin K form found in several body tissues, including bone. However, the origin of menaquinone-4 in skeletal tissue is also uncertain.

The objectives of this thesis were to investigate the tissue distribution and potential skeletal benefit of menaquinones. To meet these objectives, two experiments were conducted using male and female C57BL/6 mice. Aged (19-month-old) and young (4-month-old) mice were treated with broad-spectrum antibiotics for 12-16 weeks to determine the response of tissue menaquinone concentrations to antibiotic-induced alterations in gut menaquinone production. Young male and female mice were fed a diet containing 0.06 mg menaquinone-9 (a menaquinone form produced by bacteria) or 2.1 mg menaquinone-9 per kilogram of diet for 12 weeks, after which bone tissue quality and density were measured. During week 11, a subgroup of mice received deuterium-labeled menaquinone-9 to evaluate the conversion of dietary menaquinone-9 to menaquinone-4 in bone tissue.

Altering gut menaquinone production via antibiotics did not influence host menaquinone tissue stores in aged or young mice, as most gut-derived menaquinones were not substantially distributed to tissues other than perhaps the colon. Femoral tissue strength and whole-body bone mineral density did not differ between mice that were fed 0.06 mg or 2.1 mg of menaquinone-9/kg diet. Menaquinone-4 was the only form of vitamin K detected in bone, with over 60% of skeletal menaquinone-4 in mice fed 2.1 mg menaquinone-9/kg diet originating from deuterium labeled menaquinone-9.

Overall, these findings do not support systemic tissue uptake of bacterially produced menaquinones from the gut or a direct role of menaquinones in improving skeletal health. Additional research is needed to better define the broader health significance of gut-derived menaquinones and to clarify the biological significance of the conversion dietary vitamin K to menaquinone-4 in tissues.

Table of Contents

Tables

Figures

1. INTRODUCTION

1.1 Significance of Proposed Research

Each year in the U.S., approximately 2 million fragility fractures occur, at a cost burden of nearly $17 billion (1). Fragility fractures are caused by minimal trauma, often at home, such as a fall from a standing height (2). Risk for fragility fractures is often attributed to low bone mineral density (BMD), but fragility fractures can occur in individuals with normal BMD (3). Bone tissue quality, often characterized by bending strength and stiffness, cross-sectional geometry, , microarchitecture, and trabecular connectivity, is another critical aspect of bone health that is not reflected by BMD (4-7). Impaired bone tissue quality can increase fracture risk (8). Bone tissue quality is influenced by numerous factors, including genetic background, collagen production, medication use, and nutrition (9, 10).

Vitamin K, an essential fat-soluble nutrient, has long been linked to bone health (11). This potential role was initially linked to vitamin K's classic function as an enzymatic cofactor, required for the post-translational γ-carboxylation of certain proteins (vitamin K-dependent proteins) (12). One such protein is osteocalcin, the predominant non-collagenous protein in bone. Once carboxylated, osteocalcin binds to calcium in the bone matrix (13). Early studies suggested that osteocalcin influenced BMD (14, 15). However, findings from more precise osteocalcin knockout mouse models demonstrated that its role may be more closely related to bone tissue quality than to BMD (16-18).

Vitamin K exists in multiple naturally occurring forms all of which support γ-carboxylation. The plant-based form, phylloquinone (PK), is found in green leafy vegetables and vegetable oils (19). In addition to PK, menaquinones (MKs) are a group of vitamin K compounds that differ structurally from PK in the length and saturation of the prenylated side

chain. Most MKs (MK5-MK13) are produced by bacteria. They are found in fermented foods, meat and dairy products, and are also abundant in the gut microbiota (20). Among MKs, MK4 is unique because it is not extensively produced by bacteria. Instead, it is converted from other forms of vitamin K in several extrahepatic tissues (21-23).

The relevance of dietary vitamin K intake to bone health has been studied extensively, but findings have been inconsistent (24), leaving the role of vitamin K in bone health controversial. A systematic review and meta-analysis of randomized controlled trials that tested the effect of PK or MK4 supplementation on age-related bone loss concluded there is little evidence that vitamin K affects BMD, but indicated it may reduce clinical fracture risk (25). These findings raise the possibility that vitamin K may influence skeletal health through mechanisms related to bone tissue quality rather than BMD. In addition, among bacterially produced MKs consumed in the diet, only MK7 has been studied with respect to bone health, and the clinical evidence regarding its effect on age-related bone loss is also equivocal (26-31). It is currently not known how other dietary MK forms produced by bacteria influence skeletal health. Addressing these knowledge gaps is essential for clarifying the broader role of vitamin K in bone health.

Dietary MKs serve as precursors to MK4 in several extrahepatic tissues, including the brain, kidney, intestine, and adipose tissue (23, 32). However, it is not known whether dietary MKs can be converted to MK4 in bone tissue (**Figure 1**). MK4 has been implicated in bone homeostasis through roles in cellular response and signaling pathways (33-35), so clarifying its origin is important.

Commercial interest in vitamin K, particularly MK supplements, is rapidly growing. Many supplements marketed for bone health feature MK4 or MK7. Recent market analyses project that

the MK supplement industry will exceed approximately $265 million by 2029 (36), reflecting substantial consumer interest in the perceived skeletal benefits of vitamin K. However, evidence supporting these claimed benefits is still incomplete. This growing gap between commercial claims and scientific evidence underscores the need for investigation into how dietary MKs contribute to skeletal health.

Despite the growing abundance of MK supplements on the market, the absorption of MKs, is not well understood. Most of what is known about vitamin K absorption comes from studies of PK, which is absorbed in the small intestine through a bile-dependent mechanism (37, 38). MKs from the diet are generally assumed to follow a similar pathway, but direct evidence is scarce. In addition, there is a large reservoir of MKs in the colon, where they are produced by gut bacteria. The extent to which gut-produced MKs are absorbed and contribute to the body's overall vitamin K pool remains uncertain (**Figure 1**).

The production of MKs by gut bacteria can be altered by disrupting the composition of the gut microbiota using antibiotics (39). However, results of a recent rodent experiment found the concentrations of bacterially produced MK forms measured in the liver and kidney did not reflect the changes in the caecal MK contents (39). This raises questions regarding how alterations in gut MK production affect tissue MK stores. Importantly, intestinal tissues were not measured in this experiment, which is a notable gap, because dietary vitamin K absorption and endogenous bacterial MK production occur in the intestine. The exclusion of female mice is an additional gap, given the documented sex differences in vitamin K tissue stores (23, 40).

1.2 Hypothesis and Specific Aims

The *overall goal* of this thesis project is to investigate the tissue distribution and potential skeletal roles of menaquinones. To address this goal, we have two hypotheses and corresponding specific aims:

Hypothesis 1: Alterations in the gut menaquinone production do not influence tissue menaquinone concentrations in aged and young mice.

Specific Aim 1: To determine how oral antibiotic-induced alterations in gut menaquinone production affect tissue menaquinone contents in aged (Aim 1a) and young (Aim 1b) male and female C57BL/6 mice.

Hypothesis 2: Dietary supplementation with menaquinones positively influences bone tissue quality and density and serves as a precursor to MK4 in bone tissue.

Specific Aim 2: To determine the response of bone tissue quality and density (Aim 2a) and bone tissue MK4 accumulation (Aim 2b) to dietary manipulation of menaquinone-9, a menaquinone form also produced by bacteria, in young male and female C57BL/6 mice.

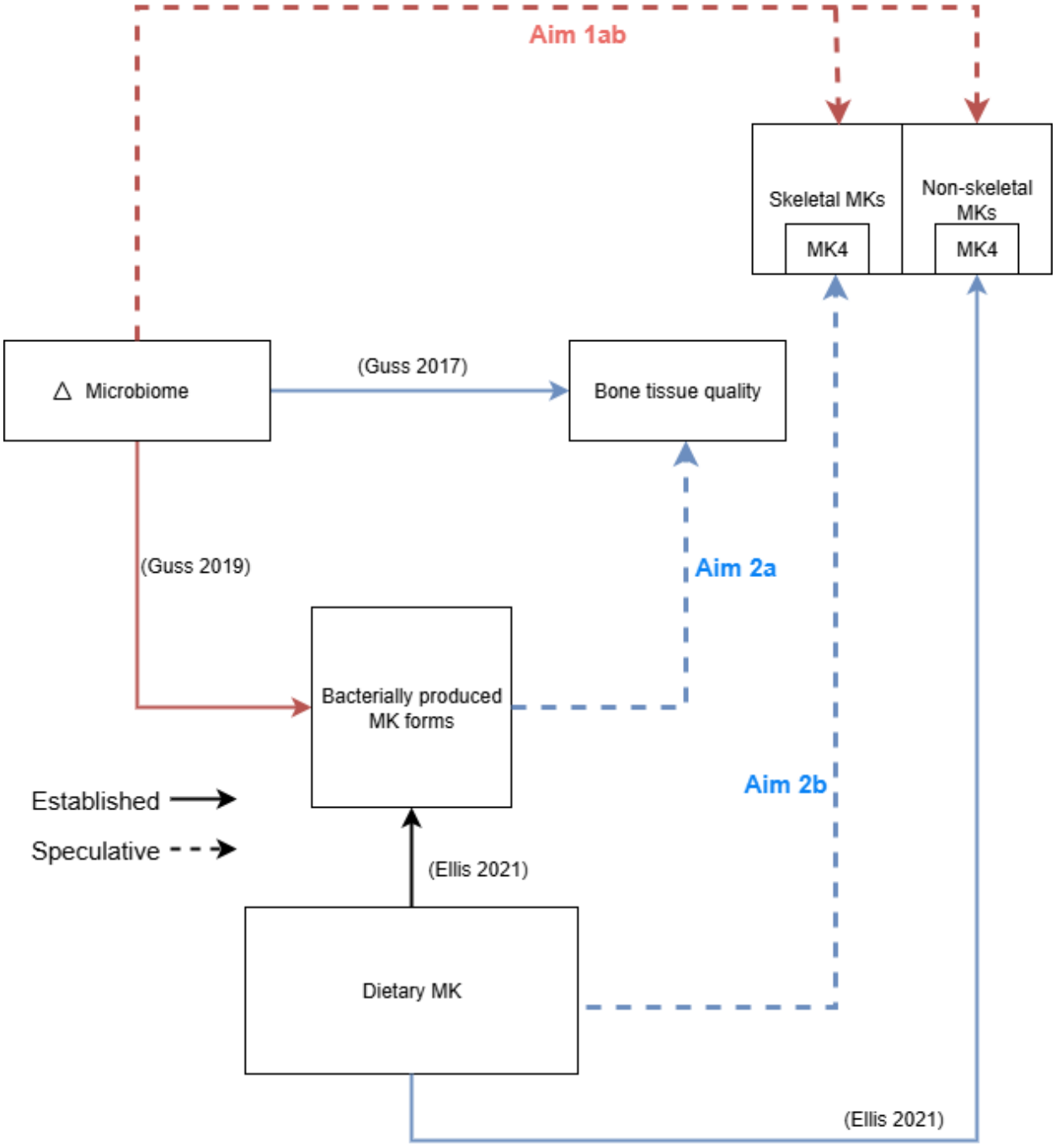

Figure 1. Theoretical framework depicting established (solid lines) and speculative components (dashed lines, representing Specific Aims 1 and 2) of the tissue stores and skeletal roles of bacterially produced MK forms.

REFERENCES

1. Burge R, Dawson-Hughes B, Solomon DH, Wong JB, King A, Tosteson A. Incidence and economic burden of osteoporosis-related fractures in the United States, 2005-2025. J Bone Miner Res. 2007;22(3):465-75.
2. Arlettaz Y. Augmented osteosynthesis in fragility fracture. Orthopaedics & Traumatology: Surgery & Research. 2023;109(1, Supplement):103461.
3. Kimmel DB, Vennin S, Desyatova A, Turner JA, Akhter MP, Lappe JM, et al. Bone architecture, bone material properties, and bone turnover in non-osteoporotic post-menopausal women with fragility fracture. Osteoporos Int. 2022;33(5):1125-36.
4. Seeman E. Bone quality: the material and structural basis of bone strength. J Bone Miner Metab. 2008;26(1):1-8.
5. Wallach S, Feinblatt JD, Carstens JH, Jr., Avioli LV. The bone "quality" problem. Calcif Tissue Int. 1992;51(3):169-72.
6. Watts NB. Bone quality: getting closer to a definition. J Bone Miner Res. 2002;17(7):1148-50.
7. Hernandez CJ, Keaveny TM. A biomechanical perspective on bone quality. Bone. 2006;39(6):1173-81.
8. Kopperdahl DL, Aspelund T, Hoffmann PF, Sigurdsson S, Siggeirsdottir K, Harris TB, et al. Assessment of incident spine and hip fractures in women and men using finite element analysis of CT scans. J Bone Miner Res. 2014;29(3):570-80.
9. Coulombe JC, Senwar B, Ferguson VL. Spaceflight-Induced Bone Tissue Changes that Affect Bone Quality and Increase Fracture Risk. Current Osteoporosis Reports. 2020;18(1):1-12.
10. Fonseca H, Moreira-Gonçalves D, Coriolano H-JA, Duarte JA. Bone Quality: The Determinants of Bone Strength and Fragility. Sports Medicine. 2014;44(1):37-53.
11. Booth SL, Dallal G, Shea MK, Gundberg C, Peterson JW, Dawson-Hughes B. Effect of vitamin K supplementation on bone loss in elderly men and women. J Clin Endocrinol Metab. 2008;93(4):1217-23.
12. Shearer MJ, Newman P. Recent trends in the metabolism and cell biology of vitamin K with special reference to vitamin K cycling and MK-4 biosynthesis. Journal of Lipid Research. 2014;55(3):345-62.
13. Booth SL, Centi AJ, Gundberg C. Bone as an Endocrine Organ Relevant to Diabetes. Current Diabetes Reports. 2014;14(12):556.
14. Boskey AL, Gadaleta S, Gundberg C, Doty SB, Ducy P, Karsenty G. Fourier transform infrared microspectroscopic analysis of bones of osteocalcin-deficient mice provides insight into the function of osteocalcin. Bone. 1998;23(3):187-96.
15. Ducy P, Desbois C, Boyce B, Pinero G, Story B, Dunstan C, et al. Increased bone formation in osteocalcin-deficient mice. Nature. 1996;382(6590):448-52.
16. Moriishi T, Ozasa R, Ishimoto T, Nakano T, Hasegawa T, Miyazaki T, et al. Osteocalcin is necessary for the alignment of apatite crystallites, but not glucose metabolism, testosterone synthesis, or muscle mass. PLoS Genet. 2020;16(5):e1008586.
17. Xu Z, Yang C, Wu F, Tan X, Guo Y, Zhang H, et al. Triple-gene deletion for osteocalcin significantly impairs the alignment of hydroxyapatite crystals and collagen in mice. Front Physiol. 2023;14:1136561.
18. Lambert LJ, Challa AK, Niu A, Zhou L, Tucholski J, Johnson MS, et al. Increased trabecular bone and improved biomechanics in an osteocalcin-null rat model created by CRISPR/Cas9 technology. Dis Model Mech. 2016;9(10):1169-79.

19. Booth SL. Vitamin K: food composition and dietary intakes. Food Nutr Res. 2012;56.
20. Karl JP, Fu X, Dolnikowski GG, Saltzman E, Booth SL. Quantification of phylloquinone and menaquinones in feces, serum, and food by high-performance liquid chromatography-mass spectrometry. J Chromatogr B Analyt Technol Biomed Life Sci. 2014;963:128-33.
21. Al Rajabi A, Booth SL, Peterson JW, Choi SW, Suttie JW, Shea MK, et al. Deuterium-labeled phylloquinone has tissue-specific conversion to menaquinone-4 among Fischer 344 male rats. J Nutr. 2012;142(5):841-5.
22. Collins MD, Jones D. Distribution of isoprenoid quinone structural types in bacteria and their taxonomic implication. Microbiol Rev. 1981;45(2):316-54.
23. Ellis JL, Fu X, Karl JP, Hernandez CJ, Mason JB, DeBose-Boyd RA, et al. Multiple Dietary Vitamin K Forms Are Converted to Tissue Menaquinone-4 in Mice. The Journal of Nutrition. 2021;152(4):981-93.
24. Shea MK, Booth SL. Update on the role of vitamin K in skeletal health. Nutrition Reviews. 2008;66(10):549-57.
25. Mott A, Bradley T, Wright K, Cockayne ES, Shearer MJ, Adamson J, et al. Effect of vitamin K on bone mineral density and fractures in adults: an updated systematic review and meta-analysis of randomised controlled trials. Osteoporos Int. 2019;30(8):1543-59.
26. Rønn SH, Harsløf T, Pedersen SB, Langdahl BL. Vitamin K2 (menaquinone-7) prevents age-related deterioration of trabecular bone microarchitecture at the tibia in postmenopausal women. Eur J Endocrinol. 2016;175(6):541-9.
27. Rønn SH, Harsløf T, Oei L, Pedersen SB, Langdahl BL. The effect of vitamin MK-7 on bone mineral density and microarchitecture in postmenopausal women with osteopenia, a 3-year randomized, placebo-controlled clinical trial. Osteoporos Int. 2021;32(1):185-91.
28. Fusaro M, Evenepoel P. Efficacy of vitamin K on bone fragility: puzzling findings from which we should learn how to design a rigorous study. Nephrol Dial Transplant. 2023;38(10):2105-8.
29. Zhang Y, Liu Z, Duan L, Ji Y, Yang S, Zhang Y, et al. Effect of Low-Dose Vitamin K2 Supplementation on Bone Mineral Density in Middle-Aged and Elderly Chinese: A Randomized Controlled Study. Calcif Tissue Int. 2020;106(5):476-85.
30. Fu X, Moreines J, Booth SL. Vitamin K supplementation does not prevent bone loss in ovariectomized Norway rats. Nutr Metab (Lond). 2012;9(1):12.
31. Iwamoto D, Masaki C, Shibata Y, Watanabe C, Nodai T, Munemasa T, et al. Microstructural and mechanical recovery of bone in ovariectomized rats: The effects of menaquinone-7. J Mech Behav Biomed Mater. 2021;120:104571.
32. Ellis JL, Karl JP, Oliverio AM, Fu X, Soares JW, Wolfe BE, et al. Dietary vitamin K is remodeled by gut microbiota and influences community composition. Gut Microbes. 2021;13(1):1-16.
33. Tabb MM, Sun A, Zhou C, Grün F, Errandi J, Romero K, et al. Vitamin K2 regulation of bone homeostasis is mediated by the steroid and xenobiotic receptor SXR. J Biol Chem. 2003;278(45):43919-27.
34. Ichikawa T, Horie-Inoue K, Ikeda K, Blumberg B, Inoue S. Steroid and xenobiotic receptor SXR mediates vitamin K2-activated transcription of extracellular matrix-related genes and collagen accumulation in osteoblastic cells. J Biol Chem. 2006;281(25):16927-34.
35. Tao L, Li H, Wang J, Liu Q, Cao W, Zhu Y. Vitamin K2 inhibits PGE2-mediated osteoblast ferroptosis by upregulation of CBR1 via the Nrf2/Keap1 pathway. Commun Biol. 2025;8(1):1116.

36. MarketsandMarkets Research Pvt. Ltd. Vitamin K2 Industry is Anticipated to Rise $265 Million by 2029. 2024.
37. Beulens JWJ, Booth SL, van den Heuvel EGHM, Stoecklin E, Baka A, Vermeer C. The role of menaquinones (vitamin K2) in human health. British Journal of Nutrition. 2013;110(8):1357-68.
38. Shearer MJ, Newman P. Recent trends in the metabolism and cell biology of vitamin K with special reference to vitamin K cycling and MK-4 biosynthesis. J Lipid Res. 2014;55(3):345-62.
39. Guss JD, Taylor E, Rouse Z, Roubert S, Higgins CH, Thomas CJ, et al. The microbial metagenome and bone tissue composition in mice with microbiome-induced reductions in bone strength. Bone. 2019;127:146-54.
40. Harshman SG, Fu X, Karl JP, Barger K, Lamon-Fava S, Kuliopulos A, et al. Tissue Concentrations of Vitamin K and Expression of Key Enzymes of Vitamin K Metabolism Are Influenced by Sex and Diet but Not Housing in C57Bl6 Mice. J Nutr. 2016;146(8):1521-7.

2. REVIEW OF LITERATURE

2.1 Bone Tissue Quality Contributes to Fragility Fractures

Each year in the U.S., approximately 2 million fragility fractures occur, at a cost burden of nearly $17 billion (1). Fragility fractures are caused by minimal trauma, often at home, such as a fall from a standing height (2). Risk for fragility fractures is often attributed to low bone mineral density (BMD), but fragility fractures can occur in individuals with normal BMD (3), suggesting that BMD may capture only one dimension of bone health. Bone tissue quality, often characterized by bending strength and stiffness, cross-sectional geometry, microarchitecture, and trabecular connectivity, is another critical aspect of bone health independent from BMD (4-7). Bone tissue quality impairment can reduce whole bone strength without altering BMD (8).

2.2 Determinants of Bone Tissue Quality

Nutrition has long been playing a crucial role in skeletal health, with well-studied contributors like vitamin D and calcium (9). Besides these, other nutritional components may also be involved, such as vitamin K.

2.3 The Focus that Links Vitamin K to Bone

2.3.1 Vitamin K functions

The classic function of vitamin K is an essential cofactor for the gamma (γ)-carboxyglutamyl carboxylase (GGCX) enzyme. GGCX catalyzes the post-translational carboxylation of glutamate (Glu) residues on specific proteins to form γ-carboxyglutamate (Gla), a modification that enables these proteins to bind calcium (10) (**Figure 1**). This enzymatic modification is part of a cyclical series of reactions commonly referred to as the "vitamin K cycle" (**Figure 1**). The hydroquinone form of vitamin K acts as the active cofactor for GGCX and is oxidized to the epoxide form, which

is then reduced back to the quinone form and subsequently to the hydroquinone form by the vitamin K reductase enzyme (10, 11).

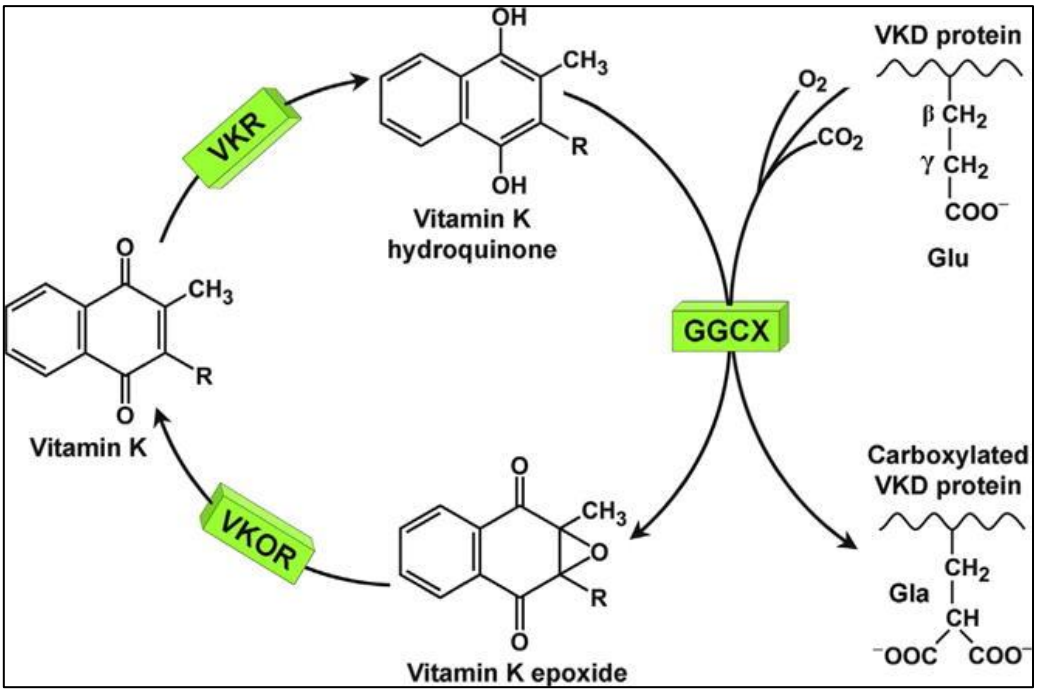

Figure 1. Vitamin K-dependent protein carboxylation - the "Vitamin K Cycle" (11).

2.3.2 Vitamin K-dependent proteins

Proteins that undergo this post-translational γ-carboxylation are collectively referred to as vitamin K-dependent proteins (VKDPs). The most well-known VKDPs are clotting factors needed for blood coagulation (11). However, VKDPs are found in several tissues throughout the body and serve other functions beyond coagulation. The most abundant non-collagenous protein in the bone - osteocalcin (OC), which is produced by osteoblasts during bone formation, is vitamin K-dependent. Once carboxylated, OC binds to calcium in the bone matrix (12). Early

studies suggested that osteocalcin was involved in regulating bone formation or quantity (13, 14). However, findings from more precise osteocalcin knockout mouse models demonstrated that its role may be more closely related to enhancing bone tissue crystallinity and bone mechanical properties (15-17).

2.4 Forms of Vitamin K

Vitamin K is an essential fat-soluble nutrient that exists in multiple naturally occurring forms. The plant-based form, PK, is found in green leafy vegetables and vegetable oils (18). MKs are a class of vitamin K compounds that differ structurally from PK in the length and saturation of their prenylated side chains. The number of prenyl units differentiates the specific MK isoforms, denoted as "n" (MKn) (19-21) (**Figure 2**). All forms of vitamin K share a common 2-methyl-1,4-naphthoquinone ring and a prenylated side chain at the 3-position (**Figure 2**). At least 13 MK forms have been identified (22). Most MKs (MK5 - MK13) are produced by bacteria. They are found in fermented foods, meat, and dairy products, and are also abundant in the gut microbiota (23-25). PK and MKs can act as a cofactor for GGCX, as the naphthoquinone ring is the functional site required for carboxylation (26).

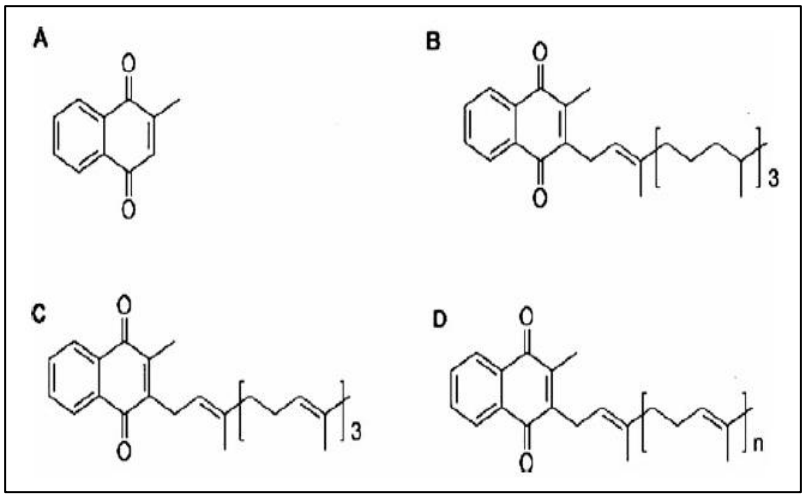

Figure 2. Forms of Vitamin K.
(A) Menadione, (B) Phylloquinone, (C) Menaquinone-4, (D) Menaquinone-n (MKn) (19)

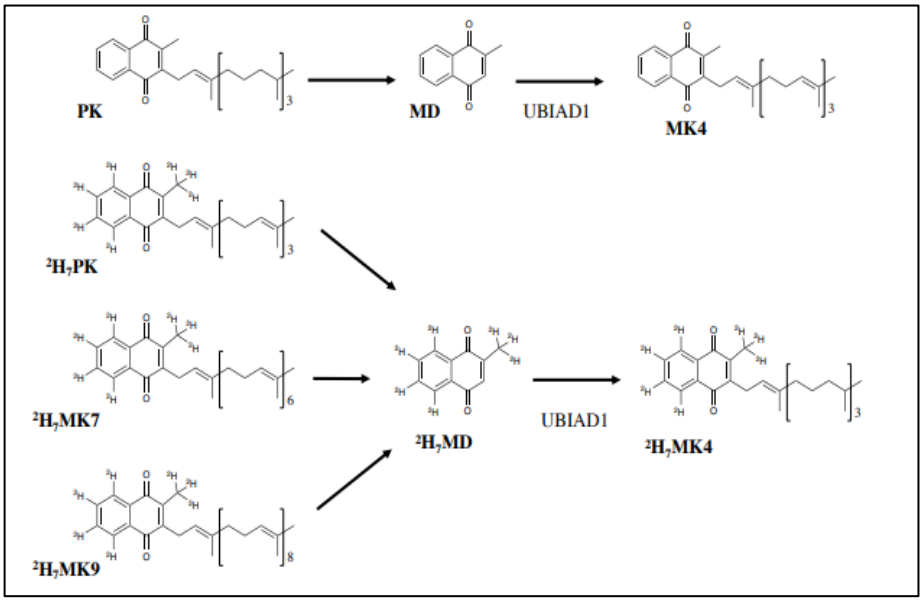

Figure 3. Mechanism of the conversion of MK4 from different vitamin K forms (31)

MK4 is the only MK form that is not produced by bacteria in large amounts. Instead, it is alkylated from menadione (MD, **Figure 2**) present in animal feeds or is the product of endogenous conversion directly from dietary PK. This process involves phytyl side chain removal, producing MD as an intermediate, which is then prenylated with a geranylgeranyl pyrophosphate side chain by the enzyme UbiA prenyltransferase domain-containing 1 (UBIAD1) (**Figure 3**) (27-30). MK4 was found to be the predominate form of vitamin K in most tissues of mice that were fed equimolar amounts of isotopically labeled PK, MK4, MK7, and MK9. Moreover, approximately 60% of MK4 measured in kidney, brain, intestinal, and adipose tissue originated from the vitamin K form consumed in the diet (31) (**Figure 3**). Bone tissue was not measured in this experiment, so it is not clear how dietary vitamin K influences skeletal tissue MK4 accumulation.

2.5 Clinical Evidence on the Role of Vitamin K in Bone Health

The relevance of vitamin K to bone health has been studied extensively, but the preponderance of studies have focused on PK and MK4, with age-related bone loss measured by BMD as the main outcome. Findings from these studies have been inconsistent (32), leaving the

role of vitamin K in bone health controversial. A systematic review and meta-analysis of randomized controlled trials that tested the effect of PK or MK4 supplementation on age-related bone loss concluded there is little evidence that vitamin K affects BMD or vertebral fractures. The authors reported a potentially beneficial effect of PK or MK4 supplementation on clinical fracture risk but concluded that additional studies are needed to confirm this (33). Therefore, vitamin K may influence skeletal health through mechanisms related to bone tissue quality rather than BMD. In addition, among bacterially produced MK forms consumed in the diet, only MK7 has been studied with respect to bone health, and the clinical evidence regarding the effect of MK7 on age-related bone loss is also equivocal (34-39). It is currently not known how other bacterially produced MK forms found in the diet influence skeletal health. Addressing these knowledge gaps is essential for clarifying the broader role of vitamin K in bone.

2.6 Importance of Menaquinone-4 in Bone Health

While MK4 is present in bone, it is unclear whether MKs consumed in the diet contribute to the MK4 stores in bone, as skeletal tissue was not measured in the prior studies that used stable isotopes (31). This is an important gap to address because MK4 appears to have a unique role in cell signaling pathways that have been implicated in bone homeostasis (40, 41). Evidence has shown that MK4 acts as an endogenous ligand for the steroid and xenobiotic receptor (SXR) to up-regulate the expression of osteoblast marker genes (40). In cell culture experiments, activation of SXR signaling by MK4 has been associated with the accumulation of collagen in osteoblastic cells, which may be beneficial in reducing fragility fractures (41). In animal models, the deletion of the pregnane X receptor (PXR, the murine homolog to the SXR) resulted in a phenotype consistent with bone fragility (42). In ovariectomized mice, MK4 treatment restored bone microarchitecture, which was accompanied by higher expression of genes involved in bone

formation and lower expression of genes involved in bone resorption (43). Conversion the conversion of dietary MKs to MK4 in skeletal tissue is uncertain but will be evaluated in this thesis research.

2.7 Absorption and Transport of Vitamin K

PK from the diet is absorbed primarily in the jejunum and ileum via bile-dependent mechanisms and enhanced in the presence of dietary fats (44). Although there is not yet a confirmed specific transport protein for vitamin K, recent evidence has also suggested vitamin K can be absorbed via an active process involving the cholesterol transporter Niemann-Pick C1-like 1 (NPC1L1) (45, 46). Within the enterocyte, absorbed PK is incorporated into chylomicrons, lipoprotein particles that carry dietary lipids. These chylomicrons are secreted into the lymphatic system and enter systemic circulation at the thoracic duct. PK is the main form of vitamin K in circulation. Plasma PK increases in response to PK intake, and this response is also influenced by triglycerides (47). In circulation, PK is concentrated within triglyceride-rich lipoproteins (TRL), which include both chylomicron remnants and very-low-density lipoproteins (VLDL). Extrahepatic tissues are believed to acquire PK primarily through low-density lipoprotein (LDL) particles via LDL receptor-mediated endocytosis (48, 49).

The absorption of MKs from the diet has not been studied as extensively as PK but is thought to follow similar lipid-mediated pathways (50, 51). However, MKs are not typically detected in circulation unless supplements or high amounts of MKs are consumed in the diet (52). There is limited evidence indicating that among MKs, the length of isoprenoid sidechain may alter cellular uptake, transport, and storage (19). Although most MKs are produced by bacteria in the colon, evidence regarding MK absorption from the colon is mixed. In canulated rats, MK9 was

reported to be absorbed passively and dose-dependently in the colon (and ileum) (53, 54). In this experiment, purified MK9 was administered directly into the intestine (54). It was subsequently reported in rats that colorectal administration of MK9 (and other vitamin K forms) did not support prothrombin carboxylation, suggesting MKs are not sufficiently absorbed from the colon to support vitamin K-dependent protein carboxylation (55).

2.8 Current Dietary Vitamin K Recommendations

Most dietary recommendations for vitamin K are based on PK, which was historically thought to be the primary form of vitamin K in the diet and is well-characterized in the food supply (18, 44, 56, 57). The current recommended adequate intakes (AI) for vitamin K in the U.S. and Canada were derived from median PK intakes reported in the National Health and Nutrition Examination Survey (NHANES) III, which are 120 μg and 90 μg per day for men and women, respectively, 19 years and older (58). Since these recommendations are based on median intakes, overall 50% of the general U.S. adult population meets the AI (59). However, vitamin K intake can vary by sex and age (59). For example, among men only 32% of those 71 years and older meet the current AI for vitamin K, compared to 49% of 31–50-year-olds. Among women, 63% of 31-50-year-olds and 56% of 71+-year-olds meet the AI (33).

Evidence has emerged that MKs are more abundant in the food supply than initially thought (60) and may account for up to 25% of total vitamin K intake in some populations (61). MK4 is found in some meats, including chicken and pork, because it is converted from MD, which is abundant in many animal feeds in some countries. MKs 5-13 are present in various fermented and dairy foods (19). For example, natto, a fermented soybean product commonly consumed in Japan, is a rich source of MK7 (19). MK9 has been identified as the predominant form of

vitamin K in dairy milk, with its concentration correlating with the milk's fat content (60). However, the form and amount of MKs in these foods is highly variable and depends on the microbial species used in the fermentation process (60). There has been discussion in the scientific community regarding a separate dietary requirement for MKs, due to potential differences in absorption and tissue stores, compared to PK (62). However, the European Food Safety Authority (EFSA) concluded that evidence on MK absorption and tissue distribution is insufficient to establish a specific dietary recommendation for MKs (56).

2.9 Gut Menaquinone Production and Tissue Stores

2.9.1 Endogenous gut bacterial menaquinone production

There is a large reservoir of MKs in the colon, where they are produced by gut bacteria. Bacteria use MKs in the electron transport chain for energy production in the gut microbiome (19). The de novo MKn synthesis in bacteria has two pathways: the "classic" pathway and the "alternative" ("futalosine") pathway (**Figure 4**). Both pathways convert the MK precursor,

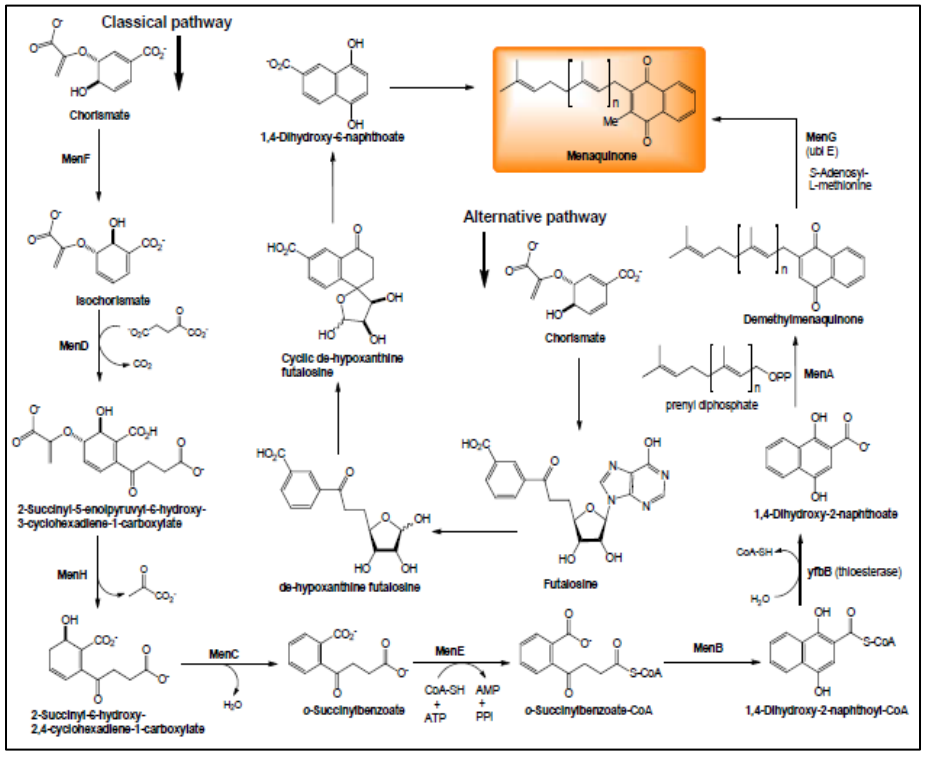

Figure 4. Menaquinone biosynthetic pathways in bacteria (63)

demethylmenaquinone, to MKs (63). In brief, the classic MK synthesis pathway uses chorismate as the substrate to synthesize 1,4-dihydroxy-2-naphthoate (DHNA) with the help of MenFDHCEB enzymes. Next, the aromatic prenylation enzyme MenA adds a side chain to DHNA to form demethylmenaquinone. Then, this prenylation reaction is followed by the methylation reaction carried out by methyltransferase (MenG) to form MK (64). Furthermore, the forms of MK produced in the human intestine vary across microbial species (65). For example, *Proteobacteria*, *Firmicutes*, and *Bacteroides* are known to be associated with the biosynthetic pathways of MK9 and MK10, whereas MK11–MK13 biosynthetic pathways are predominantly found in *Actinobacteria* and *Prevotella* (66). This implies that the bacterial composition of the microbiome influences MK content in the gut. However, the extent to which gut-derived MKs are absorbed and contribute to the body's overall vitamin K pool remains uncertain.

2.9.2 Effect of antibiotics on MK production by gut bacteria

The production of MKs by gut bacteria is affected by antibiotics, which disrupt the composition of the gut microbiota (67). In young male C57BL/6 mice, gut MK production was altered following 12 weeks of broad-spectrum antibiotic treatment (68), in which antibiotics significantly altered cecal MK content, which included reducing MK11 and MK10 while increasing MK8 concentrations (**Figure 5**). Changes in MK concentrations between treatment groups were also observed in the liver and kidney. However, the concentrations of bacterially produced MK forms measured in the liver and kidney generally did not reflect the changes in the caecal MK contents (except for MK11) (**Figure 5**). This raises questions regarding how

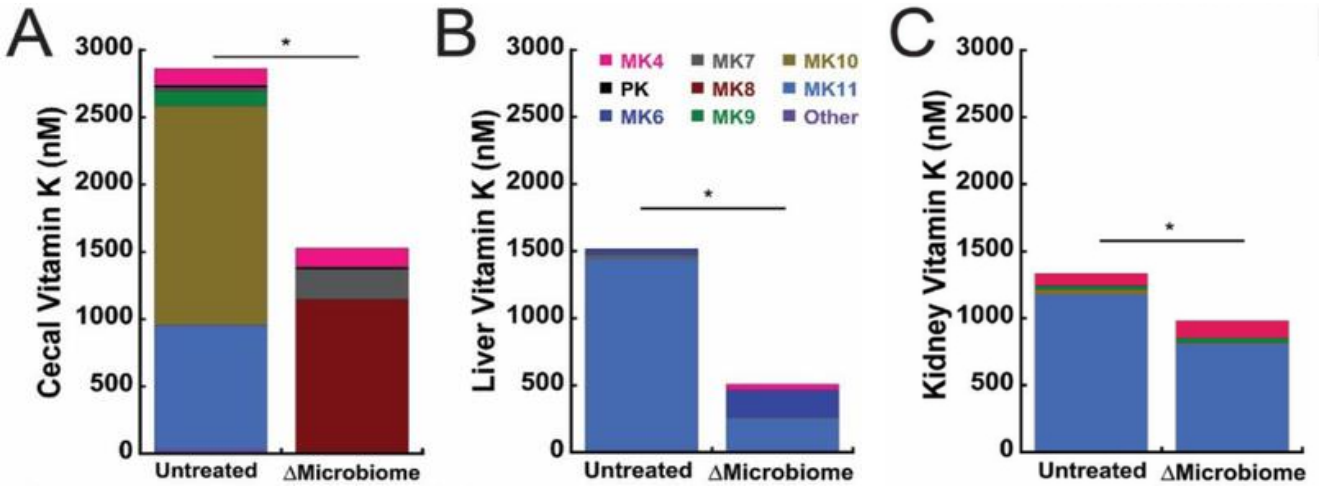

Figure 5. Vitamin K concentrations in (A) caecum, (B) liver, and (C) kidney in mice treated with antibiotics (ΔMicrobiome) and untreated controls (68)

alterations in gut MK production affect tissue MK stores. In the absence of direct measurement of intestinal tissues, the intestinal content of MKs was inferred by caecal concentrations, which is a notable gap. Moreover, the exclusion of female mice is an additional gap, given it is well-reported that female mice have higher tissue concentrations of MK4 and other MK forms than males (31, 69). To better understand how alterations in gut MK production affect MK tissue stores, it is necessary to directly quantify the MK forms in intestinal and other tissues as well as study both sexes. Furthermore, older mice could possibly respond differently due to age-related shifts in the composition of the gut microbiome (70) that could affect bacterial MK production and subsequently MK tissue stores. There also appear to be structural and functional differences in colon tissue of young and old mice (71). These age-related differences suggest it is also important to study how bacterially produced MKs contribute to vitamin K tissue stores at different life stages – which is addressed in this thesis research.

2.10 Conclusions and Opportunities for Research

Despite years of investigation, the role of vitamin K in bone physiology remains a topic of debate. Historically, research has centered on vitamin K-dependent carboxylation of osteocalcin within the bone matrix, which was thought to be important for maintaining BMD. Yet evidence remains inconsistent. A comprehensive meta-analysis and systematic review found PK and MK4 supplementation had no effect on BMD, although suggested it may be associated with reducing clinical fracture risk (33). While fragility fractures are often linked to low BMD, they can also occur in individuals with normal BMD (3). Bone tissue quality is another critical aspect of bone health not captured by bone mineral density (4-7). Therefore, vitamin K may influence skeletal health through mechanisms related to bone tissue quality rather than BMD.

More recently, attention has shifted towards dietary MKs, including those produced by bacteria. However, MK7 has been the only bacterially produced MK form studied in this regard, even though other MKs are found in the food-supply, and findings are equivocal (34-39). It is also unclear whether bacterially produced MKs forms consumed in the diet are converted to MK4 in bone tissue, which is important to clarify since MK4 appears to be involved in cell signaling in bone tissue homeostasis (40, 72). Hence, further research is needed to determine the physiological role of bacterially produced MK forms and potential conversion to MK4 in skeletal tissue.

While the colon serves as a substantial reservoir of bacterially produced MKs, the contribution of bacterially produced MKs to host vitamin K stores remains unknown. Determining how changes in gut MK production affect tissue MK stores is important to clarify how gut produced MKs participate in the physiological functions of vitamin K in bone and other host tissues.

REFERENCES

1. Burge R, Dawson-Hughes B, Solomon DH, Wong JB, King A, Tosteson A. Incidence and economic burden of osteoporosis-related fractures in the United States, 2005-2025. J Bone Miner Res. 2007;22(3):465-75.
2. Arlettaz Y. Augmented osteosynthesis in fragility fracture. Orthopaedics & Traumatology: Surgery & Research. 2023;109(1, Supplement):103461.
3. Kimmel DB, Vennin S, Desyatova A, Turner JA, Akhter MP, Lappe JM, et al. Bone architecture, bone material properties, and bone turnover in non-osteoporotic post-menopausal women with fragility fracture. Osteoporos Int. 2022;33(5):1125-36.
4. Seeman E. Bone quality: the material and structural basis of bone strength. J Bone Miner Metab. 2008;26(1):1-8.
5. Wallach S, Feinblatt JD, Carstens JH, Jr., Avioli LV. The bone "quality" problem. Calcif Tissue Int. 1992;51(3):169-72.
6. Watts NB. Bone quality: getting closer to a definition. J Bone Miner Res. 2002;17(7):1148-50.
7. Hernandez CJ, Keaveny TM. A biomechanical perspective on bone quality. Bone. 2006;39(6):1173-81.
8. Castaneda M, Strong JM, Alabi DA, Hernandez CJ. The Gut Microbiome and Bone Strength. Curr Osteoporos Rep. 2020;18(6):677-83.
9. Yao P, Bennett D, Mafham M, Lin X, Chen Z, Armitage J, et al. Vitamin D and Calcium for the Prevention of Fracture: A Systematic Review and Meta-analysis. JAMA Netw Open. 2019;2(12):e1917789.
10. Shearer MJ, Newman P. Recent trends in the metabolism and cell biology of vitamin K with special reference to vitamin K cycling and MK-4 biosynthesis. Journal of Lipid Research. 2014;55(3):345-62.
11. Tie JK, Stafford DW. Functional Study of the Vitamin K Cycle Enzymes in Live Cells. Methods Enzymol. 2017;584:349-94.
12. Booth SL, Centi AJ, Gundberg C. Bone as an Endocrine Organ Relevant to Diabetes. Current Diabetes Reports. 2014;14(12):556.
13. Boskey AL, Gadaleta S, Gundberg C, Doty SB, Ducy P, Karsenty G. Fourier transform infrared microspectroscopic analysis of bones of osteocalcin-deficient mice provides insight into the function of osteocalcin. Bone. 1998;23(3):187-96.
14. Ducy P, Desbois C, Boyce B, Pinero G, Story B, Dunstan C, et al. Increased bone formation in osteocalcin-deficient mice. Nature. 1996;382(6590):448-52.
15. Moriishi T, Ozasa R, Ishimoto T, Nakano T, Hasegawa T, Miyazaki T, et al. Osteocalcin is necessary for the alignment of apatite crystallites, but not glucose metabolism, testosterone synthesis, or muscle mass. PLoS Genet. 2020;16(5):e1008586.
16. Xu Z, Yang C, Wu F, Tan X, Guo Y, Zhang H, et al. Triple-gene deletion for osteocalcin significantly impairs the alignment of hydroxyapatite crystals and collagen in mice. Front Physiol. 2023;14:1136561.
17. Lambert LJ, Challa AK, Niu A, Zhou L, Tucholski J, Johnson MS, et al. Increased trabecular bone and improved biomechanics in an osteocalcin-null rat model created by CRISPR/Cas9 technology. Dis Model Mech. 2016;9(10):1169-79.
18. Booth SL. Vitamin K: food composition and dietary intakes. Food Nutr Res. 2012;56.

19. Walther B, Karl JP, Booth SL, Boyaval P. Menaquinones, bacteria, and the food supply: the relevance of dairy and fermented food products to vitamin K requirements. Adv Nutr. 2013;4(4):463-73.
20. Shea MK, Booth SL. Vitamin K's Role in Age-Related Bone Loss: A Critical Review. In: Holick MF, Nieves JW, editors. Nutrition and Bone Health. New York, NY: Springer New York; 2015. p. 471-86.
21. Booth SL. Roles for vitamin K beyond coagulation. Annu Rev Nutr. 2009;29:89-110.
22. Karl JP, Fu X, Dolnikowski GG, Saltzman E, Booth SL. Quantification of phylloquinone and menaquinones in feces, serum, and food by high-performance liquid chromatography-mass spectrometry. J Chromatogr B Analyt Technol Biomed Life Sci. 2014;963:128-33.
23. Barbara W, Magali C. Menaquinones, Bacteria, and Foods: Vitamin K2 in the Diet. In: Jan Oxholm G, editor. Vitamin K2. Rijeka: IntechOpen; 2017. p. Ch. 4.
24. Karl JP, Meydani M, Barnett JB, Vanegas SM, Barger K, Fu X, et al. Fecal concentrations of bacterially derived vitamin K forms are associated with gut microbiota composition but not plasma or fecal cytokine concentrations in healthy adults. Am J Clin Nutr. 2017;106(4):1052-61.
25. Ellis JL, Karl JP, Oliverio AM, Fu X, Soares JW, Wolfe BE, et al. Dietary vitamin K is remodeled by gut microbiota and influences community composition. Gut Microbes. 2021;13(1):1-16.
26. Buitenhuis HC, Soute BAM, Vermeer C. Comparison of the vitamins K1, K2 and K3 as cofactors for the hepatic vitamin K-dependent carboxylase. Biochimica et Biophysica Acta (BBA) - General Subjects. 1990;1034(2):170-5.
27. Al Rajabi A, Booth SL, Peterson JW, Choi SW, Suttie JW, Shea MK, et al. Deuterium-labeled phylloquinone has tissue-specific conversion to menaquinone-4 among Fischer 344 male rats. J Nutr. 2012;142(5):841-5.
28. Nakagawa K, Hirota Y, Sawada N, Yuge N, Watanabe M, Uchino Y, et al. Identification of UBIAD1 as a novel human menaquinone-4 biosynthetic enzyme. Nature. 2010;468(7320):117-21.
29. Hirota Y, Tsugawa N, Nakagawa K, Suhara Y, Tanaka K, Uchino Y, et al. Menadione (vitamin K3) is a catabolic product of oral phylloquinone (vitamin K1) in the intestine and a circulating precursor of tissue menaquinone-4 (vitamin K2) in rats. J Biol Chem. 2013;288(46):33071-80.
30. Davidson RT, Foley AL, Engelke JA, Suttie JW. Conversion of dietary phylloquinone to tissue menaquinone-4 in rats is not dependent on gut bacteria. J Nutr. 1998;128(2):220-3.
31. Ellis JL, Fu X, Karl JP, Hernandez CJ, Mason JB, DeBose-Boyd RA, et al. Multiple Dietary Vitamin K Forms Are Converted to Tissue Menaquinone-4 in Mice. The Journal of Nutrition. 2021;152(4):981-93.
32. Shea MK, Booth SL. Update on the role of vitamin K in skeletal health. Nutrition Reviews. 2008;66(10):549-57.
33. Mott A, Bradley T, Wright K, Cockayne ES, Shearer MJ, Adamson J, et al. Effect of vitamin K on bone mineral density and fractures in adults: an updated systematic review and meta-analysis of randomised controlled trials. Osteoporos Int. 2019;30(8):1543-59.
34. Rønn SH, Harsløf T, Pedersen SB, Langdahl BL. Vitamin K2 (menaquinone-7) prevents age-related deterioration of trabecular bone microarchitecture at the tibia in postmenopausal women. Eur J Endocrinol. 2016;175(6):541-9.

35. Rønn SH, Harsløf T, Oei L, Pedersen SB, Langdahl BL. The effect of vitamin MK-7 on bone mineral density and microarchitecture in postmenopausal women with osteopenia, a 3-year randomized, placebo-controlled clinical trial. Osteoporos Int. 2021;32(1):185-91.
36. Fusaro M, Evenepoel P. Efficacy of vitamin K on bone fragility: puzzling findings from which we should learn how to design a rigorous study. Nephrol Dial Transplant. 2023;38(10):2105-8.
37. Zhang Y, Liu Z, Duan L, Ji Y, Yang S, Zhang Y, et al. Effect of Low-Dose Vitamin K2 Supplementation on Bone Mineral Density in Middle-Aged and Elderly Chinese: A Randomized Controlled Study. Calcif Tissue Int. 2020;106(5):476-85.
38. Fu X, Moreines J, Booth SL. Vitamin K supplementation does not prevent bone loss in ovariectomized Norway rats. Nutr Metab (Lond). 2012;9(1):12.
39. Iwamoto D, Masaki C, Shibata Y, Watanabe C, Nodai T, Munemasa T, et al. Microstructural and mechanical recovery of bone in ovariectomized rats: The effects of menaquinone-7. J Mech Behav Biomed Mater. 2021;120:104571.
40. Tabb MM, Sun A, Zhou C, Grün F, Errandi J, Romero K, et al. Vitamin K2 regulation of bone homeostasis is mediated by the steroid and xenobiotic receptor SXR. J Biol Chem. 2003;278(45):43919-27.
41. Ichikawa T, Horie-Inoue K, Ikeda K, Blumberg B, Inoue S. Steroid and xenobiotic receptor SXR mediates vitamin K2-activated transcription of extracellular matrix-related genes and collagen accumulation in osteoblastic cells. J Biol Chem. 2006;281(25):16927-34.
42. Azuma K, Casey SC, Ito M, Urano T, Horie K, Ouchi Y, et al. Pregnane X receptor knockout mice display osteopenia with reduced bone formation and enhanced bone resorption. J Endocrinol. 2010;207(3):257-63.
43. Wang H, Zhang N, Li L, Yang P, Ma Y. Menaquinone 4 Reduces Bone Loss in Ovariectomized Mice through Dual Regulation of Bone Remodeling. Nutrients. 2021;13(8).
44. Institute of Medicine Panel on M. Dietary Reference Intakes for Vitamin A, Vitamin K, Arsenic, Boron, Chromium, Copper, Iodine, Iron, Manganese, Molybdenum, Nickel, Silicon, Vanadium, and Zinc. Washington (DC): National Academies Press (US)

45. Takada T, Yamanashi Y, Konishi K, Yamamoto T, Toyoda Y, Masuo Y, et al. NPC1L1 is a key regulator of intestinal vitamin K absorption and a modulator of warfarin therapy. Sci Transl Med. 2015;7(275):275ra23.
46. Shearer MJ, Okano T. Key Pathways and Regulators of Vitamin K Function and Intermediary Metabolism. Annu Rev Nutr. 2018;38:127-51.
47. Ellis JL, Fu X, Al Rajabi A, Grusak MA, Shearer MJ, Naumova EN, et al. Plasma Response to Deuterium-Labeled Vitamin K Intake Varies by TG Response, but Not Age or Vitamin K Status, in Older and Younger Adults. J Nutr. 2019;149(1):18-25.
48. Lamon-Fava S, Sadowski JA, Davidson KW, O'Brien ME, McNamara JR, Schaefer EJ. Plasma lipoproteins as carriers of phylloquinone (vitamin K1) in humans. Am J Clin Nutr. 1998;67(6):1226-31.
49. Shearer MJ, Newman P. Metabolism and cell biology of vitamin K. Thromb Haemost. 2008;100(4):530-47.
50. Beulens JWJ, Booth SL, van den Heuvel EGHM, Stoecklin E, Baka A, Vermeer C. The role of menaquinones (vitamin K2) in human health. British Journal of Nutrition. 2013;110(8):1357-68.

51. Shearer MJ, Newman P. Recent trends in the metabolism and cell biology of vitamin K with special reference to vitamin K cycling and MK-4 biosynthesis. J Lipid Res. 2014;55(3):345-62.
52. Tsugawa N, Shiraki M, Suhara Y, Kamao M, Tanaka K, Okano T. Vitamin K status of healthy Japanese women: age-related vitamin K requirement for gamma-carboxylation of osteocalcin. Am J Clin Nutr. 2006;83(2):380-6.
53. Hollander D, Muralidhara KS, Rim E. Colonic absorption of bacterially synthesized vitamin K2 in the rat. Am J Physiol. 1976;230(2):251-5.
54. Hollander D, Rim E, Ruble PE, Jr. Vitamin K2 colonic and ileal in vivo absorption: bile, fatty acids, and pH effects on transport. Am J Physiol. 1977;233(2):E124-9.
55. Groenen-van Dooren MM, Ronden JE, Soute BA, Vermeer C. Bioavailability of phylloquinone and menaquinones after oral and colorectal administration in vitamin K-deficient rats. Biochem Pharmacol. 1995;50(6):797-801.
56. Turck D, Bresson JL, Burlingame B, Dean T, Fairweather-Tait S, Heinonen M, et al. Dietary reference values for vitamin K. Efsa j. 2017;15(5):e04780.
57. U.S. Department of Agriculture ARS. FoodData Central.
58. Suttie JW. Vitamin K in health and disease: CRC Press; 2009.
59. Harshman SG, Saltzman E, Booth SL. Vitamin K: dietary intake and requirements in different clinical conditions. Curr Opin Clin Nutr Metab Care. 2014;17(6):531-8.
60. Fu X, Harshman SG, Shen X, Haytowitz DB, Karl JP, Wolfe BE, et al. Multiple Vitamin K Forms Exist in Dairy Foods. Curr Dev Nutr. 2017;1(6):e000638.
61. Kamao M, Suhara Y, Tsugawa N, Uwano M, Yamaguchi N, Uenishi K, et al. Vitamin K content of foods and dietary vitamin K intake in Japanese young women. J Nutr Sci Vitaminol (Tokyo). 2007;53(6):464-70.
62. Akbulut AC, Pavlic A, Petsophonsakul P, Halder M, Maresz K, Kramann R, et al. Vitamin K2 Needs an RDI Separate from Vitamin K1. Nutrients. 2020;12(6).
63. Ravcheev DA, Thiele I. Genomic Analysis of the Human Gut Microbiome Suggests Novel Enzymes Involved in Quinone Biosynthesis. Front Microbiol. 2016;7:128.
64. Choi S-r, Frandsen J, Narayanasamy P. Novel long-chain compounds with both immunomodulatory and MenA inhibitory activities against Staphylococcus aureus and its biofilm. Scientific Reports. 2017;7(1):40077.
65. Fernandez F, Collins MD. Vitamin K composition of anaerobic gut bacteria. FEMS Microbiology Letters. 1987;41(2):175-80.
66. Caspi R, Billington R, Ferrer L, Foerster H, Fulcher CA, Keseler IM, et al. The MetaCyc database of metabolic pathways and enzymes and the BioCyc collection of pathway/genome databases. Nucleic Acids Res. 2016;44(D1):D471-80.
67. Jernberg C, Löfmark S, Edlund C, Jansson JK. Long-term impacts of antibiotic exposure on the human intestinal microbiota. Microbiology. 2010;156(11):3216-23.
68. Guss JD, Taylor E, Rouse Z, Roubert S, Higgins CH, Thomas CJ, et al. The microbial metagenome and bone tissue composition in mice with microbiome-induced reductions in bone strength. Bone. 2019;127:146-54.
69. Harshman SG, Fu X, Karl JP, Barger K, Lamon-Fava S, Kuliopulos A, et al. Tissue Concentrations of Vitamin K and Expression of Key Enzymes of Vitamin K Metabolism Are Influenced by Sex and Diet but Not Housing in C57Bl6 Mice. J Nutr. 2016;146(8):1521-7.

70. Wu CS, Muthyala SDV, Klemashevich C, Ufondu AU, Menon R, Chen Z, et al. Age-dependent remodeling of gut microbiome and host serum metabolome in mice. Aging (Albany NY). 2021;13(5):6330-45.
71. Steegenga WT, de Wit NJW, Boekschoten MV, Ijssennagger N, Lute C, Keshtkar S, et al. Structural, functional and molecular analysis of the effects of aging in the small intestine and colon of C57BL/6J mice. BMC Medical Genomics. 2012;5(1):38.
72. Tao L, Li H, Wang J, Liu Q, Cao W, Zhu Y. Vitamin K2 inhibits PGE2-mediated osteoblast ferroptosis by upregulation of CBR1 via the Nrf2/Keap1 pathway. Commun Biol. 2025;8(1):1116.

3. MANUSCRIPTS/CHAPTERS

3.1 Responses of Tissue Menaquinone Concentrations to Alterations in Gut Bacterial Menaquinone Production in Aged and Young Male and Female Mice

Minying Liu[1], Chongshan Liu[2,3], Erika L. Cyphert[4], Declan Breen[1], Benjamin N Orbach[1], Christopher Dante Ashih [1], Christopher J Hernandez[2], Xueyan Fu[1], Jennifer Lee[1,5], Sarah L Booth[1], M Kyla Shea[1]

[1] Human Nutrition Research Center on Aging, Tufts University, Boston, MA

[2] Orthopaedic Surgery, University of California, San Francisco, CA

[3] Sibley School of Mechanical and Aerospace Engineering, Cornell University, Ithaca, NY

[4] Shu Chien-Gene Lay Department of Bioengineering, University of California, San Diego, CA

[5] Tufts University School of Medicine, Boston, MA

Correspondence: Kyla Shea, PhD, 711 Washington St., Boston, MA USA 02111; 617 556 3370; kyla.shea@tufts.edu

Supported by NIA R01 R01AG067997 and USDA Agricultural Research Service under Cooperative Agreement 58-8050-3-003. Any opinions, findings, conclusions, or recommendations expressed in this publication are those of the authors and do not necessarily reflect the view of the USDA.

ABSTRACT

Background: Menaquinones (MKs) are a class of vitamin K compounds, most of which are produced by bacteria residing in the colon. However, the contribution of gut-produced MKs to host tissue vitamin K stores remains uncertain. If these MKs are absorbed and incorporated into the host's overall vitamin K pool, altering gut MK production would be expected to influence host MK tissue stores. However, experimental evidence supporting or refuting this premise is currently limited.

Objective: To determine how altering gut MK production affects intestinal and liver tissue MK contents in aged and young mice.

Methods: Gut MK production of male and female C57BL/6 mice was altered with broad-spectrum antibiotic treatment in two experiments: (A) starting at 19 months of age for 4 months (aged mice) and (B) starting at 4 weeks of age for 3 months (young mice). Age-matched untreated controls were included in each experiment. Concentrations of 10 known MK forms (MK4-13) in feces, colon, duodenum, jejunum, ileum, and liver were quantified using mass spectrometry and compared within age-group and sex using independent samples t-tests.

Results: In aged mice, antibiotic treated males and females had higher fecal MK8–MK12 concentrations and lower MK6 and MK13 compared to untreated controls ($p<0.001$). Parallel differences were observed in colon tissue MK profiles, but not in the small intestine or liver. In young mice, antibiotic treated males and females had lower fecal MK6 and MK10–MK12 ($p<0.001$) compared to untreated controls. However, parallel differences in intestinal, liver or bone tissue MK concentrations were not detected.

Conclusion: Altering gut MK production did not correspond to changes in tissue MK concentrations, except perhaps for colon tissue. These findings raise doubt about the contribution of MKs produced by gut bacteria to vitamin K tissue stores.

INTRODUCTION

Vitamin K is a class of fat-soluble compounds that serve as an essential enzyme cofactor in the post-translational carboxylation of specific proteins, known as vitamin K-dependent proteins (1). There are multiple naturally occurring forms of vitamin K. Phylloquinone (PK, vitamin K1) is plant-based and found in green leafy vegetables and vegetable oils (2). Menaquinones (MKs, collectively referred to as vitamin K2) differ structurally from PK in the length and saturation of the side chain. Most MKs (MK5-13) are produced by bacteria. They are found in fermented foods, meat, and dairy products, and are also abundant in the gut microbiota (3). Among the MKs, however, MK4 is unique because it is not bacterially produced but is instead converted from dietary vitamin K forms in certain tissues, including the intestine and liver (4).

Most dietary recommendations for vitamin K are based on PK, which was historically thought to be the primary form of vitamin K in the diet and is well-characterized in the food supply (2, 5-7). The current recommended adequate intakes (AI) for vitamin K in the U.S. and Canada are 120 µg and 90 µg per day for men and women 19 years and older respectively (8). These AIs were derived from median PK intakes reported in the National Health and Nutrition Examination Survey (NHANES) III in 1988-1994. Since then, evidence has emerged that MKs are more abundant in the food supply than initially thought (9) and may account for up to 25% of total vitamin K intake in some populations that consume high amounts of MK-rich foods (10). There has been discussion in the scientific community about whether a separate dietary

requirement for MKs should be considered, given potential differences in absorption and tissue distribution compared to PK (11). However, this remains controversial. The European Food Safety Authority (EFSA) concluded that evidence on MK absorption and tissue distribution is insufficient to establish a specific dietary recommendation for MKs (6).

One key knowledge gap regarding MK absorption and tissue distribution is the extent to which MKs produced in the gut are absorbed and contribute to the body's overall vitamin K pool. Dietary PK is absorbed primarily in the jejunum and ileum via bile-dependent mechanisms and enhanced in the presence of dietary fats (5). Absorption of MKs from the diet is thought to follow a similar pathway (12, 13). However, there is mixed evidence regarding MK absorption from the colon (14). In canulated rats, MK9 was reported to be absorbed passively and dose-dependently in the colon (and ileum) (15, 16). In this experiment, purified MK9 was administered directly into the intestine (16). It was subsequently reported in rats that colorectal administration of MK9 (and other vitamin K forms) did not support prothrombin carboxylation, suggesting MKs are not sufficiently absorbed from the colon to support vitamin K-dependent protein carboxylation, which is vitamin K's main function (17). In a more recent experiment conducted in 4-week-old male C57BL/6 mice, gut MK production was altered via 12 weeks of treatment with broad-spectrum antibiotics. However, the concentrations of bacterially produced MK forms in the liver and kidney did not correspond to the changes in the caecum MK contents (18). This raises questions regarding how alterations in gut MK production affect tissue MK stores. MKs were not directly measured in intestinal tissue in this experiment. Instead, the intestinal MK contents were inferred by cecal concentrations, which is a notable limitation. It's possible that older mice could respond differently due to age-related shifts in the composition of the gut microbiome (19) that could affect bacterial MK production and subsequently MK tissue

stores. Evaluating how altering gut MK production contributes to tissue MK stores in young and aged animals is an important step toward improving our understanding of vitamin K metabolism over the lifespan.

To address this gap, we altered gut MK production of male and female C57BL/6 mice with broad-spectrum antibiotic treatment for up to 4 months, starting at two life stages: 19 months of age (aged mice) and 4 weeks of age (young mice). We quantified MK4–13 concentrations in feces to confirm changes in gut MK production, and in colon, duodenum, jejunum, ileum, and liver tissues to assess MK tissue distribution. We hypothesized that antibiotic-induced alterations in gut MK production would not affect intestinal, or liver tissue MK concentrations in aged or young mice.

MATERIALS AND METHODS

Study design

Experiment A – Aged Mice: Oral antibiotics treatment from 19 to 22 months of age

This animal study was conducted at the Hernandez Laboratory at Cornell University (now at University of California, San Francisco). Four-week-old male (n=45) and female (n=45) C57BL/6 mice were purchased from Jackson Laboratory (Bar Harbor; ME) and housed in plastic cages filled with 1/4-inch corn cob bedding (The Andersons' Lab Bedding, Ohio), fed with standard laboratory chow (Teklad LM-485 Mouse/Rat Sterilizable Diet, nutrient composition table see supplemental material **Figure 1S**) and water *ad libitum.* The diet contained 80 mg/kg menadione (MD), a synthetic form of vitamin K commonly used in animal feed (12). Mice were randomized into one of two groups (n=15/sex/group) and treated with oral broad-spectrum antibiotics for months using the following dosing duration regimens (**Figure 1**): (I) untreated, no

antibiotic treatment from weaning (4 weeks of age) to months 22; (II) 4 months dosing, no antibiotics from weaning to months 18, then antibiotic treatment from months 19-22.

Experiment B – Young Mice: Oral antibiotics treatment from 4 weeks to 16 weeks of age

This animal study was conducted at the Jean Mayer USDA Human Nutrition Research Center on Aging (HNRCA) at Tufts University. Three-week-old male (n=32) and female (n=32) C57BL/6 mice were acquired from Charles River Laboratories and housed in conventional plastic single cages also filled with 1/4-inch corn cob bedding at the HNRCA Comparative Biology Unit. Upon arrival, mice were acclimated to an AIN-93G diet (Inotiv, TD.94045) that contained 1mg/kg PK (per manufacturer) for one week. At 4 weeks of age, mice were divided at random into 2 experimental groups (n=16/sex/group) to receive diet containing MK9 with or without oral antibiotics for 12 weeks as follows: (1) diet containing 2.1 mg/kg MK9 with no antibiotic treatment, (2) diet containing 2.1 mg/kg MK9 with antibiotic treatment for 12 weeks (**Figure 2**). Diets were composed of a mixture of the vitamin K-free basal diet (Inotiv, TD.120060) and a molar equivalent amount of MK9 to the currently recommended concentration of vitamin K for rodents (1mg/kg PK) (20) (**Figure 2S**). It was previously demonstrated that feeding mice a diet containing MK9 (the only form of vitamin K in the diet) in an equal molar amount to the current rodent diet recommendations showed no sign of vitamin K-deficiency (4). In addition, mice were pair-fed between groups with and without oral antibiotic treatment to minimize the possibility that any outcome differences would be due to differences in the total amount of food consumed. MK9 concentrations in study diets were measured by liquid chromatography-mass spectrometry (LC-MS) (3), and diet MK9 concentrations were 2.03 ± 0.12 mg MK9/kg.

Oral antibiotics used in both experiments followed previous work (21, 22), in which a cocktail of 1.0g/L ampicillin and 0.5g/L neomycin was added to mice's drinking water in light-sensitive water bottles. Fresh antibiotic water was replaced every three days over the duration of both studies. Ampicillin and neomycin are broad-spectrum antibiotics that alter the intestinal microbiome but have poor bioavailability, which minimizes extra-intestinal effects (21, 23). Fecal pellets were collected one day before sacrifice. Tissues were selected based on their distinct roles in vitamin K metabolism: liver (primary storage site) and intestinal segments (duodenum, jejunum, and ileum for dietary absorption) and colon (where bacterial MK production occurs). Bone tissue was also included in experiment B, as an additional extrahepatic tissue. All the intestinal tissues were immediately rinsed with ice-cold phosphate-buffered saline (PBS) to remove luminal contents, snap-frozen in liquid nitrogen, and stored at -80°C until analysis.

Vitamin K analyses

MK concentrations in feces, intestinal tissues, and liver tissues from both experiments, as well as bone tissues from experiment B, were analyzed at the HNRCA. For samples collected from experiment A, tissue MK4 concentrations were measured by high-performance liquid chromatography (HPLC, to avoid co-eluting interferent peaks) and tissue MK5 through 13 concentrations were measured using LC-MS. Both assays were developed by our laboratory as described in detail elsewhere (3). For samples collected from experiment B, tissue MK4-13 concentrations were measured by Quadrupole Time-of-Flight Mass Spectrometry (Q-TOF-MS) to improve sensitivity, minimize interference, and avoid the need to switch instruments for MK4. Briefly, liver tissues (0.1–0.15 g) were homogenized in PBS using a Powergen homogenizer (Fisher Scientific) prior to extraction. Fecal pellets (0.6 g) were dispersed by sonicating in a 3:2

(v/v) mixture of 2-propanol and hexane for 1 minute. Intestinal (duodenum, jejunum, ileum, and colon; 0.1 g) tissues were homogenized with a mortar and pestle over dry ice, with the addition of liquid nitrogen to ensure thorough pulverization. Bone (left and right tibia, in total of 0.1g) tissues were fragmented using a stainless-steel tissue pulverizer (Biospec) with the addition of liquid nitrogen to ensure thorough pulverization. The resulting bone powder was transferred into 2 mL tubes pre-filled with beads, followed by the addition of 1 mL PBS. Samples were then homogenized using an Omni Bead Ruptor 24 Homogenizer, running two cycles of 1 minute each. MKs from homogenized tissue and fecal samples were then extracted using hexane, purified via solid-phase extraction, and quantified using LC-MS, HPLC, and Q-TOF-MS (Agilent series 1200 HPLC; Agilent 6130 Quadrupole MSD; Agilent 6550 iFunnel Q-TOF LC/MS). For samples measured using LC-MS and HPLC, the lowest limit of detection (LLOD) for tissue MKs are 5pmol/g for MK5, MK7, MK8, MK9, MK11-13; 10pmol/g for MK6; 1pmol/g for MK10; 0.1pmol/g for MK4 (24). For samples measured using Q-TOF-MS, the LLODs are 1pmol/g for MK4-MK8 and 5pmol/g for MK9-MK13.

Statistical analysis

Data are presented as geometric means ± SEM. Nondetectable (ND) values were handled by replacing concentrations of 0 with half of the LLOD. Statistical analyses were performed using RStudio (v. 4.3.1, 2023). The Shapiro–Wilk test was applied to assess data normality, and Levene's test was used to evaluate homogeneity of variance. Normality was tested for each MK within each tissue. When a distribution failed the Shapiro–Wilk test, concentrations were log-transformed to reduce skewness and stabilize variance, and normality was re-evaluated. Independent t-tests were then performed to compare the effects of antibiotic treatment on body weights, tissue, and fecal MK concentrations. Analyses were conducted separately by sex, with

statistical significance defined as $p<0.01$ to account for multiple comparisons within each experiment.

RESULTS

Body weight and mortality: Body weights in both experiments did not differ significantly between treatment groups in either male or female mice (all p-values$\geq$0.025, see Supplemental **Figure S3 and S4**). Eleven young mice died with no overt bleeding prior to the end of experiment B (8 males and 3 females). Of these, seven males and 2 females were from the antibiotic treatment groups. One male and 1 female in the non-treated groups were also lost. No losses were reported in experiment A.

Feces: In aged females (experiment A), fecal MK8-12 concentrations were higher following 4 months of antibiotic treatment, compared to the control (**Table 1**). In aged males, antibiotic treatment increased fecal MK7, MK8, MK9, and MK11 concentrations. Conversely, fecal MK6 and MK13 concentrations were significantly lower following antibiotic treatment in both sexes (**Table 1**). Fecal MK4 and MK5 did not differ between the treatment groups in aged males or females. In young males and females (experiment B), fecal MK6, and MK10–12 concentrations were lower following 12 weeks of antibiotic treatment compared with controls (**Table 2**). MK8 concentrations were significantly higher in antibiotic treated males compared to controls, but the between group difference in females did not achieve statistical significance. Antibiotic treatment had no effect on MK5, MK7, or MK9 concentrations and MK4 was not detected in the feces in young mice of either sex.

Colon tissue: In aged males and females, colon tissue MK8–12 concentrations were higher following antibiotic treatment, except for MK9 in females (**Table 3**). In young males and

females, 12 weeks of antibiotic treatment did not affect colon tissue MK concentrations, except for an increase in MK8 concentrations in young females. (**Table 4**).

Small intestinal tissues: In aged mice, MK6 was the only bacterially derived MK form detected in the small intestine. In males, antibiotic treatment did not alter MK4 or MK6 concentrations in the duodenum, jejunum, or ileum (**Table 3**). In females, antibiotic treatment only reduced duodenal MK4 concentrations (**Table 3**). No bacterially derived MK forms were detected in the small intestine of young males and females. In young antibiotic-treated females, MK4 concentrations in the duodenum and jejunum, but not the ileum, were lower than untreated controls (**Table 4**). Conversely, in young males, MK4 concentrations in all small intestinal segments were unaffected by antibiotic treatment (**Table 4**).

Liver: In aged mice, MK4 and MK10 were the only MKs detected in liver. However, antibiotic treatment had no effect on MK4 and MK10 concentrations, compared to the controls (**Table 3**). In young mice, MK4 and MK9 were detected in the liver. In males, liver MK4 and MK9 concentrations did not differ between antibiotic-treated and control groups (**Table 4**). In females, liver MK4 concentrations were higher following antibiotic treatment, compared to controls (**Table 4**).

Bone: MK4 was the only vitamin K form detected in the bone tissue of young mice. Antibiotic treatment had no effect on MK4 concentrations in either males or females when compared with control groups (**Table 4**).

DISCUSSION

Fecal MK concentrations were altered following antibiotic treatment in both aged and young mice. However, the magnitude and direction of the detected changes were variable. The majority of fecal MKs increased with antibiotic treatment in aged mice but decreased in young

mice. Moreover, these changes were not reflected in the MK tissue concentrations of the small intestine or liver. For example, in aged mice, fecal MK9 and MK11 concentrations increased with antibiotic treatment, yet these MKs were not detected in tissues analyzed, other than the colon. Although fecal MK10 was higher in antibiotic-treated aged female mice, liver MK10 concentrations remained unchanged. In antibiotic-treated young mice, MK6 and MK10–MK12 concentrations in feces were significantly lower compared to untreated controls. However, these MKs were not detected in the small intestine, liver, or bone tissues in the untreated or antibiotic treated young mice, which precludes determining whether corresponding alterations occurred at the tissue level.

In the aged mice, the differences in colon tissue MK concentrations generally aligned with those observed in feces. In young mice, there were similar patterns for MK8, which also increased in feces following antibiotic treatment (although statistical significance was only achieved for fecal MK8 in males and colon MK8 in females). Otherwise, antibiotic-induced changes in gut MK production generally were not reflected in colon tissue in young mice. Colon tissue is in direct contact with the gut microbiota, which endogenously produces MKs. That more MKs were detected in colon tissue of aged mice may be attributed to age-related changes in gut barrier integrity, such as increased intestinal permeability (25), amplifying the impact of antibiotic treatment on colon MKs. However, we cannot rule out the possibility that the MKs detected in the colon tissue were remnants of the fecal contents, despite our efforts to minimize contamination by the steps taken in tissue preparation.

Absorption of long-chain MKs is thought to occur primarily in ileum, where bile salts are present to facilitate their incorporation into mixed micelles and transport into the enterocyte for absorption (26). Consistent with this, long-chain MKs have been detected in ileal tissue (27).

However, because bile salts are reabsorbed before reaching the colon, where the majority of gut-produced MKs are synthesized, the absorption of MKs from the colon is questionable. Moreover, most bacterially produced MKs are bound to bacterial cell membranes, which may additionally limit their bioavailability. In older mice, MK6 was consistently detected across all intestinal tissues, though it was the only bacterially derived MK form present in the small intestine. Fecal MK6 concentrations decreased with antibiotic treatment but remained statistically unchanged in intestinal tissues. In contrast, in younger mice, no gut-derived MK forms were detected in the small intestine tissue, raising additional questions about the absorption of bacterially produced MKs.

MK4 was detected in the liver and intestinal tissues of both young and aged mice, and in feces of aged mice. Since MK4 is not bacterially produced, it is likely that MK4 mainly originated from the diet. The diet fed to the aged mice contained 80 mg menadione/kg diet. Menadione is a pro-vitamin present in standard rodent chow that can be converted to MK4 in rodent tissues (20, 28). When vitamin K-deficient rats were fed a diet that contained 20 mg menadione/kg diet for 10 days, MK4 was the predominate vitamin K form detected throughout the intestine (29). The MK4 concentrations were similar in all intestinal segments (duodenum, proximal and distal jejunum, proximal, mid-, and distal ileum, cecum, proximal and distal colon). MKs 8-10 were also detected in the rats' caecum and colon, with MK10 being the most abundant form. While these findings are generally consistent with ours, our experiment did not include a vitamin K-deficient control group, precluding our ability to determine the specific contribution of the dietary menadione to tissue MK4 levels. Moreover, the amount of MD in the diet was approximately 80-fold higher than current recommendations for laboratory animal diets (1mg/kg PK (20)), which limits the applicability of our findings to conditions of vitamin K

insufficiency. The diet given to the younger mice contained MK9 as the only form of vitamin K, which was provided at an amount molar equivalent to 1mg PK/kg diet (4, 30, 31) – which corresponds to the current recommendations for rodent chow (20). Following this diet, MK4 was not detected in feces but was detected in all examined tissues and was the only MK form present in the small intestinal tissues. This observation is consistent with previous findings that MK4 was also not detected in feces of 12-week-old mice fed MK9 for seven days, also at molar amounts equivalent to current rodent diet recommendations, but was detected in multiple tissues, including small intestine and liver (32).

Our study has several key strengths. Compared to prior studies (18, 27), our findings provide insight into how changes in gut MK production affect MK stores of several key tissues involved in MK production, absorption, and storage. We included male and female mice since males and females are known to respond differently to alterations in vitamin K intake, and our findings substantiated the sex differences reported by others (4, 31, 32). We also studied two age groups of mice to obtain insight into how bacterially produced MKs contribute to tissue vitamin K stores at different life stages. However, since our data were derived from two separate experiments in which mice were fed different forms and doses of vitamin K, we were unable to directly compare the younger and older mice. Moreover, tissue MKs were measured using different instruments in the two experiments because the aged mice were analyzed first with LC-MS/HPLC, while the young mice were analyzed later using a recently updated QTOF-based assay that offered greater sensitivity, minimized co-eluting peaks, and streamlined MK4 analysis. This methodological difference further limits direct comparisons between the age groups. However, the same antibiotics were used in both experiments. Functional measures of vitamin K status, such as PIVKA (prothrombin induced by vitamin K absence), were not available, so we were unable to

evaluate whether alterations in gut MK production affected vitamin K functional status. Emerging research suggests that gut-derived MKs may have localized roles in shaping gut microbiota composition and function (32, 33). Intestinal microbiome composition and functional data were not available in our study, and it will be important to clarify how changes in the MK production in the gut affect the composition or function of the gut microbiome and vice versa in the future. However, this limitation does not affect our primary objective, which was to evaluate how changes in gut MK production influence MK concentrations in host tissues. Both experiments A and B were respectively designed to study the effect of gut microbiome alterations and dietary MK9 on bone tissue quality (30), so the sample size calculations were based on that outcome. Our sample size provided >87% to detect antibiotic treatment group differences in caecal MK concentrations reported by Guss et al (18), using a two-tailed p-value < 0.05. We adopted a more conservative p-value of < 0.01 for statistical significance in recognition of multiple comparisons and acknowledge some of the observed comparisons would have reached statistical significance under the more conventional threshold of $p < 0.05$.

The contribution of gut-produced MKs to vitamin K tissue stores and status has been debated for quite some time (6, 12, 16, 17). Our findings suggest that most gut-produced MKs are not substantially absorbed or distributed to tissues other than perhaps the colon. However, as evidence has emerged that MKs produced in the gut may modulate gut bacteria production and function (32), additional research into the broader health implications of gut-derived MKs may be warranted.

REFERENCES

1. Shearer MJ, Newman P. Recent trends in the metabolism and cell biology of vitamin K with special reference to vitamin K cycling and MK-4 biosynthesis. Journal of Lipid Research. 2014;55(3):345-62.
2. Booth SL. Vitamin K: food composition and dietary intakes. Food Nutr Res. 2012;56.
3. Karl JP, Fu X, Dolnikowski GG, Saltzman E, Booth SL. Quantification of phylloquinone and menaquinones in feces, serum, and food by high-performance liquid chromatography-mass spectrometry. J Chromatogr B Analyt Technol Biomed Life Sci. 2014;963:128-33.
4. Ellis JL, Fu X, Karl JP, Hernandez CJ, Mason JB, DeBose-Boyd RA, et al. Multiple Dietary Vitamin K Forms Are Converted to Tissue Menaquinone-4 in Mice. The Journal of Nutrition. 2021;152(4):981-93.
5. Institute of Medicine Panel on M. Dietary Reference Intakes for Vitamin A, Vitamin K, Arsenic, Boron, Chromium, Copper, Iodine, Iron, Manganese, Molybdenum, Nickel, Silicon, Vanadium, and Zinc. Washington (DC): National Academies Press (US)

Copyright 2001 by the National Academy of Sciences. All rights reserved.; 2001.
6. Turck D, Bresson JL, Burlingame B, Dean T, Fairweather-Tait S, Heinonen M, et al. Dietary reference values for vitamin K. Efsa j. 2017;15(5):e04780.
7. U.S. Department of Agriculture ARS. FoodData Central.
8. Suttie JW. Vitamin K in health and disease: CRC Press; 2009.
9. Fu X, Harshman SG, Shen X, Haytowitz DB, Karl JP, Wolfe BE, et al. Multiple Vitamin K Forms Exist in Dairy Foods. Curr Dev Nutr. 2017;1(6):e000638.
10. Kamao M, Suhara Y, Tsugawa N, Uwano M, Yamaguchi N, Uenishi K, et al. Vitamin K content of foods and dietary vitamin K intake in Japanese young women. J Nutr Sci Vitaminol (Tokyo). 2007;53(6):464-70.
11. Akbulut AC, Pavlic A, Petsophonsakul P, Halder M, Maresz K, Kramann R, et al. Vitamin K2 Needs an RDI Separate from Vitamin K1. Nutrients. 2020;12(6).
12. Beulens JWJ, Booth SL, van den Heuvel EGHM, Stoecklin E, Baka A, Vermeer C. The role of menaquinones (vitamin K2) in human health. British Journal of Nutrition. 2013;110(8):1357-68.
13. Shearer MJ, Newman P. Recent trends in the metabolism and cell biology of vitamin K with special reference to vitamin K cycling and MK-4 biosynthesis. J Lipid Res. 2014;55(3):345-62.
14. Walther B, Karl JP, Booth SL, Boyaval P. Menaquinones, bacteria, and the food supply: the relevance of dairy and fermented food products to vitamin K requirements. Adv Nutr. 2013;4(4):463-73.
15. Hollander D, Muralidhara KS, Rim E. Colonic absorption of bacterially synthesized vitamin K2 in the rat. Am J Physiol. 1976;230(2):251-5.
16. Hollander D, Rim E, Ruble PE, Jr. Vitamin K2 colonic and ileal in vivo absorption: bile, fatty acids, and pH effects on transport. Am J Physiol. 1977;233(2):E124-9.
17. Groenen-van Dooren MM, Ronden JE, Soute BA, Vermeer C. Bioavailability of phylloquinone and menaquinones after oral and colorectal administration in vitamin K-deficient rats. Biochem Pharmacol. 1995;50(6):797-801.
18. Guss JD, Taylor E, Rouse Z, Roubert S, Higgins CH, Thomas CJ, et al. The microbial metagenome and bone tissue composition in mice with microbiome-induced reductions in bone strength. Bone. 2019;127:146-54.

19. Wu CS, Muthyala SDV, Klemashevich C, Ufondu AU, Menon R, Chen Z, et al. Age-dependent remodeling of gut microbiome and host serum metabolome in mice. Aging (Albany NY). 2021;13(5):6330-45.
20. Fu X, Booth SL, Smith DE. Vitamin K contents of rodent diets: a review. J Am Assoc Lab Anim Sci. 2007;46(5):8-12.
21. Guss JD, Horsfield MW, Fontenele FF, Sandoval TN, Luna M, Apoorva F, et al. Alterations to the Gut Microbiome Impair Bone Strength and Tissue Material Properties. J Bone Miner Res. 2017;32(6):1343-53.
22. Liu C, Cyphert EL, Stephen SJ, Wang B, Morales AL, Nixon JC, et al. Microbiome–induced increases and decreases in bone matrix strength can be initiated after skeletal maturity. Journal of Bone and Mineral Research. 2024;39(11):1621-32.
23. MacGregor RR, Graziani AL. Oral administration of antibiotics: a rational alternative to the parenteral route. Clin Infect Dis. 1997;24(3):457-67.
24. Ma J, Ding X, Sun C, Lin C, An X, Lin G, et al. Development and validation a liquid chromatography mass spectrometry for determination of solasodine in rat plasma and its application to a pharmacokinetic study. J Chromatogr B Analyt Technol Biomed Life Sci. 2014;963:24-8.
25. Thevaranjan N, Puchta A, Schulz C, Naidoo A, Szamosi JC, Verschoor CP, et al. Age-Associated Microbial Dysbiosis Promotes Intestinal Permeability, Systemic Inflammation, and Macrophage Dysfunction. Cell Host Microbe. 2017;21(4):455-66.e4.
26. Shearer MJ, Newman P. Metabolism and cell biology of vitamin K. Thromb Haemost. 2008;100(4):530-47.
27. Conly JM, Stein K. The production of menaquinones (vitamin K2) by intestinal bacteria and their role in maintaining coagulation homeostasis. Prog Food Nutr Sci. 1992;16(4):307-43.
28. Hirota Y, Tsugawa N, Nakagawa K, Suhara Y, Tanaka K, Uchino Y, et al. Menadione (vitamin K3) is a catabolic product of oral phylloquinone (vitamin K1) in the intestine and a circulating precursor of tissue menaquinone-4 (vitamin K2) in rats. J Biol Chem. 2013;288(46):33071-80.
29. Koivu-Tikkanen TJ, Schurgers LJ, Thijssen HH, Vermeer C. Intestinal, hepatic, and circulating vitamin K levels at low and high intakes of vitamin K in rats. Br J Nutr. 2000;83(2):185-90.
30. Liu M, Liu C, Cevallos N, Orbach BN, Hernandez CJ, Fu X, et al. Dietary menaquinone-9 supplementation does not influence bone tissue quality or bone mineral density during skeletal development in mice. JBMR Plus. 2025;9(6).
31. Harshman SG, Fu X, Karl JP, Barger K, Lamon-Fava S, Kuliopulos A, et al. Tissue Concentrations of Vitamin K and Expression of Key Enzymes of Vitamin K Metabolism Are Influenced by Sex and Diet but Not Housing in C57Bl6 Mice. J Nutr. 2016;146(8):1521-7.
32. Ellis JL, Karl JP, Oliverio AM, Fu X, Soares JW, Wolfe BE, et al. Dietary vitamin K is remodeled by gut microbiota and influences community composition. Gut Microbes. 2021;13(1):1-16.
33. Fenn K, Strandwitz P, Stewart EJ, Dimise E, Rubin S, Gurubacharya S, et al. Quinones are growth factors for the human gut microbiota. Microbiome. 2017;5(1):161.

Table 1. Fecal MK concentrations (pmol/g) of aged mice that received standard lab chow containing 80 mg menadione/kg diet and were treated with oral broad-spectrum antibiotics from 19-22 months of age (Experiment A)

	Male			**Female**		
MK detected	**Untreated (n=15)**	**Antibiotic Treated (n=15)**	***P values***	**Untreated (n=15)**	**Antibiotic Treated (n=15)**	***P values***
MK4	9±1	9±3	*0.287*	15±3	19±3	*0.365*
MK5	ND	ND		8±3	ND	*0.057*
MK6	263±66	35±9	*<0.001*	782±366	26±6	*0.002*
MK7	7±1	16±1	*<0.001*	15±4	24±2	*0.495*
MK8	26±2	173±22	*<0.001*	33±8	342±47	*<0.001*
MK9	196±15	593±69	*<0.001*	145±16	653±61	*<0.001*
MK10	2584±235	3186±236	*0.087*	1908±280	3544±290	*<0.001*
MK11	1123±99	2332±130	*<0.001*	961±123	2985±260	*<0.001*
MK12	284±39	434±30	*0.034*	167±26	709±100	*<0.001*
MK13	356±60	28±3	*<0.001*	124±45	30±6	*<0.001*

Values are geometric mean±SEM. Differences between treatment groups were determined using independent t-test. Males and female were analyzed separately with statistical significance set as $p<0.01$. ND, not detectable. MK5-MK13 measured by LC-MS (MK5, MK7, MK8, MK9, MK11-13 LLOD<5pmol/g; MK6 LLOD<10 pmol/g; MK10 LLOD<1 pmol/g), MK4 measured by HPLC (LLOD<0.1 pmol/g).

Table 2. Fecal MK concentrations (pmol/g) of young mice that received a diet containing 2.1 mg MK9/kg diet and were treated with oral broad-spectrum antibiotics from 4-weeks to 16-weeks of age (Experiment B)

	Male			**Female**		
MK detected	**Untreated (n=15)**	**Antibiotic treated (n=9)**	***P values***	**Untreated (n=15)**	**Antibiotic treated (n=14)**	***P values***
MK4	ND	ND		ND	ND	
MK5	1±0.3	ND	*0.087*	1±1	ND	*0.124*
MK6	249±56	1±1	*<0.001*	553±166	3±2	*<0.001*
MK7	3±2	14±7	*0.013*	13±5	22±9	*0.097*
MK8	102±11	329±27	*<0.001*	164±29	174±140	*0.025*
MK9	960±136	1251±55	*0.043*	1756±267	1523±169	*0.428*
MK10	427±55	7±3	*<0.001*	688±103	5±1	<0.001
MK11	512±46	6±2	*<0.001*	660±95	6±2	*<0.001*
MK12	218±35	ND	*<0.001*	193±88	5±1	*<0.001*
MK13	7±4	ND	*0.115*	ND	ND	

Values are geometric mean±SEM. Differences between treatment groups were determined using independent t-test. Males and female were analyzed separately with statistical significance set as $p<0.01$. ND, not detectable. MK4-MK13 measured by Q-TOF-MS (MK4-MK8 LLOD<1 pmol/g; MK9-MK13 LLOD<5 pmol/g).

Table 3. Detected tissue MK concentrations (pmol/g) of aged mice that received standard lab chow containing 80 mg menadione/kg diet and were treated with oral broad-spectrum antibiotics from 18-22 months of age (Experiment A)

		Male			Female		
Tissue	**MK Detected**	**Untreated (n=15)**	**Antibiotic Treated (n=15)**	***P values***	**Untreated (n=15)**	**Antibiotic Treated (n=15)**	***P values***
Liver	**MK4**	30±3	24±3	*0.302*	68±4	80±7	*0.143*
	MK10	33±5	24±5	*0.124*	79±16	52±13	*0.177*
Duodenum	**MK4**	204±20	193±24	*0.791*	386±46	175±61	*0.003*
	MK6	10±2	ND	*0.013*	10±4	ND	*0.208*
Jejunum	**MK4**	188±18	181±16	*0.767*	199±20	188±16	*0.668*
	MK6	11±3	ND	*0.13*	17±7	ND	*0.014*
Ileum	**MK4**	251±23	273±42	*0.604*	324±20	253±24	*0.035*
	MK6	14±4	ND	*0.037*	16±6	ND	*0.046*
Colon	**MK4**	133±5	139±7	*0.402*	245±16	199±12	*0.022*
	MK6	18±6	ND	*0.055*	43±17	ND	*0.026*
	MK8	ND	9±3	*0.001*	ND	14±4	*0.001*
	MK9	18±4	42±13	*0.009*	17±6	44±6	*0.04*
	MK10	72±12	226±46	*<0.001*	74±21	188±26	*0.002*
	MK11	108±16	210±28	*0.001*	111±24	214±26	*0.008*
	MK12	8±2	26±7	*<0.001*	ND	38±10	*<0.001*
	MK13	7±1	ND	*0.058*	6±2	ND	*0.129*

Values are geometric mean±SEM. Differences between treatment groups were determined using independent t-test. Males and female were analyzed separately with statistical significance set as $p<0.01$. ND, not detectable. MK5-MK13 measured by LC-MS (MK5, MK7, MK8, MK9, MK11-13 LLOD<5 pmol/g; MK6 LLOD<10 pmol/g; MK10 LLOD<1 pmol/g), MK4 measured by HPLC (LLOD<0.1 pmol/g).

Table 4. Detected tissue MK concentrations (pmol/g) of young mice that received a diet containing 2.1 mg MK9/kg diet and were treated with oral broad-spectrum antibiotics from 4-weeks to 16-weeks of age (Experiment B)

		Male			**Female**		
Tissue	**MK Detected**	**Untreated (n=15)**	**Antibiotic Treated (n=9)**	***P values***	**Untreated (n=15)**	**Antibiotic Treated (n=14)**	***P values***
Liver	**MK4**	5±1	5±1	*0.963*	9±1	21±3	*<0.001*
	MK9	8±2	5±1	*0.031*	30±4	26±4	*0.606*
Duodenum	**MK4**	10±1	8±1	*0.218*	30±2	20±2	*<0.001*
Jejunum	**MK4**	11±1	8±1	*0.02*	30±2	17±2	*<0.001*
Ileum	**MK4**	26±2	19±1	*0.035*	43±4	39±3	*0.32*
Colon	**MK4**	12±2	15±3	*0.174*	33±3	44±3	*0.035*
	MK6	11±4	ND	*0.032*	11±7	ND	*0.032*
	MK7	ND	1±1	*0.322*	ND	1±1	*0.315*
	MK8	2±1	4±2	*0.164*	ND	2±1	*0.006*
	MK9	11±3	16±3	*0.283*	8±2	15±3	*0.016*
Bone	**MK4**	32±4	23±4	*0.092*	54±7	55±5	*0.874*

Values are geometric mean±SEM. Differences between treatment groups were determined using independent t-test. Males and female were analyzed separately with statistical significance set as $p<0.01$. ND, not detectable. MK4-MK13 measured by Q-TOF-MS (MK4-MK8 LLOD<1 pmol/g; MK9-MK13 LLOD<5 pmol/g).

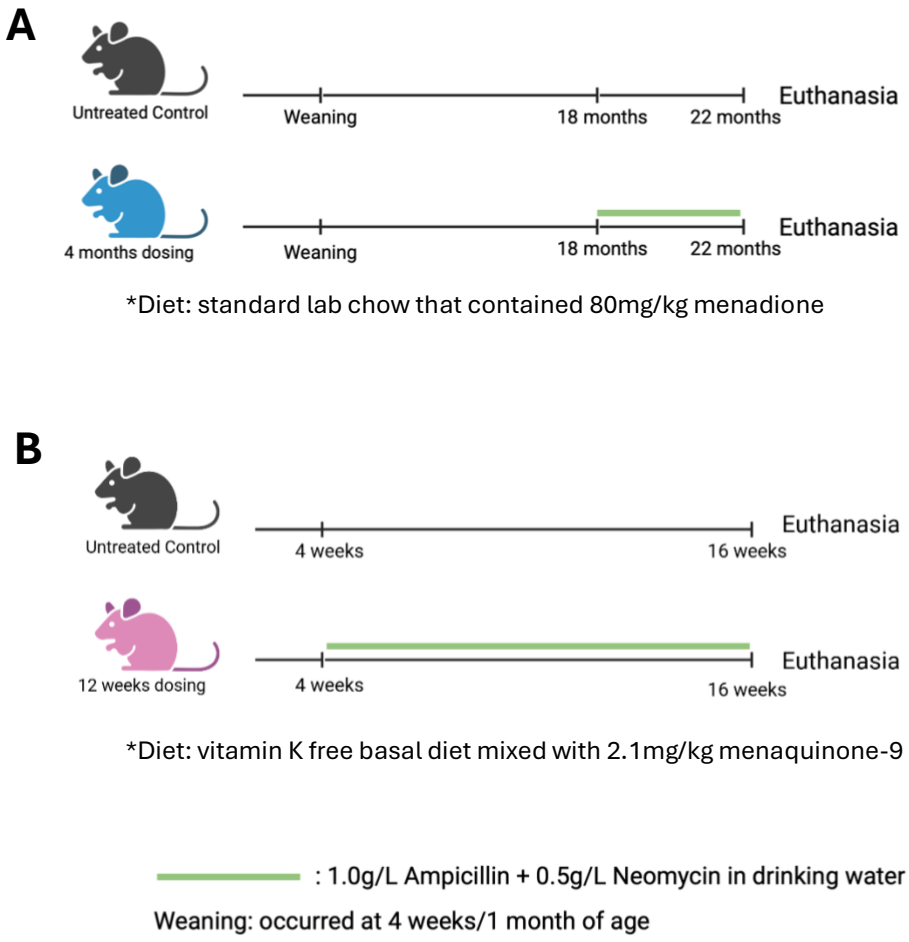

Figure 1. Animal study design, (A) Aged mice (Experiment A), four-week-old male and female (n=15/sex/group) C57BL/6 mice received standard lab chow containing 80mg menadione /kg diet and treated with oral antibiotics from 19-22 months or untreated; (B) young mice (Experiment B), four-week-old male and female (n=16/sex/group) C57BL/6 mice received diet containing 2.1mg menaquinone-9/kg diet with or without oral antibiotic treatment for 12 weeks.

Supplemental Material

Macronutrients		
Crude Protein	%	19.1
Fat (ether extract) [a]	%	5.8
Carbohydrate (available) [b]	%	44.3
Crude Fiber	%	4.6
Neutral Detergent Fiber [c]	%	13.7
Ash	%	6.1
Energy Density [d]	kcal/g (kJ/g)	3.1 (13.0)
Calories from Protein	%	25
Calories from Fat	%	17
Calories from Carbohydrate	%	58
Minerals		
Calcium	%	1.0
Phosphorus	%	0.7
Non-Phytate Phosphorus	%	0.4
Sodium	%	0.3
Potassium	%	0.8
Chloride	%	0.5
Magnesium	%	0.2
Zinc	mg/kg	63
Manganese	mg/kg	93
Copper	mg/kg	23
Iodine	mg/kg	3
Iron	mg/kg	240
Selenium	mg/kg	0.16
Amino Acids		
Aspartic Acid	%	1.8
Glutamic Acid	%	2.8
Alanine	%	1.0
Glycine	%	0.8
Threonine	%	0.8
Proline	%	1.4
Serine	%	1.3
Leucine	%	1.7
Isoleucine	%	0.8
Valine	%	0.9
Phenylalanine	%	0.9
Tyrosine	%	0.8
Methionine	%	0.4
Cystine	%	0.3
Lysine	%	1.0
Histidine	%	0.5
Arginine	%	1.2
Tryptophan	%	0.3

Standard Product Form: ***Pellet***

Vitamins		
Vitamin A [e, f]	IU/g	30.0
Vitamin D_3 [e, g]	IU/g	2.4
Vitamin E	IU/kg	150
Vitamin K_3 (menadione)	mg/kg	80
Vitamin B_1 (thiamin)	mg/kg	95
Vitamin B_2 (riboflavin)	mg/kg	14
Niacin (nicotinic acid)	mg/kg	100
Vitamin B_6 (pyridoxine)	mg/kg	17
Pantothenic Acid	mg/kg	87
Vitamin B_{12} (cyanocobalamin)	mg/kg	0.09
Biotin	mg/kg	0.77
Folate	mg/kg	7
Choline	mg/kg	2200
Fatty Acids		
C16:0 Palmitic	%	0.6
C18:0 Stearic	%	0.2
C18:1ω9 Oleic	%	1.3
C18:2ω6 Linoleic	%	2.6
C18:3ω3 Linolenic	%	0.3
Total Saturated	%	0.8
Total Monounsaturated	%	1.3
Total Polyunsaturated	%	2.9
Other		
Cholesterol	mg/kg	--

Figure 1S. Aged mice were fed a standard rodent sterilized diet (Teklad LM-485) with 80mg menadione/kg diet.

TD.120060 Vitamin K Defic. Basal Mix (95%)

Formula	g/Kg
Isolated Soy Protein	202.1
DL-Methionine	1.053
Sucrose	532.07
Corn Starch	157.9044
Cellulose	52.63
Mineral Mix, AIN-76 (170915)	36.84
Calcium Carbonate	11.84
p-Aminobenzoic Acid	0.116
Vitamin C, ascorbic acid, coated (97.5%)	1.074
Biotin	0.0004
Vitamin B12 (0.1% in mannitol)	0.0316
Calcium Pantothenate	0.069
Choline Dihydrogen Citrate	3.68
Folic Acid	0.0021
Inositol	0.116
Niacin	0.1042
Pyridoxine HCl	0.0232
Riboflavin	0.0232
Thiamin HCl	0.0232
Vitamin A Palmitate (500,000 IU/g)	0.0421
Vitamin D3, cholecalciferol (500,000 IU/g)	0.0046
Vitamin E, DL-alpha tocopheryl acetate (500 IU/g)	0.253

Footnote

This modification of TD.97053 removes corn oil to make room for tocopherol-stripped corn oil with a phylloquinone source. End user mixes 950 g of TD.120060 with 50 g of oil.

Selected Nutrient Information[1]

	% by weight	% kcal from
Protein	17.7	20.5
Carbohydrate	68.1	79.0
Fat	0.2	0.5
Kcal/g 3.5		

[1] Values are calculated from ingredient analysis or manufacturer data

Figure 2S. Young mice were fed a vitamin K-free basal diet (Inotiv, TD.120060) with 2.1mg MK9/kg diet. Purchased MK9 (IsoScience) was solubilized in tocopherol-stripped corn oil (5% diet; Inotiv, CA.160160) and then mixed into vitamin K-free basal diet mix (95% diet).

*Product form: powder

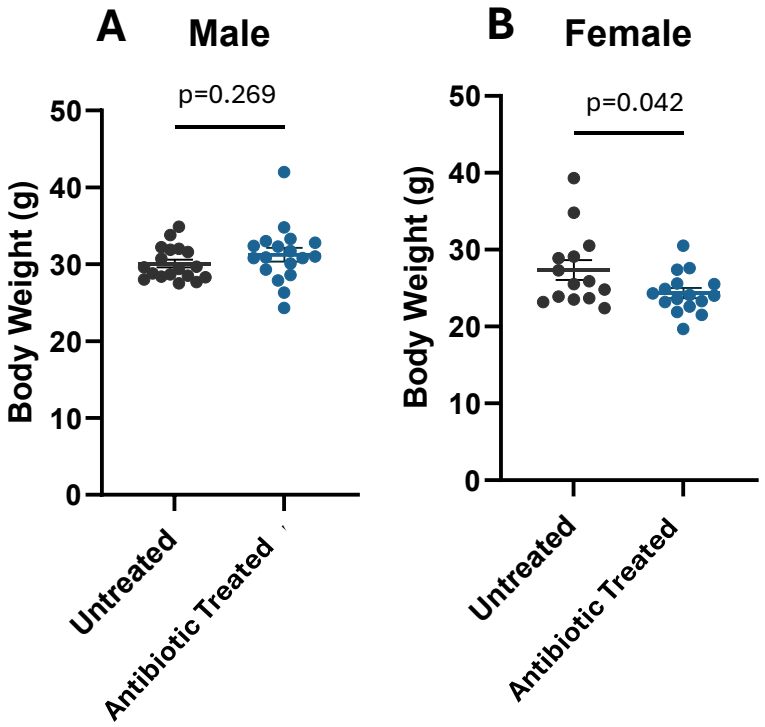

Figure 3S. Body weight (g) at 22 months of male (A) and female (B) mice that received standard lab chow containing 80 mg menadione/kg diet and were treated with broad-spectrum antibiotics from 19-22 months of age, then sacrificed (Experiment B). Differences between treatment groups were determined using an independent t-test. Males and females were analyzed separately, with statistical significance set as $p<0.01$. Data are presented as mean ±SEM.

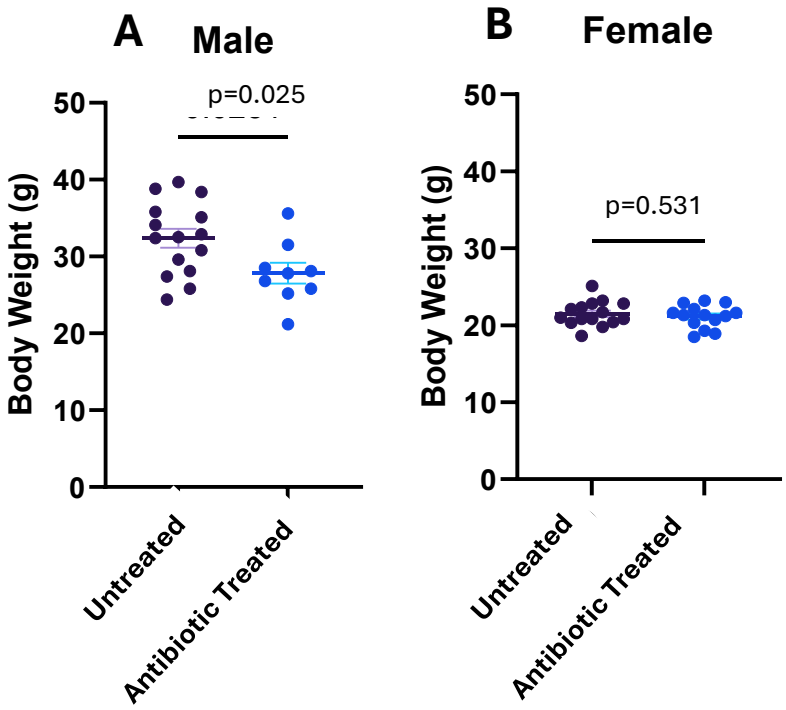

Figure 4S. Body weight (g) at 16 weeks of male (A) and female (B) mice that received a diet containing 2.1 mg MK9/kg diet and were treated with broad-spectrum antibiotics from 4 weeks to 16 weeks of age, then sacrificed (Experiment A). Differences between treatment groups were determined using an independent t-test. Males and females were analyzed separately, with statistical significance set as $p<0.01$. Data are presented as mean ±SEM.

3.2 Dietary Menaquinone-9 Supplementation Does Not Influence Bone Tissue Quality or Bone Mineral Density During Skeletal Development in Mice

Minying Liu[1], Chongshan Liu[2,3], Nicolas Cevallos[2], Benjamin N Orbach[1], Christopher J Hernandez[2], Xueyan Fu[1], Jennifer Lee[1,4], Sarah L Booth[1], M Kyla Shea[1]

[1] USDA Human Nutrition Research Center on Aging, Tufts University, Boston, MA

[2] Orthopaedic Surgery, University of California, San Francisco, CA

[3] Sibley School of Mechanical and Aerospace Engineering, Cornell University, Ithaca, NY

[4] Graduate School of Biomedical Sciences, Tufts University, Boston, MA

Correspondence: Kyla Shea, PhD, 711 Washington St., Boston MA USA 02111; 617 556 3370; kyla.shea@tufts.edu

PMID: 40386291 **PMCID:** PMC12083984 **DOI:** 10.1093/jbmrpl/ziaf059

Conflicts of interest: The authors declare no competing interests.

Data availability: The data that support the findings of this study are available from the corresponding author, upon reasonable request.

Supported by NIA R01 R01AG067997 and USDA Agricultural Research Service under Cooperative Agreement 58-8050-3-003. Any opinions, findings, conclusions, or recommendations expressed in this publication are those of the authors and do not necessarily reflect the view of the USDA.

Abbreviations:

$^{2}H_{7}$MK9 deuterium-labeled MK9

BMD bone mineral density

CBU Comparative Biology Unit

DEXA dual-energy X-ray absorptiometry

HNRCA Tufts University Human Nutrition Research Center on Aging

LC-MS liquid chromatography mass spectrometry

MK menaquinone

PBS phosphate-buffered saline

PK phylloquinone

Q-TOF-MS time-of-flight mass spectrometry

ABSTRACT

Vitamin K has been implicated in skeletal health because vitamin K-dependent proteins are present in bone. While there are multiple forms of vitamin K, most research has focused on phylloquinone, which is found mainly in plant-based foods, and its metabolite menaquinone-4 (MK4). However, there are additional forms of vitamin K that are bacterially produced that appear to influence bone health but have not yet been studied extensively. Herein, we evaluated the effects of menaquinone-9 (MK9), a bacterially produced form of vitamin K on bone tissue quality and density in young mice. Four-week-old male (n=32) and female (n=32) C57BL/6 mice were supplemented with 0.06 mg/kg diet or 2.1 mg/kg diet of MK9 for 12 weeks. During week 11, a sub-group of mice (n=7/sex/group) received daily deuterium-labeled MK9 to trace its metabolic fate in bone. Liver MK4 and MK9 were significantly higher in mice fed 2.1 mg MK9/kg compared to those receiving 0.06 mg MK9/kg, regardless of sex (all $p \leq 0.017$). MK4 was the only vitamin K form detected in bone, with 63-67% of skeletal MK4 in mice fed 2.1 mg MK9/kg derived from deuterium-labeled MK9. Femoral tissue strength, maximum bending

moment, section modulus, and bone mineral density did not differ significantly across diet groups in either sex (all $p \geq 0.083$). Cross-sectional area ($p=0.003$) and moment of inertia ($p=0.001$) were lower in female mice receiving 2.1 mg MK9/kg compared to those receiving 0.06 mg MK9/kg, but no differences were found in male mice. Higher bone MK4 concentrations did not correlate with higher bone tissue quality or density. Despite dietary MK9 being a dietary precursor to MK4 in bone, dietary MK9 supplementation did not affect bone tissue quality or bone mineral density during skeletal development.

Keywords: skeletal health, bone tissue quality, bone mineral density, vitamin K, menaquinone

Lay summary: Most vitamin K and bone health research has focused on phylloquinone, the plant-based vitamin K form, and its metabolite menaquinone-4. Interest in bacterially produced vitamin K forms is growing since they are abundant in the intestinal microbiome. We evaluated the effect of a bacterially-produced vitamin K form on skeletal health by feeding 4-week old mice diets with low and high doses of menaquinone-9 for 12 weeks. We also used stable-isotope labeled menaquinone-9 to trace its conversion to menaquinone-4 in bone. Menaquinone-9 served as a precursor to menaquinone-4 in bone, but menaquinone-9 supplementation did not improve skeletal health during skeletal development.

INTRODUCTION

Vitamin K, an essential fat-soluble nutrient, has been implicated in bone health (1) based on its role as an enzymatic cofactor required for the post-translational carboxylation of certain proteins (vitamin K-dependent proteins) (2). One such protein is osteocalcin, the predominate non-collagenous protein in bone. Once carboxylated, osteocalcin binds to calcium in the bone matrix (3). There are multiple naturally-occurring forms of vitamin K which are capable of carboxylation. The plant-based form, phylloquinone (PK) is found in green leafy vegetables and

vegetable oils (4). Menaquinones (MKs) are a class of vitamin K compounds that are primarily bacterially produced and are therefore abundant in the intestinal microbiome. At least 13 MK forms have been identified that differ structurally from PK in the length and saturation of their prenylated side chain, with the number of prenyl units differentiating among the specific MKs (MKn) (5, 6).

Among the menaquinones, MK4 is unique because it is not known to be made by bacteria. Instead, it is synthesized in several extra-hepatic tissues from other forms of vitamin K, including MKs that are bacterially synthesized (7-9). It was recently demonstrated that MK4 is found in bone (9), but the role of dietary vitamin K as a precursor to MK4 in bone has not yet been fully elucidated. This is an important gap to address because MK4 signaling pathways have been implicated in bone tissue homeostasis (10, 11).

Most observational studies and randomized clinical trials evaluating the role of vitamin K in skeletal health have focused primarily on PK and MK4, with age-related bone loss measured using bone mineral density (BMD) as the main outcome. However, these studies have yielded inconsistent results (12). A systematic review and meta-analysis of randomized controlled trials that tested the effect of PK or MK4 supplementation on age-related bone loss concluded there is little evidence that vitamin K affects BMD or vertebral fractures. The authors reported a potentially beneficial effect of PK or MK4 supplementation on clinical fracture risk, but concluded additional studies are needed to confirm this (13). While fragility fractures are often associated with low BMD, they also occur in individuals with normal BMD (14). Bone tissue quality—encompassing bone strength and mechanical properties—is another critical aspect of bone health not captured by BMD (15-18). An impairment in bone tissue quality can reduce whole bone strength without altering BMD (19). In mice, knockout of the vitamin K-dependent

protein osteocalcin results in impaired bone tissue composition and quality with only minor changes in bone geometry or BMD (20, 21). Hence, vitamin K-induced alteration of bone tissue quality may not be reflected in BMD or other indices of bone geometry and mass. Furthermore, there are limited data on the potential effects of bacterially-produced MKs on bone health outcomes. Addressing this gap is essential for understanding the broader role of vitamin K in skeletal health.

To clarify the role of bacterially-produced MK forms in bone tissue, we supplemented male and female C57BL/6 mice with two different doses of menaquinone-9 (MK9) in their diet for 12 weeks. We chose MK9 because: (I) MK9 is a MK form produced by bacteria. (II) Of the MK forms currently characterized in the food supply, MK9 is the most abundant, especially in dairy and fermented products (6). (III) Through use of stable isotopes, we have already characterized the metabolic fate of dietary MK9 in C57BL/6 mice, including the conversion of MK9 to MK4 in extra-hepatic tissues other than bone (9), which serves as a quality control from which to compare our findings. We also evaluated the conversion of dietary MK9 to MK4 in skeletal tissue using stable isotopes. We hypothesized that dietary supplementation with MK9 would positively influence bone tissue quality and density and serve as a precursor to MK4 in bone tissue.

MATERIALS AND METHODS

Study design and experimental diets

Three-week-old male (n=32) and female (n=32) C57BL/6 mice were acquired from Charles River Laboratories and housed in single cages at the Tufts University Human Nutrition Research Center on Aging (HNRCA) Comparative Biology Unit (CBU). Upon arrival, mice were acclimated to an AIN-93G diet (Inotiv, TD.94045), which contained 1mg/kg PK per

manufacture, for one week. At 4 weeks of age, mice were divided at random into 2 experimental groups to receive diets containing varying amounts of MK9 for 12 weeks (22). Males and females were randomized separately to one of the two experimental groups (**Figure 1**): (I) diet containing 2.1 mg/kg MK9, (II) diet containing 0.06 mg/kg MK9. Diets were composed of a mixture of the vitamin K-free basal diet (Inotiv, TD.120060) with two different amounts of MK9. An MK9 content of 2.1 mg/kg corresponds to the recommended vitamin K intake, which was based on the molar equivalent of MK9 to the currently recommended concentration of vitamin K for rodents (1mg/kg PK), following a protocol developed by the Vitamin K Laboratory at the HNRCA (23). In contrast, an MK9 content of 0.06 mg/kg indicates a vitamin K intake below the recommended level, which was molar equivalent to 31 ± 0.45 μg PK/kg contained in vitamin K-free basal diet (9, 24). The Vitamin K laboratory previously demonstrated that feeding mice a diet containing MK9 (as the only form of vitamin K in the diet) in an equal molar amount to the current rodent diet recommendations showed no sign of vitamin K-deficiency (9, 24). Mice were pair-fed between diet groups to minimize the possibility that any outcome differences would be due to differences in the total amount of food consumed.

To determine whether MK9 from the diet serves as a precursor to MK4 present in bone a subset of mice (n=14, 7 males and 7 females) from each group were randomly selected to receive daily diets containing deuterium-labeled MK9 ($^{2}H_{7}$MK9) (in the same amount as in the initial diet, mixed with vitamin K-free basal diet using the protocol developed by the Vitamin K Laboratory) during week 11 of the experiment (the last week prior to sacrifice) (**Figure 1**). MK9 concentrations in study diets were measured by liquid chromatography-mass spectrometry (LC-MS)(25), and diet MK9 concentrations were 0.06±0.004 mg MK9/kg, 0.07±0.006 mg $^{2}H_{7}$MK9/kg, 2.03±0.12 mg MK9/kg, and 2.47±0.18 mg $^{2}H_{7}$MK9/kg, respectively.

Animals were euthanized at 16 weeks of age. After sacrifice, mice carcasses were scanned for bone mineral density measurement, and then femurs, tibias, and liver were collected immediately after euthanasia and stored and maintained at -80 ℃ for bone biomechanical testing and vitamin K analyses. All animal experiments and procedures were approved by the Institutional Animal Care and Use Committee at the HNRCA at Tufts University.

Bone tissue quality

Right femurs were dissected and shipped to the Hernandez Laboratory at the University of California, San Francisco, where femur length, cross-sectional geometry, and maximum bending force were measured, as described elsewhere (22, 26). In brief, femur length was measured using digital calipers from the greater trochanter to the lateral condyle. The femoral diaphyseal cross-section was imaged with a micro-computed tomography scanner at a voxel size of 10 μm to assess femoral cross-sectional geometry. The measurements included cortical cross-sectional area, moment of inertia about the medial-lateral axis (I), the distance from the neutral axis to bone surface (c), and section modulus (I/c). For mechanical testing, femurs were thawed to room temperature and kept hydrated. They were then subjected to three-point bending tests in the anterior-posterior direction using the electromechanical testing instrument (ElectroForce 3200, TA instruments) until failure occurred (loading rate = 0.1 mm/s, span length = 8 mm between outer loading pins). The maximum bending force and displacement were recorded. The maximum bending force was used to calculate maximum bending moment (max force x span length/4). Bone tissue strength was calculated using maximum bending moment and cross-sectional geometric measurements (maximum bending moment / section modulus).

Bone mineral density

After sacrifice, mice carcasses were scanned using the InAlyzer2 dual-energy X-ray absorptiometry (DEXA) system, Model M (Medikors Inc., Korea) at HNRCA, with details described elsewhere (27). In brief, a quality control phantom was scanned prior to each measurement. Each carcass was positioned in the center of the scanning area in a prone position, with its arms and legs extended outward and its tail aligned straight behind the body. Scans were performed with a pixel size of 103×106 μm and a pixel pitch of 48 μm (108 μm in analysis). Total body BMD (g/cm²) was obtained using InAlyzer software version 3.2.3.

Vitamin K analyses

Measurements of MKs in bone and liver were conducted in the Vitamin K Laboratory at HNRCA as previously described (25). Briefly, liver tissues (0.15 g) were homogenized in phosphate-buffered saline (PBS) by use of a Powergen homogenizer (Fisher Scientific). Left and right tibias (in total of 0.1g) collected at sacrifice were fragmented using a stainless-steel tissue pulverizer (Biospec) with the addition of liquid nitrogen to ensure thorough pulverization. The resulting bone powder was transferred into 2 mL tubes pre-filled with beads, followed by the addition of 1 mL PBS. Samples were then homogenized using an Omni Bead Ruptor 24 Homogenizer, running two cycles of 1 minute each. Homogenized tissue samples were extracted using hexane, further purified using solid-phase extraction, and then quantified using Quadrupole Time-of-Flight Mass Spectrometry (Q-TOF-MS). To differentiate deuterium-labeled vitamin K forms, a ProntoSil C30 column is required for the separation of stereoisomers (28).

Statistical power and analyses

Sample size calculations were based on the work of Guss et al (22), who reported a decrease of 3.6 N/mm^2 in femoral peak moment bending/I/c in 4-week-old C57BL/6 male mice treated with oral antibiotics for 12 weeks compared to mice that received no antibiotic treatment

($p<0.05$). The between group standard deviation was 2.5 (22). Fifteen mice per group provided 92% power to detect a between group difference of 3.6, using a two-tailed alpha of 0.05. With 2 experimental groups, we had at least 85% power to detect differences comparable to 3.6 N/mm^2 in Peak Moment in bending/I/c, accounting for up to 6 pair-wise comparisons.

Data are presented as means ± SD. Statistical analyses were performed using RStudio (v.4.3.1, 2023). The Shapiro-Wilk test was used to assess normality, and the Levene's test was employed to evaluate equal variance. For outcome measures that satisfied parametric assumptions, an independent two-sample t-test was conducted to compare femoral tissue strength (primary outcome), other skeletal outcomes, liver, and bone vitamin K concentrations between diet groups. When parametric assumptions were not met, data were log-transformed to achieve normality, and parametric assumptions were reassessed. The correlations between bone MK4 concentrations and bone biomechanical and geometry outcomes were assessed using the Pearson correlation coefficient. Analyses were conducted separately for males and females, with statistical significance set at $p < 0.05$. Normalization by body weight was achieved by dividing bone biomechanical measurements by body weight.

RESULTS

Eight mice died prior to the end of the study (7 males and 1 female). The highest mortality rate, 38%, was observed among male mice receiving 0.06 mg/kg MK9. In contrast, all female mice receiving 0.06 mg/kg MK9 treatment survived. Additionally, one mouse of each sex was lost among those receiving 2.1 mg/kg MK9, corresponding to a mortality rate of 1% (See Supplemental **Figure S1**).

Bone tissue quality and density

Femoral tissue strength was not different across diet groups for either sex (male p=0.725; female p=0.302, **Table 1**). Similarly, there were no differences in maximum bending moment between diet groups for either male or female mice (p=0.763 and 0.083 respectively, **Table 1**) or in sectional modulus in male or female mice between the diet groups (p=0.873 and 0.277 respectively, **Table 1**).

Female mice receiving 0.06 mg/kg MK9 had higher moment of inertia and cross-sectional area compared to female mice receiving 2.1mg/kg MK9 (all p-values≤0.003). No significant differences in these two measurements were observed among the male mice across diet groups (all p-values≥0.205, **Table 1**). No significant differences were observed in femur length across diet groups for either male or female mice (p-values≥0.288, **Table 1**). In addition, total body bone mineral density did not differ between diet groups in either sex (all p-values≥0.306, **Table 1**).

Body weight did not differ between diet groups for either male or female mice (all p-values≥0.345, see Supplemental **Figure S2**). When normalized to body weight, femoral tissue strength, maximum moment, section modulus, moment of inertia, and femur length in both male and female mice remained unchanged (see Supplemental **Table S1**). The difference in femoral cross-sectional area for female mice was not statistically significant (p=0.060, **Table S1**).

Tissue Vitamin K Content

We detected MK4 and MK9 in the liver, with significantly higher concentrations of both observed in mice fed 2.1 mg MK9/kg compared to those receiving 0.06 mg MK9/kg, regardless of sex (all $p \leq 0.017$, **Figure 2A–D**). Furthermore, liver concentrations of MK9 were higher than those of MK4. MK4 was the only vitamin K form detected in bone. Mice receiving 0.06 mg/kg MK9 had significantly lower bone MK4 concentrations compared to mice receiving 2.1mg/kg

MK9 in both sexes (all p values<0.001; **Figure 3 AB**). In the subset of mice fed deuterium-labeled MK9 for the week prior to sacrifice, deuterium-labeled MK4 was detected in bone tissue of both male and female mice that received 2.1 mg/kg labeled MK9 (mean ± SD at 22 ± 9 pmol/g for males and 37 ± 21 pmol/g for females, **Table 2**). In addition, 63-67% of MK4 measured in bone was derived from labeled MK9 (**Table 2**). In female mice, bone tissue MK4 concentrations were significantly inversely correlated with cross-sectional area (Pearson r = -0.55, p = 0.008) and nearly significantly inversely correlated with moment of inertia (Pearson r = -0.40, p = 0.066). Otherwise, bone tissue MK4 concentrations did not correlate with any other bone outcome analyzed (Pearson r coefficients range -0.25 to +0.29, all p values ≥ 0.25; **Figure S3**), and bone MK4 concentrations were not correlated with any bone outcome in male mice (Pearson r range + 0.01 to + 0.30, all p ≥ 0.35; **Figure S3**).

DISCUSSION

Our findings did not support our hypothesis that dietary supplementation with MK9 will positively influence bone tissue quality and density in mice. In both sexes of mice, femoral tissue strength, section modulus, maximum bending moment, femur length, and bone mineral density did not differ between those fed 0.06 mg MK9/kg diet and those fed 2.1 mg MK9/kg diet. In male mice, moment of inertia and cross-sectional area also did not differ between the diet groups. In female mice, the moment of inertia and cross-sectional area were higher in those receiving 0.06 mg MK9 /kg diet compared to those receiving 2.1 mg MK9 /kg diet. These findings further contradict our hypothesis that higher dietary MK9 intake improves skeletal health.

MK4 and MK9 were found in liver tissues of both sexes. MK9 detected in liver reflects the absorption of vitamin K form supplemented in diet, aligning with a prior study that demonstrated that orally supplemented vitamin K forms accumulated in liver (9). MK4 was the only form of

vitamin K detected in bone tissue, with significantly higher concentrations observed in mice receiving the higher dose of MK9. These findings suggest that bone MK4 concentrations respond to dietary MK9 intakes, consistent with what has been reported in other tissues. It was recently demonstrated using stable isotopes that multiple dietary vitamin K forms, including MK9, convert to MK4 in certain tissues (9). However, bone was not measured in that experiment (9). Here we used stable isotopes to evaluate the conversion of dietary MK9 to MK4 in skeletal tissue, and found 63 to 67 % of the MK4 in bone was derived from the labeled MK9 - supporting our hypothesis that dietary MK9 serves as a precursor to MK4 in bone tissue. However, the MK4 concentrations in bone tissue were, for the most part, not correlated with bone tissue quality or density. Moreover, in female mice, higher bone MK4 correlated with a smaller femoral cross-sectional area and a lower moment of inertia (although statistical significance was borderline). Collectively these findings challenge the premise that higher MK4 in bone is beneficial to skeletal health, and the importance of dietary vitamin K conversion to MK4 in bone is unclear.

Results of previous studies focused on MKs and bone health have been inconsistent. In ovariectomized rats, bone strength and BMD were not affected by six weeks of dietary supplementation with 147 mg MK4/ kg diet or 201 mg MK7 /kg diet (equimolar doses) (29). (Like MK9, MK7 is also a bacterially produced form of vitamin K.) In aged female rats, bone formation and histomorphometry did not differ between those fed a diet containing 500 mg MK4/kg diet and those fed a control diet for 98 days (30). However, bone resorption decreased, and bone formation increased in ovariectomized mice fed diets supplemented with 20 and 40 mg MK4/kg body weight (31).

A meta-analysis of randomized clinical trials conducted primarily in post-menopausal women and older adults with osteoporosis found little evidence that vitamin K supplementation

has beneficial effects on BMD and inconclusive evidence with respect to fracture risk (13). Most of the included trials supplemented with 45 mg/d of MK4, which is a pharmacological dose that has been prescribed as an anti-osteoporotic medication in Japan (32). Evidence is also mixed regarding the protective effects of MK7. In postmenopausal osteopenic women, BMD and bone microarchitecture did not differ between those who received 375 mcg/d MK7 with 800 mg/d calcium and 1500 IU/d vitamin D for 3 years, and those who received calcium and vitamin D without MK7 (33). Supplementation with 360 µg/d MK7 alone for one year also did not affect BMD in healthy women within five years of menopause (34). However, 180 µg/d MK7 supplementation for 3 years reduced bone mineral density loss at the lumbar spine and femoral neck, but not the total hip, in healthy post-menopausal women. Compression strength and impact strength were also favorably affected by MK7 supplementation (35). This study also did not include calcium or vitamin D supplementation – two nutrients that have been repeatedly shown to protect against age-related bone loss (36, 37). Overall, the available evidence regarding the clinical benefit of MKs with respect to bone health is weak and our findings provide further support for no protective role of MK9 in skeletal health.

Our study has several key strengths. We conducted a comprehensive evaluation of skeletal health in a mouse model, assessing bone tissue quality through multiple measurements as well as bone mineral density. The use of isotopically labeled MK9 allowed us to trace the origin of skeletal tissue MK4 back to dietary MK9, providing robust evidence that MK9 provided in the diet was a source of MK4 in skeletal tissue. However, we acknowledge certain limitations. We studied mice from 4 – 16 weeks of age – a period during which skeletal development occurs. The generalizability of our findings to aging, when bone loss is more common, is uncertain. Some mice, most of which were male, did not survive for the 16-week study. There were no signs of

overt bleeding, and the cause of death is unknown. However, this is a consistent finding in male mice when fed low doses of vitamin K for prolonged periods of time (38). Multiple MK forms are produced by bacteria, and it is possible that supplementation with other forms of MK would yield different results. However, previous studies found MK7, a form that has been extensively studied, and MK9 similarly convert to MK4 in extra-hepatic tissues (9), there is no known unique biochemical mechanism for individual MK forms, and evidence regarding the skeletal benefit of MK7 is similarly inconclusive (29, 33-35).

In summary - these findings do not support a role for vitamin K in enhancing skeletal health during growth and development. Further research is needed to verify whether our results can be generalized to aging or other conditions when bone loss tends to occur.

Author Contributions:

Minying Liu (conceptualization, formal analysis, investigation, writing – original draft, review, and editing), Chongshan Liu (formal analysis, investigation, writing – review and editing), Nicolas Cevallos (investigation, writing – review and editing), Benjamin Orbach (investigation, writing – review and editing), Christropher Hernandez (conceptualization, formal analysis, investigation, writing – review and editing), Xueyan Fu (conceptualization, formal analysis, investigation, writing – review and editing), Jennifer Lee (conceptualization, formal analysis, writing – review and editing), Sarah Booth (conceptualization, formal analysis, investigation, writing – original draft, review, and editing), Kyla Shea (conceptualization, formal analysis, investigation, writing – original draft, review, and editing).

REFERENCES

1. Booth SL, Dallal G, Shea MK, Gundberg C, Peterson JW, Dawson-Hughes B. Effect of vitamin K supplementation on bone loss in elderly men and women. J Clin Endocrinol Metab. 2008;93(4):1217-23.
2. Shearer MJ, Newman P. Recent trends in the metabolism and cell biology of vitamin K with special reference to vitamin K cycling and MK-4 biosynthesis. Journal of Lipid Research. 2014;55(3):345-62.
3. Berezovska O, Yildirim G, Budell WC, Yagerman S, Pidhaynyy B, Bastien C, et al. Osteocalcin affects bone mineral and mechanical properties in female mice. Bone. 2019;128:115031.
4. Booth SL. Vitamin K: food composition and dietary intakes. Food Nutr Res. 2012;56.
5. Booth SL. Roles for vitamin K beyond coagulation. Annu Rev Nutr. 2009;29:89-110.
6. Walther B, Karl JP, Booth SL, Boyaval P. Menaquinones, bacteria, and the food supply: the relevance of dairy and fermented food products to vitamin K requirements. Adv Nutr. 2013;4(4):463-73.
7. Al Rajabi A, Booth SL, Peterson JW, Choi SW, Suttie JW, Shea MK, et al. Deuterium-labeled phylloquinone has tissue-specific conversion to menaquinone-4 among Fischer 344 male rats. J Nutr. 2012;142(5):841-5.
8. Collins MD, Jones D. Distribution of isoprenoid quinone structural types in bacteria and their taxonomic implication. Microbiol Rev. 1981;45(2):316-54.
9. Ellis JL, Fu X, Karl JP, Hernandez CJ, Mason JB, DeBose-Boyd RA, et al. Multiple Dietary Vitamin K Forms Are Converted to Tissue Menaquinone-4 in Mice. The Journal of Nutrition. 2021;152(4):981-93.
10. Tabb MM, Sun A, Zhou C, Grün F, Errandi J, Romero K, et al. Vitamin K2 regulation of bone homeostasis is mediated by the steroid and xenobiotic receptor SXR. J Biol Chem. 2003;278(45):43919-27.
11. Ichikawa T, Horie-Inoue K, Ikeda K, Blumberg B, Inoue S. Steroid and xenobiotic receptor SXR mediates vitamin K2-activated transcription of extracellular matrix-related genes and collagen accumulation in osteoblastic cells. J Biol Chem. 2006;281(25):16927-34.
12. Shea MK, Booth SL. Update on the role of vitamin K in skeletal health. Nutrition Reviews. 2008;66(10):549-57.
13. Mott A, Bradley T, Wright K, Cockayne ES, Shearer MJ, Adamson J, et al. Effect of vitamin K on bone mineral density and fractures in adults: an updated systematic review and meta-analysis of randomised controlled trials. Osteoporos Int. 2019;30(8):1543-59.
14. Kimmel DB, Vennin S, Desyatova A, Turner JA, Akhter MP, Lappe JM, et al. Bone architecture, bone material properties, and bone turnover in non-osteoporotic post-menopausal women with fragility fracture. Osteoporos Int. 2022;33(5):1125-36.
15. Seeman E. Bone quality: the material and structural basis of bone strength. J Bone Miner Metab. 2008;26(1):1-8.
16. Wallach S, Feinblatt JD, Carstens JH, Jr., Avioli LV. The bone "quality" problem. Calcif Tissue Int. 1992;51(3):169-72.
17. Watts NB. Bone quality: getting closer to a definition. J Bone Miner Res. 2002;17(7):1148-50.
18. Hernandez CJ, Keaveny TM. A biomechanical perspective on bone quality. Bone. 2006;39(6):1173-81.

19. Castaneda M, Strong JM, Alabi DA, Hernandez CJ. The Gut Microbiome and Bone Strength. Curr Osteoporos Rep. 2020;18(6):677-83.
20. Moriishi T, Ozasa R, Ishimoto T, Nakano T, Hasegawa T, Miyazaki T, et al. Osteocalcin is necessary for the alignment of apatite crystallites, but not glucose metabolism, testosterone synthesis, or muscle mass. PLoS Genet. 2020;16(5):e1008586.
21. Diegel CR, Hann S, Ayturk UM, Hu JCW, Lim KE, Droscha CJ, et al. An osteocalcin-deficient mouse strain without endocrine abnormalities. PLoS Genet. 2020;16(5):e1008361.
22. Guss JD, Horsfield MW, Fontenele FF, Sandoval TN, Luna M, Apoorva F, et al. Alterations to the Gut Microbiome Impair Bone Strength and Tissue Material Properties. J Bone Miner Res. 2017;32(6):1343-53.
23. Fu X, Booth SL, Smith DE. Vitamin K contents of rodent diets: a review. J Am Assoc Lab Anim Sci. 2007;46(5):8-12.
24. Harshman SG, Fu X, Karl JP, Barger K, Lamon-Fava S, Kuliopulos A, et al. Tissue Concentrations of Vitamin K and Expression of Key Enzymes of Vitamin K Metabolism Are Influenced by Sex and Diet but Not Housing in C57Bl6 Mice. J Nutr. 2016;146(8):1521-7.
25. Karl JP, Fu X, Dolnikowski GG, Saltzman E, Booth SL. Quantification of phylloquinone and menaquinones in feces, serum, and food by high-performance liquid chromatography-mass spectrometry. J Chromatogr B Analyt Technol Biomed Life Sci. 2014;963:128-33.
26. Cyphert EL, Liu C, Morales AL, Nixon JC, Blackford E, Garcia M, et al. Effects of high dose aspartame-based sweetener on the gut microbiota and bone strength in young and aged mice. JBMR Plus. 2024;8(8):ziae082.
27. Coulombe JC, Maridas DE, Chow JL, Bouxsein ML. Small animal DXA instrument comparison and validation. Bone. 2024;178:116923.
28. Fu X, Peterson JW, Hdeib M, Booth SL, Grusak MA, Lichtenstein AH, et al. Measurement of deuterium-labeled phylloquinone in plasma by high-performance liquid chromatography/mass spectrometry. Anal Chem. 2009;81(13):5421-5.
29. Fu X, Moreines J, Booth SL. Vitamin K supplementation does not prevent bone loss in ovariectomized Norway rats. Nutr Metab (Lond). 2012;9(1):12.
30. Sakamoto W, Isomura H, Fujie K, Iizuka T, Nishihira J, Tatebe G, et al. The effect of vitamin K2 on bone metabolism in aged female rats. Osteoporos Int. 2005;16(12):1604-10.
31. Wang H, Zhang N, Li L, Yang P, Ma Y. Menaquinone 4 Reduces Bone Loss in Ovariectomized Mice through Dual Regulation of Bone Remodeling. Nutrients. 2021;13(8).
32. Orimo H, Nakamura T, Hosoi T, Iki M, Uenishi K, Endo N, et al. Japanese 2011 guidelines for prevention and treatment of osteoporosis--executive summary. Arch Osteoporos. 2012;7(1):3-20.
33. Rønn SH, Harsløf T, Oei L, Pedersen SB, Langdahl BL. The effect of vitamin MK-7 on bone mineral density and microarchitecture in postmenopausal women with osteopenia, a 3-year randomized, placebo-controlled clinical trial. Osteoporos Int. 2021;32(1):185-91.
34. Emaus N, Gjesdal CG, Almås B, Christensen M, Grimsgaard AS, Berntsen GK, et al. Vitamin K2 supplementation does not influence bone loss in early menopausal women: a randomised double-blind placebo-controlled trial. Osteoporos Int. 2010;21(10):1731-40.
35. Knapen MH, Drummen NE, Smit E, Vermeer C, Theuwissen E. Three-year low-dose menaquinone-7 supplementation helps decrease bone loss in healthy postmenopausal women. Osteoporos Int. 2013;24(9):2499-507.

36. Bischoff-Ferrari HA, Willett WC, Orav EJ, Lips P, Meunier PJ, Lyons RA, et al. A pooled analysis of vitamin D dose requirements for fracture prevention. N Engl J Med. 2012;367(1):40-9.
37. Tang BM, Eslick GD, Nowson C, Smith C, Bensoussan A. Use of calcium or calcium in combination with vitamin D supplementation to prevent fractures and bone loss in people aged 50 years and older: a meta-analysis. Lancet. 2007;370(9588):657-66.
38. Shea MK, Booth SL, Harshman SG, Smith D, Carlson CS, Harper L, et al. The effect of vitamin K insufficiency on histological and structural properties of knee joints in aging mice. Osteoarthr Cartil Open. 2020;2(3):100078.

Table 1. Femoral biomechanics, geometry and total body bone mineral density measurements of male and female mice receiving diets supplemented with MK9.

	Male		Female	
	0.06mg/kg (n=7)	2.1mg/kg (n=11)	0.06mg/kg (n=13)	2.1mg/kg (n=11)
Tissue strength (Mpa)	153.3±13.6	156±16.3	171.8±16.7	164.6±14.8
P values	0.725		0.302	
Maximum moment (N*mm)	33.3±2.4	33.7±3.5	37.9±3	35.4±3.7
P values	0.763		0.083	
Section modulus (mm^3)	0.22±0.02	0.22±0.01	0.22±0.02	0.21±0.02
P values	0.873		0.277	
Moment of inertia (mm^4)	0.13±0.01	0.13±0.01	0.14±0.01	0.13±0.01
P values	0.46		0.003	
Cross sectional area (mm^2)	0.86±0.07	0.9±0.04	0.95±0.07	0.87±0.03
P values	0.205		0.001	
Femur length (mm)	15.6±0.3	15.6±0.5	15.6±0.4	15.8±0.3
P values	0.774		0.288	
Bone mineral density (g/cm^2)	0.06±0.004	0.06±0.004	0.06±0.002	0.06±0.003
P values	0.306		0.947	

Values are mean±SD. Differences between diet groups were determined using parametric unpaired two sample t-test. Males and female were analyzed separately with statistical significance set as $p<0.05$. Total body bone mineral density is presented, with all other measurements analyzed using femurs.

Table 2. Bone MK4 concentrations of male and female mice receiving diets supplemented with deuterium-labeled MK9.

VK form	Male			Female		
	0.06mg/kg (n=4)	2.1mg/kg (n=6)	*P values*	0.06mg/kg (n=7)	2.1mg/kg (n=7)	*P values*
Unlabeled MK4 (pmol/g)	4 ± 2	11 ± 3	0.009	12 ± 5	23 ± 15	0.066
Labeled MK4 (pmol/g)	ND	22 ± 9	0.002	ND	37 ± 21	<0.001
Total MK4 (pmol/g)	5 ± 2	32 ± 12	0.002	13 ± 5	60 ± 35	<0.001
% of labeled MK4 (of total VK)	NC	66.6 ± 3.4	<0.001	NC	62.6 ± 6.2	<0.001

Values are mean±SD. Differences between diet groups were determined using parametric unpaired two sample t-test. Males and female were analyzed separately with statistical significance set as $p<0.05$. ND, not detectable; NC, not calculable. The lowest detectable limit for both MK4 and deuterium-labeled MK4 was 1pmol/g.

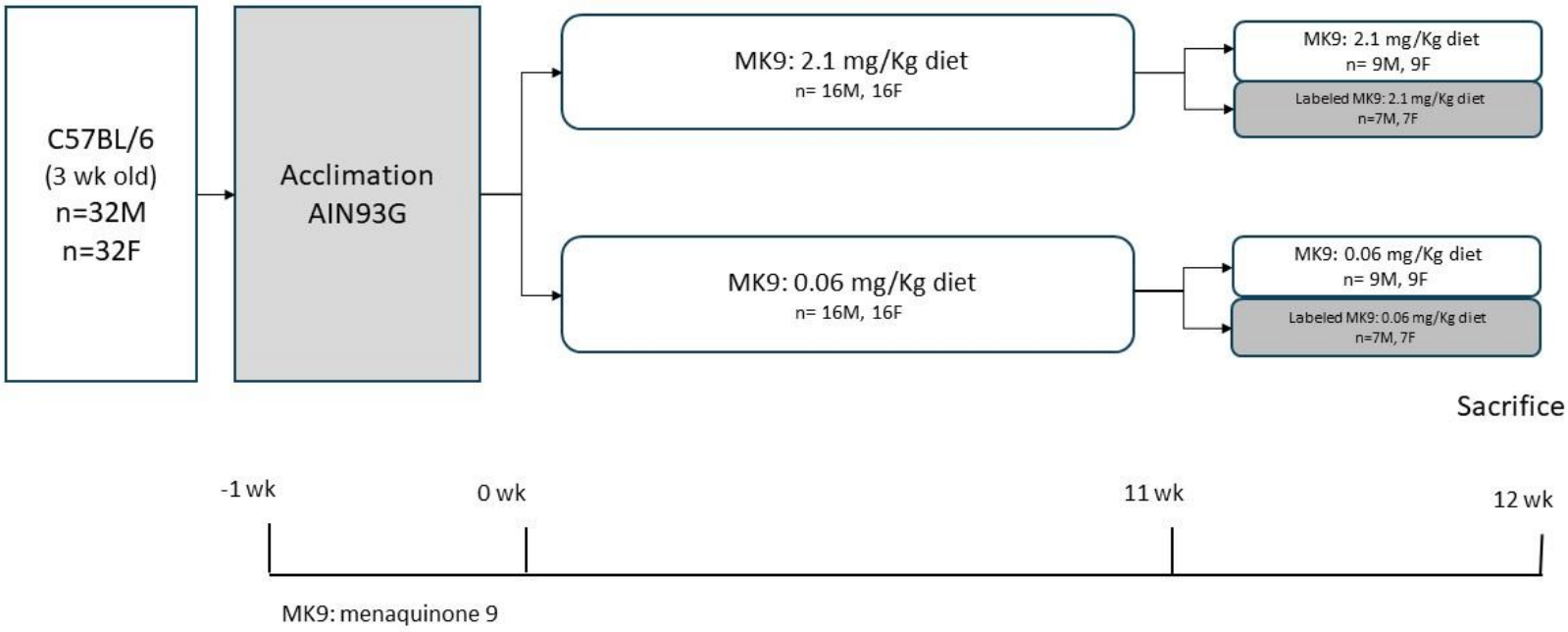

Figure 1. Animal Study Design.

Four-week-old male (n=32) and female (n=32) C57BL/6 mice were supplemented with 0.06 mg/kg and 2.1 mg/kg of menaquinone-9 (MK9) for 12 weeks. During the final week, a sub-group of mice (n=7/sex/group) received deuterium-labeled MK9 to trace its metabolic fate in bone.

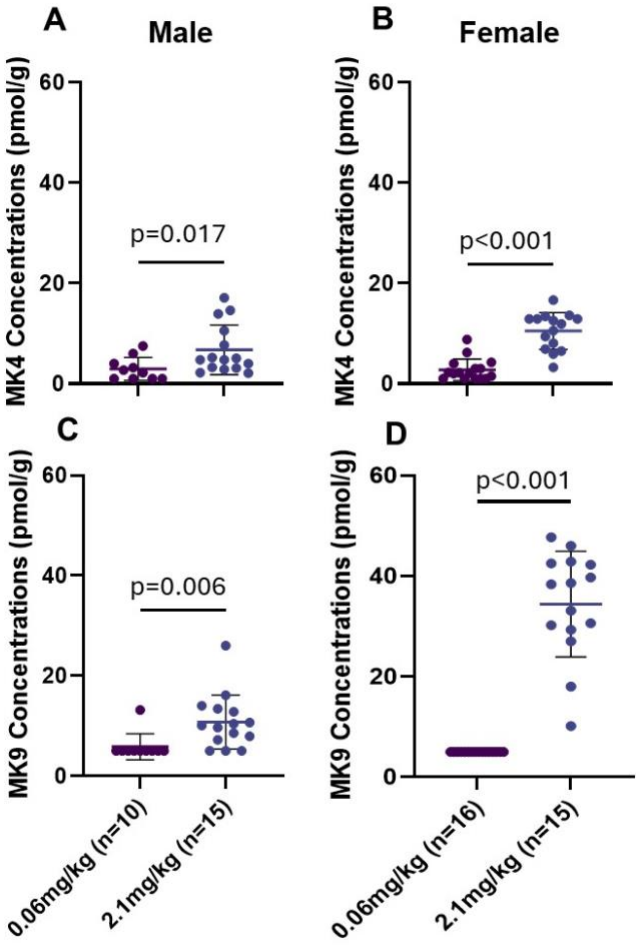

Figure 2. Liver MK4 (A, B) and MK9 (C, D) concentrations (pmol/g) of male (A, C) and female (B, D) mice receiving diets supplemented with MK9.

Differences between diet groups were determined using parametric unpaired two sample t-test. Males and female were analyzed separately with statistical significance set as $p<0.05$. Data are presented as mean ±SD.

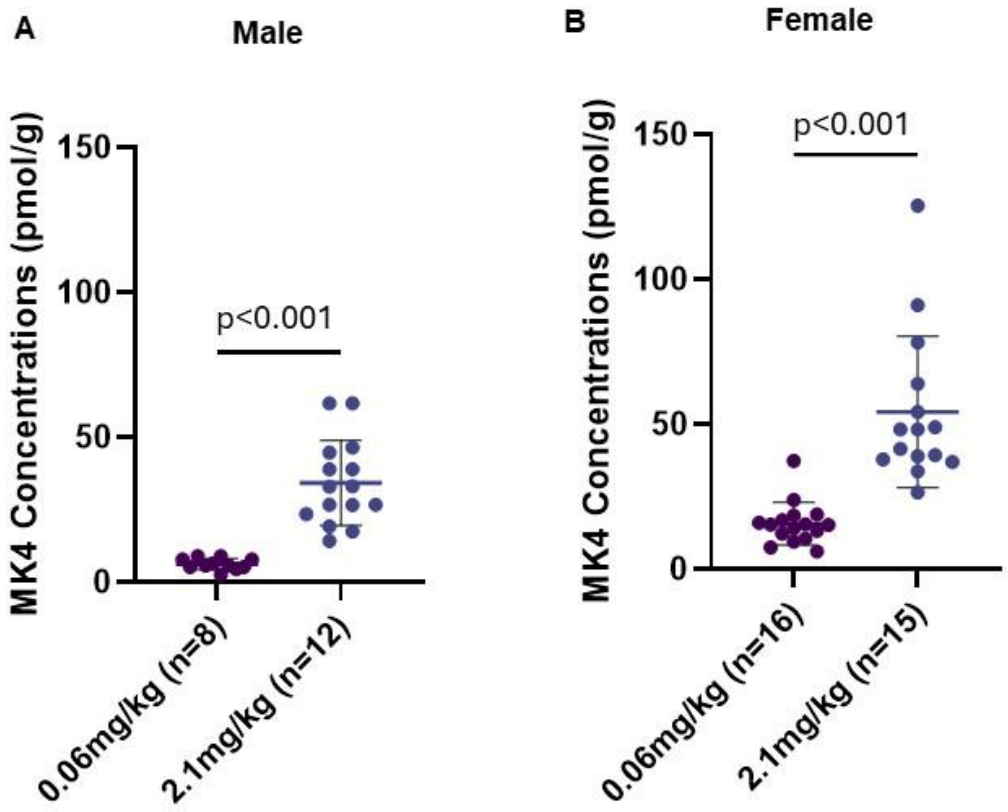

Figure 3. Bone MK4 concentrations (pmol/g) of male (A) and female (B) mice receiving diets supplemented with MK9.

Differences between diet groups were determined using parametric unpaired two sample t-test. Males and female were analyzed separately with statistical significance set as $p<0.05$. Data are presented as mean ±SD.

Supplemental Materials

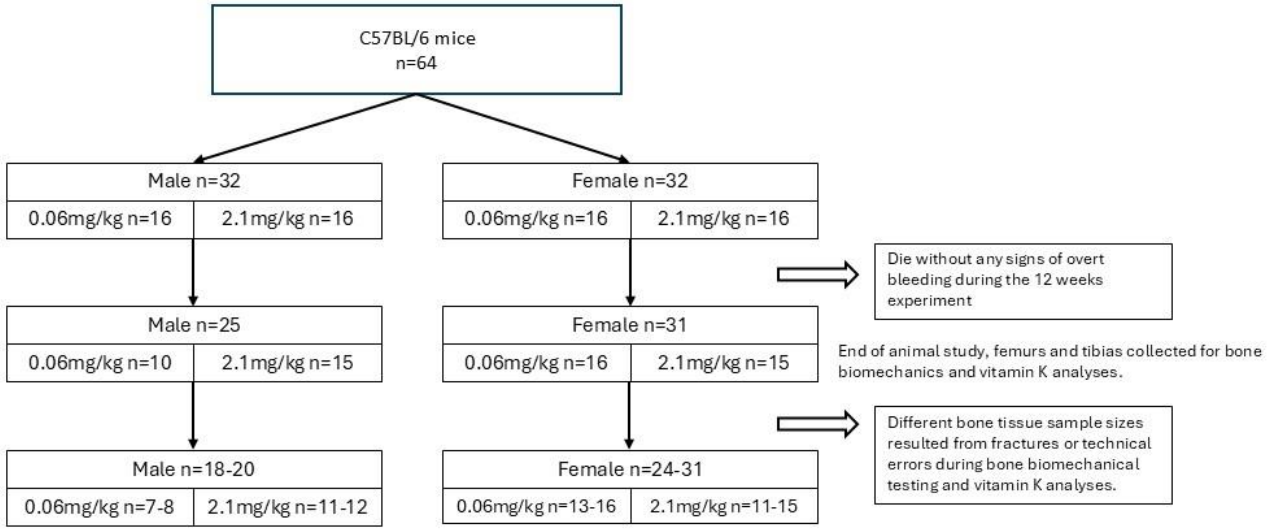

Figure S1. Animal Disposition Flowchart. Eight mice died prior to the end of the study (7 males and 1 female) with no signs of overt bleeding. Femurs were unavailable from 7 male and 7 female mice due to bone fractures or technical errors during biomechanical testing. Additionally, tibias from 5 male mice and 0 female mice were lost during vitamin K analyses.

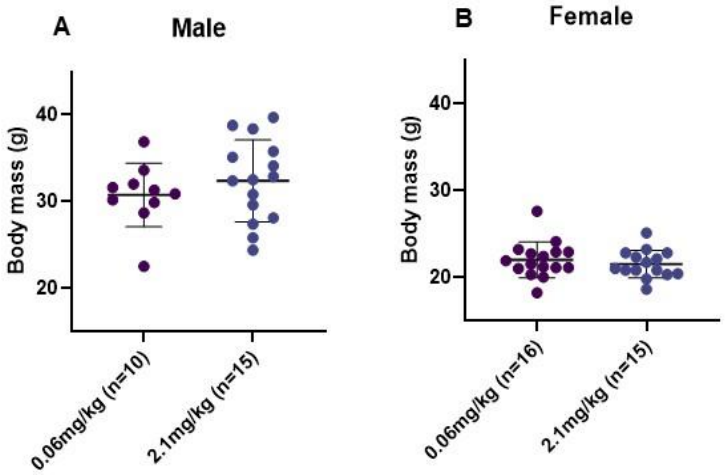

Figure S2. Body weight (g) of male **(A)** and female **(B)** mice receiving diets supplemented with MK9. Differences between diet groups were determined using parametric unpaired two sample t-test. Males and female were analyzed separately with statistical significance set as $p<0.05$. Data are presented as mean ±SD. No difference between diet groups in body weight were observed for both sexes (all p values ≥ 0.345).

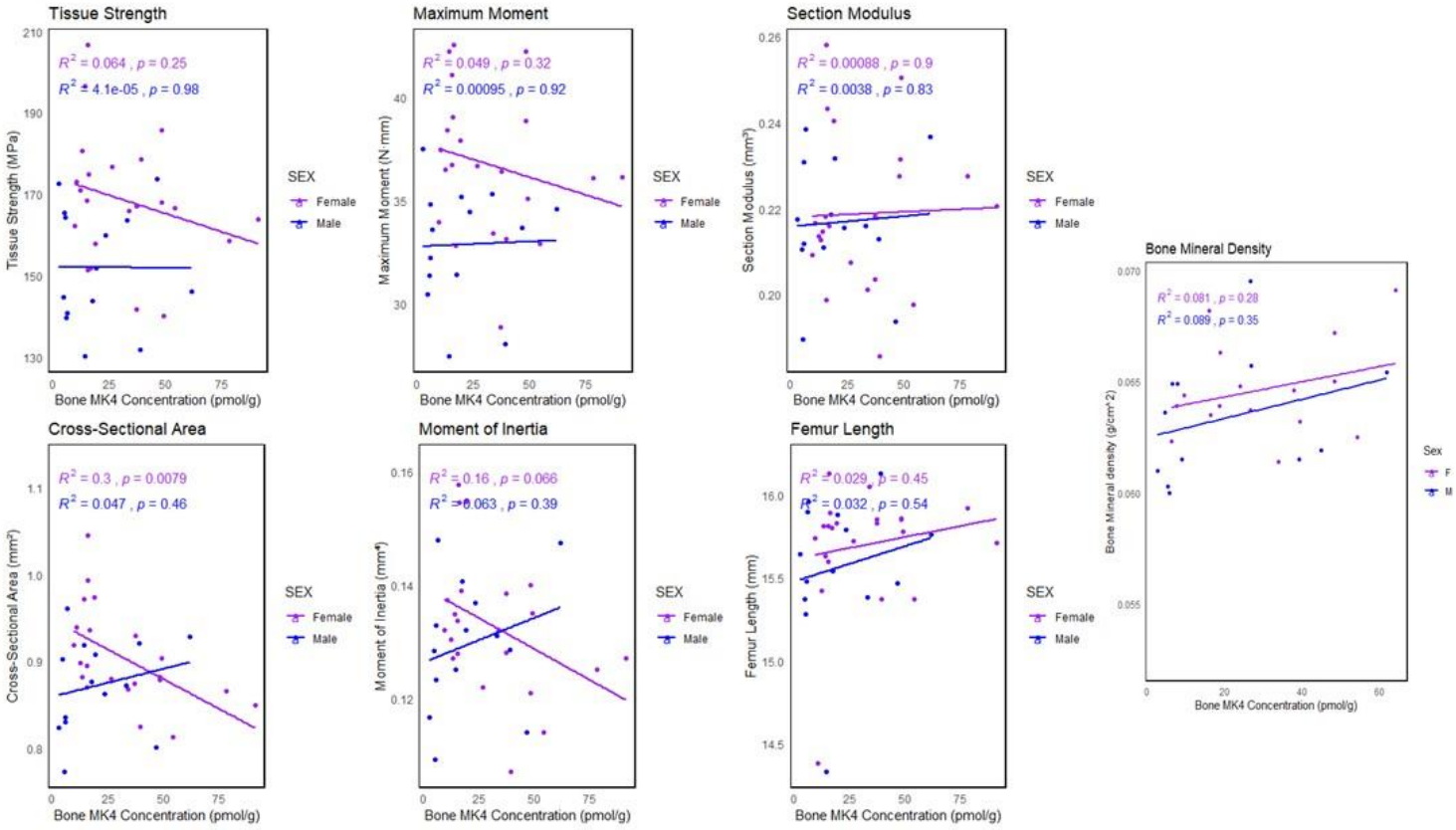

Figure S3. Correlations between bone MK4 concentrations (pmol/g) and bone biomechanical and geometry outcomes of male **(blue)** and female **(purple)** mice receiving diets supplemented with MK9. Correlations were assessed using the Pearson correlation coefficient with statistical significance set as $p<0.0$

Table S1. Femoral biomechanics and geometry measurements normalized with body weight of male and female mice receive diets supplemented with MK9.

	Male		Female	
	0.06mg/kg (n=7)	2.1mg/kg (n=11)	0.06mg/kg (n=13)	2.1mg/kg (n=11)
Tissue strength (Mpa)	153.3±13.6	156±16.3	171.8±16.7	164.6±14.8
P values	0.758		0.84	
Maximun moment (N*mm)	33.3±2.4	33.7±3.5	37.9±3	35.4±3.7
P values	0.667		0.309	
Section modulus (mm^3)	0.22±0.02	0.22±0.01	0.22±0.02	0.21±0.02
P values	0.45		0.842	
Moment of inertia (mm^4)	0.13±0.01	0.13±0.01	0.14±0.01	0.13±0.01
P values	0.788		0.01	
Cross sectional area (mm^2)	0.86±0.07	0.9±0.04	0.95±0.07	0.87±0.03
P values	0.937		0.06	
Femur length (mm)	15.6±0.3	15.6±0.5	15.6±0.4	15.8±0.3
P values	0.458		0.161	

The data are presented as original values, mean ± SD. Differences between diet groups were assessed using a parametric unpaired two-sample t-test using **data normalized to body weight**. Males and female were analyzed separately with statistical significant set as $p<0.05$.

4. SUMMARY AND DISCUSSION

4.1 Research Summary

The role of vitamin K in skeletal health remains a topic of debate. Interest in vitamin K's potential skeletal benefits stems primarily from its classic role as an enzymatic cofactor in the carboxylation of OC in the bone matrix (1). However, the current evidence base is inconsistent (2). While clinical studies have shown that PK and MK4 supplementation do not significantly affect BMD (3), little is known about its role in influencing bone tissue quality, a critical aspect of bone health not captured by BMD. Recently, attention has shifted towards dietary MKs, including those forms produced by bacteria, which are found in fermented foods, animal meat, and dairy products (4). However, the effect of bacterially produced MKs from diet on bone tissue quality remains poorly understood.

In addition to being present in the diet, MKs are also produced by gut bacteria (5-7). The contribution of bacterially produced MKs to the host's overall vitamin K stores remains debated largely because the extent of their absorption from the colon is uncertain (8-11). Although gut bacterial MK production is altered with antibiotic treatment, experimental evidence linking these changes to host MK tissue stores is currently limited (12).

The objective of this thesis research was to investigate the tissue distribution and potential skeletal roles of MKs. We utilized two experiments conducted in male and female C57BL/6 mice to determine: (I) the response of tissue MK concentrations to antibiotic-induced alterations in gut MK production in aged and young mice, and (II) the effect of dietary MK9 (a MK form produced by bacteria) on bone tissue quality and density in young mice. We also determined the conversion of dietary MK9 to MK4 in bone tissue using stable isotopes.

Altering gut MK production via antibiotics did not appreciably influence host MK tissue stores in aged or young mice. Moreover, in young mice, bone tissue quality did not differ appreciably between those fed a diet containing 0.06 mg MK9/kg or 2.1 mg MK9/kg for 12 weeks. However, in these mice, MK4 was the only form of vitamin K detected in bone tissue, and its concentration in bone corresponded to the MK9 dose in the diet. In mice fed the diet containing 2.1 mg MK9/kg, over 60% of MK4 in bone was derived from dietary MK9 – extending the finding of prior research that dietary vitamin K is converted to MK4 in skeletal tissue as well (7).

4.2 Discussion and Future Directions

The results of this thesis research showed that bacterially produced MKs contributed minimally to systemic vitamin K tissue stores. This finding is somewhat unsurprising because bile salts, which facilitate vitamin K absorption from the small intestine, are largely reabsorbed before reaching the colon (13). Moreover, most bacterially produced MKs are bound to bacterial cell membranes, where they participate in the electron transfer chain for energy production (14), and may therefore remain largely available to the microbes rather than the host. The parallel trends observed between fecal MKs and colon tissue MK concentrations in aged mice may be attributable to age-related increases in intestinal permeability (15) or inevitable remnants of the fecal contents resulting from direct contact with the gut microbiota. Since most gut-derived MKs do not appear to reach liver, small intestinal tissues, or bone their relevance to vitamin K tissue stores remain questionable.

We also investigated the potential role of MK9, a MK form produced by bacteria and the predominant form in dairy products, on bone health. Dietary MK9 was absorbed, as supported by its accumulation in the liver, but it was not detected in bone. Instead, dietary MK9 serves as a

precursor to MK4, which was the only form present in bone, and its concentration responded to dietary supplementation (16). While MK4 appears to have additional functions beyond its established role as an enzyme cofactor, including in cell-signaling pathways involved in bone formation (17, 18, 19), higher MK4 concentrations in bone did not confer measurable benefits to bone tissue quality or density in young mice.

In conclusion, the findings of this thesis do not support systemic tissue uptake of bacterially produced MKs from the gut or a direct role of MKs in skeletal health. The biological significance of the conversion of dietary vitamin K to MK4 in bone is uncertain and in need of further investigation. Moreover, as emerging evidence demonstrates gut-derived MKs influence microbial composition and function (20, 21), further research into their broader health implications is also warranted.

REFERENCES

1. Booth SL, Centi AJ, Gundberg C. Bone as an Endocrine Organ Relevant to Diabetes. Current Diabetes Reports. 2014;14(12):556.
2. Shea MK, Booth SL. Update on the role of vitamin K in skeletal health. Nutrition Reviews. 2008;66(10):549-57.
3. Mott A, Bradley T, Wright K, Cockayne ES, Shearer MJ, Adamson J, et al. Effect of vitamin K on bone mineral density and fractures in adults: an updated systematic review and meta-analysis of randomised controlled trials. Osteoporos Int. 2019;30(8):1543-59.
4. Karl JP, Fu X, Dolnikowski GG, Saltzman E, Booth SL. Quantification of phylloquinone and menaquinones in feces, serum, and food by high-performance liquid chromatography-mass spectrometry. J Chromatogr B Analyt Technol Biomed Life Sci. 2014;963:128-33.
5. Al Rajabi A, Booth SL, Peterson JW, Choi SW, Suttie JW, Shea MK, et al. Deuterium-labeled phylloquinone has tissue-specific conversion to menaquinone-4 among Fischer 344 male rats. J Nutr. 2012;142(5):841-5.
6. Collins MD, Jones D. Distribution of isoprenoid quinone structural types in bacteria and their taxonomic implication. Microbiol Rev. 1981;45(2):316-54.
7. Ellis JL, Fu X, Karl JP, Hernandez CJ, Mason JB, DeBose-Boyd RA, et al. Multiple Dietary Vitamin K Forms Are Converted to Tissue Menaquinone-4 in Mice. The Journal of Nutrition. 2021;152(4):981-93.
8. Turck D, Bresson JL, Burlingame B, Dean T, Fairweather-Tait S, Heinonen M, et al. Dietary reference values for vitamin K. Efsa j. 2017;15(5):e04780.
9. Beulens JWJ, Booth SL, van den Heuvel EGHM, Stoecklin E, Baka A, Vermeer C. The role of menaquinones (vitamin K2) in human health. British Journal of Nutrition. 2013;110(8):1357-68.
10. Hollander D, Rim E, Ruble PE, Jr. Vitamin K2 colonic and ileal in vivo absorption: bile, fatty acids, and pH effects on transport. Am J Physiol. 1977;233(2):E124-9.
11. Groenen-van Dooren MM, Ronden JE, Soute BA, Vermeer C. Bioavailability of phylloquinone and menaquinones after oral and colorectal administration in vitamin K-deficient rats. Biochem Pharmacol. 1995;50(6):797-801.
12. Guss JD, Taylor E, Rouse Z, Roubert S, Higgins CH, Thomas CJ, et al. The microbial metagenome and bone tissue composition in mice with microbiome-induced reductions in bone strength. Bone. 2019;127:146-54.
13. Shearer MJ, Newman P. Metabolism and cell biology of vitamin K. Thromb Haemost. 2008;100(4):530-47.
14. Walther B, Karl JP, Booth SL, Boyaval P. Menaquinones, bacteria, and the food supply: the relevance of dairy and fermented food products to vitamin K requirements. Adv Nutr. 2013;4(4):463-73.
15. Thevaranjan N, Puchta A, Schulz C, Naidoo A, Szamosi JC, Verschoor CP, et al. Age-Associated Microbial Dysbiosis Promotes Intestinal Permeability, Systemic Inflammation, and Macrophage Dysfunction. Cell Host Microbe. 2017;21(4):455-66.e4.
16. Liu M, Liu C, Cevallos N, Orbach BN, Hernandez CJ, Fu X, et al. Dietary menaquinone-9 supplementation does not influence bone tissue quality or bone mineral density during skeletal development in mice. JBMR Plus. 2025;9(6):ziaf059.
17. Tie JK, Stafford DW. Functional Study of the Vitamin K Cycle Enzymes in Live Cells. Methods Enzymol. 2017;584:349-94.

18. Tabb MM, Sun A, Zhou C, Grün F, Errandi J, Romero K, et al. Vitamin K2 regulation of bone homeostasis is mediated by the steroid and xenobiotic receptor SXR. J Biol Chem. 2003;278(45):43919-27.
19. Tao L, Li H, Wang J, Liu Q, Cao W, Zhu Y. Vitamin K2 inhibits PGE2-mediated osteoblast ferroptosis by upregulation of CBR1 via the Nrf2/Keap1 pathway. Commun Biol. 2025;8(1):1116.
20. Ellis JL, Karl JP, Oliverio AM, Fu X, Soares JW, Wolfe BE, et al. Dietary vitamin K is remodeled by gut microbiota and influences community composition. Gut Microbes. 2021;13(1):1-16.
21. Fenn K, Strandwitz P, Stewart EJ, Dimise E, Rubin S, Gurubacharya S, et al. Quinones are growth factors for the human gut microbiota. Microbiome. 2017;5(1):161.
22. Liu M, Matuszek G, Azcarate-Peril MA, Loeser RF, Shea MK. An Exploratory Case-Control Study on the Associations of Bacterially-Derived Vitamin K Forms with the Intestinal Microbiome and Obesity-Related Osteoarthritis. Current Developments in Nutrition. 2023;7(3):100049.
23. Cyphert EL, Liu C, Chu VT, Dubey A, Liu M, Zhong Z, et al. Commensal taxa in gut microbiota limit antibiotic resistance during extended oral antibiotic use. bioRxiv. 2025:2025.08.13.670183.
24. Kim M, Wang J, Pilley SE, Lu RJ, Xu A, Kim Y, et al. Estropausal gut microbiota transplant improves measures of ovarian function in adult mice. bioRxiv. 2025.

5. APPENDIX A: ASSAYS and PROTOCOLS

5.1 Quantification of menaquinone-5 through 13 in feces and food by LC-APCI-MS

1. Select samples to be analyzed. Allow samples to defrost at room temperature.

2. While samples are defrosting, write the assay plan in your lab notebook:

a. Include 2 controls (baby food and freeze-dried human feces controls)

b. Number samples according to identifiers; # tubes for each sample depending on if running singles, duplicates, triplicates, etc.

c. Determine amount of sample you will use for the analysis.

i. For feces: 0.06 g dry wt often used

ii. For food: 0.1 g – 0.15 g

3. Label 50mL polypropylene centrifuge tubes.

4. Stir or mix defrosted samples to ensure homogeneity. Use a mortar and pestle if necessary. Freeze-dried fecal samples MUST be ground with a mortar and pestle.

5. Weigh amount of sample determined in step 2c. Record the exact amount, to the nearest thousandth of a gram, in lab notebook.

6. Use the weight recorded in step 5 to calculate the dilution factor. Divide 1 by the exact weight of food used so that results calculated by the will be pmol/g or ng/g. For serum, the unit is pmol/mL or nM. Record this dilution factor to the nearest hundredth in the notebook.

7. Add Internal Standard (about 25 pmol)

8. Add 10 mL dH_2O to each tube

9. Vortex for about 30 seconds to suspend the food

10. Add 15mL 2-propanol:hexane (3:2 V/V) to each sample

11. Vortex samples for 2-3 minutes making sure they form a funnel

12. Sonicate each sample at continuous output 40% duty cycle, output control # 4 for 1 minute

13. Vortex all samples for 2-3 minutes

14. Centrifuge at 20ºC and 3000 RPM for 5 minutes

15. Aspirate the top layer of each tube using a Pasteur pipette and transfer it to a labeled, glass 16 x 100 culture tube.

16. Warm samples while evaporating to dryness under a gentle nitrogen stream (<10 psi) using the NEvap. It usually takes about 45 min.

Stage 2: Solid phase extraction

18. Label a set of 16 x 100 culture tubes and put into Vac-Elute manifold rack. Place 500 mg silica SPE columns (we use Varian part # 12113036) on the Vac Elute SPS 24, one column for each sample

19. Reconstitute each sample with calculated amount 4mL hexane

20. Prepare 3.5% ethyl ether in hexane (make fresh daily) - a minimum of 12mL per tube is required

21. Be sure the Vac-Elute is set on “WASTE”

22. Condition each column with 4mL of 3.5% ethyl ether in hexane –vacuum to dry

23. Condition each column with 4mL hexane-vacuum to dry

24. Vortex each sample (making sure to achieve a funnel-affect) for about 5 seconds and then add predetermined amount to column (often 0.5 mL – 1.0 mL) **–** vacuum to dry

25. Wash each column with 4mL hexane-vacuum to dry

26. Switch Vac-Elute to “COLLECT”

27. Wash each column with 8mL 3.5% ethyl ether in hexane – vacuum to dry

28. Warm eluates while evaporating to dryness under a gentle nitrogen stream (<10 psi) using the NEvap. It usually takes about 45-60 min.

Stage 3: Dissolve sample for injection on the chromatograph

Prior to beginning sample analysis, the LC-MS should be balanced, by purging the system of air caught in the tubing, stabilizing pressure and temperature, and followed with a test injection including a blank mobile phase and/or calibration standard injections.

29. Reconstitute using 30 uL of methylene chloride; vortex for 5 seconds.

30. Evaporate to dryness at 60°C in a hot water bath (10 min).

29. Reconstitute using 30 uL of methylene chloride; vortex for 5 seconds.

30. After all the tubes have been reconstituted add 170 uL of methanol; lightly vortex another 5 seconds.

31. Transfer the reconstituted sample to a labeled amber sample vial with conical insert. Cap each vial with an aluminum crimp cap.

32. Centrifuge the sample vials at 20°C and 3,000 rpm for 5 minutes to precipitate undissolved material.

33. Inject 25-100 uL of sample. (The volume of sample injected may be varied to accommodate the amount of vitamin K vitamers in the sample).

-25 uL should be injected for fecal samples.

APCI-LC-MS settings:

Column temperature was maintained at 20°C. The mobile phase consisted of methanol (solvent A) and methylene chloride (solvent B).

Solvent conditions: isocratic at 100% solvent A for 2.5 min, linear gradient to 70% solvent A at 10 min, isocratic at 70% solvent A to 14.0 min. At 15.5 min the mobile phase was returned to 100% solvent A for 4.5 min to prepare the column for the next sample. Flow rate was maintained at 1.0 mL/min throughout.

Time (minutes)	%solvent B	Flow rate (ml/min)	Pressure (max)
2.5	0	1.0	600
10	30	1.0	600
14	30	1.0	600
15.5	0	1.0	600
20	0	1.0	600
19.5	0	1.0	600
23.5	0	1.0	600

Solvents:

During each run, check solvents that correct solvents are selected. Always select A1, and B1 when running the method.

A: Methanol

B: Methylene Chloride

HPLC conditions	
Approximate pressure	410 bar
Temperature of column	20 degrees C

Injection volume	< 100uL
Total time of 1 run	23.5 minutes

MSD settings:

ion source, positive APCI; spray chamber gas temperature, 350°C; vaporizer temperature, 400°C; drying nitrogen, 7.0 L/min; nitrogen nebulizer pressure, 45 psig; capillary voltage, 3800V; and corona current, 5 μA. Selected ion monitoring was used to detect PK, dPK and MK4 through MK13 at the following mass-to-charge ratios: *m/z* 451 (PK), *m/z* 458 (dPK), *m/z* 445 (MK4), *m/z* 513 (MK5), *m/z* 582 (MK6), *m/z* 650 (MK7), *m/z* 718 (MK8), *m/z* 786 (MK9), *m/z* 854 (MK10), *m/z* 923 (MK11), *m/z* 991 (MK12), and *m/z* 1059 (MK13).

Lower limit of detection, recovery, and inter/intra-assay variability

The limit of detection (LOD) and limit of quantification (LOQ) for PK and each individual MKn were determined by spiking baby food with incrementally diluted calibration standards. Baby food was used instead of feces because feces contain multiple MKn whereas the baby food contained only MK4 and PK. As such, using the baby food eliminated an inherent source of error attributable to endogenous MKn in the fecal material. The LOD was defined as the lowest analyte concentration statistically different from zero with an RSD of ≤ 20% over triplicate measurements. The LOQ was defined as the lowest analyte concentration within ± 20% of the expected concentration, and with a CV of ≤ 20% over triplicate measurements.

Table 2 Linearity and detection limits of an LC-APCI-MS assay for measuring vitamin K vitamers.

	Slope	**R^2**	**IDL (fmol/injection)**	**LOD (pmol/g)**	**LOQ (pmol/g)**
PK	1294.2	0.9996	50	30	30
MK4	1385.1	0.9997	100	30	90
MK5	881.4	0.9987	50	5	10
MK6	230.8	0.9992	200	10	10
MK7	166.6	0.9995	100	5	40
MK8	262.2	0.9993	100	5	60
MK9	897.8	0.9997	200	5	30
MK10	1605.4	0.9996	3	1	5
MK11	1372.5	0.9997	12	5	20
MK12	1345.6	0.9995	12	5	10
MK13	1396.4	0.9997	25	5	10

[a]dPK, deuterium-labeled phylloquinone; IDL, instrument detection limit; LOD, limit of detection; LOQ; limit of quantification; MK, menaquinone; PK, phylloquinone.

Reference:

Karl JP, Fu X, Dolnikowski GG, Saltzman E, Booth SL. Quantification of phylloquinone and menaquinones in feces, serum, and food by high-performance liquid chromatography-mass spectrometry. J Chromatogr B Analyt Technol Biomed Life Sci [Internet]. 2014 [cited 2014 Jun 25];963C:128–33. Available from: http://www.ncbi.nlm.nih.gov/pubmed/24956079

5.2 Quantification of phylloquinone and menaquinone-4 in serum or plasma by by Agilent HPLC with fluorimetric detection

Stage 1: Precipitation of proteins and extraction of plasma lipids:

(perform in biosafety cabinet)

1. pipet 0.20 mL of plasma/serum into 16 X 100 borosilicate screw cap culture tubes
2. add 20 µL of internal standard ($K_{1(25)}$)
3. add 0.5 mL of ethanol to each tube
4. vortex vigorously for 5 seconds to denature proteins
5. add 0.5 mL of DI water to each tube
6. add 3 mL of hexane to each tube, cap tubes with Teflon lined caps.

   (perform on lab bench)
7. vortex vigorously for 5 minutes
8. centrifuge for 5 minutes at 3,000 rpm
9. remove upper, hexane layer with a Pasteur pipet and aspirate into a clean tube
10. evaporate hexane layer to dryness in a N2 evaporator
11. add 0.5 mL of hexane to each tube
12. cap and store at –80^{o} C or proceed with solid phase extraction (SPE) procedure

Stage 2: Solid phase extraction

(perform in fume hood)

1. prepare 3.5% ethyl ether in hexane (3.5 mL ether + 96.5 mL hexane), prepare 12 mL for

each sample, use within 8 hours

2. place 3 mL (500 mg) silica SPE columns (we use Varian part # 12113036) on the Vac Elute SPS 24, one column for each sample
3. wash each column with 4 mL of 3.5% ether/hexane
4. wash each column with 4 mL of hexane (Do NOT let the column totally dry)
5. pick up a sample in 0.5 mL of hexane and add it to a column
6. wash each column with 4 mL of hexane (Totally dry)
7. elute vitamin K with 8 mL of 3.5% ether/hexane
8. collect eluate and evaporate ether/hexane to dryness in a centrifugational evaporator

Stage 3: Dissolve sample for injection on the chromatograph

Prior to beginning sample analysis, the HPLC should be balanced, by purging the air caught in the tubing system, stabilizing pressure and temperature, and followed with a test injection including a blank mobile phase and/or calibration standard injections.

HPLC gradient table:

Time (minutes)	%solvent B	Flow rate (ml/min)	Pressure (max)
0	0	0.6	400
7	10	0.6	400
11	10	0.6	400
11.5	30	0.8	400
19	30	0.8	400

19.5	0	0.8	400
23.5	0	0.8	400

Solvents:

During each run, check solvents that correct solvents are selected. Always select A1, and B1 when running the method.

A:

A1 = Mobile phase

A2 = Methanol

B:

B1 = Methylene Chloride

B2 = Methanol

HPLC conditions	
Approximate pressure	55 bar
Temperature of column	30 degrees C
Injection volume	< 100uL
Total time of 1 run	24.1 minutes

1. Re-dissolve sample for injection on the chromatograph. Reconstitute first in 30 µL of methylene chloride with vertexing for 5 seconds
2. Quickly followed with 150 µL mobile phase – vortex another 5 seconds.

3. Transfer the reconstituted sample to an amber sample vial with conical insert.

4. Cap each vial with Teflon lined rubber septum and an aluminum crimp cap.

5. Centrifuge the sample vials at 3,000 rpm for 5 minutes to precipitate undissolved material.

6. Program the Agilent to inject 100 µL (or preferred volume) of sample

Reference:

Davidson WK and Sadowski JA. Determination of Vitamin K Compounds in Plasma or Serum by High-Performance Liquid Chromatography Using Postcolumn Chemical Reduction and Fluorimetric Detection. *Methods in Enzymology*. 1997;**282**:408-421.

5.3 LC-MS and HPLC method adaptations for extraction from tissues

For soft tissues (most organs)

Homogenization in preparation for extraction

1. Weigh out tissue sample approximately 0.1-0.15g depending on tissue.
    a. Liver- 0.15g
    b. Kidney- 0.15g
2. Add between 0.5-1.0mL of PBS to sample in small cryotube.
3. Homogenize tissue using bench top PowerGen 125 Fisher Scientific homogenizer, at power setting 6.
4. Homogenize for approximately 30 seconds.
5. Wash the homogenizer in between samples, and wipe with chemwipe.
6. Continue until all samples are homogenized.
7. Vortex sample, then pipet 0.250-0.5 mL of homogenate into 16 X 100 borosilicate screw cap culture tubes
8. Resume LC-MS or HPLC extraction methods at the step of adding internal standard

For elastic (intestine) tissues

1. Collect materials
    a. Small Styrofoam cooler, fill with dry ice
    b. Mortar, pestle, and small spatula; place in cooler and keep cold throughout procedure
    c. Liquid nitrogen
    d. Frozen tissue sample to be homogenized
2. Add frozen tissue sample to mortar

3. Pour liquid nitrogen over tissue sample

4. Homogenize sample with pestle

5. Use the cold spatula to transfer homogenized tissue sample to storage tube

6. Return to freezer for storage, or resume with extraction procedure at the weighing step

    a. Duodenum- 0.1g

    b. Jejunum- 0.1g

    c. Ileum- 0.1g

5.4 Q-TOF-MS method adaptations for extraction from tissues and feces

Purpose: tissue MK4-13 concentrations were measured by Quadrupole Time-of-Flight Mass Spectrometry (Q-TOF-MS) to improve sensitivity, minimize interference, and avoid the need to switch instruments for MK4.

Q-TOF-MS operation

1. Before adjusting the Q-TOF, check the lights for all parts of the Q-TOF – lights should be either orange or yellow.
2. Pull the needle out of the ion source and unlatch the ion source to expose the inside column. Clean the ion source with methanol and Kim wipes and use the grey sandpaper to clean the needle.
3. Put the needle back and close the ion source. On the top of the ion source, swap the red line for the beige line to calibrate the Q-tof.
4. To start the calibration, select the tab with the name “APCI Positive Menaquinones.”
5. Turn on the Q-TOF and change the context from “Acquisition” to “Tune.” Prompts about saving the layout and method should be rejected, but the worklist should be saved.
6. Wait until the vaporizer hits a temperature of 350 to start the “TOF Mass Calibration” and click yes.
7. After the calibration is done, save the report as a file and convert it to PDF.
8. Change the context from “Tune” to “Acquisition” and change the top of the ion source from the beige line to the red line.

9. Turn on the the system, purge lines A (methanol) for 5 minutes at flow rate of 1.0 ml/min and line B (methyl chloride) for 5 minutes at flow rate of 5.0 mL/min, and update the worklist with the correct sample name, sample position, method, data file (must be unique).
    a. Always have a blank as the first sample and flush/shutdown method last.
10. Click the check box to the left of each sample to ensure they are being analyzed.
11. Save the worklist and once the pressure is at an acceptable level of ~500 bar, click the start.

APCI-LC-MS settings - C_{18} run:

Column temperature was maintained at 20°C. The mobile phase consisted of methanol (solvent A) and methylene chloride (solvent D).

Solvent conditions: isocratic at 100% solvent A for 2.5 min, linear gradient to 70% solvent A at 10 min, isocratic at 70% solvent A to 14.0 min. At 15.5 min the mobile phase was returned to 100% solvent A for 4.5 min to prepare the column for the next sample. Flow rate was maintained at 1.0 mL/min throughout.

Time (minutes)	%solvent D	Flow rate (ml/min)	Pressure (max)
2.5	0	1.0	600
10	30	1.0	600
14	30	1.0	600
15.5	0	1.0	600
20	0	1.0	600
19.5	0	1.0	600
23.5	0	1.0	600

Solvents:

During each run, check solvents that correct solvents are selected. Always select A1, and B1 when running the method.

A: Methanol

D: Methylene Chloride

QTOF conditions	
Approximate pressure	410 bar
Temperature of column	20 degrees C
Injection volume	< 100uL
Total time of 1 run	23.5 minutes

MSD settings:

ion source, positive APCI; spray chamber gas temperature, 350°C; vaporizer temperature, 400°C; drying nitrogen, 7.0 L/min; nitrogen nebulizer pressure, 45 psig; capillary voltage, 3800V; and corona current, 5 μA. Selected ion monitoring was used to detect PK and MK4 through MK13 at the following mass-to-charge ratios: *m/z* 451 (PK), *m/z* 445 (MK4), *m/z* 513 (MK5), *m/z* 582 (MK6), *m/z* 650 (MK7), *m/z* 718 (MK8), *m/z* 786 (MK9), *m/z* 854 (MK10), *m/z* 923 (MK11), *m/z* 991 (MK12), and *m/z* 1059 (MK13). Stable-isotope (deuterium) labelled PK and MK4 through MK13 were also selected at the following mass-to-charge ratios: *m/z* 458 (d7PK), *m/z* 452 (d7MK4), *m/z* 520 (d7MK5), *m/z* 590 (d7MK6), *m/z* 664 (d7MK7), *m/z* 725 (d7MK8), *m/z* 793 (d7MK9), *m/z* 861 (d7MK10), *m/z* 930 (d7MK11), *m/z* 998 (d7MK12), and *m/z* 1066 (d7MK13).

<u>APCI-LC-MS settings – C_{30} run:</u>

Column temperature was maintained at 7°C. The mobile phase consisted of methanol (solvent A) and methylene chloride (solvent D).

Solvent conditions: isocratic at 98% solvent A for 14.00 min, linear gradient to 90% solvent A at 14.10 min (flow rate also increased to 1.2 mL/min), linear gradient to 70% solvent A at 21.00

min, isocratic at 70% solvent A to 26.00 min. At 26.10 min the mobile phase was returned to 100% solvent A for ~4 min to prepare the column for the next sample. At 32.00 min, flow rate was is returned to1.0 mL/min.

Time (minutes)	%solvent D	Flow rate (ml/min)	Pressure (max)
14.00	2	1.0	600
14.10	10	1.2	600
21.00	30	1.2	600
26.00	30	1.2	600
26.10	0	1.2	600
32.00	0	1.0	600

Solvents:

During each run, check solvents that correct solvents are selected. Always select A1, and B1 when running the method.

A: Methanol

D: Methylene Chloride

QTOF conditions	
Approximate pressure	100 bar
Temperature of column	7 degrees C
Injection volume	< 100uL
Total time of 1 run	32.0 minutes

MSD settings:

ion source, positive APCI; spray chamber gas temperature, 350°C; vaporizer temperature, 400°C; drying nitrogen, 7.0 L/min; nitrogen nebulizer pressure, 45 psig; capillary voltage, 3800V; and corona current, 5 μA. Selected ion monitoring was used to detect PK, d7PK, MK4, and d7MK4 at the following mass-to-charge ratios: *m/z* 451 (PK), *m/z* 458 (d7PK), *m/z* 445 (MK4), and *m/z* 452 (d7MK4).

QTOF calibration standard preparation

1. Prepare four glass tubes (12*75, white)
2. Add 200ul standard for each concentration [2.5, 5, 10, 100pmol/ml] (R718 3mL brown vials)
3. Add 40ul IS0823
4. Vortex for 30 seconds
5. Evaporate
6. Add 30ml methylene chloride
7. Vortex for 10 seconds
8. Incubate in water bath (60℃) for five minutes
9. Add 30ml methylene chloride
10. Add 170ml methanol
11. Prepare 8 MS brown bottles, make duplicates for each concentration

Aliquot 100ul per concentration

Std	MW	Wavelengh	Abs	$e_{1cm}^{1\%}$	New (ug/ml)	Old (ug/ml)	% new/old	New (nmol/ml)
MK4	444.7	249	0.558	436	12.80	12.41	103.1%	28.78
VK1	450.7	249	0.454	420	10.81	11.07	97.6%	23.98
MK5	512.8	249	0.787	363	21.68	21.63	100.3%	42.28
MK6	580.9	249	0.815	320	25.47	25.47	100.0%	43.84
MK7	649	249	0.976	295	33.08	32.95	100.4%	50.98
MK8	717.1	249	0.527	268	19.66	20.49	96.0%	27.42
MK9	785.2	249	0.769	246	31.26	32.20	97.1%	39.81
MK10	853.4	249	0.48	224	21.43	19.96	107.4%	25.11
MK11	921.6	249	0.15	202	7.43	10.94	67.9%	8.06
MK12	989.7	249	0.168	180	9.33	11.39	82.0%	9.43
MK13	1057.8	249	0.494	158	31.27	25.06	124.7%	29.56

Componant	MW	Ref	C (nmol/ml)	Vol added(ul)	Added amount (nmol)	Final C (pmol/ml)	Final C (ng/ml)
MK4	444.7		28.78	86.9	2.5	100	44.47
VK1	450.7		23.98	104.2	2.5	100	45.07
MK5	512.8		42.28	59.1	2.5	100	51.28
MK6	580.9		43.84	57.0	2.5	100	58.09
MK7	649		50.98	49.0	2.5	100	64.9
MK8	717.1		27.42	91.2	2.5	100	71.71
MK9	785.2		39.81	62.8	2.5	100	78.52
MK10	853.4		25.11	99.6	2.5	100	85.34
MK11	921.6		8.06	310.3	2.5	100	92.16
MK12	989.7		9.43	265.1	2.5	100	98.97
MK13	1057.8		29.56	84.6	2.5	100	105.78

5.5 Lipase treatment

Purpose: To break down lipids in fatty tissues (e.g., intestines) in order to minimize interference peaks caused by lipids with molecular masses similar to MK4 during HPLC and Q-TOF-MS analysis.

1. Prepare Lipase in Tris buffer (3.4 mg/mL): calculate the amount of Lipase solution needed for the day by multiplying the number of samples (n) by 1.2-ml and then adding 2 to 4 ml extra to the number. Then calculate amount of crude Lipase needed (Total mL x [3.4 mg/mL]).
2. Bring solution up to volume, by weighing Tris buffer directly into a 15-ml polypropylene centrifuge tube on the scale. Vortex 30 seconds or until lipase fully dissolved.
3. Thaw and weigh food samples (0.05-0.2g) to 50mL polypropylene centrifuge tube.
4. Add 250-µL PBS and vortex for a few seconds
5. Add 10-µL of 200-g/L albumin solution to each sample
6. Add 200-µL of an aqueous solution of sodium taurocholate (0.05 mol/L, calcium chloride (0.1 mol/L), and sodium chloride (0.15 mol/L) to each sample.
7. Add 1200-µL of 0.2 mol/L Tris buffer (pH 7.7) that contains 4.08-mg of porcine pancreas, type II lipase, to each sample
8. Incubate samples in 37ºC shaking water bath for 45-min at 100 strokes/min.
9. Add 200-µL of an ammonium hydroxide solution (50 g/L)
10. Add IS to each sample
11. Continue with sample preparation starting from adding 10 mL dH_2O to each tube.

Working Solutions – 100 samples

Tris Buffer

Add 4.85 g Tris Base to 200 ml of dH2O

1.ml of 0.2 ml/L Tris buffer to each sample

1.2 ml x 100 samples = 120ml → 200ml (0.2 L)

0.2 mol/L x 0.2 L = 0.04 mol

0.04 mol x 121.14 g/mol (MW) = 4.85g

Using pH meter, add hydrochloric acid until pH of 7.7 is reached

Albumin Solution (200-g/L)

Add 1g of albumin to 5 ml of dH2O

10-µL (per sample) x 100 samples = 1 ml → 5 ml

5 ml x 200mg/mL = 1000 mg (1 g)

Aqueous Solution

Add 0.672g of Sodium taurocholate (0.05mol/L), 0.219 g sodium chloride (0.15 mol/L), 0.277 g calcium chloride (0.1 mol/L) to 25 ml of dH2O

200-µL (per sample) x 100 samples = 20 ml total solution → 25ml (0.025L)

Add 0.672g of Sodium taurocholate (0.05mol/L)

0.05 mol/L x 0.02 5L = 0.0012 5mol

0.00125 mol x 537.7 g/mol (MW) = 0.672 g

Add 0.219 g sodium chloride (0.15 mol/L)

0.15 mol/L x 0.025 L – 0.00375 mol

0.00373 mol x 58.44 g/mol (MW) = 0.219 g

Add 0.277 g calcium chloride (0.1 mol/L)

0.1 mol/L x 0.025L = 0.0025 mol

0.0025 mol x 110.98 g/mol (MW) = 0.277 g

Ammonium Hydroxide Solution (50g/L)

Add 18 ml of ammonium hydroxide to 82ml ml of dH2O

200-µL (per sample) x 100 samples = 20ml → 100 ml

50 g/L → 5 g

Using ammonium hydroxide concentration of 28%

5 g / 280 x 1000 = 18 ml

6. APPENDIX B: ADDITIONAL MANUSCRIPTS

During my doctoral training, I also contributed to several projects outside my dissertation. Collectively, these studies provide additional context for understanding the physiological relevance of gut-derived menaquinones. First, fecal menaquinone cluster profiles did not differ between individuals with and without osteoarthritis (see **Section 6.1**), suggesting that the contribution of gut bacterially produced menaquinones to osteoarthritis in humans remains uncertain. Second, long-term treatment of aged male and female mice with broad-spectrum antibiotics for 22 months did not significantly alter gut permeability (**Section 6.2**). This finding indicates that antibiotic exposure may not induce a "leaky gut" that would facilitate passive absorption of gut microbially produced menaquinones. Third, in young and estropausal female mice receiving fecal microbiota transplants, bacterially produced menaquinone forms were largely undetectable in extrahepatic tissues such as ovary, brain, and muscle (**Section 6.3**). Taken together, these findings further support my dissertation work by suggesting that the direct physiological relevance of gut-derived menaquinones to host's health appears to be limited.

6.1 An exploratory case-control study on associations of bacterially derived vitamin K forms with the intestinal microbiome and obesity-related osteoarthritis

Minying Liu [1], Gregory Matuszek [1], M. Andrea Azcarate-Peril [2], Richard F Loeser [3] *, M Kyla Shea [1] *

[1] USDA Human Nutrition Research Center on Aging at Tufts University, Boston, MA

[2] Division of Gastroenterology and Hepatology and UNC Microbiome Core, Center for Gastrointestinal Biology and Disease, University of North Carolina School of Medicine, Chapel Hill, North Carolina, USA

[3] Division of Rheumatology, Allergy, and Immunology and the Thurston Arthritis Research Center, University of North Carolina School of Medicine, Chapel Hill, NC

* These authors have contributed equally to this work.

Correspondence: Kyla Shea, PhD, 711 Washington St., Boston MA USA 02111; 617 556 3370; kyla.shea@tufts.edu

PMID: 37181928 **PMCID:** PMC10111584 **DOI:** 10.1016/j.cdnut.2023.100049

Supported by the Tufts University Clinical and Translational Science Institute National Institutes of Health Clinical and Translational Science Award (UL1TR002544), the United States Department of Agriculture (cooperative agreement 58-8050-9-004), the Arthritis Foundation, the National Center for Advancing Translational Sciences (UL1TR002489), and the National Institute of Arthritis and Musculoskeletal and Skin Diseases (P30AR072580). The Johnston County Osteoarthritis Project is funded in part by the Centers for Disease Control and Prevention (U01 DP006266). The University of North Carolina Microbiome Core is supported in part by

the National Institute of Diabetes and Digestive and Kidney Diseases (P30 DK034987 and P30 DK056350).

Disclosures: Minying Liu, Greg Matuszek, Andrea Azcarate-Peril, Richard F Loeser, Kyla Shea have nothing to disclose.

Teaser text: This study evaluated the associations among intestinally derived forms of vitamin K (menaquinones), microbial composition of the intestinal microbiome, and osteoarthritis in obese adults.

Short title: Intestinally derived vitamin K and osteoarthritis

Abbreviations

BMI body mass index

EU

HNRCA Tufts University Human Nutrition Research Center on Aging

LC-MS liquid chromatography mass spectrometry

LPS lipopolysaccharide

LBP lipopolysaccharide binding protein

MK menaquinone

OA osteoarthritis

PCA principal components analysis

PERMANOVA permutational multivariate analysis of variance

PK phylloquinone

Abstract

Background: Evidence suggests natural metabolites produced by intestinal microorganisms may have beneficial or harmful effects on osteoarthritis (OA). This could include menaquinones, which are bacterially-synthesized biologically active vitamin K forms abundant in the intestinal microbiome.

Objective: The overall goal of this study was to evaluate the association of intestinally-derived menaquinones with obesity-related OA.

Methods: This case-control study used data and biospecimens derived from a sub-group of Johnston County Osteoarthritis Study participants. Fecal menaquinone concentrations and microbial composition were determined in 52 obese participants with hand and knee OA and 42 age- and sex-matched obese participants without OA. The inter-relationships between the fecal menaquinones were evaluated using principal component analysis. Differences in alpha and beta diversity and microbial composition across menaquinone clusters were evaluated using analysis of variance.

Results: Samples clustered into three groups: cluster 1 characterized by higher fecal menaquinone -8, -9, and -10 concentrations, cluster 2 characterized by lower overall menaquinone concentrations, and cluster 3 characterized by higher menaquinone-12 and -13. Overall, fecal menaquinone clusters did not differ between participants with or without OA ($p=0.707$). Microbial diversity did not differ across the fecal menaquinone clusters (all F-test $p>0.12$). However, the relative abundance of bacterial taxa differed among clusters, with a higher abundance of *Coprococcus*, *Prevotella*, and *Eggerthella* in cluster 2 compared to cluster 1, a higher abundance of *Oscilospira, Dorea* and *Eubacterium,* and *Bacteroides* in cluster 3

compared to cluster 1, and a higher abundance of *Prevotella, Sutterella* and *Dorea* in cluster 3 compared to cluster 2 (all $p<0.001$).

Conclusion: Menaquinones were variable and abundant in the human gut, but the fecal menaquinone clusters did not differ with OA status. While the relative abundance of specific bacterial taxa differed among fecal menaquinone clusters, the relevance of these differences with respect to vitamin K status and human health is uncertain.

Key words: Vitamin K, menaquinone, microbiome, osteoarthritis, aging

Introduction

Osteoarthritis (OA), a debilitating disease that causes joint pain and loss of mobility, affects nearly 30 million Americans (1). There are currently no therapies known to mitigate OA progression. Therefore, the identification of novel pathways involved in OA is an important step toward identifying effective treatment strategies.

Evidence is accumulating that suggests deficiency of the lipid-soluble vitamer, vitamin K, may contribute to the development and progression of OA. In epidemiological studies, low vitamin K status has been associated with a greater incidence and progression of knee OA (2, 3). Vitamin K functions as a co-factor in the carboxylation of vitamin K-dependent proteins. Vitamin K-dependent proteins are present in joint tissues (4, 5) and are involved in inhibition of cartilage calcification, which can be characteristic of OA. Additionally, vitamin K is reported to have anti-inflammatory effects (6, 7). Since joint tissue inflammation contributes to OA progression (8), vitamin K's involvement in OA may additionally involve inflammatory pathways (4, 5).

There are multiple forms of vitamin K. The plant-based phylloquinone (PK), found in green leafy vegetables and vegetable oils, is the primary dietary form in Western diets. Menaquinones (MKs) are a class of vitamin K compounds that differ structurally from phylloquinone in the length and saturation of their prenylated side chain, with the number of prenyl units differentiating among the specific MKs (MK-n). At least 13 MK forms have been identified (17). The majority of MKs are synthesized by bacteria and are abundant in the intestinal tract (9). There is evidence suggesting that alterations in the intestinal microbiome are implicated in OA (10-12). Because many natural metabolites synthesized by the intestinal bacteria are biologically active and essential for the host health (13), it is possible that intestinally-derived menaquinones represent a mechanistic link

between the intestinal microbiome and OA. Thus, the purpose of this study was to test the hypothesis that the fecal menaquinone profiles differ between adults with and without hand and knee OA. The association of fecal menaquinone profiles with fecal microbial composition was also evaluated.

Methods

Study design and participants

This exploratory ancillary case-control study used data and biospecimens derived from a sub-group of Johnston County OA Study (JoCo) participants. Details of subject recruitment, fecal sample collection, and fecal microbiome analysis have been described previously (14, 15). Briefly, 52 obese adults ≥45 years old with hand and knee OA (cases) and 42 age- and sex-matched obese adults without hand or knee OA (controls) were recruited between July 2016 to July 2018. Cases had at least 3 hand joints with clinical and/or radiographic OA plus moderate to severe OA in at least one knee (defined as Kellgren Lawrence grade 3-4 or prior knee replacement for OA) (16). Controls did not have hand OA or definitive knee OA. All participants were obese based on having a BMI of at least 30 kg/m^2. The study was approved by institutional review boards of University of North Carolina Chapel Hill and Tufts University and all participants provided informed consent.

Measurements

Fecal vitamin K forms: Fecal samples were collected and stored at the University of North Carolina Chapel Hill as described in detail previously (15). Frozen aliquots were shipped to the

Vitamin K Laboratory at the Tufts University Human Nutrition Research Center on Aging (HNRCA), where fecal vitamin K formswere measured using the LC/MS assay developed by that lab, as detailed elsewhere (17). The lower limit of detection for fecal menaquinones ranges from 0.001 (menaquinone-10) to 0.03 (menaquinone-4 and phylloquinone) nmol/g (17).

Fecal microbiome: Fecal samples were analyzed for microbial composition using the Illumina MiSeq 16S rRNA amplicon sequencing at the University of North Carolina Chapel Hill Microbiome Core, as described and previously reported (15).

Lipopolysaccharide and lipopolysaccharide binding protein: Plasma lipopolysaccharide (LPS) was measured using the EndoZyme Assay (Hygios), and plasma lipopolysaccharide binding protein (LBP) was measured using ELISA (Hycult), as described and previously reported (15, 18).

Statistical analysis

Individual menaquinone measures were log transformed, centererd, and scaled prior to analysis. Menaquinone clusters were identified using k-mediods clustering with the partitioning around mediods (pam) function in the cluster() R-package. The optimum number of clusters used was selected based on the peak average silhouette width.

Principal component analysis with partitioning around mediod clusters was used to examine the inter-relationships among the fecal menaquinone forms. Participant characteristics were compared across menaquinone clusters using general linear models. Microbial alpha diversity was evaluated using the Shannon and Simpson Indexes in the phyloseq R-package (19). The Shannon index is a measure of the diversity of the microbial population in each group and the

Simpson index measures the relative abundance of species. Beta diversity was measured using the Bray-Curtis dis-similarity index and PERMANOVA (20). Differences in alpha and beta diversity across menaquinone clusters were evaluated using analysis of variance. Initial broad inter-omic relationships between the fecal microbiome and fecal menaquinones were evaluated and detected using Procrustes analysis and partial least squares regression using a q-value cutoff of 0.2. All analyses were performed in R version 4.0.*.

Results

Characteristics of the study participants are provided in **Table 1**. Participants were 72 ± 7 years old (mean ± SD), and their BMI was 35±4 kg/m^2. Nearly 74% were female and 63% were non-Hispanic white.

Overall, menaquinones 10 through 13 (MK10-MK13) were the predominant menaquinone forms detected in human feces (**Figure 1A**). Using PCA, three fecal menaquinone clusters were identified two of which explained approximately 50% of the variability in fecal menaquinone abundance (**Figure 1B**). Cluster 1 was characterized by higher MK9 and MK10. Cluster 2 was characterized by overall lower menaquinone concentrations. Cluster 3 was characterized collectively by higher concentrations of MK12 and MK13. However, fecal menaquinone clusters did not differ between participants with OA and those without ($p = 0.707$). Except for age ($p=0.032$), participants' demographic characteristics and BMI were similar across the identified fecal menaquinone clusters (**Table 1**). The plasma LPS and LBP were also similar across the fecal menaquinone clusters (**Table 1**).

Neither the Shannon alpha diversity index of the overall microbial communities nor the Simpson index of microbial species abundance differed across the three fecal menaquinone clusters (**Figures 2A and 2B**) (both F-test $p>0.12$). However, both indices showed similar microbial diversity across all three clusters. Beta diversity across the menaquinone clusters, calculated using bray-curtis distance measure and PERMANOVA, showed no significant differences among menaquinone clusters (all $p>0.13$).

The relative abundance of microbial genera differed among the fecal menaquinone clusters (**Figure 3**). *Coprococcus*, *Prevotella*, and *Eggerthella* were among the microbial genera significantly more abundant in cluster 2 compared to cluster 1 (**Figure 3A).** *Oscilospira, Dorea* and *Eubacterium,* and were among the microbial genera significantly more abundant in cluster 3 compared to cluster 1 (**Figure 3B).** *Prevotella, Sutterella* and *Dorea* were among the microbial genera significantly more abundant in cluster 3 compared to cluster 2 (**Figure 3C**) (all $p<0.001$).

Discussion

Our hypothesis that intestinally produced MKs would be associated with OA stemmed from previous observational studies linking vitamin K and the intestinal microbiome to OA (2, 3, 21, 22). However, we found no significant differences in fecal MK profiles between obese adults with OA and age-matched obese adults without OA. Although accumulating evidence suggests vitamin K status is associated with OA (2-5), the results of this study indicate this association does not involve intestinally derived MKs. Moreover, while evidence suggests the intestinal microbiome may contribute to OA (21, 22), our findings suggest intestinally derived MKs are not part of the underlying mechanism. In previous analyses of this same cohort, intestinal

microbial diversity did not differ between OA cases and controls (15), but distinct fecal metabolomes characterized by metabolites reflecting dysregulated proteolysis differentiated the cases from controls (10) as did serum LPS levels which were higher in the cases (15). This suggests some microbial metabolites are relevant to OA. However, based on our findings, microbially derived MKs do not appear among them.

In this study, fecal MKs were partitioned into three clusters. Cluster 1 with high MK9 ($p<0.01$), and MK10 ($p<0.001$), cluster 2 with low overall menaquinone concentrations, and cluster 3 with higher MK12 ($p< 0.001$) and MK13 ($p<0.001$). The partitioning pattern for MK12-13 are generally consistent with previous studies. In separate human feeding studies, Karl et al identified two fecal MK clusters – one generally enriched with MK5, and 11-13, and one generally enriched with MK9 and MK10 (23, 24). However, we observed low amounts of MK5 in all three clusters. We identified an additional cluster characterized by overall low amounts of MKs. The results of a rodent feeding study indicate the amount of dietary vitamin K influences the intestinal microbial composition more than the form of vitamin K in the diet (9). It is possible the participants characterized by lower fecal MKs (cluster 2) consumed lower amounts of vitamin K in the diet. Unfortunately, dietary intake data were not available, so we were not able to account for potential dietary contributors to the identified fecal MK clusters. Fecal phylloquinone concentrations were did not differ across the three clusters. As phylloquinone is the primary vitamin K form in the western diet and is not produced by the gut microbiota, this could suggest that phylloquinone intakes were similar among participants across the three menaquinone clusters.

The overall microbial diversity was similar across the identified fecal MK clusters. However, we detected differences in the relative abundance of specific microbial phyla and genera among the

MK clusters. For example, the relative abundance of bacteria in the *Bacteroides*, and *Firmicutes* phyla was significantly lower in the cluster characterized by low overall menaquinone concentrations (cluster 2), relative to cluster 3. In the studies conducted by Karl et al, the relative abundance of *Bacteroides* was linked to MK9 and MK10, and a strong association between *Prevotella* and MK5-MK7/MK11-MK13 was also apparent (23, 24). Our findings are generally consistent with data demonstrating that *Proteobacteria*, *Firmicutes*, and *Bacteroides* are predominantly associated with the biosynthetic pathways of MK9 and MK10, whereas MK11–MK13 biosynthetic pathways are predominantly found in phyla *Prevotella* and *Actinobacteria* (24).

Results of the parent study indicated OA cases had significantly higher circulating LPS concentrations compared to controls, suggesting individuals with OA might have a more permeable gut barrier (15). The extent to which intestinally derived MKs are absorbed from the colon is currently unclear. Although some have suggested one possibility is through the leaky gut pathway carried by the triacylglycerol-rich lipoprotein fraction (17, 25), our findings do not support this since we did not detect any associations between fecal MKs and plasma LPS.

Our findings should be interpreted in the context of the study's strengths and limitations. To the best of our knowledge, there are no studies that have reported the association between intestinally derived MKs and OA. Fecal MKs were measured using a sensitive and validated state-of-the-art LC-MS assay (17). Moreover, participants were well phenotyped for hand and knee OA. However, they were all obese, which may limit generalizability. We do not have circulating measures of vitamin K status so were unable to correlate fecal MKs with circulating concentrations. However, MKs are not typically detected in the circulation (17), which further

limits our understanding of the contribution of intestinally derived MKs to overall vitamin K status. Differences in fecal MKs were evaluated as an exploratory analysis to a parent study designed to evaluate differences in the intestinal microbiome composition between OA cases and controls (15), and the sample size was relatively small (n=90), so the results should be considered exploratory. The 16S RNA amplicon sequencing identifies bacterial genera but not necessarily species or functional attributes directly. Imputing microbiota function from 16S RNA using PICRUSt is possible but limited as recent metagenomics studies show that taxonomy features and vitamin K functional pathways are not directly related (26). However, metagenomic sequencing could provide additional insight into screening possible functional pathways carried by microbes that were found in high abundances in fecal MK clusters.

In summary, MKs were abundant in the human gut and the abundance of individual MK forms was variable. However, MK abundance did not differ with OA status. Although the relative abundance of some bacterial phyla differed between the MK clusters identified, the implications of these observed differences with respect to vitamin K status and human health remains to be determined.

Author's Responsibilities: GM, RFL, MKS designed the study; GM analyzed the data; MAA-P conducted microbiome analyses; ML wrote the manuscript; GM, MAA-P, RFL, MKS contributed critically to data interpretation and manuscript revision; MKS and RFL share responsibility for final content; all authors read and approved the final manuscript.

Data Availability: The data and analytic code that support these findings will be made available upon request pending approval of shared agreement contracts.

References

1. Lawrence RC, Felson DT, Helmick CG, Arnold LM, Choi H, Deyo RA, Gabriel S, Hirsch R, Hochberg MC, Hunder GG, et al. Estimates of the prevalence of arthritis and other rheumatic conditions in the United States. Part II. Arthritis Rheum. 2008;58(1):26-35.

2. Misra D, Booth SL, Tolstykh I, Felson DT, Nevitt MC, Lewis CE, Torner J, Neogi T. Vitamin K Deficiency Is Associated with Incident Knee Osteoarthritis. The American Journal of Medicine. 2013;126(3):243-8.

3. Shea MK, Kritchevsky SB, Hsu FC, Nevitt M, Booth SL, Kwoh CK, McAlindon TE, Vermeer C, Drummen N, Harris TB, et al. The association between vitamin K status and knee osteoarthritis features in older adults: the Health, Aging and Body Composition Study. Osteoarthritis Cartilage. 2015;23(3):370-8.

4. Wallin R, Schurgers LJ, Loeser RF. Biosynthesis of the vitamin K-dependent matrix Gla protein (MGP) in chondrocytes: a fetuin-MGP protein complex is assembled in vesicles shed from normal but not from osteoarthritic chondrocytes. Osteoarthritis Cartilage. 2010;18(8):1096-103.

5. Cavaco S, Viegas CS, Rafael MS, Ramos A, Magalhães J, Blanco FJ, Vermeer C, Simes DC. Gla-rich protein is involved in the cross-talk between calcification and inflammation in osteoarthritis. Cell Mol Life Sci. 2016;73(5):1051-65.

6. Ohsaki Y, Shirakawa H, Miura A, Giriwono PE, Sato S, Ohashi A, Iribe M, Goto T, Komai M. Vitamin K suppresses the lipopolysaccharide-induced expression of inflammatory cytokines in cultured macrophage-like cells via the inhibition of the activation of nuclear factor κB through the repression of IKKα/β phosphorylation. J Nutr Biochem. 2010;21(11):1120-6.

7. Ohsaki Y, Shirakawa H, Hiwatashi K, Furukawa Y, Mizutani T, Komai M. Vitamin K suppresses lipopolysaccharide-induced inflammation in the rat. Biosci Biotechnol Biochem. 2006;70(4):926-32.

8. Sanchez-Lopez E, Coras R, Torres A, Lane NE, Guma M. Synovial inflammation in osteoarthritis progression. Nature Reviews Rheumatology. 2022.

9. Ellis JL, Karl JP, Oliverio AM, Fu X, Soares JW, Wolfe BE, Hernandez CJ, Mason JB, Booth SL. Dietary vitamin K is remodeled by gut microbiota and influences community composition. Gut Microbes. 2021;13(1):1-16.

10. Rushing BR, McRitchie S, Arbeeva L, Nelson AE, Azcarate-Peril MA, Li YY, Qian Y, Pathmasiri W, Sumner SCJ, Loeser RF. Fecal metabolomics reveals products of dysregulated proteolysis and altered microbial metabolism in obesity-related osteoarthritis. Osteoarthritis and Cartilage. 2022;30(1):81-91.

11. Guss JD, Ziemian SN, Luna M, Sandoval TN, Holyoak DT, Guisado GG, Roubert S, Callahan RL, Brito IL, van der Meulen MCH, et al. The effects of metabolic syndrome, obesity, and the gut microbiome on load-induced osteoarthritis. Osteoarthritis Cartilage. 2019;27(1):129-39.

12. Ulici V, Kelley KL, Azcarate-Peril MA, Cleveland RJ, Sartor RB, Schwartz TA, Loeser RF. Osteoarthritis induced by destabilization of the medial meniscus is reduced in germ-free mice. Osteoarthritis Cartilage. 2018;26(8):1098-109.

13. Postler TS, Ghosh S. Understanding the Holobiont: How Microbial Metabolites Affect Human Health and Shape the Immune System. Cell Metabolism. 2017;26(1):110-30.

14. Jordan JM, Helmick CG, Renner JB, Luta G, Dragomir AD, Woodard J, Fang F, Schwartz TA, Abbate LM, Callahan LF, et al. Prevalence of knee symptoms and radiographic and symptomatic knee osteoarthritis in African Americans and Caucasians: the Johnston County Osteoarthritis Project. J Rheumatol. 2007;34(1):172-80.

15. Loeser RF, Arbeeva L, Kelley K, Fodor AA, Sun S, Ulici V, Longobardi L, Cui Y, Stewart DA, Sumner SJ, et al. Association of Increased Serum Lipopolysaccharide, But Not Microbial Dysbiosis, With Obesity-Related Osteoarthritis. Arthritis Rheumatol. 2022;74(2):227-36.

16. Kellgren JH, Lawrence JS. Radiological assessment of osteo-arthrosis. Ann Rheum Dis. 1957;16(4):494-502.

17. Karl JP, Fu X, Dolnikowski GG, Saltzman E, Booth SL. Quantification of phylloquinone and menaquinones in feces, serum, and food by high-performance liquid chromatography-mass spectrometry. J Chromatogr B Analyt Technol Biomed Life Sci. 2014;963:128-33.

18. Huang ZY, Stabler T, Pei FX, Kraus VB. Both systemic and local lipopolysaccharide (LPS) burden are associated with knee OA severity and inflammation. Osteoarthritis Cartilage. 2016;24(10):1769-75.

19. McMurdie PJ, Holmes S. phyloseq: an R package for reproducible interactive analysis and graphics of microbiome census data. PLoS One. 2013;8(4):e61217.

20. Bray JR, Curtis JT. An Ordination of the Upland Forest Communities of Southern Wisconsin. Ecological Monographs. 1957;27(4):325-49.

21Biver E, Berenbaum F, Valdes AM, Araujo de Carvalho I, Bindels LB, Brandi ML, Calder P, Castronovo V, Cavalier E, Cherubini A, et al. Gut microbiota and osteoarthritis management: An expert consensus of the European society for clinical and economic aspects of osteoporosis, osteoarthritis and musculoskeletal diseases (ESCEO). Ageing Res Rev. 2019;55:100946.

22. Hao X, Shang X, Liu J, Chi R, Zhang J, Xu T. The gut microbiota in osteoarthritis: where do we stand and what can we do? Arthritis Res Ther. 2021;23(1):42.

23. Karl JP, Meydani M, Barnett JB, Vanegas SM, Barger K, Fu X, Goldin B, Kane A, Rasmussen H, Vangay P, et al. Fecal concentrations of bacterially derived vitamin K forms are associated with gut microbiota composition but not plasma or fecal cytokine concentrations in healthy adults. Am J Clin Nutr. 2017;106(4):1052-61.

24. Karl JP, Fu X, Wang X, Zhao Y, Shen J, Zhang C, Wolfe BE, Saltzman E, Zhao L, Booth SL. Fecal menaquinone profiles of overweight adults are associated with gut microbiota composition during a gut microbiota-targeted dietary intervention. Am J Clin Nutr. 2015;102(1):84-93.

25. Schurgers LJ, Vermeer C. Differential lipoprotein transport pathways of K-vitamins in healthy subjects. Biochimica et Biophysica Acta (BBA). 2002;1570(1):27-32.

26. Das P, Babaei P, Nielsen J. Metagenomic analysis of microbe-mediated vitamin metabolism in the human gut microbiome. BMC Genomics. 2019;20(1):208.

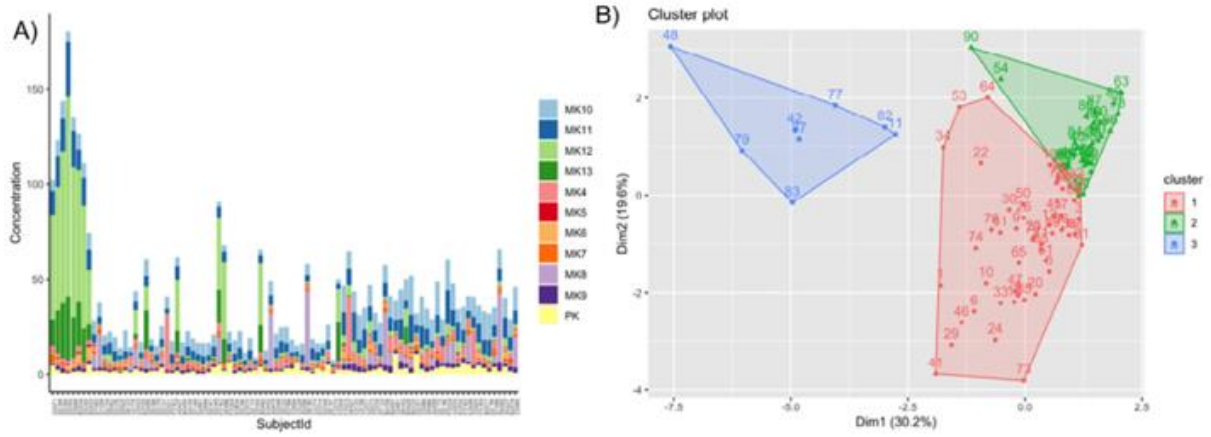

Figure 1. Fecal menaquinone profiles of study participants (n=90) (A), and fecal menaquinone K-mediods clustering (B).

(**A**) Bars represent individual participants. Colors represent different fecal vitamin K forms.

(**B**) Partitioning around mediod analysis of fecal menaquinones identified three clusters: cluster 1 (shown in red, n=34) characterized by higher MK9 and MK10; cluster 2 (shown in green, n=48) characterized by overall lower menaquinone concentrations; cluster 3 (shown in blue, n=8) characterized by higher concentrations of MK12 and MK13.

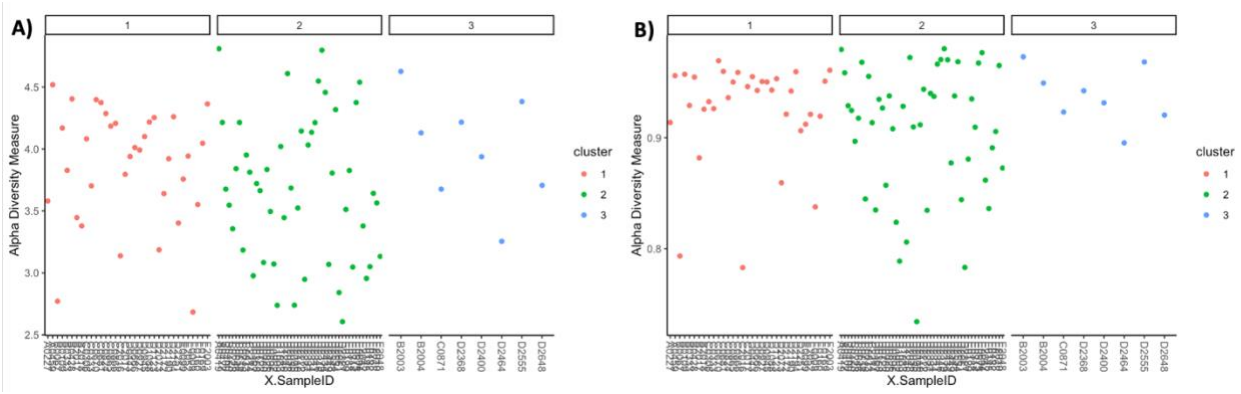

Figure 2. Microbial alpha diversity indexes of obese adults with and without osteoarthritis according the fecal menaquinone cluster.

Column represents individual participants. Microbial alpha diversity evaluated using the (**A**) Shannon and (**B**) Simpson Indexes did not differ among three fecal menaquinone clusters (ANOVA F-test p>0.12).

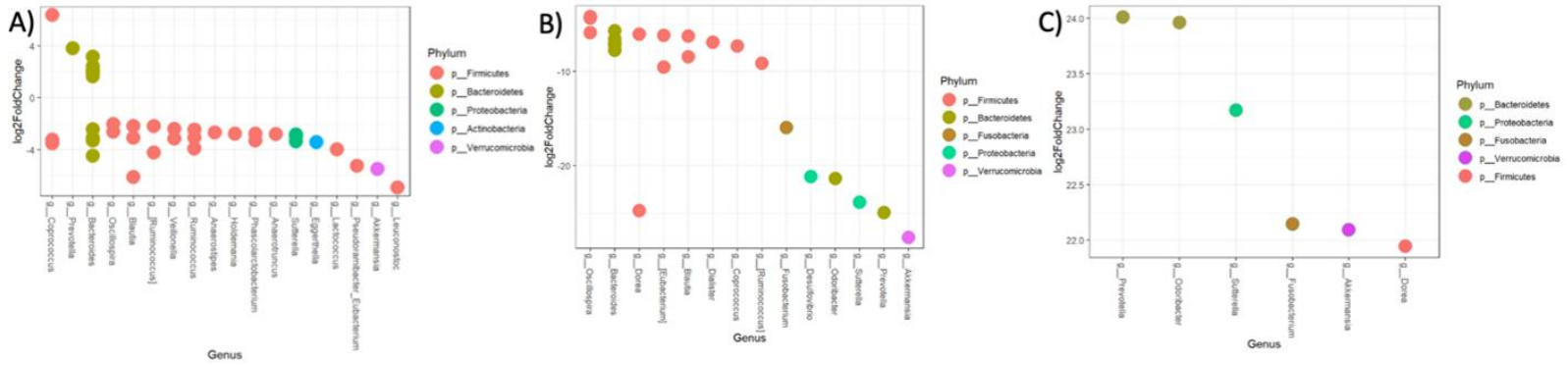

Figure 3. Differentially abundant microbiota between fecal menaquinone clusters 1 and 2 (A), 1 and 3 (B), 2 and 3 (C).

Dotplot showing significantly differently abundant microbiota (using a q-value cutoff of 0.2) among fecal menaquinone clusters. Effect size is represented on the y-axis as $\log_2$-fold difference between **(A)** cluster 1 and cluster 2, **(B)** cluster 1 and cluster 3, and **(C)** cluster 2 and cluster 3. Genera are shown on the x-axis. Colors represent phyla.

Table 1. Participant characteristics and fecal vitamin K concentrations according to fecal menaquinone clusters. Data are n (%) or mean (SD).

	Overall (n=90)	**Cluster 1 (n=34)**	**Cluster 2 (n=48)**	**Cluster 3 (n=8)**	**p-value**
OA group Case	48 (53.3%)	19 (55.9%)	26 (54.2%)	3 (37.5%)	NS
Control	42 (46.7%)	15 (44.1%)	22 (45.8%)	5 (62.5%)	
Sex Female	67 (74.4%)	27 (79.4%)	35 (72.9%)	5 (62.5%)	NS
Male	23 (25.6%)	7 (20.6%)	13 (27.1%)	3 (37.5%)	
Race Black	33 (36.7%)	15 (44.1%)	13 (27.1%)	5 (62.5%)	NS
White	57 (63.3%)	19 (55.9%)	35 (72.9%)	3 (37.5%)	
BMI, kg/m^2	35.0 (4.1)	34.6 (4.3)	35.3 (3.9)	34.4 (4.8)	NS
Age, years	72.4 (6.83)	75.2 (7.5)	71.3 (5. 6)	67.4 (6.9)	*
Plasma LPS, EU/ml	83.9 (46.3)	80.3 (38.8)	90.3 (47.5)	58.2 (60.1)	NS
Plasma LBP, µg/ml	12.1 (5.6)	11.9 (5.7)	11.9 (4.7)	14.6 (9.7)	NS
Fecal vitamin K forms , nmol/g					
PK	2.53 (1.96)	3.21 (2.37)	2.10 (1.53)	2.18 (1.78)	NS
MK4	3.18 (4.49)	4.34 (5.55)	2.49 (3.86)	2.35 (0.55)	NS

MK5	0.19 (0.19)	0.19 (0.13)	0.13 (0.12)	0.57 (0.32)	**
MK6	1.00 (1.04)	1.21 (0.94)	0.61 (0.41)	2.50 (2.14)	**
MK7	1.07 (0.75)	1.25 (0.69)	0.92 (0.68)	1.23 (1.25)	NS
MK8	3.73 (7.50)	5.15 (8.02)	3.24 (7.61)	0.64 (0.28)	NS
MK9	1.71 (0.92)	2.53 (0.86)	1.11 (0.42)	1.78 (0.57)	**
MK10	8.18 (3.75)	11.81 (3.02)	5.72 (2.03)	7.51 (1.37)	**
MK11	6.71 (4.55)	8.25 (3.29)	4.04 (1.38)	16.27 (5.90)	**
MK12	9.60 (20.68)	2.84 (2.15)	4.65 (9.76)	68.08 (21.82)	**
MK13	3.32 (7.34)	0.58 (1.53)	2.27 (5.41)	21.23 (8.17)	**

* P<0.05 Hochberg-adjusted

** P<0.001, Hochberg-adjusted

EU endotoxin unit; LBP lipopolysaccharide binding protein; LPS Lipopolysaccharide; NS not statistically significant (all NS P>0.70, Hochberg adjusted); OA osteoarthritis

6.2 Commensal Taxa in Gut Microbiota Limit Antibiotic Resistance During Extended Oral Antibiotic Use

https://doi.org/10.1101/2025.08.13.670183 (full text in PDF version)

Title: Commensal taxa in gut microbiota limit antibiotic resistance during extended oral antibiotic use

Authors: Erika L. Cyphert[1]*†, Chongshan Liu[2,3]†, Victoria T. Chu[4], Aditi Dubey[2], Minying Liu[5], Zhe Zhong[6,7,8], James R. Cockey[9], Eva C. González Díaz[2], Angie L. Morales[3], Jacob C. Nixon[3], Matthew Garcia[3], Susana Zeng[3], Sidhant Rohatgi[1], Joan Wong[10], Ritwicq Arjyal[10], Honey Mekonen[10], Norma Neff[10], Jennifer Lee[5,11], M. Kyla Shea[5], Xueyan Fu[5], Sarah L. Booth[5], Cynthia A. Leifer[9], Ankur Singh[6,7,8], Charles R. Langelier[10,12], Christopher J. Hernandez[2,10,13,14]*

Affiliations:

[1]Shu Chien-Gene Lay Department of Bioengineering, University of California San Diego; San Diego, CA, USA.

[2]Department of Orthopaedic Surgery, University of California San Francisco; San Francisco, CA, USA.

[3]Sibley School of Mechanical & Aerospace Engineering, Cornell University; Ithaca, NY, USA.

[4]Division of Infectious Diseases and Global Health, Department of Pediatrics, University of California San Francisco; San Francisco, CA, USA.

[5]USDA Human Nutrition Research Center on Aging at Tufts University; Boston, MA, USA.

[6]Coulter Department of Biomedical Engineering, Georgia Institute of Technology and Emory University; Atlanta, GA, USA.

[7]Woodruff School of Mechanical Engineering, Georgia Institute of Technology; Atlanta, GA, USA.

[8]Parker H. Petit Institute for Bioengineering and Bioscience, Georgia Institute of Technology; Atlanta, GA, USA.

[9]Department of Microbiology and Immunology, Cornell University; Ithaca, NY, USA.

[10]Chan Zuckerberg Biohub; San Francisco, CA, USA.

[11]Tufts University School of Medicine; Boston, MA, USA.

[12]Division of Infectious Diseases, Department of Medicine, University of California San Francisco; San Francisco, CA, USA.

[13]Department of Bioengineering and Therapeutic Sciences, University of California San Francisco; San Francisco, CA, USA.

[14]Department of Bioengineering, University of California Berkeley; Berkeley, CA, USA.

*Co-Corresponding authors. Email: ecyphert@ucsd.edu, christopher.hernandez@ucsf.edu

† These authors contributed equally to this work

Title: Commensal taxa in gut microbiota limit antibiotic resistance during extended oral antibiotic use

Authors: Erika L. Cyphert[1]*†, Chongshan Liu[2,3]†, Victoria T. Chu[4], Aditi Dubey[2], Minying Liu[5], Zhe Zhong[6,7,8], James R. Cockey[9], Eva C. González Díaz[2], Angie L. Morales[3], Jacob C. Nixon[3], Matthew Garcia[3], Susana Zeng[3], Sidhant Rohatgi[1], Joan Wong[10], Ritwicq Arjyal[10], Honey Mekonen[10], Norma Neff[10], Jennifer Lee[5,11], M. Kyla Shea[5], Xueyan Fu[5], Sarah L. Booth[5], Cynthia A. Leifer[9], Ankur Singh[6,7,8], Charles R. Langelier[10,12], Christopher J. Hernandez[2,10,13,14]*

Affiliations:

[1]Shu Chien-Gene Lay Department of Bioengineering, University of California San Diego; San Diego, CA, USA.

[2]Department of Orthopaedic Surgery, University of California San Francisco; San Francisco, CA, USA.

[3]Sibley School of Mechanical & Aerospace Engineering, Cornell University; Ithaca, NY, USA.

[4]Division of Infectious Diseases and Global Health, Department of Pediatrics, University of California San Francisco; San Francisco, CA, USA.

[5]USDA Human Nutrition Research Center on Aging at Tufts University; Boston, MA, USA.

[6]Coulter Department of Biomedical Engineering, Georgia Institute of Technology and Emory University; Atlanta, GA, USA.

[7]Woodruff School of Mechanical Engineering, Georgia Institute of Technology; Atlanta, GA, USA.

[8]Parker H. Petit Institute for Bioengineering and Bioscience, Georgia Institute of Technology; Atlanta, GA, USA.

[9]Department of Microbiology and Immunology, Cornell University; Ithaca, NY, USA.

[10]Chan Zuckerberg Biohub; San Francisco, CA, USA.

[11]Tufts University School of Medicine; Boston, MA, USA.

[12]Division of Infectious Diseases, Department of Medicine, University of California San Francisco; San Francisco, CA, USA.

[13]Department of Bioengineering and Therapeutic Sciences, University of California San Francisco; San Francisco, CA, USA.

[14]Department of Bioengineering, University of California Berkeley; Berkeley, CA, USA.

*Co-Corresponding authors. Email: ecyphert@ucsd.edu, christopher.hernandez@ucsf.edu

† These authors contributed equally to this work

Abstract: Certain bacterial infections, such as those involving prosthetics, can require antimicrobial therapy over months to years, potentially increasing the burden of antimicrobial resistance. Here we longitudinally track the antimicrobial resistome in mice during continuous antibiotic dosing over 21 months. The burden of antibiotic resistance genes (ARGs) initially increases, but, surprisingly, declines in later months, approaching levels observed in untreated animals. ARG burden is regulated by taxonomy and declines as ARG-harboring taxa that initially bloom are replaced by commensals. Furthermore, we find that the dynamics of antibiotic-induced ARG burden are influenced by age-related differences in microbial taxonomy and can be removed by fecal microbiota transplantation. We show that commensals may regulate the resistome by limiting the growth of ARG-harboring taxa, thereby providing antimicrobial expansion resistance.

Main Text:

Antibiotic-resistant infections are a global threat responsible for an estimated 1.5 million deaths annually (*1*). Widespread antibiotic use exerts selective pressure that drives the emergence of resistance among both commensal and pathogenic bacterial species (*2*). Collectively, antimicrobial resistance genes (ARGs) in an ecosystem are known as the "resistome." While most antibiotic resistance mechanisms are naturally present, antibiotic use in humans and domestic animals has increased the collective reservoir of antibiotic resistance (*3-4*). Within hosts, the gut microbiome is the largest population of microbes and serves as an ecosystem for ARGs (*5-8*).

The abundance and richness of ARGs in the gut microbiome increases immediately after the start of oral antibiotics (*8-11*). A short course of oral antibiotics (e.g. < 10 days) results in changes in the composition of the microbiome and ARG abundance that reverses within several weeks to months after cessation (*8, 12-14*). However, there are certain clinical conditions in which prolonged antibiotic therapy of months to years is required, such as infections of prosthetic materials, endocarditis, or mycobacterial infections including tuberculosis (*15-18*). Although prolonged antibiotic exposure during infection treatment is presumed to select for accumulation of resistance, this has not been rigorously studied with respect to the microbiome resistome (*18, 19*).

Here, we use a mouse model to longitudinally assess community dynamics within the gut microbiome over 21 months of exposure to oral antibiotics. Surprisingly, after a year of continuous antibiotic dosing, the burden of ARGs decreases toward levels seen in treatment-naïve mice primarily due to shifts in taxonomic abundance. Furthermore, the dynamics of ARG abundance depend on age at antibiotic initiation; the transient increase in ARG abundance is shorter when antibiotics are initiated late in life. Lastly, we show that the abundance and richness of ARGs can return to baseline through administration of a fecal microbiota transplant (FMT) from treatment-naïve mice. Collectively, our findings illustrate how members of a microbial community with intrinsic resistance can regulate the resistome, thereby providing antimicrobial expansion resistance in a community.

Abundance of antimicrobial resistance genes declines during prolonged exposure to oral antibiotics

To capture the dynamics of the microbiota community in mice throughout life, fecal samples were collected from mice longitudinally, from one month of age until 22 months of age (near the natural lifespan), to observe changes in the gut microbiome during normal aging (Unaltered) or during sustained dosing with oral antibiotics in drinking water (the beta-lactam ampicillin and the aminoglycoside neomycin, Continuous Dose; Fig. 1A). Only a portion of the microbiota is susceptible to one or both antibiotics; hence, many taxa are not directly affected by the applied antibiotics, as is true with most antibiotics used clinically (*21*). Chronic administration of these antibiotics did not have detectable effects on gut permeability, serum biomarkers of inflammation or systemic immunity (fig. S1-2, table S1-2).

In the first few months of continuous antibiotic dosing, ARG abundance and diversity increased, peaking at three months of age. The abundance of ARGs subsequently declined, approaching levels similar to those of the Unaltered group by 18 months of age (Fig. 1B, fig. S3). The richness of ARGs also peaked at three months of age and declined thereafter, but remained elevated relative to the Unaltered group for the remainder of the experiment (Fig. 1C, fig. S3).

The enrichment of ARGs only partially reflected the administered antibiotics (table S3-4). Prior to antibiotic exposure (at one month of age), the abundance of ARGs was low and primarily consisted of tetracycline resistance (*tet(Q)* > 90% relative abundance); ARGs for beta-lactam, aminoglycoside and multidrug resistance genes together were less than 4% of relative abundance. Two months after the start of antibiotic exposure, ARG abundance was increased, primarily due to enrichment of ARGs conferring resistance to the administered antibiotics (49.29 ± 2.18% associated with beta-lactam, aminoglycoside or multidrug resistance genes effective against either drug). By 22 months of age, only 26.28 ± 9.75% of ARG abundance was associated with applied antibiotics (as compared to 3.18 ± 2.27% in Unaltered mice) (Fig. 1D-E, fig. S3-4). These findings show that after years of continuous exposure to antibiotics, the majority of ARGs in a gut microbial community do not confer resistance to the applied antibiotics.

Although the abundance of ARGs decreased late in life in the Continuous Dose group, ARG richness remained elevated. The increase in ARG richness was due to the presence of ARGs that were not detected prior to the start of dosing (Fig. 1F, fig. S3). Several ARGs were first detected months after the start of antibiotic exposure. These "new" ARGs conferred resistance to multiple antibiotic classes including beta-lactam, aminoglycoside, tetracycline, and fluoroquinolone (Fig. 1, fig. S3). Additionally, during continuous dosing, the resistome composition shifted over time to be more similar to baseline as indicated by reductions in Bray-Curtis distance (Fig. 1G, fig. S3). Together, these findings show that during prolonged exposure to antibiotics, the majority of enriched ARGs confer resistance to unrelated antibiotic classes and total ARG abundance can be similar to that in Untreated individuals.

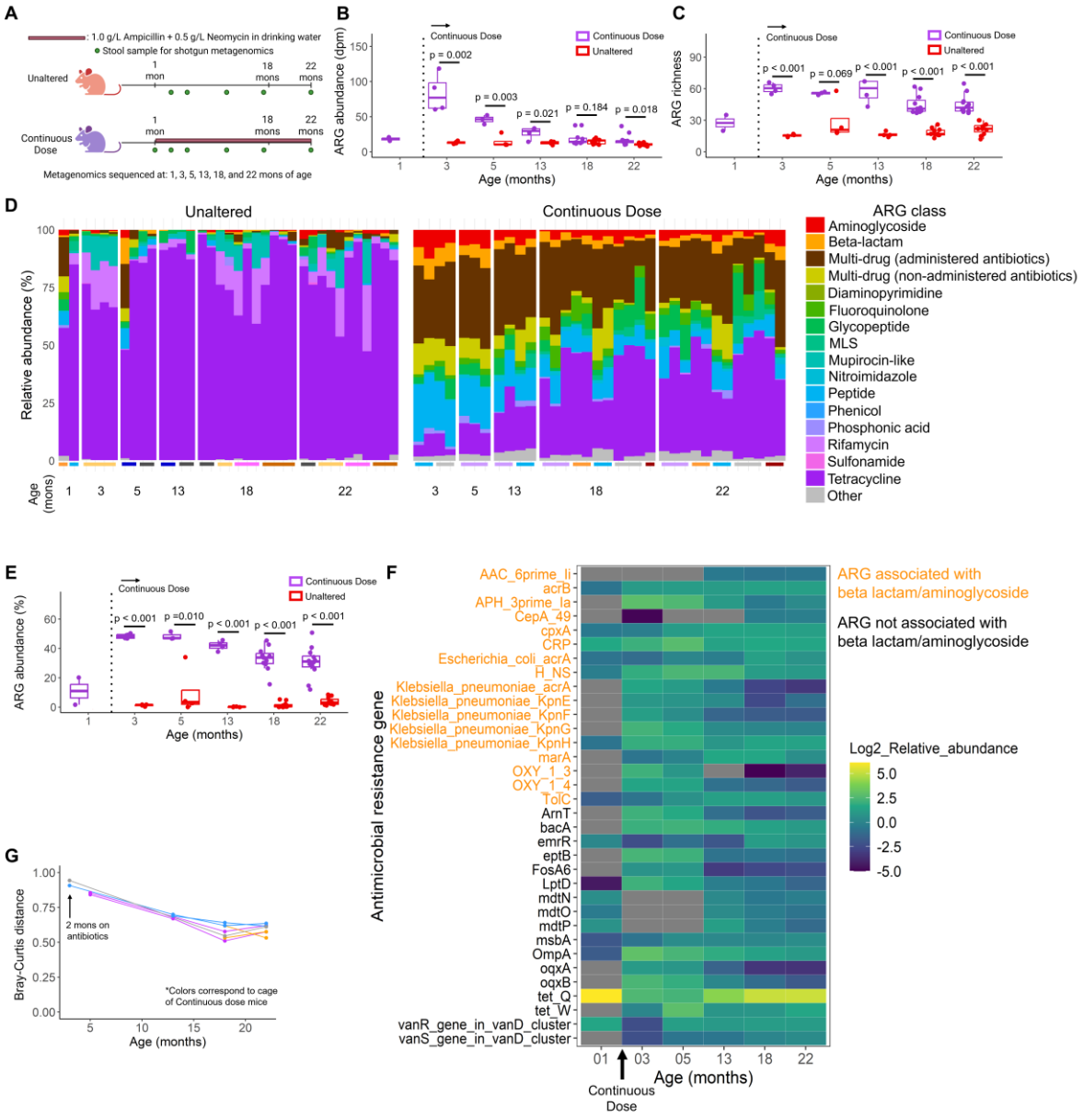

Fig. 1. Abundance of antimicrobial resistance genes declines during prolonged exposure to oral antibiotics. (**A**) Study design. (B) Changes in ARG abundance over time are shown. (C) Changes in ARG richness are shown. (D) Bar charts for each animal show changes in ARGs. Colors at the bottom represent the same cage. (E) Two months after the start of antibiotic exposure < 50% of the ARG abundance conferred resistance to beta-lactams or aminoglycosides. (F) The increase in ARG richness was primarily due to the sustained presence of ARGs that were first detected shortly after the start of antibiotic dosing. (G) Longitudinal tracking in individual mice showed changes in the Bray-Curtis resistome composition over time that decreased. Lines connect data points from the same individual and represent Bray-Curtis distance to baseline (1 month of age prior to antibiotic exposure); colors correspond to the cages as shown in D. Results from female mice are shown here, the corresponding results from male mice are in Figure S3.

Whiskers of the box plots represent the range of the data and the boxes represent the middle 50% of data.

Taxonomic changes explain declines in ARG abundance during prolonged oral antibiotics

The observed ARGs were attributed to several different taxa based on the CARD ontology, leading us to examine the changes in taxonomic composition in more detail. Consistent with prior work (*21, 22*), oral antibiotics resulted in a drastic change in gut microbial composition compared to mice without antibiotic exposure. Although antibiotic perturbation was continuous, the gut microbial population was dynamic, with significant differences observed in the taxonomic composition between three and 22 months of age (PERMANOVA: female – $p < 0.001$, male – $p = 0.003$; Fig. 2A, fig. S5). Specifically, the Bray-Curtis distance of taxonomic composition in individual animals decreased over time, becoming more similar to the Unaltered baseline (Fig. 2B, fig. S5).

Short term antibiotic dosing reduces the alpha diversity of the gut microbiome (*22*). Consistent with this fact, in the two months after the start of continuous antibiotic dosing, Shannon diversity was reduced relative to baseline (Fig. 2C). After 12 months of continuous dosing, however, Shannon diversity had unexpectedly increased in females, nearly reaching baseline by 22 months of age (Fig. 2C, in males, Shannon diversity remained low, fig. S5). The increase in Shannon diversity in females was attributed to the increased abundance of more than 100 genera. We speculate that Shannon diversity recovered in females because females tend to have a greater microbiome diversity than males (*23*). Genus-level analysis revealed complex dynamics of taxonomic composition during continuous antibiotic dosing (Fig. 2D-E, fig. S5-6). The dynamic changes in taxonomic abundance followed four different responses to antibiotic exposure: colonization, dynamic colonization, sustained change in abundance, and dynamic change in abundance. Representative genera that followed these trends include *Citrobacter*, *Klebsiella*, and *Phocaeicola* (Fig. 2F-H, fig. S5).

Prior to antibiotic exposure, *Muribaculaceae spp.* occupied the largest proportion of taxonomic abundance (29.81 ± 2.13%). Shortly after the onset of antibiotic exposure, the abundance of *Muribaculaceae spp.* declined (14.27 ± 8.86%). Concurrently, the relative abundance of *Enterobacteriaceae* rapidly increased and peaked at three months of age (29.35 ± 8.67%) and later declined to 2.66% by 22 months of age (still greater than the pre-antibiotic baseline of 0.26 ± 0.32%). The changes in *Enterobacteriaceae* abundance in the Continuous Dose group were predominantly driven by two classic pathobionts that frequently harbor ARGs: *Klebsiella spp.* and *Citrobacter spp.* (table S5). The decline in *Enterobacteriaceae* coincided with the gradual increase in the relative abundance of *Bacteroides*. Before exposure to antibiotics, *Bacteroides* had a relatively low abundance (6.56 ± 3.16%). Prolonged exposure to antibiotics gradually increased the relative abundance of *Bacteroides* which peaked at 16.24 ± 2.97% in females. *Bacteroides* are not susceptible to aminoglycosides and commonly carry resistance against beta-lactams and aminoglycosides (*24, 25*).

The changes in taxa over time in the Continuous Dose group were substantially larger than the age-related changes observed in the Unaltered group, which experienced subtle changes in taxonomy during aging (table S6). The changes in taxonomic composition explained the majority of changes in ARG abundance. Changes in the relative abundance of *Klebsiella* alone explain more than 85% of the variance in total ARG abundance (Fig. 2I, fig. S5,7-8). Overall, the transient increase in ARG burden aligned with the combined relative abundance of *Klebsiella*, *Citrobacter*, and *Bacteroides* (Fig. 2J, fig. S5). These three genera harbor 82% of the

differentially abundant ARGs (based on CARD ontology/pathogen of origin prediction). As the abundance of *Klebsiella* and *Citrobacter* increased upon exposure to antibiotics, the abundance of ARGs increased. When the abundance of *Klebsiella* decreased, ARG abundance also decreased but was partially replaced by ARGs associated with *Bacteroides*. Together, these results show that fluctuations in the abundance of ARGs during continuous antibiotic exposure are explained primarily by shifts in taxonomy as ARG-harboring organisms are replaced by commensals of varying susceptibilities.

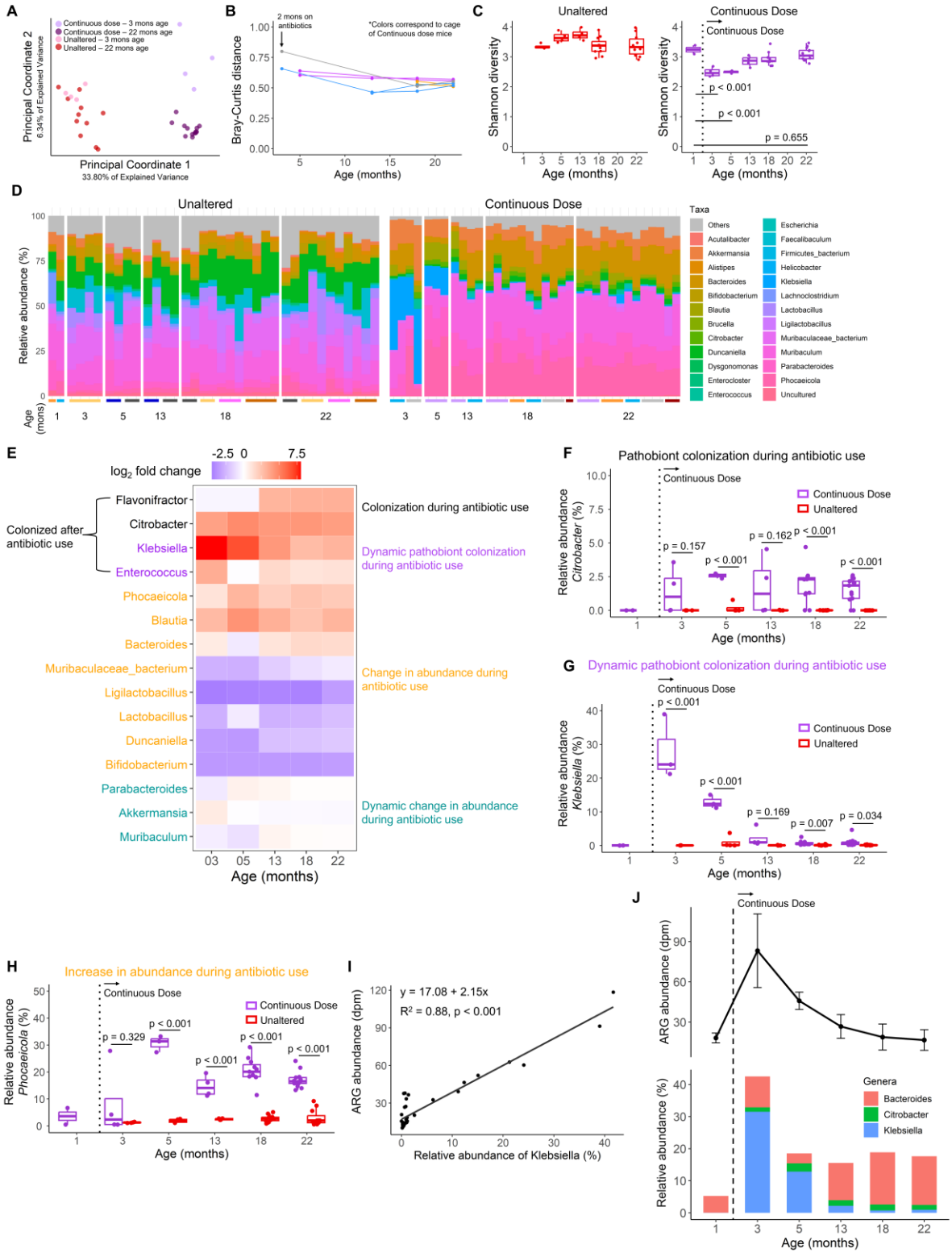

Fig. 2. Taxonomic changes explain declines in ARG abundance during prolonged oral antibiotics. (**A**) Continuous oral antibiotics resulted in a rapid change in gut microbial composition compared to Unaltered mice. (B) During continuous dosing, the microbial

composition shifted slightly toward the Unaltered state seen in the Bray-Curtis distance from baseline. (C) Shannon diversity initially decreased in Continuous Dose mice but recovered afterwards. (D) Genus-level analysis revealed complex dynamics of taxa during antibiotic dosing. (E) Log-fold change of most abundant genera during antibiotic dosing relative to one month of age before antibiotics. Representative pathobionts that (F) colonized, (G) dynamically colonized; or (H) increased in abundance during antibiotic use. (I) The relative abundance of *Klebsiella* is strongly correlated with ARG abundance in Unaltered and Continuous Dose mice (Pearson correlation: 0.88). (J) Shifts in the relative abundance of ARG harboring taxa (*Bacteroides*, *Citrobacter*, *Klebsiella*) directly align with shifts in ARG abundance. Whiskers in the line plot represent the standard deviation of data. Whiskers of the box plots represent the range of the data and the boxes represent the middle 50% of data. Results from female mice are shown here; corresponding results from male mice are in Figure S5.

Age-related change in the gut microbiota influences ARG dynamics following initiation of oral antibiotics

The response of the gut microbiota to oral antibiotics is influenced by host age (*26*). As the composition of the gut microbiota is more malleable in younger than in older mice (*27, 28*), we hypothesized that oral antibiotics would have less effect on the microbiota and the resistome in older mice. To test this idea, we initiated oral antibiotics in mice who were treatment-naïve until 18 months of age (considered elderly in mice) (Fig. 3A).

The initiation of antibiotic dosing at 18 months of age (Delayed Dose groups) resulted in an increase in ARG abundance that was more heterogeneous than in Continuous Dose mice exposed to the antibiotics for the same period of time (Fig. 3C,D, table S8-9). Prior to antibiotic exposure, most ARGs were associated with tetracycline but after antibiotic exposure ARGs were primarily multidrug resistant and associated with aminoglycoside and beta-lactam (Fig. 3H, table S7). Unlike the Continuous Dose mice, however, the resistome of Delayed Dose mice showed more variability among animals within the same groups, as indicated by Bray-Curtis distance from baseline (Fig. 3J, fig. S9).

The initial shifts in taxonomy after the start of oral antibiotics followed a similar pattern to that seen in the Continuous Dose animals (Fig. 3I, fig. S9). As observed in the Continuous Dose groups, antibiotic dosing initiated a transient increase in the relative abundance of *Klebsiella*: The relative abundance of *Klebsiella* prior to antibiotic dosing was initially less than 1%, increased substantially within the first two months of antibiotic exposure, then declined (Fig. 3B, fig. S9). The decline in *Klebsiella* abundance in Delayed Dose mice followed an exponential decay that was much faster than in Continuous Dose mice exposed to antibiotics for the same duration (decay rate constant between two and four months of dosing 0.537/month in Delayed Dose mice versus 0.184/month in Continuous Dose, $p < 0.001$) (Fig. 3B) suggesting a more resilient microbiome in the aged Delayed Dose mice, consistent with prior reports and clinical findings (*8*, *29*). The taxonomic beta diversity in the Delayed Dose mice after the start of antibiotics was more variable, mirroring the differences in ARG diversity (Fig. 3J-K, fig. S9).

The relative abundance of *Klebsiella* was strongly correlated with ARG burden in the Delayed Dose mice but there were several outliers that showed larger than expected ARG burden (Fig. 3F). The outliers were a subset of animals with increased abundance of the ARG carrier *E. coli* and ARGs associated with *E. coli* (Fig. 3G, fig. S10). The presence of ARGs harbored by *E. coli* contributed to the maintenance of a higher total ARG burden in Delayed Dose mice, even

when *Klebsiella* abundance declined (fig. S11). These findings further show that taxonomic differences drive variations in ARG abundance, even in aged hosts.

A secondary cause for variability in ARG abundance in Delayed Dose mice was the accumulation of ARGs in the microbiota in the months prior to the start of antibiotic dosing. At one month of age, more than 95% of ARG abundance was associated with tetracycline. By 18 months of age, the abundance of ARGs associated with tetracycline declined; *tet(Q)*, accounted for more than 70% of ARG abundance at one month of age but only 47% of ARG abundance at 18 months (fig. S12). Several "new" ARGs not detected at one month of age, but present at 18 months of age confer resistance to aminoglycoside, beta-lactam, glycopeptide, MLS, mupirocin-like, peptide, and multidrug resistance (Fig. 3H, fig. S10). These "new" ARGs were likely associated with changes in taxonomy (fig. S13). This observation is consistent with recent cross-sectional studies in aging humans that show increases in ARG abundance in older individuals (*30*). Although increased abundance of ARGs in older humans is often attributed to the accumulated effects of doses of antibiotics throughout life (*22*), our findings in mice suggest such shifts can occur in the absence of antibiotic exposure. Collectively, our findings show that subtle changes in the gut microbiota during aging can change the response to oral antibiotics in terms of taxonomic composition and associated ARGs.

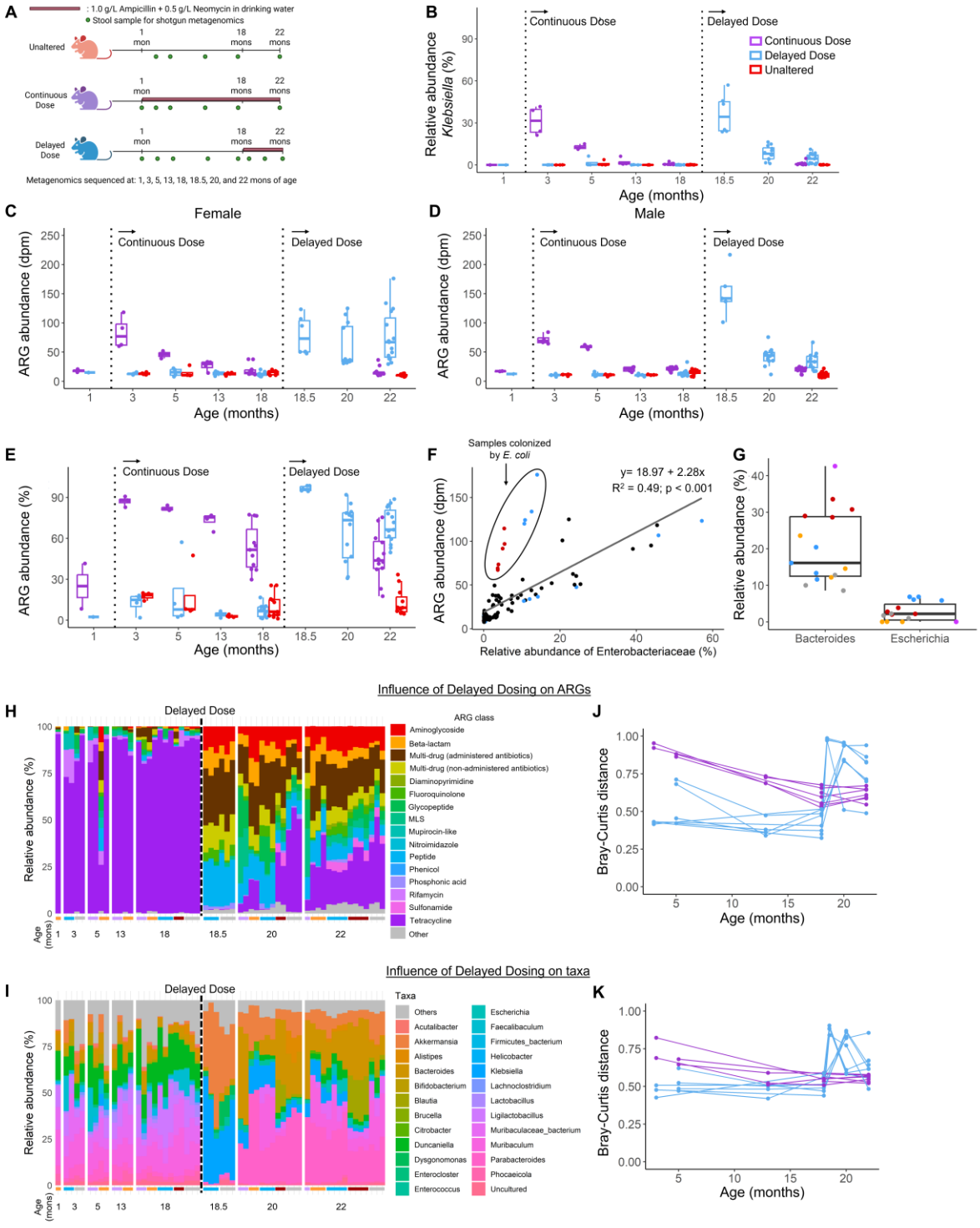

Fig. 3. Age-related change in the gut microbiota influences ARG dynamics following initiation of oral antibiotics. (**A**) Study design. (B) Mice initiating antibiotic dosing at 18 months of age (Delayed Dose group) had a transient increase in *Klebsiella* and a more rapid decline in *Klebsiella* relative to younger mice in the Continuous Dose group that were exposed to the antibiotics for the same period. (C) In contrast to Continuous Dose mice, female Delayed

Dose mice did not exhibit a decreased ARG abundance with prolonged antibiotic exposure. (D-E) Changes in ARG abundance in Delayed Dose mice. (F) The relative abundance of *Enterobacteriaceae* was strongly correlated with the abundance of ARGs with the exception of animals colonized with *E. coli*. (G) The relative abundance of *Bacteroides* and *Escherichia* in Delayed Dose mice (indicated by color). (H-I) The variability in the resistome and microbiota composition. (J-K) Variability in the Bray-Curtis distance from baseline (pre-antibiotic) in the Delayed Dose mice at 22 months of age was greater than that in Continuous Dose. Whiskers of the box plots represent the range of the data and the boxes represent the middle 50% of data. Additional results are shown in Figure S9.

Fecal microbiota transplantation mitigates collateral ARGs acquired through lifelong antibiotic exposure

The accumulation of ARGs in response to antibiotic exposure has the potential to provide a reservoir of antibiotic resistance that can be transmitted through communities or complicate management of bacterial infections (*31*). Fecal microbiota transplantation (FMT) has been proposed as a means of displacing resistant organisms from the microbiome (*9*). We thus evaluated the utility of FMT for reducing ARG burden in mice continuously exposed to antibiotics from one to 18 months of age. At 18 months of age, antibiotic dosing was suspended, and mice received FMT from age- and sex-matched donors with an Unaltered microbiome (Initial Dose group, Fig. 4A). Within two weeks after the FMT, the taxonomic composition of the gut microbiota became indistinguishable from that of similarly aged treatment-naïve animals (Fig. 4B, fig. S14-15). Similarly, the composition, abundance, and richness of ARGs matched that of age- and sex-matched Unaltered animals (Fig. 4C-E, fig. S14). After the FMT, species that had colonized as a result of antibiotic dosing were no longer detectable after FMT (Fig. 4G, fig. S14). Therefore, the introduction of treatment-naïve microbiota not only replenished the microbial taxa to an Unaltered state but also removed ARGs that were enriched during prolonged antibiotic dosing.

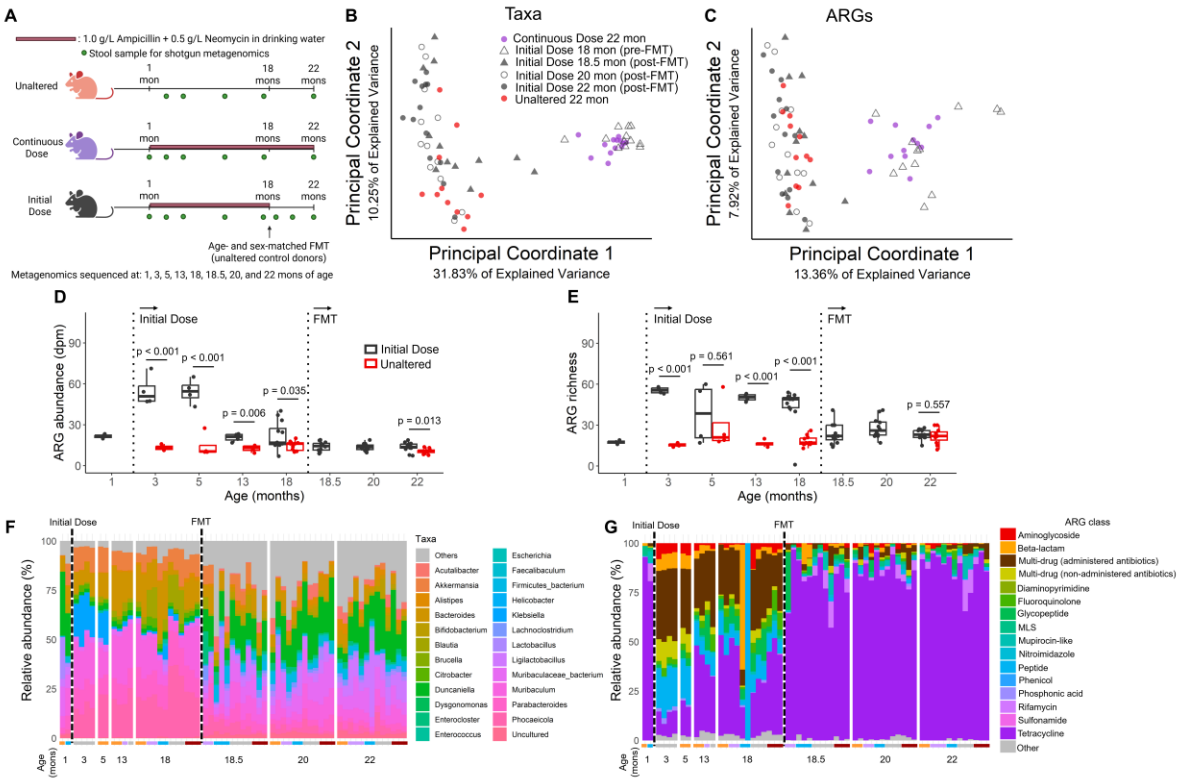

Fig. 4. Fecal microbiota transplantation mitigates collateral ARGs acquired through lifelong antibiotic exposure. (**A**) Study design. (B-C) Receiving the FMT from the Unaltered donor at 18 months of age restored the microbiota and resistome composition to its Unaltered state. (D-E) The total abundance and richness of ARGs decreased, returning to the level of Unaltered mice after receiving the FMT. (F-G) Composition of the microbiota and resistome prior to and after receiving the FMT. Whiskers of the box plots represent the range of the data and the boxes represent the middle 50% of data.

Discussion

Extended exposure to antibiotics has been implicated in promoting antibiotic resistance by selecting for resistant organisms and thus increasing the abundance of ARG in the microbiome. Antibiotic stewardship strategies that limit excessive or inappropriate antibiotic use reduce the incidence of antibiotic resistant infections (*32*). Certain types of infections, however, require prolonged antibiotic treatment for months or years (*15-18*), raising the risk that commensals and/or pathogens in the gut microbiota will develop antibiotic resistance. Our findings demonstrate that the ARG burden increases most strikingly following initiation of antibiotic treatment, and then recedes after months of exposure, but never fully normalizes. This likely represents an initial fitness advantage of taxa harboring relevant ARGs that ultimately get outcompeted by community members with intrinsic resistance or other growth advantages in the presence of antibiotics. Our findings illustrate how members of the community that are not susceptible to an antibiotic can provide expansion resistance limiting the abundance of ARGs and emergence of resistant pathogens.

Studies of antibiotic resistance in the gut microbiota report increases in ARG abundance and richness during and immediately after short-term (fewer than 10 days) antibiotic dosing (*22*,

33-35) and/or cross-sectional studies in humans (*36-38*). These studies have shown that short-term antibiotic exposures can have a lasting effect on the gut microbiota and resistome, although some components of the microbiota and resistome eventually return to pre-treatment states (*8*, *22*, *39-42*). Consistent with prior reports (*10*, *43*), we observed increases in ARG abundance and reductions in taxonomic diversity soon after antibiotic dosing. However, unlike prior reports that have been cross-sectional, our study is unique in performing a longitudinal analysis for most of the natural lifespan of the mice. We were therefore able to observe dynamic changes in the gut microbiota and ARG abundance over almost two years of dosing. Our findings show that the early increases in ARG abundance can eventually fade.

A common concern related to excessive antibiotic dosing is the possibility that horizontal gene transfer could confer resistance to antibiotics among organisms in the gut microbiota (*3*, *44*, *45*). Although we did not directly examine horizontal gene transfer, our finding that fluctuations in taxonomic abundance explain over 85% of ARG abundance suggests that the majority of the ARGs in our study were taxonomically stable, making it unlikely that horizontal gene transfer had a significant effect on the overall ARG profile.

Our findings that FMT eliminates the detection of ARGs and taxa acquired after prolonged antibiotic use aligns with clinical findings that FMT reduces the abundance of ARGs (*9*, *46*, *47*). Collectively, our findings support the idea that FMTs can reduce the abundance of ARGs even after prolonged antibiotic exposure. However, our findings highlight the importance of the microbiota before perturbation.

There are some important limitations to our study. First, identification, classification and association with host taxa of ARGs was limited to the databases used. Although the CZ-ID pipeline uses the most updated National Center for Biotechnology Information (NCBI) and Comprehensive Antibiotic Resistance Database (CARD) databases (*48*), it only includes ARGs that have been previously sequenced and classified and is therefore biased to the most commonly studied organisms (e.g., the *Enterobacteriaceae* family). It is unclear how much of our findings are specific to the murine host, diet, the breadth of the antibiotic spectrum, or the specific antibiotics used in this study.

Our findings show that the impact on ARG abundance is greatest in the first weeks after antibiotic exposure. As a result, risks of transmission of antibiotic-resistant taxa and/or antibiotic-resistant infections from the gut microbiota may be greatest in the first few weeks to months of exposure, while steadily declining if antibiotic dosing continues for longer periods. In situations requiring prolonged antibiotics, the risk presented by increased ARG abundance in the gut microbiota may decline after the first few months of dosing. Our findings demonstrate that the presence of commensal microbes that are not sensitive to the dosed antibiotic provides a limit to the accumulation of antibiotic resistance within the community, an effect we term expansion resistance. Taken together, our results demonstrate that a more diverse gut microbiome not only helps to promote colonization resistance but can also moderate the abundance of antibiotic-resistant microbes.

References and Notes

1. Antimicrobial Resistance Collaborators, Global burden of bacterial antimicrobial resistance in 2019: a systematic analysis. *Lancet* **399**, 629-655 (2022). doi: 10.1016/S0140-6736(21)02724-0.
2. V.T. Chu, A. Glascock, D. Donnell, C. Grabow, C.E. Brown, R. Ward, C. Love, K.L. Kalantar, S.E. Cohen, C. Cannon, M.H. Woodworth, C.F. Kelley, C. Celum, A.F Leutkemeyer, C.R. Langelier, Impact of doxycycline post-exposure prophylaxis for sexually transmitted infections on the gut microbiome and antimicrobial resistome. *Nat. Med.* **31**, 2017-217 (2025). doi: 10.1038/s41591-024-03274-2.
3. R.S. McInnes, G.E. McCallum, L.E. Lamberte, W. van Schaik, Horizontal transfer of antibiotic resistance genes in the human gut microbiome. *Curr. Opin. Microbiol.* **53**, 35-43 (2020). doi: 10.1016/j.mib.2020.02.002.
4. D.G.J. Larsson, C.F. Flach, Antibiotic resistance in the environment. *Nat. Rev. Microbiol.* **20**, 257-269 (2022). doi: 10.1038/s41579-021-00649-x.
5. I.L. Brito, S. Yilmaz, K. Huang, L. Xu, S.D. Jupiter, A.P. Jenkins, W. Naisilisili, M. Tamminen, C.S. Smillie, J.R. Wortman, B.W. Birren, R.J. Xavier, P.C. Blainey, A.K Singh, D. Gevers, E.J. Alm, Mobile genes in the human microbiome are structured from global to individual scales. *Nature* **535**, 435-439 (2016). doi: 10.1038/nature18927.
6. P.J. Diebold, M.W. Rhee, Q. Shi, N.V. Trung, F. Umrani, S. Ahmed, V. Kulkarni, P. Deshpande, M. Alexander, N.T. Hoa, N.A. Christakis, N.T. Iqbal, S.A. Ali, J.S. Mathad, I.L. Brito, Clinically relevant antibiotic resistance genes are linked to a limited set of taxa within gut microbiome worldwide. *Nat. Comm.* **14**, 7366 (2023). doi: 10.1038/s41467-023-42998-6.
7. E.C. Pehrsson, P. Tsukayama, S. Patel, M. Mejía-Bautista, G. Sosa-Soto, K.M. Navarrete, M. Calderon, L. Cabrera, W. Hoyos-Arango, M.T. Bertoli, D.E. Berg, R.H. Gilman, G. Dantas, Interconnected microbiomes and resistomes in low-income human habitats. *Nature* **533**, 212-216 (2016). doi: 10.1038/nature17672.
8. A. Palleja, K.H. Mikkelsen, S.K Forslund, A. Kashani, K.H. Allin, T. Nielsen, T.H. Hansen, S. Liang, Q. Feng, C. Zhang, P.T. Pyl, L.P. Coelho, H. Yang, J. Wang, A. Typas, M.F. Nielsen, H.B. Nielsen, P. Bork, J. Wang, T. Vilsbøll, T. Hansen, F.K. Knop, M. Arumugam, O. Pedersen, Recovery of gut microbiota of healthy adults following antibiotic exposure. *Nat. Microbiol.* **3**, 1255-1265 (2018). doi: 10.1038/s41564-018-0257-9.
9. A. Rashidi, M. Ebadi, T.U. Rehman, H. Elhusseini, D. Kazadi, H. Halaweish, M.H. Khan, A. Hoeschen, Q. Cao, X. Luo, A.J. Kabage, S. Lopez, S.G. Holtan, D.J. Weisdorf, C. Liu, S. Ishii, A. Khoruts, C. Staley, Long- and short-term effects of fecal microbiota transplantation on antibiotic resistance genes: results from a randomized placebo-controlled trial. *Gut Microbes* **16**, 2327442 (2024). doi: 10.1080/19490976.2024.2327442.
10. K. Lee, S. Raguideau, K. Sirén, F Asnicar, F. Cumbo, F. Hildebrand, N. Segata, C.J. Cha, C. Quince, Population-level impacts of antibiotic usage on the human gut microbiome. *Nat. Comm.* **14**, 1191 (2023). doi: 10.1038/s41467-023-36633-7.
11. A.M. Turner, L. Li, I.R. Monk, J.Y.H. Lee, D.J. Ingle, S. Portelli, N.L. Sherry, N. Isles, T. Seemann, L.K. Sharkey, C.J. Walsh, G.E Reid, S. Nie, B.A. Eijkelkamp, N.E. Holmes, B.

Collis, S. Vogrin, A. Hiergeist, D. Weber, A. Gessner, E. Holler, D.B. Ascher, S. Duchene, N.E. Scott, T.P. Stinear, J.C. Kwong, C.L. Gorrie, B.P. Howden, G.P. Carter, Rifaximin prophylaxis causes resistance to the last-resort antibiotic daptomycin. *Nature* **635**, 969-977 (2024). doi: 10.1038/s41586-024-08095-4.

12. K.S. Xue, S.J. Walton, D.A. Goldman, M.L. Morrison, A.J. Verster, A.B. Parrott, F.B. Yu, N.F. Neff, N.A. Rosenberg, B.D. Ross, D.A. Petrov, K.C. Huang, B.H. Good, D.A. Relman, Prolonged delays in human microbiota transmission after a controlled antibiotic perturbation. *bioRxiv* 2023.09.26.559480 (2023). doi: 10.1101/2023.09.26.559480.

13. J. Suez, N. Zmora, G. Zilberman-Schapira, U. Mor, M. Dori-Bachash, S. Bashiardes, M. Zur, D. Regev-Lehavi, R.B.Z. Brik, S. Federici, M. Horn, Y. Cohen, A.E. Moor, D. Zeevi, T. Korem, E. Kotler, A. Harmelin, S. Itzkovitz, N. Maharshak, O. Shibolet, M. Pevsner-Fischer, H. Shapiro, I. Sharon, Z. Halpern, E. Segal, E. Elinav, Post-antibiotic gut mucosal microbiome reconstitution is impaired by probiotics and improved by autologous FMT. *Cell* **174**, 1406-1423 (2018). doi: 10.1016/j.cell.2018.08.047.

14. A.J. Gasparrini, B. Wang, X. Sun, E.A. Kennedy, A. Hernandez-Leyva, I.M. Ndao, P.I. Tarr, B.B. Warner, G. Dantas, Metagenomic signatures of early life hospitalization and antibiotic treatment in the infant gut microbiota and resistome persist long after discharge. *Nat. Microbiol.* **4**, 2285-2297 (2019). doi: 10.1038/s41564-019-0550-2.

15. J.S.Y. Lau, T.M. Korman, I. Woolley, Life-long antimicrobial therapy: where is the evidence? *J. Antimicrob. Chemother.* **73**, 2601-2612 (2018). doi: 10.1093/jac.dky174.

16. T.R. Weiner, D.B. El-Najjar, C.L. Herndon, C.C. Wyles, H.J. Cooper, How are oral antibiotics being used in total joint arthroplasty? A review of the literature. *Orthop. Rev.* **16**, 92287 (2024). doi: 10.52965/001c.92287.

17. K.S. O'Brien, A.M. Arzika, A. Amza, R. Maliki, B. Aichatou, I.M. Bello, D. Beidi, N. Galo, N. Harouna, A.M. Karamba, S. Mahamadou, M. Abarchi, A. Ibrahim, E. Lebas, B. Peterson, Z. Liu, V. Le, E. Colby, T. Doan, J.D. Keenan, C.E. Oldenburg, T.C. Porco, B.F. Arnold, T.M. Lietman, AVENIR study group, Azithromycin to reduce mortality – an adaptive cluster-randomized trial. *N. Engl. J. Med.* **391**, 699-709 (2024). doi: 10.1056/NEJMoa2312093.

18. S.K. Bhattarai, M. Du, A.L. Zeamer, B.M. Morzfeld, T.D. Kellogg, K. Firat, A. Benjamin, J.M. Bean, M. Zimmerman, G. Mardi, S.C. Vilbrun, K.F. Walsh, D.W. Fitzgerald, M.S. Glickman, V. Bucci, Commensal antimicrobial resistance mediates microbiome resilience to antibiotic disruption. *Sci. Transl. Med.* **16**, eadi9711 (2024). doi: 10.1126/scitranslmed.adi9711.

19. M. Bakhit, T. Hoffmann, A.M. Scott, E. Beller, J. Rathbone, C. Del Mar, Resistance decay in individuals after antibiotic exposure in primary care: a systematic review and meta-analysis. *BMC Medicine* **16**, 126 (2018). doi: 10.1186/s12916-018-1109-4.

20. C. Roubaud-Baudron, V.E. Ruiz, A.M. Swan, B.A. Vallance, C. Ozkul, Z. Pei, J. Li, T.W. Battaglia, G.I. Perez-Perez, M.J. Blaser, Long-term effects of early-life antibiotic exposure on resistance to subsequent bacterial infection. *mBio* **10**, e02820-19 (2019). doi: 10.1128/mBio.02820-19.

21. C. Liu, E.L. Cyphert, S.J. Stephen, B. Wang, A.L. Morales, J.C. Nixon, N.R. Natsoulas, M. Garcia, P. Blazquez Carmona, A.C. Vill, E. Donnelly, I.L. Brito, D. Vashishth, C.J.

Hernandez, Microbiome-induced increases and decreases in bone matrix strength can be initiated after skeletal maturity. *J. Bone Miner. Res.* **39**, 1621-1632 (2024). doi: 10.1093/jbmr/zjae157.

22. W.E. Anthony, B. Wang, K.V. Sukhum, A.W. D'Souza, T. Hink, C. Cass, S. Seiler, K.A. Reske, C. Coon, E.R. Dubberke, C.A.D. Burnham, G. Dantas, J.H. Kwon, Acute and persistent effects of commonly used antibiotics on the gut microbiome and resistome in healthy adults. *Cell Rep.* **39**, 110649 (2022). doi: 10.1016/j.celrep.2022.110649.

23. J de la Cuesta-Zuluaga, S.T. Kelley, Y. Chen, J.S. Escobar, N.T. Mueller, R.E. Ley, D. McDonald, S. Huang, A.D. Swafford, R. Knight, V.G. Thackray, Age- and sex-dependent patterns of gut microbial diversity in human adults. *mSystems* **4**, e00261-19 (2019). doi: 10.1128/mSystems.00261-19.

24. L.E. Bryan, S.K. Kowand, H.M. Van Den Elzen, Mechanism of aminoglycoside antibiotic resistance in anaerobic bacteria: Clostridium perfringens and Bacteroides fragilis. *Antimicrob. Agents Chemother.* **15**, 7-13 (1979). doi: 10.1128/aac.15.1.7.

25. R. Edwards, Resistance to beta-lactam antibiotics in Bacteroides spp. *J. Med. Microbiol.* **46**, 979-986 (1997). doi: 10.1099/00222615-46-12-979.

26. D.J. Schwartz, A.E. Langdon, G. Dantas, Understanding the impact of antibiotic perturbation on the human microbiome. *Genome Med.* **12**, 82 (2020). doi: 10.1186/s13073-020-00782-x.

27. M. Derrien, A.S. Alvarez, W.M. de Vos, The gut microbiota in the first decade of life. *Trends Microbiol.* **27**, 997-1010 (2019). doi: 10.1016/j.tim.2019.08.001.

28. A. Parker, S. Romano, R. Ansorge, A. Aboelnour, G. Le Gall, G.M. Savva, M.G. Pontifex, A. Telatin, D. Baker, E. Jones, D. Vauzour, S. Rudder, L.A. Blackshaw, G. Jeffery, S.R. Carding, Fecal microbiota transfer between young and aged mice reverses hallmarks of the aging gut, eye, and brain. *Microbiome* **10**, 68 (2022). doi: 10.1186/s40168-022-01243-w.

29. D.V. Patangia, G. Grimaud, C.A. O'Shea, C.A. Ryan, E. Dempsey, C. Stanton, R.P. Ross, Early life exposure of infants to benzylpenicillin and gentamicin is associated with a persistent amplification of the gut resistome. *Microbiome* **12**, 19 (2024). doi: 10.1186/s40168-023-01732-6.

30. T. Tavella, S. Turroni, P. Brigidi, M. Candela, S. Rampelli, The human gut resistome up to extreme longevity. *mSphere* **6**, e00691-21 (2021). doi: 10.1128/msphere.00691-21.

31. H. Todman, S. Arya, M. Baker, D.J. Stekel, A model of antibiotic resistance genes accumulation through lifetime exposure from food intake and antibiotic treatment. *PLoS One* **18**, e0289941 (2023). doi: 10.1371/journal.pone.0289941.

32. D. Baur, B.P. Gladstone, F. Burkert, E. Carrara, F. Foschi, S. Döbele, E. Tacconelli, Effect of antibiotic stewardship on the incidence of infection and colonization with antibiotic-resistant bacteria and Clostridium difficile infection: a systematic review and meta-analysis. *Lancet Infect. Dis.* **17**, 990-1001 (2017). doi: 10.1016/S1473-3099(17)30325-0.

33. C. Munck, R.U. Sheth, E. Cuaresma, J. Weidler, S.L. Stump, P. Zachariah, D.H. Chong, A.C. Uhlemann, J.A. Abrams, H.H. Wang, D.E. Freedberg, The effect of short-course antibiotics on the resistance profile of colonizing gut bacteria in the ICU: a prospective cohort study. *Crit. Care* **24**, 404 (2020). doi: 10.1186/s13054-020-03061-8.

34. Y. Hong, H. Li, L. Chen, H. Su, B. Zhang, Y. Luo, C. Li, Z. Zhao, Y. Shao, L. Guo, Short-term exposure to antibiotics begets long-term disturbance in gut microbial metabolism and molecular ecological networks. *Microbiome* **12**, 80 (2024). doi: 10.1186/s40168-024-01795-z.

35. C.W. MacPherson, O. Mathieu, J. Tremblay, J. Champagne, A. Nantel, S.A. Girard, T.A. Tompkins, Gut bacterial microbiota and its resistome rapidly recover to basal state levels after short-term amoxicillin-clavulanic acid treatment in healthy adults. *Sci. Rep.* **8**, 11192 (2018). doi: 10.1038/s41598-018-29229-5.

36. B.G. Bell, F. Schellevis, E. Stobberingh, H. Goossens, M. Pringle, A systematic review and meta-analysis of the effects of antibiotic consumption on antibiotic resistance. *BMC Infect. Dis.* **14**, 13 (2014). doi: 10.1186/1471-2334-14-13.

37. K. Kandelaki, C.S. Lundborg, G. Marrone, Antibiotic use and resistance: a cross-sectional study exploring knowledge and attitudes among school and institution personnel in Tbilisi, Republic of Georgia. *BMC Res. Notes* **8**, 495 (2015). doi: 10.1186/s13104-015-1477-1.

38. S.W. Olesen, M.L. Barnett, D.R. MacFadden, J.S. Brownstein, S. Hernández-Díaz, M. Lipsitch, Y.H. Grad, The distribution of antibiotic use and its association with antibiotic resistance. *eLife* **7**, e39435 (2018). doi: 10.7554/eLife.39435.

39. A. Dhariwal, L.C.H. Braten, K. Sturød, G. Salvadori, A. Bargheet, H. Amdal, R. Junges, D. Berild, J.A. Zwart, K. Storheim, F.C. Petersen, Differential response to prolonged amoxicillin treatment: long-term resilience of the microbiome versus long-lasting perturbations in the gut resistome. *Gut Microbes* **15**, 2157200 (2023). doi: 10.1080/19490976.2022.2157200.

40. K. Kang, L. Imamovic, M.A. Misiakou, M.B. Sørensen, Y. Heshiki, Y. Ni, T. Zheng, J. Li, M.M.H. Ellabaan, M. Colomer-Lluch, A.A. Rode, P. Bytzer, G. Panagiotou, M.O.A. Sommer, Expansion and persistence of antibiotic-specific resistance genes following antibiotic treatment. *Gut Microbes* **13**, 1-19 (2021). doi: 10.1080/19490976.2021.1900995.

41. C. d'Humieres, M. Delavy, L. Alla, F. Ichou, E. Gauliard, A. Ghozlane, F. Levenez, N. Galleron, B. Quinquis, N. Pons, J. Mullaert, A. Bridier-Nahmias, B. Condamine, M. Touchon, D. Rainteau, A. Lamaziere, P. Lesnik, M. Ponnaiah, M. Lhomme, N. Sertour, S. Devente, J.D. Docquier, M.E. Bougnoux, O. Tenaillon, M. Magnan, E. Ruppé, N. Grall, X. Duval, D. Ehrlich, F. Mentré, E. Denamur, E.P.C. Rocha, E. Le Chatelier, C. Burdet for the PrediRes study group, Perturbation and resilience of the gut microbiome up to 3 months after β-lactams exposure in healthy volunteers suggest an important role of microbial β-lactamases. *Microbiome* **12**, 50 (2024). doi: 10.1186/s40168-023-01746-0.

42. L. Liu, M.E. Kirst, L. Zhao, E. Li, G.P. Wang, Microbiome resilience despite a profound loss of minority microbiota following clindamycin challenge in humanized gnotobiotic mice. *Microbiol. Spectr.* **10**, e0196021 (2022). doi: 10.1128/spectrum.01960-21.

43. Y. Hu, X. Yang, N. Lu, B. Zhu, The abundance of antibiotic resistance genes in human guts has correlation to the consumption of antibiotics in animal. *Gut Microbes* **5**, 245-249 (2014). doi: 10.4161/gmic.27916.

44. J.R. Huddleston, Horizontal gene transfer in the human gastrointestinal tract: potential spread of antibiotic resistance genes. *Infect. Drug Resist.* **7**, 167-176 (2014). doi: 10.2147/IDR.S48820.

45. K. Forslund, S. Sunagawa, J.R. Kultima, D.R. Mende, M. Arumugam, A. Typas, P. Bork, Country-specific antibiotic use practices impact the human gut resistome. *Genome Res.* **23**, 1163-1169 (2013). doi: 10.1101/gr.155465.113.

46. M.H. Woodworth, R.E. Conrad, M. Haldopoulos, S.M. Pouch, A. Babiker, A.K. Mehta, K.L. Sitchenko, C.H. Wang, A. Strudwick, J.M. Ingersoll, C. Philippe, S. Lohsen, K. Kocaman, B.G. Lindner, J.K. Hatt, R.M. Jones, C. Miller, A.S. Neish, R. Friedman-Moraco, G. Karadkhele, K.H. Liu, D.P Jones, C.C. Mehta, T.R. Ziegler, D.S. Weiss, C.P. Larsen, K.T. Konstantinidis, C.S. Kraft, Fecal microbiota transplantation promotes reduction of antimicrobial resistance by strain replacement. *Sci. Transl. Med.* **15**, eabo2750 (2023). doi: 10.1126/scitranslmed.abo2750.

47. J. Hyun, S.K. Lee, J.H. Cheon, D.E. Yong, H. Koh, Y.K. Kang, M.H. Kim, Y. Sohn, Y. Cho, Y.J. Baek, J.H. Kim, J.Y. Ahn, S.J. Jeong, J.S. Yeom, J.Y. Choi, Faecal microbiota transplantation reduces amounts of antibiotic resistance genes in patients with multidrug-resistant organisms. *Antimicrob. Resist. Infect. Control* **11**, 20 (2022). doi: 10.1186/s13756-022-01064-4.

48. K.L. Kalantar, T. Carvalho, C.F.A. de Bourcy, B. Dimitrov, G. Dingle, R. Egger, J. Han, O.B. Holmes, Y.F. Juan, R. King, A. Kislyuk, M.F. Lin, M. Mariano, T. Morse, L.V. Reynoso, D.R. Cruz, J. Sheu, J. Tang, J. Wang, M.A. Zhang, E. Zhong, V. Ahyong, S. Lay, S. Chea, J.A. Bohl, J.E. Manning, C.M. Tato, J.L. DeRisi, IDseq-an open source cloud-based pipeline and analysis service for metagenomic pathogen detection and monitoring. *Gigascience* **9**, giaa111 (2020). doi: 10.1093/gigascience/giaa111.

49. B.W. Ma, N.A. Bokulich, P.A. Castillo, A. Kananurak, M.A. Underwood, D.A. Mills, C.L. Bevins, Routine habitat change: a source of unrecognized transient alteration of intestinal microbiota in laboratory mice. *PLoS ONE* **7**, e47416 (2012). doi: 10.1371/journal.pone.0047416.

50. K.E. Fujimura, A.R. Sitarik, S. Havstad, D.L. Lin, S. Levan, D. Fadrosh, A.R. Panzer, B. LaMere, E. Rackaityte, N.W. Lukacs, G. Wegienka, H.A. Boushey, D.R. Ownby, E.M. Zoratti, A.M. Levin, C.C. Johnson, S.V. Lynch, Neonatal gut microbiota associates with childhood multisensitized atopy and T cell differentiation. *Nat. Med.* **22**, 1187-1191 (2016). doi: 10.1038/nm.4176.

Funding:

National Institutes of Health grant R01AG067996 (CJH)

National Institutes of Health grant F32AG076244 (ELC)

National Institutes of Health grant 1R01AI181282-01A1 (AS)

USDA Agricultural Research Service Cooperative Agreement No. 58-8050-3-003 (ML, MKS, XF, SLB)

Author contributions: Each author's contribution(s) to the paper should be listed [we encourage you to follow the CRediT model]. Each CRediT role should have its own line, and there should not be any punctuation in the initials.

Examples:

Conceptualization: ELC, CL, VTC, CRL

Methodology: ELC, CL, VTC, AD, ML, ZZ, JRC, RA, HM, NN, JL, MKS, XF, SLB, CAL, AS, CRL

Investigation: ELC, CL, AD, ML, ZZ, JRC, ECGD, ALM, JCN, MG, SZ, JW, JL, MKS, XF, SLB, CAL, AS, CRL

Visualization: ELC, VTC, ML, ZZ, SR, CRL

Funding acquisition: CJH

Project administration: CJH

Supervision: CJH

Writing – original draft: ELC, VTC, CRL, CJH

Writing – review & editing: ELC, CL, VTC, AD, ML, ZZ, JRC, ECGD, ALM, JCN, MG, SZ, SR, JW, RA, HM, NN, JL, MKS, XF, SLB, CAL, AS, CRL, CJH

Competing interests: Authors declare that they have no competing interests. Any opinions, findings, conclusions, or recommendations expressed in this publication are those of the authors and do not necessarily reflect the views of the USDA.

Data and materials availability: Raw shotgun metagenomics fastq.gz files can be accessed on Dryad database.

Supplementary Materials

Materials and Methods

Figs. S1 to S15

Tables S1 to S10

SUPPLEMENTARY

Materials and Methods

Mouse strains

All animal procedures received prior approval from the local Institutional Animal Care and Use Committee. Male and female C57Bl/6J mice were purchased from Jackson Laboratory (Bar Harbor, ME, USA) and bred using trio breeding Pups were weaned at three weeks of age and housed by sex (n = 4/cage). Second-generation pups from breeders were used in the study. Sterile cages contained ¼-inch corn cob bedding (The Andersons' Lab Beddin, Maumee, OH, USA), standard laboratory chow (Teklad LM-485 Mouse/Rat Sterilizable Diet Irradiated, Envigo Diets, Madison, WI, USA), reverse osmosis sterilized water *ad libitum*, and cardboard hut (Ketchum Manufacturing, Brockville, Canada).

Study design

Male and female pups were divided into four treatment groups (n > 15/sex/group) over two breeding rounds (same dams, two months apart). Treatment groups included: 1) Unaltered control from birth-22 months of age, 2) Continuous alteration from 1-22 months of age, 3) Initial alteration from 1-18 months of age that received an age- and sex-matched Unaltered donor fecal microbiota transplant at 18 months of age, and 4) Delayed alteration from 18-22 months of age only. Antibiotic dosing (microbiome alteration) consisted of reverse osmosis sterilized water or reverse osmosis sterilized water containing 0.5 g/L neomycin (N6386, Millipore Sigma, Burlington, MA, USA) and 1 g/L ampicillin (A0166, Millipore Sigma, Burlington, MA, USA) in light-sensitive water bottles. Fresh antibiotic water was replaced every three days over the duration of the study. Antibiotics were selected due to their poor oral bioavailability and limited spectrum of activity, capable of acting directly on gut microbes. Weekly bedding mixing was performed between cages of the same sex and treatment groups from 1-3 months of age. Specifically, a sample of dirty bedding was collected from each cage within a treatment group, pooled together and redistributed back to the cages to normalize gut microbiota composition across cages of the same treatment and sex (*49*).

FMT to antibiotic-treated mice

Male and female C57Bl/6J mice (n = ~15/sex) that had been treated with ampicillin and neomycin in their drinking water from 1-18 months of age received a fecal microbiota transplant (FMT) at 18 months of age to repopulate microbes. Mice were fasted for three hours prior to receiving the transplant with *ad libitum* access to water. Fresh stool samples were collected from age- and sex-matched unaltered control mice with two pellets being placed in sterile 1.5 mL microcentrifuge tubes. Fecal samples were immediately transferred to an anaerobic chamber (Coy Laboratory Products, Grass Lake, MI, USA) and suspended in 1 mL anoxic PBS with 0.05% L-cysteine. Pellets were allowed to soften for 15 minutes and were vortexed for three minutes until the pellets were fully broken apart and homogeneous. Suspended bacteria were separated from fibrous material by centrifuging for five minutes (150 rpm). Supernatant was aliquoted into a sterile bottle and fecal slurries were pooled from multiple animals to create two separate solutions: male and female. The prepared bacterial solutions were placed in an anaerobic jar (BD BBL™ GasPak™ jar, Franklin Lakes, NJ, USA) and transported to the conventional vivarium. Each mouse received 150 µL donor material from the corresponding age- and sex-matched donor pooled sample. The remaining solution was frozen at -80ºC. Mice

received a single transplant and afterwards were placed in cages with dirty bedding from sex-matched Unaltered control donor mice.

DNA extraction of the fecal metagenome

Shotgun metagenomic sequencing was employed to determine the composition of the microbiota from fecal samples collected at 1, 3, 5, 13, 18, 18.5, 20, and 22 months of age. DNA extraction was conducted at the Benioff Center for Microbiome Medicine Microbial Genomics CoLab Plug-in at the University of California, San Francisco. Frozen fecal pellets were placed in 500 µL of cetyltrimethylammonium bromide (CTAB) extraction buffer (Lysing Matrix E tube, MP Biomedicals, Burlingame, CA, USA), vortexed and incubated (65ºC, 15 min) (*50*). A mixture of 500 µL phenol, chloroform, and isoamyl alcohol (in a ratio of 25:24:1) was placed in the tube and the sample was subjected to bead-beating (5.5 m/s; 30 sec) and centrifuged (16,000 g, 5 min, 4ºC). 400 µL of supernatant was placed in a 2 mL Eppendorf tube and 500 µL CTAB buffer was added. This process was repeated until the extraction volume reached 800 µL, after which 800 µL chloroform was added and centrifuged (3,000 g, 10 min). The supernatant (600 µL) was then placed in a 2 mL Eppendorf tube, 2-volume polyethylene glycol was added and the mixture was kept at 4ºC overnight to allow for DNA precipitation. The samples were subsequently centrifuged (3,000 g, 60 mins), washed twice with chilled 70% ethanol, and placed in 100 µL of sterile water. Extracted DNA was quantified with Qubit 2.0 Fluorometer using dsDNA BR Assay Kit (Life Technologies, Grand Island, NY, USA).

Library preparation and quality control of fecal metagenome

Library preparation was performed at the Chan Zuckerberg Biohub San Francisco Genomics Platform. All materials and samples were processed in a post-PCR lab. Six 96-well plates containing extracted cDNA were quadrant pooled into two 384 deep-well plates, cDNA wells were normalized to 2 ng/µL and further diluted 1:10 to achieve a concentration of 0.2 ng/µL using SPT Labtech Firefly Liquid Handler. 0.5 µL of diluted cDNA was transferred to a regular 384 well plate using SPT Firefly and Integra ViaFLO384 liquid handlers, to be used as input for library preparation. Library preparation was completed using a modified Nextera XT DNA Library Kit protocol. This protocol has volumes that were miniaturized for high throughput processing in plate format. In summary, 0.5 µL (~0.1 ng) of cDNA used as the input was tagmented at 55ºC for 5 minutes using Tagment DNA Buffer (0.2 µL) and Amplicon Tagment mix (1.2 µL). The tagmentation reaction was neutralized by adding 0.4 µL of Neutralize Tagment Buffer (NT) followed by 2000 RCF centrifugation for 5 minutes. Index PCR was performed by adding 1.2 µL of Nextera PCR mix (NPM), 0.4 µL of 5 µM i5 and i7 indexing primers while ensuring each library received a unique combination of i5 and i7. Libraries were amplified according to the following cycling parameters: 72ºC for 3 min; 95ºC for 30 sec; 12 cycles (95ºC for 10 sec, 55ºC for 30 sec, 72ºC for 30 sec) and final extension at 72ºC for 5 min. Barcoded libraries were pooled to a 1.5 mL lo-bind Eppendorf tube using SPT Labtech MosquitoLV. Pooled libraries were processed through two 0.7 X SPRI cleanups and were quality controlled for sequencing using Aligent 4150 Tapestation System and D5000 ScreenTape and via qPCR using Bio-Rad CFX96 RT System. All libraries were pooled equimolar for loading on a Novaseq 6000 instrument.

Shotgun metagenomic sequencing of fecal metagenome

Sequencing was performed at the Chan Zuckerberg Biohub San Francisco Genomics Platform. All libraries were sequenced using the loading guidelines provided by Illumina. The Illumina sequencing library was loaded with a NovaSeq 6000 instrument using two S4 kits (2 x 10 billion reads) flow cells using PE150 run parameter.

Quality control, taxonomic profiling metagenomes, and antimicrobial resistance gene identification

The open-source CZ ID pipeline (https://czid.org/) was used for quality control processing, the taxonomic classification of microbes (mNGS pipeline version 8.3), and antimicrobial resistance genes (AMR pipeline version 1.4.2; CARD Database version 3.2.6; Wildcard Database version 4.0.0). Microbial identification in the CZ ID pipeline involved subtractive alignment to mouse host genome (Bowtie2) using raw FASTQ files and fastq quality control (*2*). Microbial reads were aligned to the NCBI NT database (National Center for Biotechnology Information Nucleotide Database) using minimap2 (assembly-based alignment) (*2*). Microbial reads were also aligned to the NCBI NR database (non-redundant protein) (*2*). Prior to quality control processing samples had an average number of 62,212,731± 30,371,926 reads. Samples that had more than 150,000 reads were kept for downstream microbial and antimicrobial resistance genes analyses. After quality control, samples had an average number of 30,557,604 ± 13,488,671 reads (table S9). Following taxonomic alignment, samples were run through CZ ID's antimicrobial resistance pipeline (Comprehensive Antibiotic Resistance Database Resistance Gene Identifier tool) and antimicrobial resistance genes that had ≥ 5% read coverage breadth were kept for resistance analyses (*2*). A table of identified antimicrobial resistance genes and their microbial origin and resistance classification are provided (table S10).

Flow cytometry immune profiling

Spleens were collected at euthanasia in individual tubes on ice with 5 mL complete RMPI medium, which contained 10% fetal bovine serum, 2 mM L-glutamine, 1% penicillin-streptomycin (Corning), 2.5 µg/mL amphotericin B (Gibco), 1 mM sodium pyruvate (Corning), and 10 mM HEPES (Corning). The spleens were processed through a 70 µm cell strainer with isolation buffer comprising PBS supplemented with 2% fetal bovine serum, 1% penicillin-streptomycin, and 1 mM EDTA. The resulting single-cell suspension was centrifuged at 350×g for five minutes at room temperature. The pellet was then resuspended in 1 mL of ACK lysis buffer (Thermo Fisher Scientific) and incubated for three minutes. Additional isolation buffer was added to adjust the total volume to 10 mL, followed by another centrifugation. After washing in isolation buffer, the cells were resuspended in 1 mL of freezing medium consisting of 90% fetal bovine serum and 10% DMSO, and stored in a liquid nitrogen tank until subsequent thawing for analytical procedures.

Frozen splenocytes were thawed and analyzed for T cell, B cell, and myeloid populations using multicolor spectral flow cytometry. All antibodies were used at a 1:200 dilution in FACS buffer (PBS with 2% FBS and 1 mM EDTA). Dead cells were excluded using Zombie UV viability dye. The specific staining panels are detailed below:

T cell			**Myeloid**			**B cell**		
Biomarker	**Fluorophore**	**Clone**	**Biomarker**	**Fluorophore**	**Clone**	**Biomarker**	**Fluorophore**	**Clone**
CD4	FITC	RM4-5	CD4	BUV615	RM4-5	B220	BUV395	RA3-6B2
B220	BUV395	RA3-6B2	B220	BUV395	RA3-6B2	GL7	FITC	GL-7
CD3	APC	17A2	CD3	APC	17A2	FAS	BV421	Jo2
PD1	PE-CY7	J43	CD8	AF700	53-6.7	CD138	BV711	281-2
CD25	PE	PC61.5	CD19	BV711	6D5	CD38	APC	90
CXCR5	PERCP-eFluo710	SPRCL5	F4/80	PE	BM8	CXCR4	PE	2B11
CD8	AF700	53-6.7	CD11b	PE-Cy7	M1/70	CD86	BV605	GL-1
CD62L	BV650	MEL-14	I-A/I-E(MHCII)	FITC	M5/114.15.2	IgM	APC-eFluo780	II/41
CD69	SuperBright 600	H1.2F3	CD11c	BV605	N418	IgG1	PE-Cy7	M1-14D12
FAS(CD95)	BV421	Jo2						
CD44	AF532	IM7						

CCR7	BUV737	4B12
LAG3	APC-eFluo780	eBioC9B7W
CD127	BV711	A7R34

Gut permeability histology

Fresh colon tissue was harvested from mice and stored at -80˚C before processing for RNA extraction using Trizol and cDNA synthesis. Real-time quantitative PCR was performed using the QuantStudio 7 Real-Time PCR system using TaqMan Universal PCR Master Mix and TaqMan Gene Expression Assays for the following genes: *ppia* (housekeeping), *cldn2*, *occluding*, *tip1*, and *muc2* (Applied Biosystems). Relative expression of transcript levels were measured using the $2^{-\Delta\Delta Ct}$ method using amplified C_t values.

Serum/plasma biomarker content

Whole blood was collected using cardiac puncture at euthanasia under anesthesia. For serum collection, whole blood was placed in sterile 1.5 mL microcentrifuge tubes, allowed to clot, centrifuged for 10 minutes, and placed in 25 µL aliquots and frozen at -80ºC. For plasma collection, whole blood was placed in EDTA (ethylenediaminetetraacetic acid)-coated microcentrifuge tubes (BD Microtainer® Blood Collection Tubes, 365992, Franklin Lakes, NJ, USA), centrifuged at 4ºC for 10 minutes, and placed in 25 µL aliquots and frozen at -80ºC. An ELISA (enzyme-linked immunosorbent assay) was carried out at Duke Molecular Physiology Institute Biomarkers Shared Resource. Serum was collected from fasted mice and was measured for adiponectin, leptin, and insulin. Plasma was collected from unfasted mice and was measured for estrogen (females only), interleukin 6 (IL-6), tumor necrosis factor-α (TNF-α), and insulin-like growth factor 1 (IGF-1).

Statistics

Principal coordinate analyses (PCoA) were performed on rarefied Bray-Curtis dissimilarity matrices on ARGs and taxa to discern differences in composition amongst treatment groups, timepoints, and cage assignments. Differences in Shannon diversity, body weight, fat pad mass, and serum/plasma biomarkers were evaluated using a one-way analysis of variance (ANOVA) with a post hoc Dunnett test to evaluate significance between each treatment group relative to the Unaltered sex-matched control. Correlations between individual ARGs and microbial species were determined using a pairwise Spearman correlation calculation followed by a Benjamini-Hochberg FDR correction. To determine ARGs and genera that significantly changes with time within individual treatment groups by sex Microbiome Multivariate Associations with Linear Models (MaAsLin2) was performed in which cage assignment was accounted for as a random effect. Post hoc Benjamini-Hochberg FDR q-values were reported along with p-values. Taxa heatmaps were generated by averaging the relative abundance of 15 top taxa within each timepoint from the Continuous Dose group. A pseudocount of 0.1 was used and the fold change of the relative abundance of each taxa was calculated relative to the baseline value at 1 month of age with a $\log_2$ transform. Here, we defined colonization as the detection of genera that were not observed prior to antibiotic exposure (less than 0.1% relative abundance) (*12*). Colonizers were not detected prior to antibiotic exposure and remained at an increased abundance with prolonged antibiotic exposure. Dynamic colonizers were not detected prior to antibiotic exposure and exhibited temporary increases or decreases in abundance with prolonged antibiotic exposure. Genera that changed in abundance were present prior to antibiotic exposure and remained increased or decreased with prolonged antibiotic exposure. Genera with a dynamic

change in abundance were present prior to antibiotic exposure and exhibited temporary increases or decreases in abundance with prolonged antibiotic exposure. ARG heatmaps were generated by averaging the relative abundance of top ARGs within each timepoint from the Continuous Dose group with a $\log_2$ transform. Variance of % ARG abundance associated with *Enterobacteriaceae*, ARG richness, ARG abundance, and relative abundance of taxa was calculated and followed with Shapiro's test to confirm normality and a Likelihood Ratio Test was used to compare two Generalized Least Squares models with homoscedastic and heteroscedastic residual variance to determine changes in variance over time. Rate constants associated with changes in taxonomy in the first four months after the start of antibiotic dosing were determined with regression models. All statistical testing was completed using R Statistical Software (v 4.0.3; R Core Team 2020).

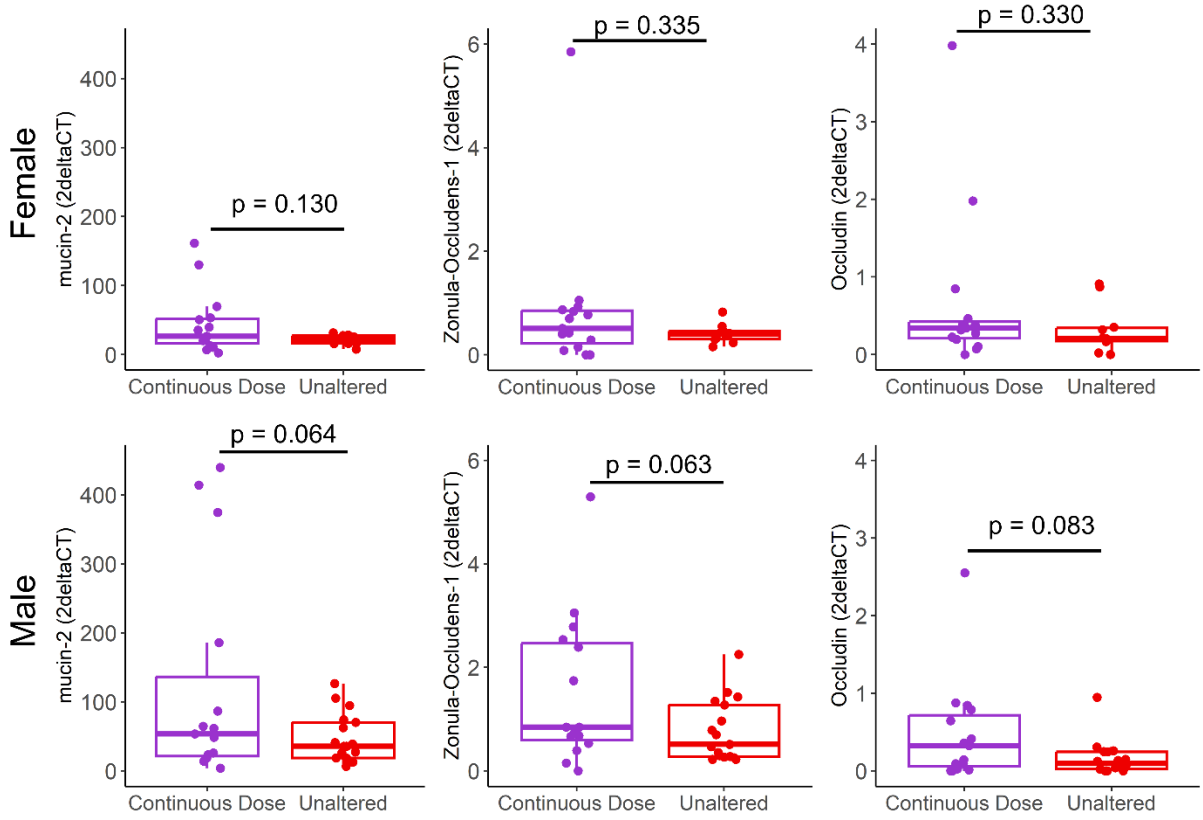

Fig. S1.

Gut permeability for Unaltered and Continuous Dose mice. Continuous antibiotic exposure did not significantly influence gut permeability.

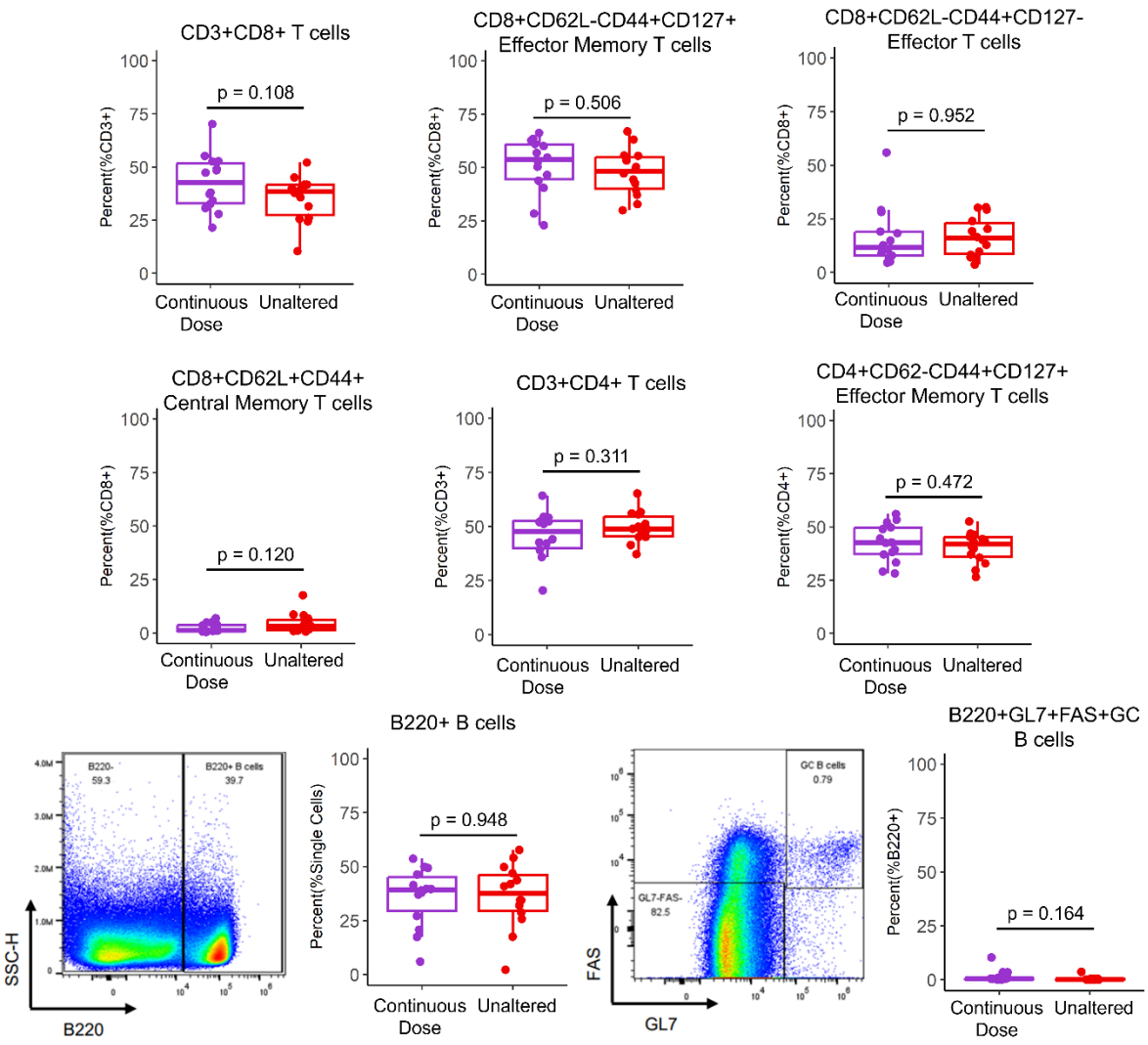

Fig. S2.

Splenic immune cell profiling for Unaltered and Continuous Dose mice. Continuous antibiotic exposure did not significantly influence splenic immune cell profile.

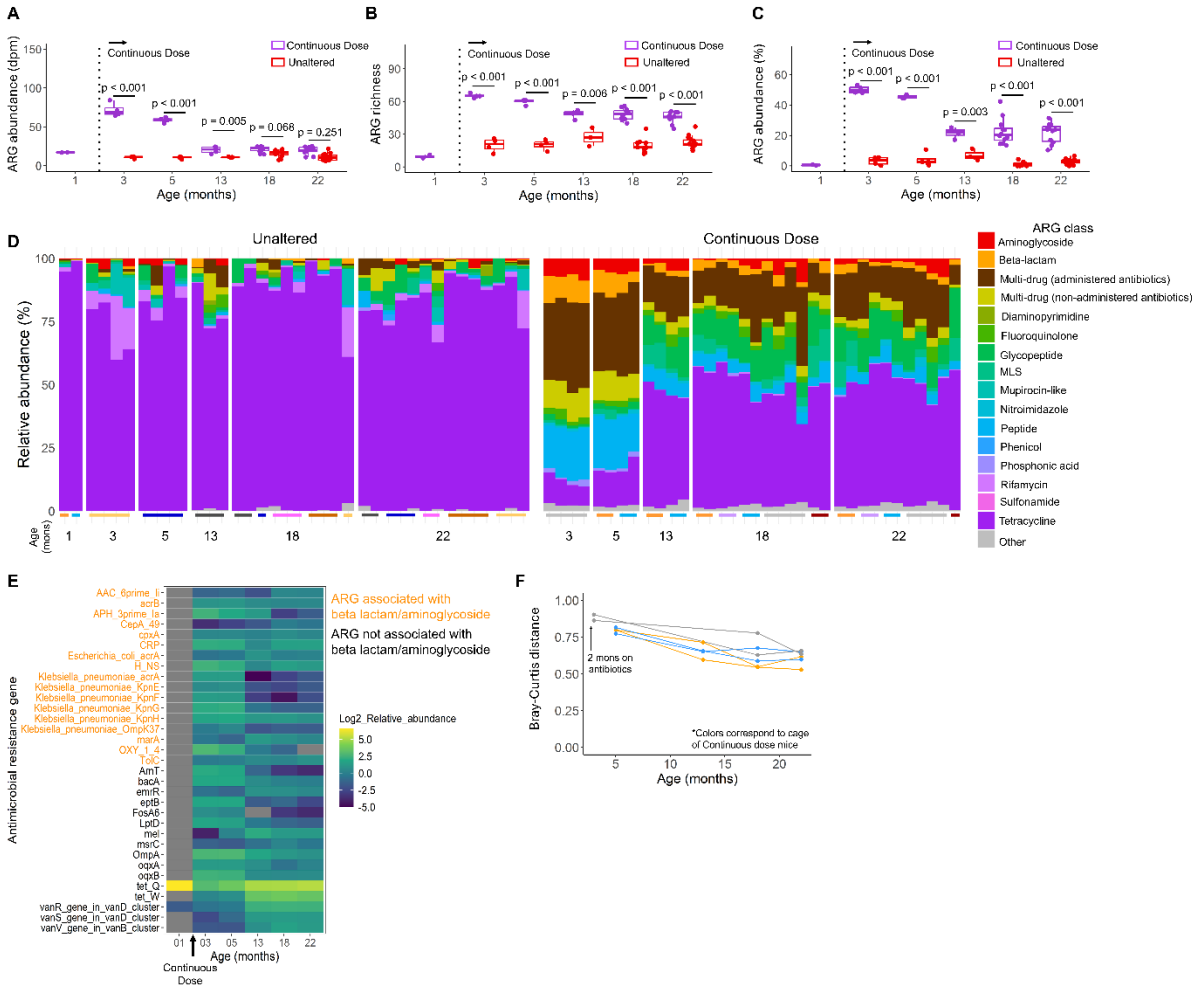

Fig. S3.

Effects of Continuous exposure to antibiotics on the resistome of male mice. (A) In the first few months of antibiotic dosing there was an increase in ARG abundance that peaked at three months of age, however, the abundance of ARGs declined and reached levels indistinguishable from that of the Unaltered group by 18 months of age. (B) In the first few months of antibiotic dosing there was an increase in ARG richness that peaked at three months of age and declined shortly after but remained increased relative to the Unaltered group for the remainder of life. (C) Two months after the start of antibiotic exposure < 50% of the ARG burden was attributed to resistance to the classes of antibiotics that were administered (beta-lactams and aminoglycosides). (D) Continuous exposure to antibiotics resulted in dynamic changes in the resistome composition. (E) The increase in ARG richness was primarily due to the sustained presence of ARGs that were first detected shortly after the start of antibiotic dosing. (F) Longitudinal tracking in individual mice showed that Continuous antibiotic exposure resulted in changes in the Bray-Curtis resistome composition over time that shifted towards the baseline Unaltered composition. Lines connect data points from the same individual and represent Bray-Curtis distance to baseline (one month of age prior to antibiotic exposure).

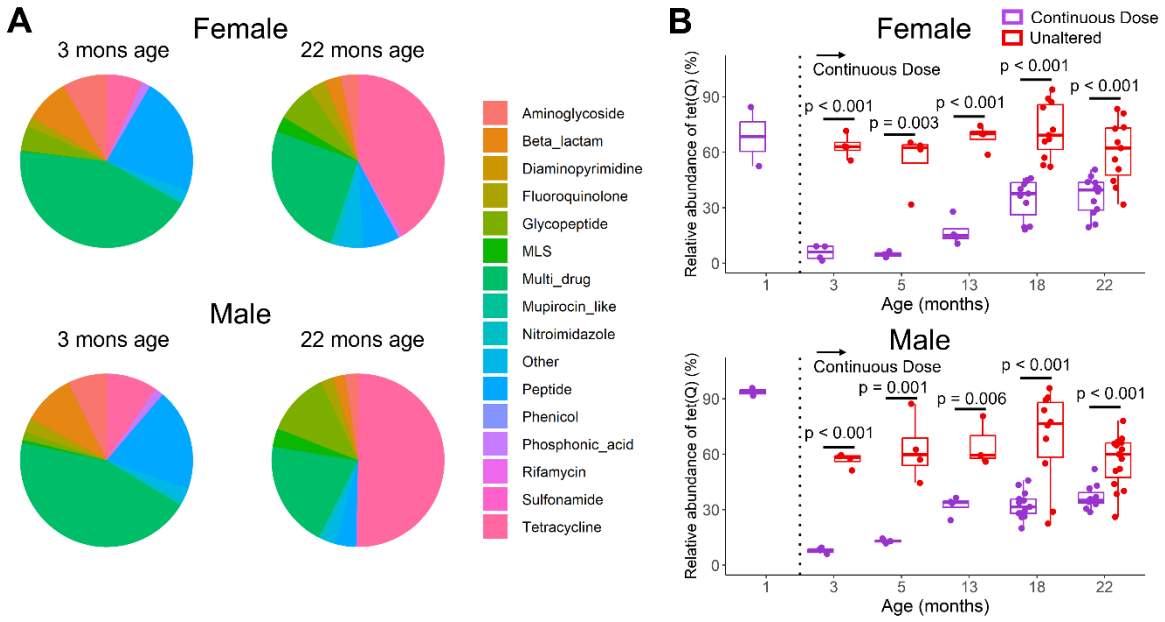

Fig. S4.

(A) Average abundance of ARGs associated with different classes of antibiotics in Continuous Dose mice revealed a decrease in ARGs associated with multidrug resistance and increase in ARGs associated with tetracycline over time. (B) The relative abundance of *tet(Q)* constituted the majority of the resistome in mice prior to antibiotic exposure, was significantly decreased with antibiotic exposure, and gradually increased with prolonged antibiotic exposure.

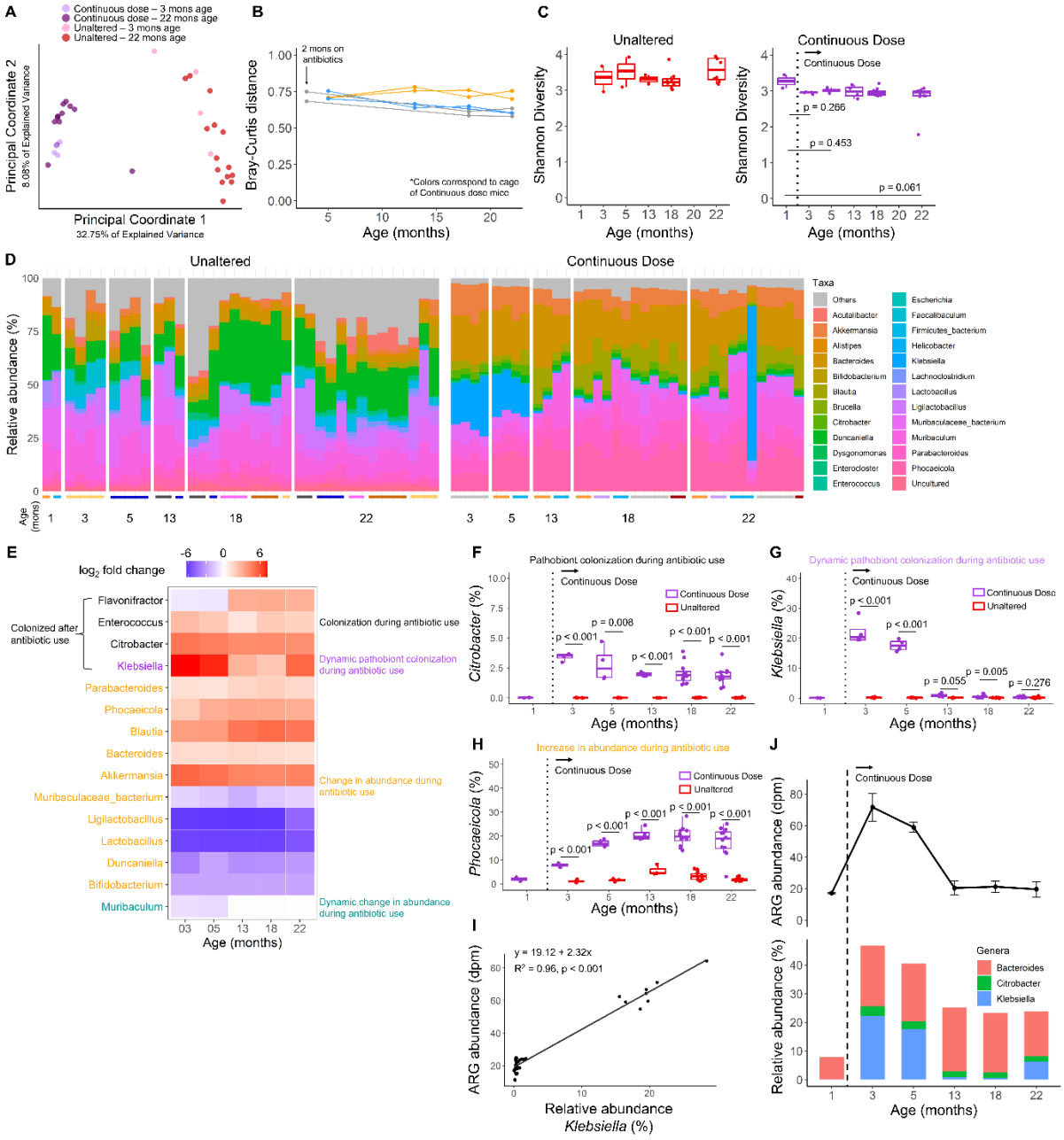

Fig. S5.

Effects of Continuous exposure to antibiotics on the microbiota of male mice. (A-B) Continuous exposure to oral antibiotics resulted in a rapid, drastic change in gut microbial composition compared to mice without antibiotic exposure and composition changed over time. (C) Shortly after the start of Continuous antibiotic dosing the Shannon diversity of the taxa decreased. (D-E) Genera-level analysis revealed complex dynamics of taxa during antibiotic dosing. (F-H) Representative plots in males with relative abundance of genera classified based on their response to antibiotics. (I) Regression of the relative abundance of *Klebsiella* against ARG abundance in Unaltered and Continuous Dose mice demonstrated that changes in ARG abundance were strongly linked with abundance of *Klebsiella* (Pearson correlation: 0.98). (J) Shifts in relative abundance of ARG harboring taxa directly align with shifts in ARG abundance.

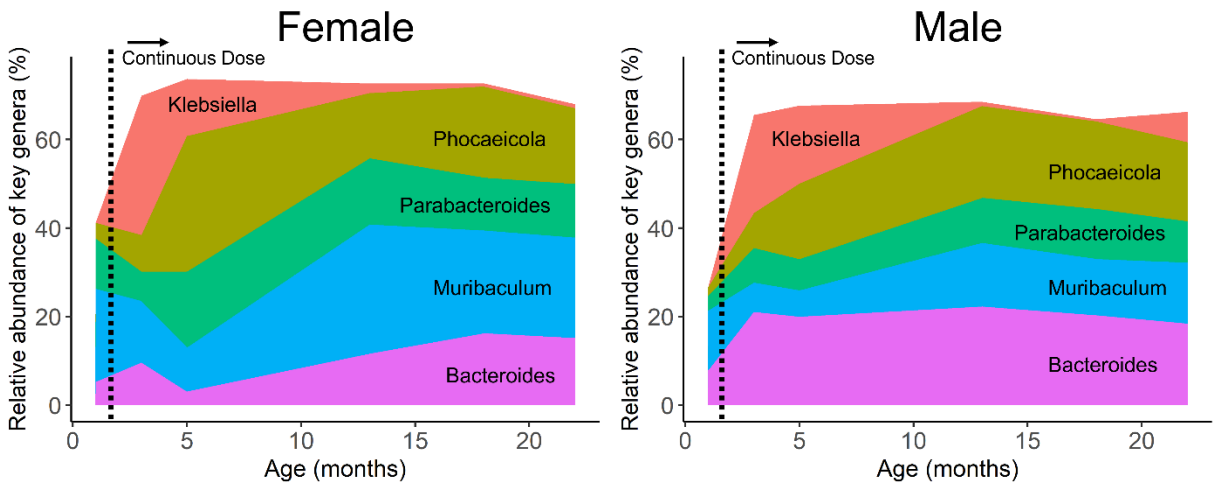

Fig. S6.
Average relative abundance of key genera (*Bacteroides*, *Klebsiella*, *Muribaculum*, *Parabacteroides*, *Phocaeicola*) over time in Continuous Dose mice revealed a dynamic shift amongst microbes.

5

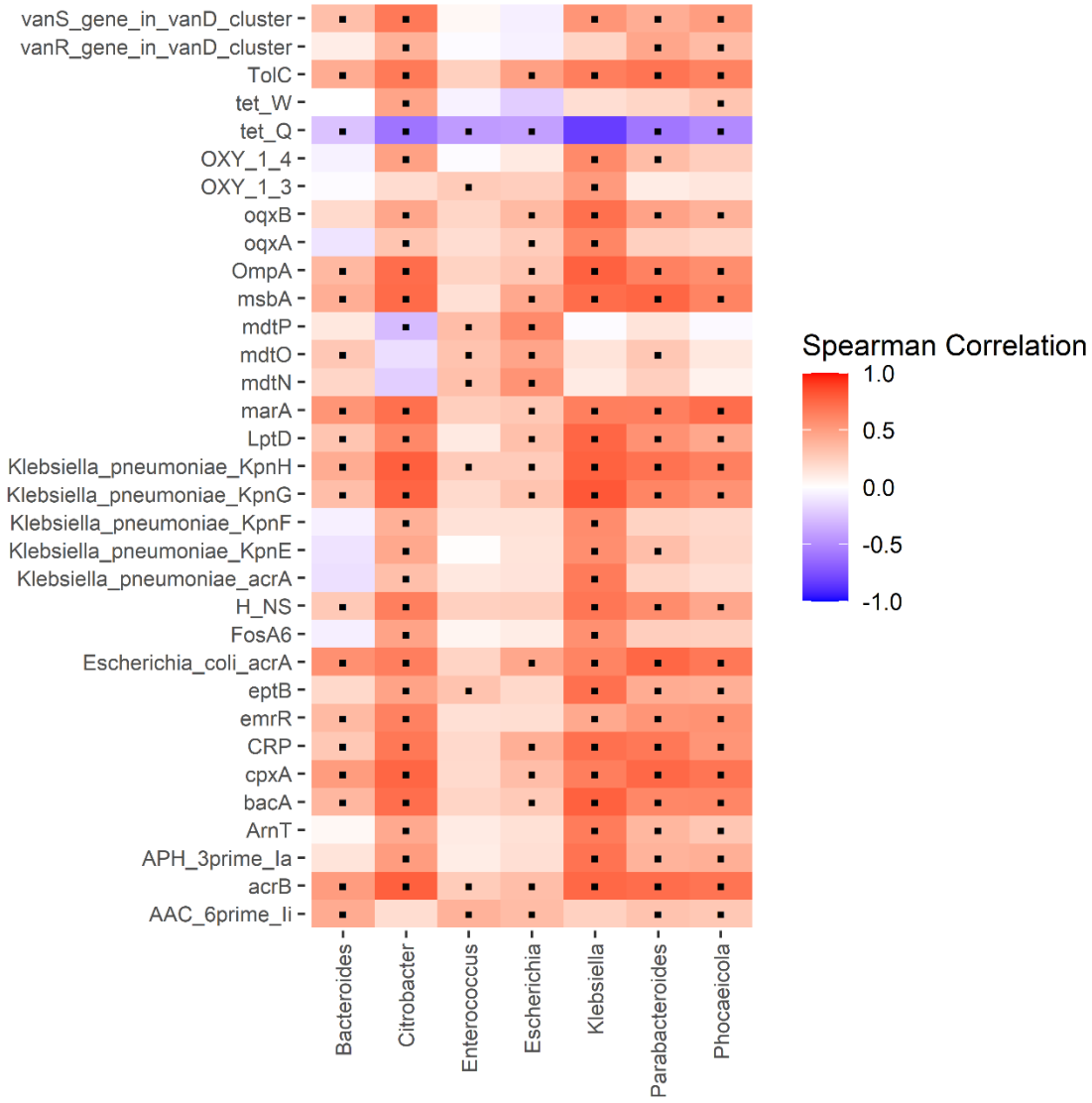

Fig. S7.
Pairwise Spearman correlation between genera and ARGs in Continuous Dose female mice; ▪ indicates a significant correlation ($p < 0.05$, Benjamini-Hochberg correction FDR).

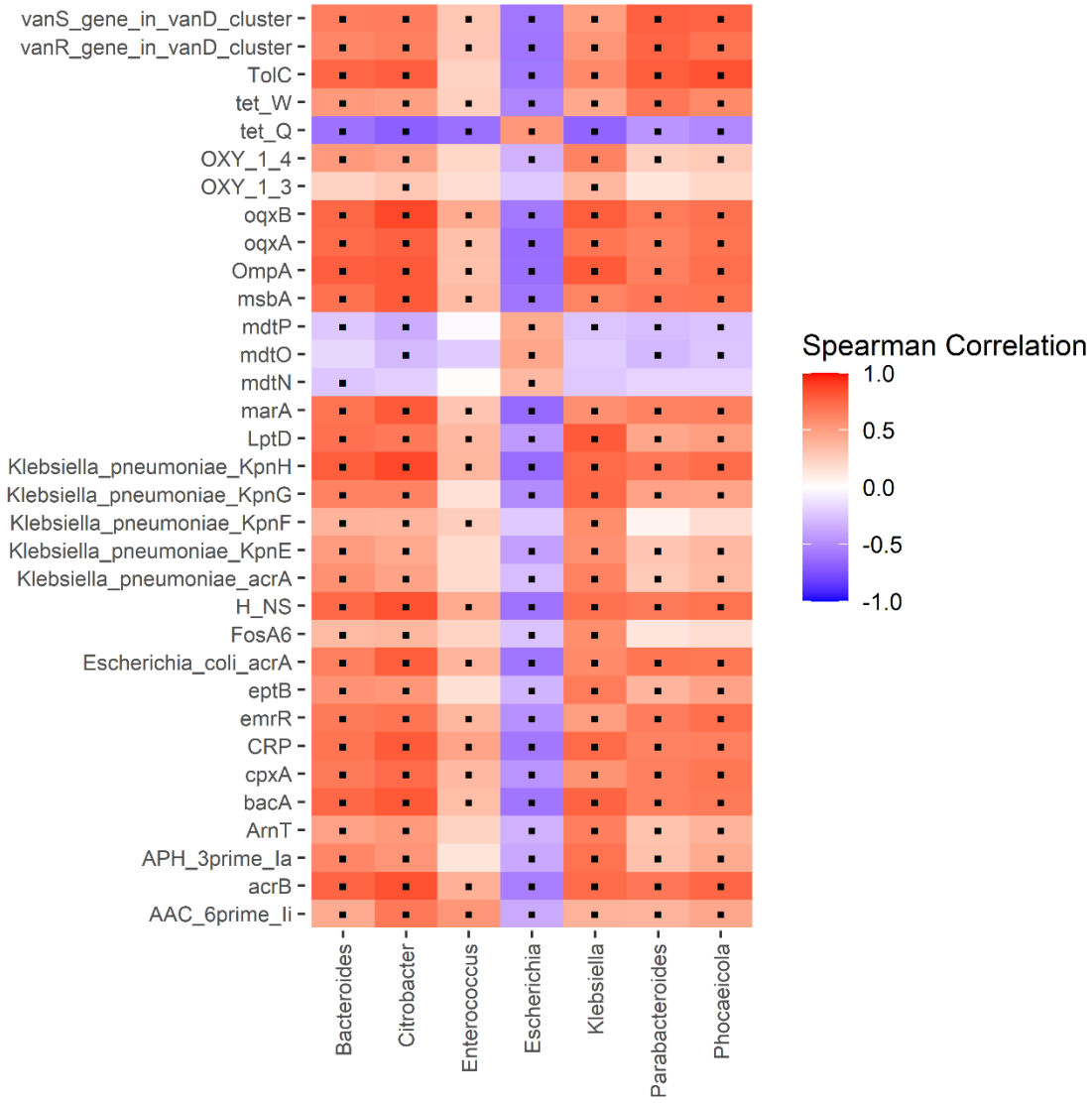

Fig. S8.
Pairwise Spearman correlation between genera and ARGs in Continuous Dose male mice; ▪ indicates a significant correlation ($p < 0.05$, Benjamini-Hochberg correction FDR).

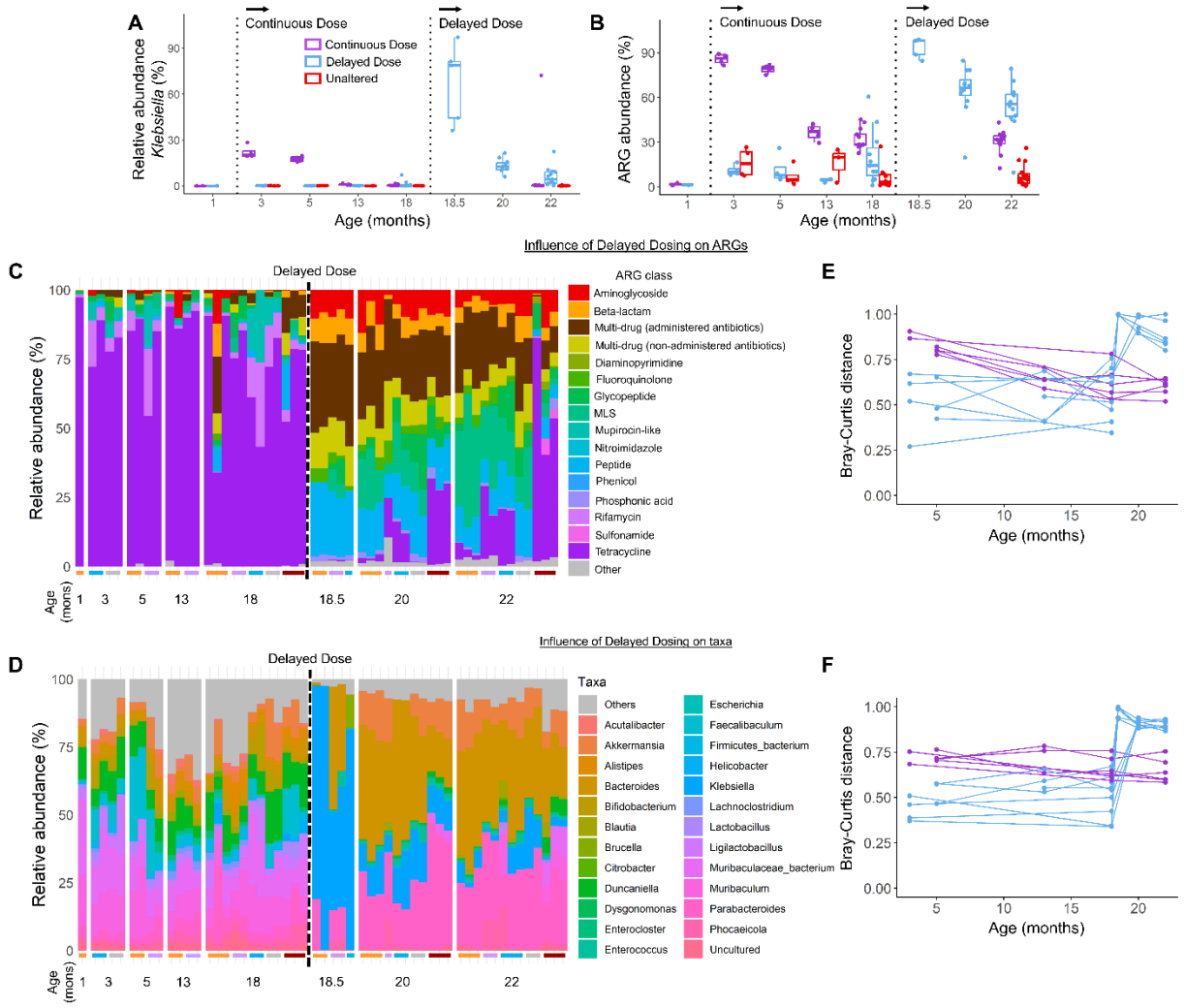

Fig. S9.

Effects of Delayed Dose antibiotic exposure on the microbiota and resistome of male mice. (A) Mice in the Delayed Dose group had a transient increase in *Klebsiella* and more rapid decline in *Klebsiella* relative to mice in the Continuous Dose group that were exposed to antibiotics for the same duration. (B) Delayed Dose mice had a transient increase in the relative abundance of ARGs that were associated with *Enterobacteriaceae*. (C-D) Composition of the resistome and microbiota over time in individual mice. (E-F) Bray-Curtis distance from baseline in the resistome and microbiota composition of Delayed Dose male mice.

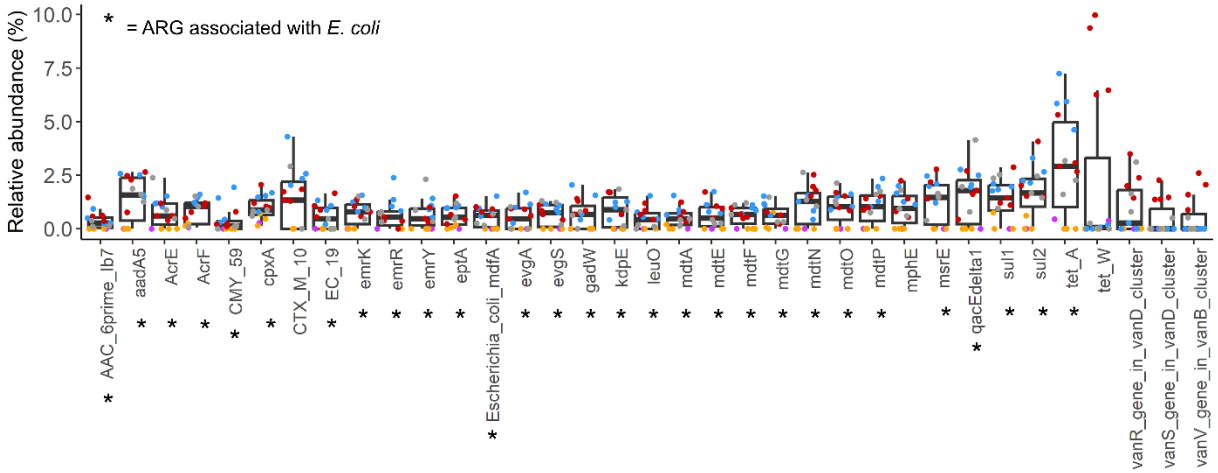

Fig. S10.
Outliers in the relationship between *Klebsiella* abundance and ARG burden in Figure 3F had increased relative abundance of more than 29 ARGs associated with *E. coli* and more than 5 ARGs associated with other taxa. Colored dots indicate mice housed in the same cage.

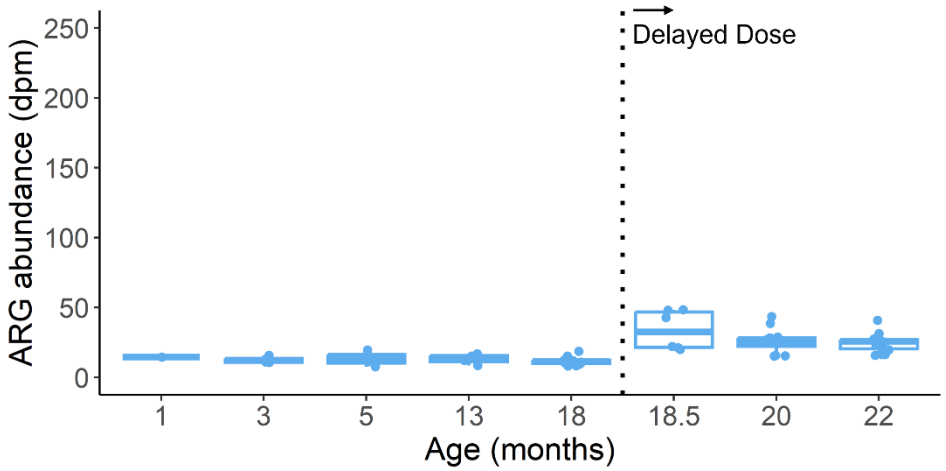

Fig. S11.
After subtracting off contributions of ARGs associated with *E. coli* from total ARG abundance in Delayed Dose female mice, ARG abundance declined after exposure to antibiotics as observed in male mice.

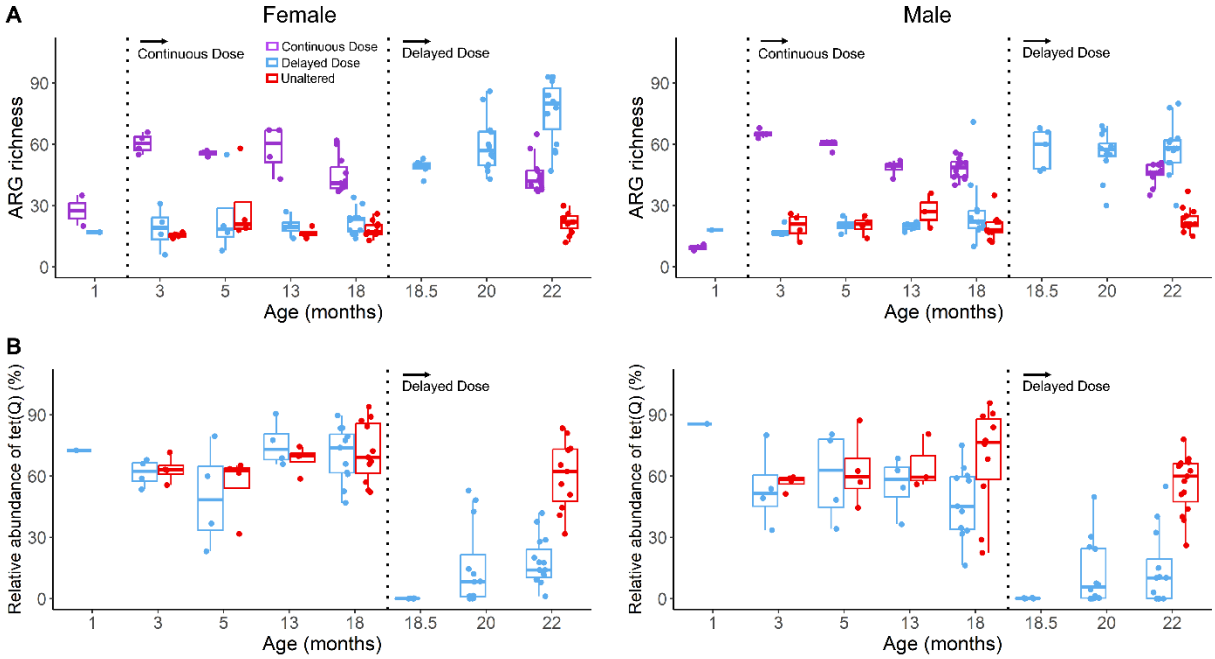

Fig. S12.
(A) ARG richness in Delayed Dose, Continuous Dose, and Unaltered groups over time. (B) *tet(Q)* dominated the resistome prior to antibiotic exposure and slowly increased in abundance after prolonged antibiotic exposure.

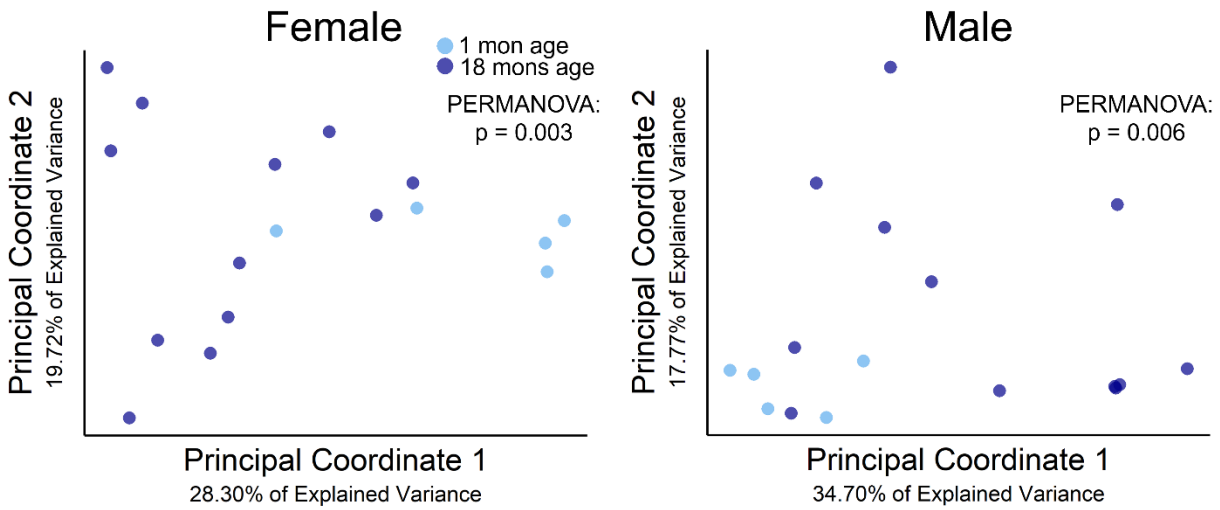

Fig. S13.
Taxonomic composition of the gut microbiota in Delayed Dose mice significantly shifted over aging from one to 18 months of age in both females and males.

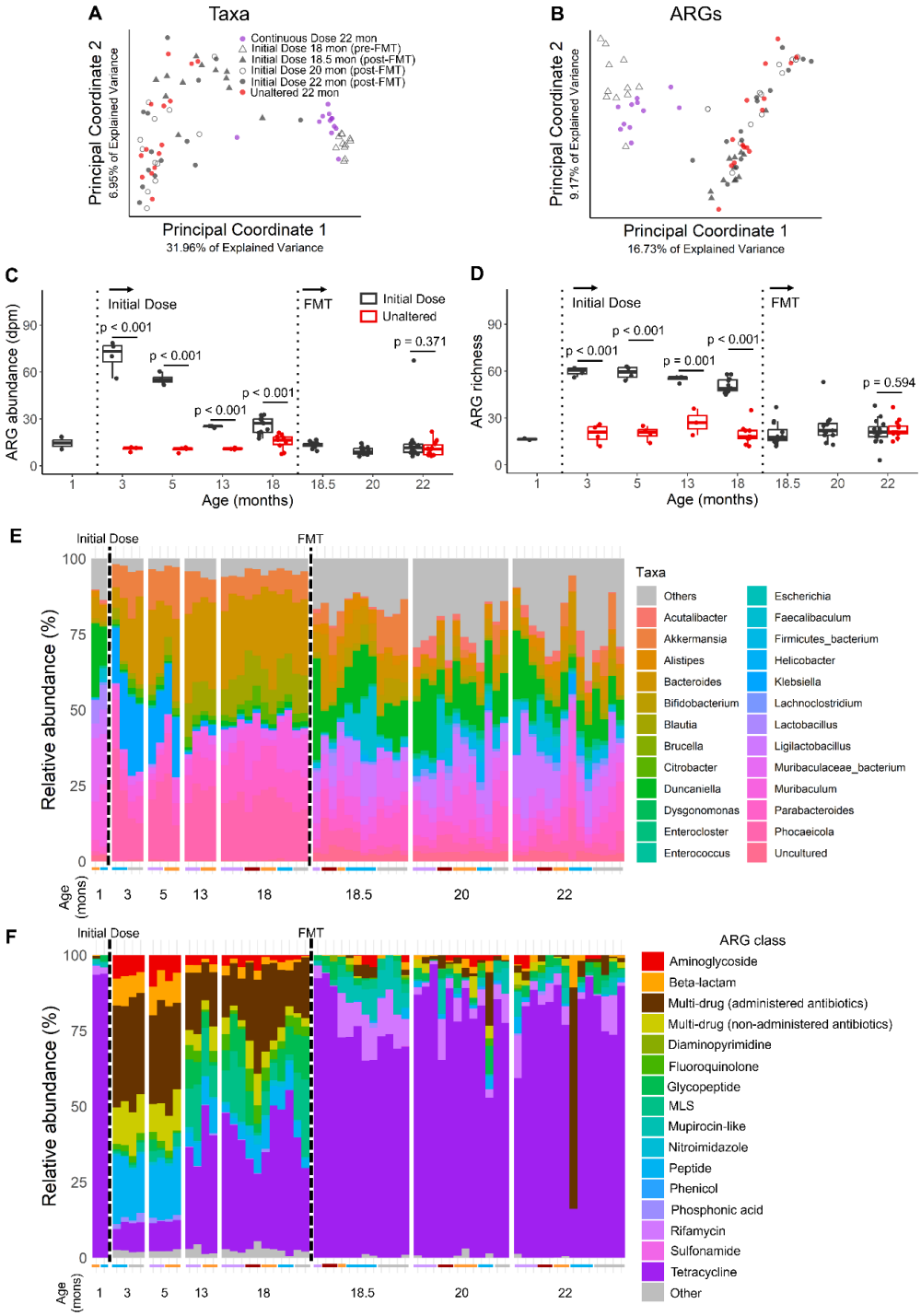

Fig. S14. (A-B) As observed in female mice, male mice that received the FMT after prolonged antibiotic exposure had their microbiota composition and resistome restored to the Unaltered state. (C-D) As observed in female mice, male mice that receive the FMT after prolonged antibiotic exposure had their total ARG burden and richness restored to the Unaltered state. (E-F) Composition of the microbiota and resistome prior to and after receiving the FMT.

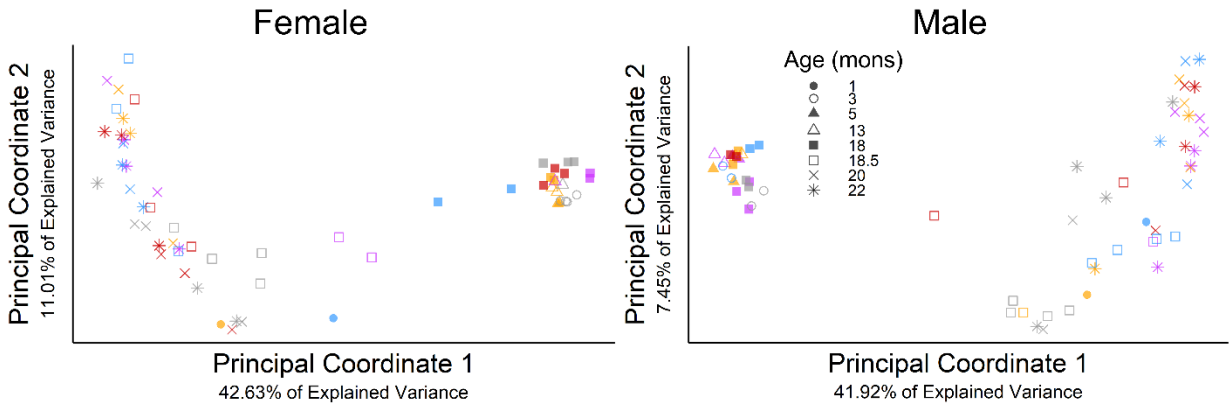

Fig. S15.
Longitudinally tracking the Bray-Curtis distance principal coordinate analysis of the Initial Dose group.

Table S1.

Circulating fasted serum (adiponectin, leptin, insulin) and non-fasted plasma (IL-6, IGF-1, TNF-α, estrogen – female only) biomarkers. Average values with standard deviation are shown. Dunnett test performed relative to Unaltered sex-matched control.

Treatment Group	Adiponectin (ng/mL)	Leptin (pg/mL)	Insulin (pg/mL)	IL-6 (pg/mL)	IGF-1 (pg/mL)	TNF-α (pg/mL)	Estrogen (pg/mL)
Female							
Unaltered	11791.600 ± 1854.456	6664.927 ± 4513.005	328.640 ± 284.080	59.407 ± 40.367	323744.286 ± 30842.775	25.336 ± 17.843	739.319 ± 414.776
Continuous Dose	11603.600 ± 1316.444 p = 0.994	3155.279 ± 2115.732 p = 0.012	233.815 ± 229.871 p = 0.516	95.657 ± 94.067 p = 0.612	264990.000 ± 34082.415 p = 0.007	20.651 ± 5.155 p = 0.998	1240.004 ± 892.425 p = 0.204
Delayed Dose	11601.000 ± 1365.696 p = 0.993	3532.141 ± 1990.284 p = 0.027	197.989 ± 113.136 p = 0.268	70.281 ± 67.956 p = 0.980	293688.571 ± 42610.087 p = 0.226	25.148 ± 15.417 p = 1.000	833.631 ± 274.280 p = 0.974
Initial Dose	10307.100 ± 1173.284 p = 0.281	3160.301 ± 1975.363 p = 0.012	202.444 ± 107.547 p = 0.294	102.700 ± 48.065 p = 0.481	359667.143 ± 17646.433 p = 0.123	74.361 ± 114.718 p = 0.295	640.484 ± 239.664 p = 0.971
Male							
Unaltered	6399.000 ± 304.501	3374.644 ± 2181.318	290.774 ± 186.042	87.982 ± 64.059	293718.571 ± 23523.576	11.359 ± 3.214	--
Continuous Dose	6002.960 ± 935.092 p = 0.834	2283.911 ± 1341.219 p = 0.219	327.804 ± 197.484 p = 0.883	48.077 ± 29.648 p = 0.236	288605.714 ± 20158.671 p = 0.979	16.119 ± 5.251 p = 0.180	--
Delayed Dose	5962.880 ± 1396.125 p = 0.794	2099.470 ± 1129.790 p = 0.126	238.974 ± 99.210 p = 0.743	73.761 ± 39.391 p = 0.876	295170.000 ± 27974.134 p = 0.999	8.669 ± 5.436 p = 0.599	--
Initial Dose	5274.200 ± 654.134 p = 0.165	2277.777 ± 1359.676 p = 0.215	242.443 ± 99.685 p = 0.779	63.823 ± 34.160 p = 0.611	298610.000 ± 44024.678 p = 0.981	13.854 ± 4.967 p = 0.650	--

Table S2.

Body weight at euthanasia and perigonadal fat pad mass. Average values with standard deviations are shown. Dunnett test performed compared to Unaltered sex-matched control.

Treatment group	Body weight at euthanasia (g)	Perigonadal fat pad mass (g)
Female		
Unaltered	27.343 ± 4.863	0.773 ± 0.386
Continuous Dose	24.194 ± 2.073 p = 0.015	0.452 ± 0.180 p = 0.003
Delayed Dose	24.356 ± 2.619 p = 0.025	0.495 ± 0.235 p = 0.014
Initial Dose	24.353 ± 2.149 p = 0.022	0.443 ± 0.203 p = 0.002
Male		
Unaltered	30.094 ± 2.180	0.621 ± 0.207
Continuous Dose	28.500 ± 2.384 p = 0.176	0.461 ± 0.182 p = 0.154
Delayed Dose	31.239 ± 3.735 p = 0.432	0.635 ± 0.422 p = 0.997
Initial Dose	29.710 ± 2.115 p = 0.944	0.512 ± 0.156 p = 0.424

Table S3.

ARGs that significantly changed with time (3-22 months) in the Continuous Dose group with an abundance greater than 1%.

ARG	Change over time	p-value	q-value
Female			
Klebsiella pneumoniae acrA	Decrease	< 0.001	< 0.001
oqxB	Decrease	< 0.001	< 0.001
ArnT	Decrease	< 0.001	< 0.001
oqxA	Decrease	< 0.001	< 0.001
eptB	Decrease	< 0.001	< 0.001
LptD	Decrease	< 0.001	< 0.001
tet(Q)	Increase	< 0.001	< 0.001
APH(3')-Ia	Decrease	< 0.001	< 0.001
Klebsiella pneumoniae KpnG	Decrease	< 0.001	< 0.001
OmpA	Decrease	< 0.001	< 0.001
OXY-1-3	Decrease	< 0.001	< 0.001
FosA6	Decrease	< 0.001	< 0.001
OXY-1-4	Decrease	< 0.001	< 0.001
Klebsiella pneumoniae KpnF	Decrease	< 0.001	< 0.001
Klebsiella pneumoniae KpnE	Decrease	0.001	0.006
bacA	Decrease	0.001	0.006
Klebsiella pneumoniae OmpK37	Decrease	0.003	0.015
H-NS	Decrease	0.007	0.029
emrK	Increase	0.007	0.030
mdtO	Increase	0.008	0.030
mdtA	Increase	0.009	0.034
mdtN	Increase	0.010	0.037
gadW	Increase	0.012	0.043
mdtC	Decrease	0.013	0.044
AcrS	Increase	0.013	0.044
Escherichia coli mdfA	Increase	0.018	0.057
CRP	Decrease	0.020	0.058
vanS gene in vanD cluster	Increase	0.019	0.058
evgA	Increase	0.020	0.058
mdtF	Increase	0.021	0.061
emrY	Increase	0.025	0.067
leuO	Increase	0.027	0.071
mdtE	Increase	0.035	0.089
CepA-49	Increase	0.040	0.091
emrR	Increase	0.040	0.091
PmrF	Increase	0.049	0.108
Male			
APH(3')-Ia	Decrease	< 0.001	< 0.001
LptD	Decrease	< 0.001	< 0.001
tet(Q)	Increase	< 0.001	< 0.001
ArnT	Decrease	< 0.001	< 0.001
eptB	Decrease	< 0.001	< 0.001
Klebsiella pneumoniae KpnG	Decrease	< 0.001	< 0.001

oqxB	Decrease	< 0.001	< 0.001
OXY-1-4	Decrease	< 0.001	< 0.001
Klebsiella pneumoniae acrA	Decrease	< 0.001	< 0.001
bacA	Decrease	< 0.001	< 0.001
OmpA	Decrease	< 0.001	< 0.001
Klebsiella pneumoniae KpnF	Decrease	< 0.001	< 0.001
FosA6	Decrease	< 0.001	< 0.001
Klebsiella pneumoniae KpnE	Decrease	< 0.001	< 0.001
oqxA	Decrease	< 0.001	< 0.001
vanR gene in vanD cluster	Increase	< 0.001	< 0.001
Klebsiella pneumoniae KpnH	Decrease	< 0.001	< 0.001
Klebsiella pneumoniae OmpK37	Decrease	< 0.001	0.001
vanS gene in vanD cluster	Increase	< 0.001	0.001
emrA	Decrease	< 0.001	0.002
OXY-1-3	Decrease	< 0.001	0.002
tet(W)	Increase	0.002	0.006
tet(W/N/W)	Increase	0.004	0.012
vanH gene in vanD cluster	Increase	0.008	0.024
vanV gene in vanB cluster	Increase	0.010	0.027
H-NS	Decrease	0.022	0.058
mdtC	Decrease	0.033	0.081
TolC	Increase	0.039	0.095
msrC	Increase	0.050	0.117

Table S4.

ARGs with an abundance greater than 1% that significantly change with time (1-22 months) in the Unaltered group. No genera changed significantly over time in the Unaltered female mice.

ARG	Change over time	p-value	q-value
Female			
tet(O/32/O)	Increase	0.006	0.159
tet(W/N/W)	Increase	0.006	0.159
Male			
tet(40)	Increase	0.002	0.100

Table S5.

Genera that significantly changed with time (3-22 months) in the Continuous Dose group with a relative abundance greater than 1%.

Genera	Change over time	p-value	q-value
Female			
Caudoviricetes	Increase	< 0.001	< 0.001
Klebsiella	Decrease	< 0.001	< 0.001
Duncaniella	Increase	< 0.001	< 0.001
Flavonifractor	Increase	< 0.001	< 0.001
Bacteroides	Increase	< 0.001	< 0.001
Akkermansia	Decrease	< 0.001	0.007
Muribaculum	Increase	0.006	0.034
Blautia	Decrease	0.011	0.050
Escherichia	Increase	0.012	0.054
Enterococcus	Decrease	0.018	0.064
Male			
Flavonifractor	Increase	< 0.001	< 0.001
Akkermansia	Decrease	< 0.001	0.001
Citrobacter	Decrease	< 0.001	0.010
Muribaculum	Increase	0.002	0.032
Phocaeicola	Increase	0.004	0.074
Blautia	Increase	0.012	0.165
Klebsiella	Decrease	0.013	0.165

Table S6.

Genera that significantly changed with time (1-22 months) in the Unaltered group with an abundance greater than 1%. Unaltered female mice did not have any genera that significantly changed with time.

Genera	Change over time	p-value	q-value
Male			
Muribaculaceae bacterium	Decrease	< 0.001	< 0.001
Faecalibaculum	Decrease	0.001	0.056
[Clostridium]	Increase	0.019	0.165
Blautia	Increase	0.018	0.165
Caudoviricetes	Increase	0.019	0.165
Muribaculum	Decrease	0.017	0.165
Lachnoclostridium	Increase	0.028	0.185
Roseburia	Increase	0.030	0.190
Acutalibacter	Increase	0.035	0.204
Enterocloster	Increase	0.038	0.208

Table S7.

Variance in the % of ARG abundance associated with *Enterobacteriaceae* family amongst treatment groups over time. Shapiro's test was used to check for the normality of each dataset. A Likelihood Ratio Test was used comparing two Generalized Least Squares models with homoscedastic and heteroscedastic residual variance to determine changes in variance over time.

Sex	**Group**	**Age (Months)**								**p value**
		1	3	5	13	18	18.5	20	22	
Female	Unaltered		7.044	398.242	0.821	81.225			99.571	<0.001
	Continuous Dose	550.624	10.871	1122.147	31.780	296.521			311.983	0.003
	Delayed Dose		55.596	814.657	4.248	20.991	3.127	457.193	159.998	<0.001
	Initial Dose	27.876	14.713	392.422	83.987	368.685	63.367	42.202	43.186	<0.001
Male	Unaltered		94.663	46.378	132.576	63.907			54.000	0.866
	Continuous Dose	1.342	13.083	60.052	31.834	47.476			65.539	0.385
	Delayed Dose		14.805	72.633	1.182	337.242	44.286	275.398	297.194	<0.001
	Initial Dose	2.233	6.099	49.266	59.217	213.520	59.571	129.980	447.772	<0.001

Table S8.

Variance in the ARG richness and abundance amongst treatment groups over time. Shapiro's test was used to check for the normality of each dataset. A Likelihood Ratio Test was used comparing two Generalized Least Squares models with homoscedastic and heteroscedastic residual variance to determine changes in variance over time.

Sex	Group	Age (Months)								p value
		1	3	5	13	18	18.5	20	22	
ARG richness										
Female	Unaltered		1.667	365.667	6.333	14.054			32.691	< 0.001
	Continuous Dose	112.500	24.333	2.333	134.250	81.200			74.992	0.213
	Delayed Dose		110.250	426.000	28.667	37.242	14.167	180.515	222.981	0.004
	Initial Dose	4.500	5.667	489.667	7.583	199.788	58.447	55.242	12.692	< 0.001
Male	Unaltered		40.000	21.583	72.333	42.233			30.374	0.867
	Continuous Dose	4.500	4.250	6.250	15.000	26.386			26.218	0.369
	Delayed Dose		9.000	13.667	4.917	268.691	97.200	121.356	165.474	0.006
	Initial Dose	0.500	8.250	18.000	4.000	22.164	51.818	106.750	63.381	0.007
ARG abundance										
Female	Unaltered		4.102	74.315	6.383	11.449			3.484	0.002
	Continuous Dose	13.468	750.200	41.709	77.982	93.890			58.519	0.011
	Delayed Dose		3.740	45.690	13.091	11.236	1118.776	1378.560	1946.852	< 0.001
	Initial Dose	5.848	128.480	83.415	9.152	105.099	11.877	7.222	10.566	< 0.001
Male	Unaltered		2.026	2.735	0.417	21.294			20.488	0.014
	Continuous Dose	0.120	78.237	10.136	19.831	12.289			23.834	0.065
	Delayed Dose		4.927	12.675	4.615	45.944	1805.357	246.861	195.395	< 0.001
	Initial Dose	31.920	103.841	13.030	0.337	29.421	4.299	6.183	221.139	< 0.001

Table S9.

Quality control processing of shotgun metagenomic paired-end samples using the Chan Zuckerberg ID pipeline.

Sample name	Total reads (combined paired-end)	Reads post bowtie2 ercc filter	Reads post fastp	Reads post bowtie2 host filter	Reads post hisat2 host filter	Reads post czid-dedup
431283_1_S385	98254790	98254256	86252768	81456210	81456120	42313340
435068_1_S47	78174480	78174348	66048086	64746448	64746428	34557762
431277_1_S235	38130396	38130374	36550942	36384350	36384344	18848960
431242_1_S396	110199866	110199694	98085530	96529696	96529650	47698584
431218_1_S142	50575594	50575540	48313664	47956910	47956894	24908656
431228_1_S373	68101464	68101422	64511926	64290002	64289992	33349054
431287_1_S281	83195204	83194958	78995442	76871444	76871370	36780318
431293_1_S94	23059416	23059380	22146096	21909206	21909206	13708014
435090_1_S374	63552618	63552592	58636430	58462610	58462610	36383398
435085_1_S190	64606822	64606788	61511926	61375426	61375426	32233710
439799NP_3_S325	70625354	70624954	66536922	63278524	63278454	33666686
435071LP_3_S88	19694508	19694498	18864946	18759846	18759846	12470880
439790LP_3_S276	56593580	56593524	52449186	52389208	52389196	28018656
439790NP_3_S230	39783532	39783356	38202670	38181948	38181938	19562470
435090NP_3_S323	89979696	89979652	82272354	82244112	82244104	45336820
435090LP_3_S368	67049752	67049662	62738884	62704372	62704368	32815768
435082LP_3_S278	49348462	49348378	46608018	45947900	45947894	23532006
435082NP_3_S232	72160594	72160536	68105120	67778314	67778306	35208504
435075RP_3_S326	90953166	90952116	84344956	74542538	74542298	37076218
435075BP_3_S371	46738462	46738264	44147760	43141066	43141046	22422508
435075LP_3_S279	85329562	85328312	78888864	66112308	66111998	33475500
435075NP_3_S233	87107260	87106922	81417080	78224640	78224578	38421918
435073LP_3_S90	47714912	47714816	45451542	44984060	44984042	24995956
435073RP_3_S44	34679472	34679112	32868008	30609250	30609186	18215590
435071RP_3_S136	28387586	28387562	27226090	27108638	27108638	16005218
435068NP_3_S134	39411840	39411776	37942260	37548918	37548882	19331922
435068LP_3_S182	27366870	27366840	26289722	26256168	26256166	15909022
439795BP_3_S366	70421666	70421550	64910016	64658918	64658900	33900318
439795LP_3_S274	33030312	33030300	31640968	31627680	31627680	17264466
439795NP_3_S228	76647368	76647278	70343378	70268348	70268330	36728702
439795RP_3_S321	82721652	82721002	77348306	73301284	73301122	37406040
439799LP_3_S370	54884196	54883994	51858506	50693228	50693202	27879372
435071BP_3_S184	94862402	94862344	90184714	89838924	89838902	41150758
435071NP_3_S42	17482554	17482538	16817078	16781376	16781372	11987542
439818LP_3_S86	22328292	22328256	21423304	21289496	21289486	11563198
439823LP_3_S138	12107004	12106826	11458274	10402940	10402892	7001186
439823BP_3_S186	83343730	83343128	77338350	72365246	72365128	36659748
439824BP_3_S46	80020526	80020278	75040356	72954552	72954516	37883270
439824RP_3_S92	13721136	13720694	12745684	10178486	10178386	6587030
439824NP_3_S140	101642052	101641248	95352048	86514928	86514764	38823566
439824LP_3_S188	49876346	49876222	47262730	46338278	46338232	25810910
439818NP_3_S40	81169152	81169116	76796784	76716394	76716394	39970016
431281NP_5_S78	130670442	130670252	116678872	114561092	114561016	54534028
431283RP_5_S130	45839370	45839276	43576630	42688676	42688664	22813686
431283LP_5_S178	51375088	51374714	48663066	45688624	45688536	25104760
431281LP_5_S126	79767512	79767422	75861434	75105696	75105672	37169570

431277NP_5_S128	102949688	102949620	92634786	92099756	92099740	47253550
431277LP_5_S176	47616706	47616692	44810230	44669476	44669468	26782770
431242NP_5_S317	45861968	45861448	42397614	38700184	38700086	20426886
431242BP_5_S363	60542198	60541580	57193866	52592408	52592264	27774400
431218NP_5_S313	59836326	59836232	56721284	56301518	56301482	30614976
431218LP_5_S359	80472128	80472006	73759756	73435088	73435058	39847822
431233LP_5_S272	70354834	70354632	65686384	64237444	64237430	33365432
431233NP_5_S226	41089840	41089750	38992514	38234808	38234774	20379204
431230NP_5_S319	52041496	52041374	48932798	47869886	47869850	26686596
431230LP_5_S365	65303188	65303076	61116694	60523824	60523812	33721604
431229NP_5_S224	44492996	44492888	42165154	41077066	41077032	22691544
431229LP_5_S270	74311146	74310990	69395218	67830252	67830216	35528354
431226RP_5_S315	114336990	114336888	105808102	104979856	104979768	52005514
431226NP_5_S222	97329166	97329050	91925368	90823984	90823890	43567798
431226BP_5_S361	108504794	108504620	100572374	98599430	98599352	51957586
431289RP_5_S38	89059470	89059408	81870004	81729480	81729452	41226918
431289BP_5_S84	40144578	40144458	38021608	37415374	37415342	23184402
431289LP_5_S180	58280444	58280372	55584744	55325712	55325694	27823440
431289NP_5_S132	56974378	56974264	54184568	53471600	53471580	27264998
431287LP_5_S80	94042744	94042718	89289430	89170960	89170960	43845824
431287NP_5_S34	80437234	80437174	76400396	75983520	75983510	40807292
431290LP_5_S82	45404792	45404538	43169354	41526282	41526256	20387960
431290NP_5_S36	70035412	70035344	64089742	63785924	63785912	35097116
431293LP_5_S267	34852960	34852914	33388500	33056328	33056326	20439086
431293NP_5_S174	46360700	46360582	43875130	42740280	42740234	21775620
431281NP_13_S93	35302692	35302622	33803224	33230374	33230340	20247714
431287LP_13_S120	76812082	76811826	71399824	71240498	71240498	38432252
431284NP_13_S172	32448348	32448336	30495522	30426016	30426016	20037520
431284BP_13_S219	98828472	98828274	90160086	88163754	88163702	46049670
431283NP_13_S170	34685982	34685870	30507716	29523520	29523468	19377100
431283LP_13_S217	68469168	68468870	60703410	58944246	58944196	31185070
431281LP_13_S141	82421384	82421272	78551386	77449054	77449010	39843888
431277NP_13_S168	53890556	53890478	51483582	50929024	50929018	30664094
431277LP_13_S215	80896454	80896364	76670144	75969072	75969048	43497722
431242BP_13_S30	88090768	88090196	81532184	76509786	76509672	40372750
431242NP_13_S355	69108762	69108366	64654222	61186342	61186224	34265870
431218NP_13_S280	13811288	13811258	13256982	13114772	13114772	8464228
431218LP_13_S327	75188974	75188812	70322208	69943572	69943530	41291928
431233NP_13_S265	85632122	85632024	78762242	78014930	78014914	40503762
431233LP_13_S311	94597132	94596744	86333786	83323776	83323708	44013926
431230NP_13_S357	88923086	88922780	81447462	78913070	78913026	42863396
431230LP_13_S32	77078750	77078594	72498144	71156438	71156414	38408004
431229NP_13_S309	40359746	40359536	38394222	37212272	37212222	21646366
431229LP_13_S263	62054876	62054476	54860572	51209788	51209684	30146966
431226NP_13_S261	103433794	103433336	95800106	93613178	93613120	51088788
431226LP_13_S307	96142134	96141922	88696870	88349758	88349624	46731332
431289LP_13_S124	54358070	54357994	51591856	51301678	51301676	29191516
431287NP_13_S73	69984808	69984506	66682692	66645022	66645020	37077570
431290LP_13_S122	81111610	81111260	75275630	72402844	72402774	38092096
431290NP_13_S75	66914596	66914328	62068764	59784670	59784590	33142618
431293LP_13_S234	62435464	62435430	58671678	58478866	58478854	34183608
431293NP_13_S189	94701924	94701812	89379708	88294684	88294654	46169382
435090BP_13_S353	49110614	49110414	46853698	46123916	46123896	26393496
435090LP_13_S28	89917874	89917464	85788688	85148430	85148412	42000828
439795NP_13_S26	99504984	99504722	93602388	93326420	93326356	49121016

431236LP_13_S372	70942654	70942448	67320002	66752348	66752318	33729104
431283BP_18_S316	42637134	42637060	40441668	40159310	40159300	22930452
431281NP_18_S24	107277332	107277304	99759282	99619134	99619132	52275612
431287LP_18_S262	110634028	110633644	103398662	103349578	103349576	57229868
439799RP_18_S133	31150608	31150242	29369716	26561088	26561002	15126988
439825RP_18_S362	50967930	50967842	48365146	47887254	47887248	25761748
431284NP_18_S320	93104654	93104298	85943814	83763618	83763584	42417764
431284BP_18_S41	51719540	51719280	48579140	46697886	46697850	26914100
431283LP_18_S360	65811422	65811044	60824946	57618420	57618322	32560786
435069NP_18_S275	48130118	48129946	45923658	44864770	44864762	24099626
435069BP_18_S367	59199640	59199518	55648912	54614170	54614140	27619018
435069LP_18_S322	75884534	75884336	70647608	68964554	68964534	38521456
431283NP_18_S314	63460622	63460470	57210262	55893260	55893230	31256630
431281BP_18_S305	140572758	140572716	131685010	131517914	131517914	60391630
431281LP_18_S71	97414410	97414384	92425004	92379138	92379138	45678618
431279LP_18_S264	85397480	85397428	73951368	73608944	73608932	42139294
431277NP_18_S308	110456924	110456888	99694278	99657528	99657528	50219650
431279NP_18_S218	79155222	79155166	75709280	75528362	75528348	38484790
431277LP_18_S354	124008234	124008174	113038354	112863600	112863594	56261304
431242BP_18_S179	35787524	35787516	33999738	33962534	33962532	20560642
431242NP_18_S131	59157036	59156898	56358784	55448346	55448328	28601420
431236LP_18_S119	88693000	88692990	84401338	84292394	84292374	46479108
431218NP_18_S25	56461874	56461528	53338398	51728878	51728838	30833552
431218LP_18_S72	89542420	89542186	84931166	84879354	84879324	47490196
431233NP_18_S89	39492910	39492602	37159918	34765328	34765254	20378254
431233LP_18_S137	35905464	35905296	34051230	32782862	32782812	20166946
431229NP_18_S37	55741888	55741806	53070022	52785934	52785914	30161046
431229LP_18_S83	46038268	46038228	43648188	43502228	43502228	23500090
431228NP_18_S312	99834756	99834528	93920578	93389354	93389292	47948252
431228LP_18_S358	114035432	114035128	104635416	102837834	102837744	52153796
431226NP_18_S31	91829636	91829376	86633326	86239524	86239486	46333028
431226BP_18_S127	9487548	9487484	9066058	8864542	8864528	6438586
431226LP_18_S77	126854744	126854464	119545976	118721596	118721450	57631230
431236BP_18_S74	85141238	85141222	80321478	80238474	80238434	46328602
431289LP_18_S273	33161328	33161276	31587618	31226454	31226446	19152942
431287NP_18_S216	125150556	125150124	115829626	115781040	115781036	58869894
431290NP_18_S221	54365800	54365764	47705186	47670654	47670654	25686608
431290LP_18_S268	52433466	52433434	49455348	49408818	49408818	26394018
431293LP_18_S166	72591302	72591274	68811816	68794854	68794854	37856324
431293NP_18_S118	39981258	39981238	38319220	38266686	38266686	21657580
431292LP_18_S259	105126688	105126676	99266648	99211944	99211944	47405116
431292NP_18_S213	59572354	59572336	57219234	57177130	57177128	28864002
439791NP_18_S185	27747412	27747400	26529856	26359406	26359384	15872648
439791BP_18_S187	74423150	74422994	70792366	69820860	69820838	32843582
439791LP_18_S231	30657652	30657558	29303732	28814836	28814822	17042452
439790NP_18_S220	15042138	15042106	14438834	14382506	14382498	9500212
439790RP_18_S175	64849596	64849500	61795810	61766154	61766146	31704462
439790LP_18_S266	33722774	33722686	32326508	32012714	32012706	19931988
435090LP_18_S173	43962858	43962588	41902442	41697652	41697644	25501046
435090BP_18_S125	15309890	15309810	14713064	14614324	14614320	10050156
435085RP_18_S306	25786	25786	24532	23496	23496	20616
435085LP_18_S260	49261494	49261300	47151530	46536870	46536838	27233168
435083NP_18_S39	73578164	73577920	70030574	68004114	68004074	34100116
435083LP_18_S85	74293796	74293730	69388236	68790738	68790724	39289908
435082RP_18_S181	74650636	74650480	70324286	68746630	68746588	36591708

435082LP_18_S271	77469316	77469106	73272188	71432364	71432330	34154300
435082NP_18_S225	20579832	20579802	19554736	19502842	19502842	11813508
435075NP_18_S369	60337602	60337374	56760486	55113774	55113728	28538902
435073RP_18_S35	80093366	80093246	75560840	74521108	74521072	38777762
435073LP_18_S81	16884996	16884952	16156108	15991924	15991922	9844798
435071NP_18_S29	98860718	98860648	91112130	91047972	91047966	50851560
435071RP_18_S123	85335750	85335604	81192514	81095996	81095996	43151180
435071LP_18_S76	69025232	69025172	64715294	64624994	64624986	38401306
435068NP_18_S303	111051900	111051814	105101240	104256186	104256144	52688390
435068LP_18_S349	44869682	44869628	42415788	42083642	42083634	26692860
435075LP_18_S45	92269082	92268884	87356760	85741534	85741498	43775612
439794RP_18_S33	43413842	43413684	41799576	41569328	41569316	23693908
439795RP_18_S169	54731218	54731190	52521692	52233812	52233772	28623186
439795NP_18_S167	105010924	105010742	98526654	96750686	96750622	50876298
439795LP_18_S214	2031928	2031922	1674434	1628356	1628350	921926
439797BP_18_S121	68372666	68372466	65213010	64973130	64973126	36540364
439797LP_18_S27	90791376	90791104	86028410	85589544	85589520	47714034
439797NP_18_S352	64704628	64704442	60748030	60646892	60646866	36782792
439799LP_18_S364	89898468	89898248	84779504	82792480	82792408	43494560
439799NP_18_S318	48026412	48026314	45677454	44976884	44976830	23151980
439821RP_18_S356	88127636	88127614	82211770	81972994	81972990	47378734
439821NP_18_S310	91364042	91363876	85798136	84451768	84451752	45983900
435071BP_18_S171	55028772	55028708	52781396	52657952	52657948	30467016
439818LP_18_S257	85833878	85833674	81396162	79447724	79447660	41548032
439818NP_18_S211	38300032	38299994	36739468	36249302	36249296	24934214
439824NP_18_S183	103787204	103787050	97125806	95727096	95727052	44471892
439816LP_18_S135	86930970	86930726	82330530	80577920	80577838	41837012
439816NP_18_S87	87137468	87137048	82343524	79302090	79302008	39036124
439825LP_18_S269	40458002	40457940	38659198	38382832	38382820	19790698
439825NP_18_S223	55283454	55283442	52017524	51981840	51981836	29173514
439823BP_18_S177	23869638	23869606	22770500	22658650	22658648	13444008
439823LP_18_S129	65189220	65189150	60677638	59876832	59876824	31742794
439801BP_18_S139	77096134	77096008	73372060	72551092	72551074	36528640
439801RP_18_S91	64947954	64947880	61479000	60881578	60881568	36240082
439801LP_18_S324	54081394	54081322	51419932	51216900	51216894	26787196
439801NP_18_S277	28394310	28394266	27134304	26851524	26851520	15779312
439816RP_18_S43	55319984	55319830	52604520	51416246	51416196	28570726
439799RP_18_5_S22	50525718	50525682	48182488	47998690	47998690	25206208
431283NP_18_5_S114	117622334	117622062	101374788	99218620	99218542	51358898
431283LP_18_5_S162	136357708	136357424	116273656	113490028	113489966	53036904
431281BP_18_5_S110	91414458	91414336	86001888	85571532	85571518	41942578
431236BP_18_5_S253	79505020	79504494	74431338	69991558	69991446	36980040
431290LP_18_5_S67	62008226	62008166	59141738	58779822	58779814	31870424
431290NP_18_5_S20	43799956	43799938	41999956	41906548	41906548	24893284
431293RP_18_5_S158	67362738	67362606	62920442	62240704	62240680	35938130
431292LP_18_5_S63	97864270	97864108	92279292	90788960	90788920	46696306
431292NP_18_5_S16	55352108	55352038	52906698	52641470	52641470	27833910
435085BP_18_5_S206	73459346	73458872	68385676	64584318	64584228	32598216
435085LP_18_5_S65	12321644	12321590	10373974	9826596	9826586	5276048
435085RP_18_5_S112	8230358	8230326	7812744	7578282	7578268	5086238
435082RP_18_5_S69	125249018	125248480	116057110	109913828	109913684	51963304
435082LP_18_5_S164	129981410	129981332	118085156	117436170	117436160	58171596
435082NP_18_5_S116	39306718	39306682	37585140	37320166	37320148	20278162
435073LP_18_5_S255	77555338	77552718	69526926	51035218	51034394	26133466

435068RP_18_5_S295	19854228	19854178	18890758	18618476	18618470	11970964
435068NP_18_5_S108	16906450	16906324	16031370	15094598	15094574	9780992
435068BP_18_5_S341	47973422	47973334	45154164	44793416	44793404	21945304
435068LP_18_5_S156	28294712	28294604	26979490	26313056	26313042	14649678
439795BP_18_5_S297	83055458	83054708	76564076	70198816	70198664	34882756
439795LP_18_5_S18	86316720	86316416	79993726	77231600	77231524	38719512
439795NP_18_5_S343	25694320	25694226	24433158	23693956	23693938	13080224
439795RP_18_5_S345	41117106	41117006	38645748	38084850	38084834	21049300
439797BP_18_5_S299	39278004	39277962	37119122	36974616	36974608	21933990
439797LP_18_5_S208	22763032	22762776	21425056	19383994	19383908	12277888
439797NP_18_5_S160	11619896	11619892	11097280	11048286	11048284	7576928
439799LP_18_5_S347	112508234	112507966	104936028	102623962	102623912	44913566
439799NP_18_5_S301	117709404	117709314	108049306	107100064	107100028	55006536
439818BP_18_5_S249	41054120	41053986	38934822	38147796	38147776	22224230
439818LP_18_5_S61	103808066	103807936	96414642	95230478	95230426	48578900
439818NP_18_5_S14	41540004	41539980	39611674	39368594	39368588	24793516
439818RP_18_5_S204	42436516	42436162	40189042	37347422	37347338	20585722
431236LP_18_5_S251	120757452	120757086	110610512	107432544	107432468	54817786
431281NP_20_S192	34418776	34418228	32200628	28038496	28038410	16522014
431281LP_20_S237	15860794	15860474	14851996	12895216	12895192	8813696
431283LP_20_S150	31494556	31494430	30118126	29789018	29789002	19917280
431283NP_20_S102	10853448	10853416	10428968	10317002	10316996	6916306
431283BP_20_S104	64428848	64428676	61579144	61537204	61537204	32258856
431281BP_20_S98	28559834	28559736	27160546	26230950	26230944	16311218
431242NP_20_S291	73202718	73202626	69607000	68823898	68823878	36806174
431242BP_20_S337	74405946	74405864	67496046	66913442	66913420	35332118
431236LP_20_S285	21757430	21756702	19999134	14815376	14815212	9364218
431218NP_20_S194	70183512	70182702	65008696	58034114	58033972	30962448
431218LP_20_S239	33410996	33410654	31442100	29142162	29142086	16852854
431229NP_20_S200	57093572	57093514	54749744	54452608	54452604	29555502
431229LP_20_S245	90851600	90851276	85370972	81224920	81224800	42588952
431236BP_20_S241	25295354	25294786	23588020	19631172	19631094	12289602
431290LP_20_S55	344614	344614	331694	329296	329296	275062
431293RP_20_S146	15410518	15410146	14310762	11441092	11440994	7694854
431293LP_20_S329	50995168	50994000	47121424	38530220	38529998	21154482
431293NP_20_S283	34679586	34679018	32355376	27431456	27431332	16240650
431292NP_20_S4	25997998	25997886	24748198	24227706	24227700	15129058
431292LP_20_S51	52732584	52731826	48894320	42450038	42449854	24668994
435085RP_20_S100	47830034	47829400	45049188	40022626	40022426	22153000
435085LP_20_S53	53350388	53349922	50252378	45928124	45928048	24833886
435083LP_20_S247	113136254	113136222	105116332	104637228	104637208	56473924
435083NP_20_S202	111828640	111828502	105559062	104489214	104489192	51765136
435082RP_20_S339	104502354	104502272	97268782	96620774	96620724	46635630
435082LP_20_S59	150000000	149999830	141542408	140915502	140915472	60441244
435082NP_20_S12	79594868	79594746	73127990	72324496	72324480	43550154
435073RP_20_S198	86310248	86310020	81518666	79467644	79467582	39884034
435073LP_20_S243	64677798	64677490	60684082	58018132	58018040	33626626
439795RP_20_S333	67809692	67809614	63695764	63036568	63036548	31986076
439795LP_20_S6	31278502	31278372	28811262	27884154	27884140	18835254
439795NP_20_S331	40642534	40642304	38480844	37136060	37136044	20655370
439797BP_20_S287	59850538	59849684	55863520	47470886	47470716	25819166
439797LP_20_S196	61448322	61447878	57962144	54028140	54028030	29118480
439797NP_20_S148	25060324	25060264	23940892	23584976	23584976	14638640
439799NP_20_S106	58248340	58248274	55609240	55143810	55143804	31526938
439799LP_20_S154	54696690	54696612	52218510	51730328	51730318	27930104

435068LP_20_S144	33617430	33616952	31446084	27708698	27708526	17201834
435068NP_20_S96	45772466	45771726	42755832	36410770	36410596	21662008
439799RP_20_S293	111588440	111588242	101512934	99495340	99495300	51559166
439818LP_20_S49	34467452	34467264	32922422	31673062	31673016	18714378
439818NP_20_S2	39054626	39054386	37138098	35160902	35160876	21650948
439823BP_20_S335	89221764	89221696	83628052	83220222	83220208	44490496
439823LP_20_S289	29284638	29284588	28014708	27798492	27798490	17328324
439825LP_20_S57	129749152	129749028	120377336	119288894	119288868	58508152
439825NP_20_S10	79468250	79468194	75831818	75378456	75378454	38895970
439825RP_20_S152	74755038	74754872	71200924	70205424	70205408	34885632
431218LP_22_S238	25356730	25356448	22936304	20724500	20724456	13225768
431281NP_22_S191	29358128	29357988	27773928	26687680	26687642	17829934
431281LP_22_S236	29302682	29302538	27796536	26999898	26999880	16020890
431287LP_22_S54	71164220	71163862	67464676	65439994	65439910	36754608
439799NP_22_S111	76151474	76151412	71154578	70692718	70692714	40918934
439825NP_22_S15	60242466	60242392	57481042	57337386	57337382	31240252
431284NP_22_S113	65083870	65083440	60942900	58027164	58027092	30091578
431283NP_22_S107	76218216	76218032	72985856	72660880	72660878	38253788
431284BP_22_S161	58859938	58859508	55512444	52411530	52411462	29726830
431283LP_22_S155	80698212	80697902	70401930	70000910	70000896	45858476
435069LP_22_S68	28050116	28050082	26767792	26648968	26648968	15057008
435071BP_22_S334	60058152	60057706	56986388	53738442	53738358	29135786
435069NP_22_S21	49738452	49738416	47238794	47127718	47127718	24772840
431283BP_22_S109	64697392	64697202	60916190	60432752	60432734	39916486
431281BP_22_S97	71667210	71666882	67021232	64241110	64241074	34865612
431277NP_22_S101	85822986	85822880	79207834	78067890	78067856	41863758
431279LP_22_S56	78364054	78364032	74893134	74727902	74727896	41435430
431279NP_22_S9	84632548	84632514	79994742	79941374	79941370	42552586
431277LP_22_S149	5906440	5906398	5659540	5465178	5465148	4320156
431242BP_22_S342	108510596	108510514	99323356	98739172	98739160	49806680
431242NP_22_S296	70706174	70706150	67498660	67404956	67404956	37675920
431242RP_22_S250	85115628	85115596	80433678	80116354	80116340	46007408
431236LP_22_S284	61137774	61137338	57301318	53575370	53575288	30623766
431236RP_22_S427	39328068	39327836	34067774	31988028	31987972	17733414
431218NP_22_S193	25713698	25713510	24323924	23090430	23090410	14020148
431233NP_22_S210	13628290	13628076	12852306	11488720	11488700	7635060
431233LP_22_S256	40604892	40604228	37774702	32700688	32700524	18391512
431229NP_22_S205	109210398	109210354	102122978	102071414	102071408	52695510
431228NP_22_S105	94346374	94346054	88264074	87227982	87227918	46408758
431228LP_22_S153	88200580	88200398	83711846	82912806	82912782	44621050
431226NP_22_S199	104361150	104360628	96508672	94370426	94370330	50932250
431226LP_22_S244	57996928	57996750	55423882	55319298	55319258	30242668
431226BP_22_S292	60585296	60585122	58010134	57454542	57454518	26895830
431236BP_22_S240	32165908	32165766	30165702	29315798	29315776	18425560
431289NP_22_S19	34317082	34316998	32602184	32162678	32162666	18181988
431289RP_22_S454	7360974	7360880	6974168	6623770	6623756	4421434
431289LP_22_S66	18984004	18983866	17940518	17037908	17037872	12076856
431287NP_22_S7	74231010	74230818	70819976	70491000	70490990	39202804
431290NP_22_S13	69932916	69932518	66382552	65522912	65522892	39110124
431290LP_22_S60	91142888	91142554	83406666	82863176	82863164	49454364
431293BP_22_S445	23246188	23246108	22059660	21596810	21596794	11562752
431293LP_22_S328	34719352	34719222	33135112	32637200	32637178	18633704
431292NP_22_S3	50680128	50679982	48187928	47048550	47048518	25717186
431292LP_22_S50	53241714	53240786	49643630	41889660	41889438	23756664
439791LP_22_S348	32894330	32893804	30756858	26905968	26905864	15580876

439791NP_22_S302	48380214	48379688	45483076	41659136	41659052	23745072
439791BP_22_S304	24125354	24125256	23015462	22303380	22303366	13705492
439790NP_22_S11	66481630	66481420	62980294	62702518	62702500	37053852
439790RP_22_S338	56696246	56696092	53424580	52788170	52788156	29705322
439790LP_22_S58	41070346	41070206	39336492	38996284	38996256	23617984
435090LP_22_S336	74617654	74617278	70727042	70457058	70457054	38376004
435090BP_22_S290	78905752	78905310	74541022	72961608	72961538	40104000
435085RP_22_S99	37765894	37765816	35702776	34795078	34795054	21250302
435085LP_22_S52	15361318	15361020	14389666	12203088	12203036	8117194
435083LP_22_S252	72714580	72714538	69324980	69192038	69192030	35036238
435083NP_22_S207	110668820	110668734	105240264	104617354	104617326	49755244
435083RP_22_S412	93056374	93056334	85364688	85093140	85093140	44309218
435083BP_22_S380	71774886	71774860	65304124	64962780	64962776	35665214
435082RP_22_S344	104181868	104181688	96292656	94196418	94196254	43657878
435082BP_22_S423	99042056	99041982	90799928	90429706	90429698	43396298
435082LP_22_S64	130126308	130126210	121681200	121466820	121466818	60358670
435082NP_22_S17	109087806	109087754	102312544	101878544	101878526	55980482
435075NP_22_S117	26196706	26196672	24984082	24861996	24861994	13973698
435075BP_22_S350	33079864	33079692	31543828	30387420	30387374	15997472
435075LP_22_S165	85399192	85398940	81089132	78828164	78828088	41048546
435073RP_22_S203	42978534	42978348	40998964	39522282	39522252	22086230
435073LP_22_S248	35217874	35217810	33691922	32914210	32914176	20011254
435071NP_22_S197	30443508	30443478	28874470	28621540	28621540	19437656
435071RP_22_S288	70266806	70266708	66270008	65818172	65818150	36852340
435071LP_22_S242	88406210	88406004	82606016	81050912	81050876	44131182
435068RP_22_S402	39206744	39206594	36188346	35214928	35214902	19215336
435068LP_22_S143	7006750	7006698	6647168	6391498	6391490	4799288
439821NP_22_S103	42515466	42515330	40655560	39587512	39587482	23679834
439818BP_22_S425	36182760	36182588	31623852	29790250	29790198	17263188
439795LP_22_S5	60502400	60502066	44224052	41034536	41034466	32120616
439795NP_22_S330	25322034	25321888	24021238	23254038	23254000	13484514
439795RP_22_S332	30437898	30437616	28447816	26455654	26455608	14523352
439797BP_22_S286	38224082	38223890	36190192	34384582	34384534	20628392
439797LP_22_S195	32047746	32047614	30031236	29046150	29046108	18499224
439797NP_22_S147	36509442	36508630	34022170	27919886	27919714	16317940
439799RP_22_S298	85418802	85418654	81118774	80089756	80089740	40601418
439799LP_22_S159	100964896	100964608	94873840	92108876	92108822	48008496
439825BP_22_S434	65366756	65366732	59302938	59291026	59291026	32221544
439825LP_22_S62	39254082	39254062	37579292	37573924	37573922	22211504
439823BP_22_S340	49340394	49340382	46914732	46899770	46899770	23464328
439794LP_22_S246	148370616	148369984	137894444	136131444	136131342	65114192
439794RP_22_S201	68063070	68062742	62640878	62519014	62519010	37860924
439824NP_22_S300	38087272	38087158	36349322	35519804	35519768	20713954
439801BP_22_S258	39904094	39903956	38125042	37227902	37227884	19445294
439801LP_22_S70	15547898	15547882	14898538	14805234	14805234	9713694
439801RP_22_S212	24302426	24302332	23180998	22413830	22413814	13056242
439816RP_22_S163	11782176	11782096	11194898	10803630	10803616	7277458
439816NP_22_S209	23440642	23440600	15215636	14842844	14842824	12540600
439816LP_22_S254	41814792	41814632	39915510	39534060	39534050	22502556
439823LP_22_S294	103496308	103496028	97531756	97480044	97480044	49767778
439824BP_22_S414	34436298	34435916	30159074	26984296	26984216	16122990
439824LP_22_S346	50362526	50362262	47612190	45986758	45986734	23618428
439816BP_22_S391	53515976	53515880	49164538	48628058	48628042	25332446
439818LP_22_S48	81440142	81439820	75497866	72254086	72254036	38685290
439818NP_22_S1	56690526	56689886	53325476	48149584	48149436	29728446

439818RP_22_S444	16539528	16539474	13466802	13146384	13146382	6794026

Table S10.

Microbial origin and classification of antimicrobial resistance genes (> 1% relative abundance) detected in female and male mice in overall study.

Antimicrobial resistance gene	Microbial origin	Class of resistance drug	Mechanism of resistance
AAC(6')-Ii	*E. faecium*	Aminoglycoside	Antibiotic inactivation
acrB	*P. distasonis,* *C. amalonaticus,* *K. michiganensis,* *K. pneumoniae,* *C. koseri,* *C. freundii,* *E. coli,* *S. flexneri*	Phenicol, Rifamycin, Tetracycline, Beta-lactam, Fluoroquinolone, Disinfecting agents and antiseptics	Efflux pump
acrD	*K. oxytoca,* *K. michiganensis,* *C. amalonaticus,* *E. coli,* *K. pneumoniae,* *C. koseri,* *B. thetaiotaomicron*	Aminoglycoside	Efflux pump
AcrE	*E. coli,* *C. amalonaticus*	Beta-lactam, Fluoroquinolone	Efflux pump
APH(3')-Ia	*S. enterica,* *K. pneumoniae,* *M. tuberculosis,* *K. michiganensis,* *A. nosocomialis,* *P. multocida,* *E. coli,* *A. baumannii,* *K. aerogenes*	Aminoglycoside	Antibiotic inactivation
APH(3')-VIIa	--	Aminoglycoside	Antibiotic inactivation
ArnT	*K. oxytoca,* *K. michiganensis,* *K. pneumoniae*	Peptide	Antibiotic target alteration
bacA	*C. amalonaticus,* *E. coli*	Peptide	Antibiotic target alteration
baeR	*K. michiganensis,* *K. oxytoca,* *E. coli,* *C. koseri,* *C. amalonaticus,* *K. pneumoniae*	Aminoglycoside, Aminocoumarin	Efflux pump
baeS	*C. amalonaticus,* *E. coli*	Aminoglycoside, Aminocoumarin	Efflux pump
Bifidobacterium adolescentis rpoB mutants conferring resistance to rifampicin	*B. longum,* *B. animalis,* *K. pneumoniae,* *E. coli,* *E. hormaechei*	Rifamycin	Antibiotic target alteration
Bifidobacterium bifidum ileS conferring resistance to mupirocin	--	Mupirocin	Antibiotic target alteration
CepA-49	--	Beta-lactam	Antibiotic inactivation
cpxA	*C. amalonaticus,*	Aminoglycoside,	Efflux pump

	E. coli, *C. koseri*, *C. freundii*	Aminocoumarin	
CRP	*C. amalonaticus*, *K. oxytoca*, *C. koseri*, *K. pneumoniae*, *E. coli*, *M. morganii*	Beta-lactam, Fluoroquinolone, Macrolide	Efflux pump
Escherichia coli acrA	*C. amalonaticus*, *E. coli*, *C. koseri*	Fluoroquinolone, Beta-lactam, Phenicol, Tetracycline, Rifamycin, Disinfecting agents and antiseptics	Efflux pump
emrA	*K. michiganensis*, *E. coli*, *K. oxytoca*, *E. albertii*	Fluoroquinolone	Efflux pump
emrR	*C. amalonaticus*, *K. oxytoca*, *C. koseri*, *K. pneumoniae*, *E. coli*	Fluoroquinolone	Efflux pump
eptB	*K. oxytoca*, *K. michiganensis*, *K. pneumoniae*	Peptide	Antibiotic target alteration
evgS	*E. coli*, *S. dysenteriae*	Beta-lactam, Fluoroquinolone, Macrolide, Tetracycline	Efflux pump
FosA6	*K. oxytoca*, *K. michiganensis*, *K. huaxiensis*, *K. quasipneumoniae*, *K. pneumoniae*	Phosphonic acid	Antibiotic inactivation
gadX	*E. coli*	Beta-lactam, Fluoroquinolone, Macrolide	Efflux pump
H-NS	*K. michiganensis*, *C. amalonaticus*, *K. oxytoca*, *C. koseri*, *K. pneumoniae*, *S. boydii*	Beta-lactam, Fluoroquinolone, Macrolide, Tetracycline	Efflux pump
Klebsiella pneumoniae acrA	*S. enterica*, *C. amalonaticus*, *K. pneumoniae*	Beta-lactam, Fluoroquinolone, Rifamycin, Phenicol, Tetracycline, Disinfecting agents and antiseptics	Efflux pump
Klebsiella pneumoniae KpnE	*C. amalonaticus*, *K. oxytoca*, *K. pneumoniae*, *C. koseri*,	Rifamycin, Tetracycline, Aminoglycoside, Peptide,	Efflux pump

	K. michiganensis, *E. coli*	Beta-lactam, Macrolide, Disinfecting agents and antiseptics	
Klebsiella pneumoniae KpnF	*K. oxytoca,* *K. pneumoniae,* *K. michiganensis*	Rifamycin, Tetracycline, Aminoglycoside, Peptide, Beta-lactam, Macrolide, Disinfecting agents and antiseptics	Efflux pump
Klebsiella pneumoniae KpnG	*K. oxytoca,* *K. michiganensis,* *K. pneumoniae*	Aminoglycoside, Peptide, Beta-lactam, Fluoroquinolone, Macrolide	Efflux pump
Klebsiella pneumoniae KpnH	*K. oxytoca,* *C. amalonaticus,* *K. michiganensis,* *E. coli,* *C. koseri,* *K. pneumoniae*	Fluoroquinolone, Beta-lactam, Peptide, Aminoglycoside, Macrolide	Efflux pump
Klebsiella pneumoniae OmpK37	*K. pneumoniae*	Beta-lactam	Reduced permeability to antibiotic
LptD	*K. oxytoca,* *K. michiganensis,* *K. pneumoniae*	Rifamycin Aminocoumarin Peptide	Efflux pump
marA	*C. amalonaticus,* *E. coli,* *C. koseri*	Rifamycin, Phenicol, Beta-lactam, Tetracycline, Fluoroquinolone, Disinfecting agents and antiseptics	Efflux pump
mdtA	*E. coli*	Aminocoumarin	Efflux pump
mdtB	*C. amalonaticus,* *E. coli,* *C. koseri*	Aminocoumarin	Efflux pump
mdtC	*E. coli,* *C. amalonaticus,* *C. koseri*	Aminocoumarin	Efflux pump
MdtK	--	Fluoroquinolone	Efflux pump
mdtN	*E. coli*	Nucleoside, Disinfecting agents and antiseptics	Efflux pump
mdtO	*E. coli*	Nucleoside, Disinfecting agents and antiseptics	Efflux pump
mdtP	*E. coli*	Nucleoside, Disinfecting agents and antiseptics	Efflux pump
mel	*P. vulgatus,* *S. suis,* *E. faecium*	Macrolide, Lincosamide, Streptogramin	Antibiotic target protection
msbA	*K. oxytoca,*	Nitroimidazole	Efflux pump

	C. amalonaticus, *E. coli,* *C. koseri,* *K. michiganensis,* *K. pneumoniae*		
msrC	*E. faecium*	Macrolide, Lincosamide, Streptogramin	Antibiotic target protection
OmpA	*K. michiganensis,* *K. oxytoca,* *K. pneumoniae*	Peptide	Reduced permeability to antibiotic
oqxA	*K. oxytoca,* *K. pneumoniae,* *C. amalonaticus,* *K. michiganensis*	Fluoroquinolone, Tetracycline, Diaminopyrimidine, Nitrofuran	Efflux pump
oqxB	*K. oxytoca,* *K. michiganensis,* *K. pneumoniae,* *C. amalonaticus,* *A. xylosoxidans,* *P. distasonis*	Fluoroquinolone, Tetracycline, Diaminopyrimidine, Nitrofuran	Efflux pump
OXY-1-1	*K. michiganensis*	Beta-lactam	Antibiotic inactivation
OXY-1-3	*K. michiganensis*	Beta-lactam	Antibiotic inactivation
OXY-1-4	*K. michiganensis*	Beta-lactam	Antibiotic inactivation
ramA	*Enterobacter (chromosome)*	Phenicol, Rifamycin, Beta-lactam, Tetracycline, Fluoroquinolone, Disinfecting agents and antiseptics	Efflux pump
tet(M)	*S. suis,* *E. faecium*	Tetracycline	Antibiotic target protection
tet(O)	*S. suis,* *A. hadrus,* *G. urolithinfaciens*	Tetracycline	Antibiotic target protection
tet(O/M/O)	*G. urolithinfaciens*	Tetracycline	Antibiotic target protection
tet(O/32/O)	*E. ramosum,* *E. hirae,* *S. suis,* *E. clostridioformis,* *M. mulieris*	Tetracycline	Antibiotic target protection
tet(Q)	*B. thetaiotaomicron,* *P. vulgatus,* *B. fragilis,* *B. ovatus,* *B. caccae,* *P. distasonis*	Tetracycline	Antibiotic target protection
tet(W)	*B. longum,* *C. aerofaciens,* *B. breve*	Tetracycline	Antibiotic target protection
tet(W/N/W)	*T. pyogenes,* *E. lenta,* *B. breve,* *S. suis,*	Tetracycline	Antibiotic target protection

	L. johnsonii, *C. aerofaciens*		
tet(W/32/O)	*T. pyogenes*	Tetracycline	Antibiotic target protection
tet(32)	*E. hirae,* *E. clostridioformis,* *E. ramosum,* *B. longum*	Tetracycline	Antibiotic target protection
tet(40)	--	Tetracycline	Efflux pump
tet(44)	*E. clostridioformis,* *C. perfringens*	Tetracycline	Antibiotic target protection
TolC	*E. coli*	Beta-lactam, Rifamycin, Aminocoumarin, Fluoroquinolone, Macrolide, Tetracycline, Aminoglycoside, Peptide, Phenicol, Disinfecting agents and antiseptics	Efflux pump
vanR gene in vanD cluster	--	Glycopeptide	Antibiotic target alteration
vanR gene in vanG cluster	--	Glycopeptide	Antibiotic target alteration
vanS gene in vanD cluster	--	Glycopeptide	Antibiotic target alteration
vanV gene in vanB cluster	--	Glycopeptide	Antibiotic target alteration
vanY gene in vanG cluster	--	Glycopeptide	Antibiotic target alteration
YojI	*E. coli,* *S. flexneri,* *S. sonnei*	Peptide	Efflux pump

5

6.3 Estropausal gut microbiota transplant improves measures of ovarian function in adult mice

https://doi.org/10.1101/2024.05.03.592475 ((full text in PDF version)

Estropausal gut microbiota transplant improves measures of ovarian function in adult mice

Minhoo Kim[1], Justin Wang[1,2,3], Steven E. Pilley[4], Ryan J. Lu[1,5], Alan Xu[1,6], Younggyun Kim[1,7], Minying Liu[8], Xueyan Fu[8], Sarah L. Booth[8], Peter J. Mullen[1,4,9], and Bérénice A. Benayoun[1,9, 10,11,12]

1. Leonard Davis School of Gerontology, University of Southern California, Los Angeles, CA 90089, USA.
2. Department of Quantitative and Computational Biology, University of Southern California, Los Angeles, CA 90089, USA.
3. Department of Chemistry, University of Southern California, Los Angeles, CA 90089, USA.
4. Department of Molecular Microbiology and Immunology, Keck School of Medicine, University of Southern California, Los Angeles, CA, USA
5. Graduate Program in the Biology of Aging, University of Southern California, Los Angeles, CA 90089, USA.
6. Thomas Lord Department of Computer Science, USC Viterbi School of Engineering, Los Angeles, CA 90089, USA.
7. Alfred E. Mann Department of Biomedical Engineering, University of Southern California, Los Angeles, CA 90089, USA.
8. Jean Mayer USDA Human Nutrition Research Center on Aging at Tufts University, Boston, MA 02111, USA
9. Norris Comprehensive Cancer Center, Keck School of Medicine, University of Southern California, Los Angeles, CA, USA
10. Molecular and Computational Biology Department, USC Dornsife College of Letters, Arts and Sciences, Los Angeles, CA 90089, USA.
11. Biochemistry and Molecular Medicine Department, USC Keck School of Medicine, Los Angeles, CA 90089, USA.
12. USC Stem Cell Initiative, Los Angeles, CA 90089, USA.

*Correspondence: berenice.benayoun@usc.edu

Estropausal gut microbiota transplant improves measures of ovarian function in adult mice

Minhoo Kim[1], Justin Wang[1,2,3], Steven E. Pilley[4], Ryan J. Lu[1,5], Alan Xu[1,6], Younggyun Kim[1,7], Minying Liu[8], Xueyan Fu[8], Sarah L. Booth[8], Peter J. Mullen[1,4,9], and Bérénice A. Benayoun[1,9, 10,11,12]

1. Leonard Davis School of Gerontology, University of Southern California, Los Angeles, CA 90089, USA.

2. Department of Quantitative and Computational Biology, University of Southern California, Los Angeles, CA 90089, USA.

3. Department of Chemistry, University of Southern California, Los Angeles, CA 90089, USA.

4. Department of Molecular Microbiology and Immunology, Keck School of Medicine, University of Southern California, Los Angeles, CA, USA

5. Graduate Program in the Biology of Aging, University of Southern California, Los Angeles, CA 90089, USA.

6. Thomas Lord Department of Computer Science, USC Viterbi School of Engineering, Los Angeles, CA 90089, USA.

7. Alfred E. Mann Department of Biomedical Engineering, University of Southern California, Los Angeles, CA 90089, USA.

8. Jean Mayer USDA Human Nutrition Research Center on Aging at Tufts University, Boston, MA 02111, USA

9. Norris Comprehensive Cancer Center, Keck School of Medicine, University of Southern California, Los Angeles, CA, USA

10. Molecular and Computational Biology Department, USC Dornsife College of Letters, Arts and Sciences, Los Angeles, CA 90089, USA.

11. Biochemistry and Molecular Medicine Department, USC Keck School of Medicine, Los Angeles, CA 90089, USA.

12. USC Stem Cell Initiative, Los Angeles, CA 90089, USA.

*Correspondence: berenice.benayoun@usc.edu

Abstract

Decline in ovarian function with age not only affects fertility but is also linked to a higher risk of age-related diseases in women (*e.g.* osteoporosis, dementia). Intriguingly, earlier menopause is linked to shorter lifespan; however, the underlying molecular mechanisms of ovarian aging are not well understood. Recent evidence suggests the gut microbiota may influence ovarian health. In this study, we characterized ovarian aging associated microbial profiles in mice and investigated the effect of the gut microbiome from young and estropausal female mice on ovarian health through fecal microbiota transplantation. We demonstrate that the ovarian transcriptome can be broadly remodeled after heterochronic microbiota transplantation, with a reduction in inflammation-related gene expression and trends consistent with transcriptional rejuvenation. Consistently, these mice exhibited enhanced ovarian health and increased fertility. Using metagenomics-based causal mediation analyses and serum untargeted metabolomics, we identified candidate microbial species and metabolites that may contribute to the observed effects of fecal microbiota transplantation. Our findings reveal a direct link between the gut microbiota and ovarian health.

Keywords

Microbiome, ovarian aging, menopause, 16S amplicon sequencing, ovarian RNA-seq

Main

Women are born with a definitive number of ovarian follicles and the gradual decrease in the number of the follicles ultimately leads to menopause[1-3]. The onset of menopause has been linked with an elevated risk of numerous age-related conditions, including osteoporosis and dementia[4-6]. Moreover, a later onset of menopause has been identified as a potential predictor of extended lifespan[7,8]. While the profound effects of menopause on the health- and lifespan of women are well-documented, the factors that contribute to ovarian aging and the strategies for its prevention remain poorly understood.

During the reproductive years, the hypothalamus-pituitary-ovarian hormone axis ensures the proper production and release of hormones necessary for ovulation and menstruation[9]. However, as menopause progresses, ovaries become less responsive due to reduced follicle numbers, ultimately leading to the hormonal imbalances characteristic of menopause[10]. Specifically, the serum concentrations of follicle-stimulating hormone (FSH) and luteinizing hormone (LH) increase, whereas anti-Müllerian hormone (AMH) and Inhibin A (INHBA) decrease with menopause progression[11-13]. These hormonal adjustments are hallmarks of the menopausal transition and highlight the diminished function of the ovaries[10]. Importantly, this disrupted feedback mechanism has been attributed to the wide array of menopausal symptoms and health risks associated with this transition phase[14,15]. For instance, recent studies have shown FSH receptor activation by FSH in the brain increases susceptibility for Alzheimer's disease pathogenesis in women and blockade of FSH improves cognition in a mouse model of Alzheimer's disease[14,16].

The adult human gut microbiome is composed of approximately 10^{13} to 10^{14} micro-organisms[17,18]. The microbiome consists of bacteria, viruses and fungi, with bacteria representing the largest proportion of the microbial population[19]. Perturbations in the gut microbiota configuration are reported to lead to development and/or progression of serious disease, including diabetes and depression[20,21]. Interestingly, reported health effects of fecal microbiota derived from aged individuals have been inconsistent[22,23]. For example, one study demonstrated that fecal microbiota transplantation (FMT) from 24-month-old mice to 3-month-old mice led to the acceleration of age-associated phenotypes in the brain, retina, and gut of the recipient mice[22]. In contrast, another study found that grafting of fecal microbiota from 24-month-old mice to 5- to 6-week-old germ-free mice enhanced neurogenesis in the hippocampus and induced intestinal

growth[23]. These findings underscore the microbiome's complex, multifaceted effects on various organ systems throughout life, significantly affecting host health.

A recent study discovered that women with premature ovarian insufficiency exhibited significantly altered gut microbial profiles compared to healthy women[24]. Notably, alternations in the gut microbiome in premature ovarian insufficiency patients were associated with changes in serum hormone levels of key ovarian endocrine markers, including FSH, LH and AMH[24]. Similarly, the composition of the gut microbiome has been implicated in the development of polycystic ovary syndrome (PCOS), a disorder characterized by hyperandrogenism and polycystic ovaries[25]. Specifically, FMT of samples from PCOS patients to mice resulted in ovarian dysfunction in otherwise healthy recipient mice[25]. Consistent with the importance of a healthy microbiome for ovarian function, another study has shown that 17β-estradiol levels are significantly lowered in the germ-free female mice[26]. Moreover, transcriptome analysis of sexual development marker genes of the liver and histological studies of ovarian follicle development in germ-free female mice indicated that sexual maturation is perturbed in microbiota-depleted mice[26]. Importantly, the gut microbiota has been shown to modulate serum estrogen levels (through the “estrobolome”), further highlighting the potential role of the gut microbiota in female reproductive health[27]. The gut microbiota regulates action of estrogens through the secretion of β-glucuronidase, an enzyme that deconjugates estrogens into their active forms[27-29]. Dysbiosis of the gut microbiota can impair this process, leading to a reduction in circulating estrogens and potentially contributing to the development of estrogen-modulated conditions[27]. Collectively, these findings highlight a significant causal relationship between the gut microbiota and ovarian function and health, suggesting a pivotal role for microbial communities in modulating female reproductive conditions.

In this study, we analyzed the gut microbial profiles of young and estropausal (post-reproductive phase in rodents, analogous to human menopause) female mice via 16S rRNA amplicon sequencing and explored how the distinct microbial communities affect ovarian health through FMT experiments in young female mice. Unbiased RNA-seq analyses revealed that modifying the gut microbiota leads to profound changes in the ovarian transcriptomic landscape. Surprisingly, heterochronic gut microbiota transplant from estropausal mice to young female recipients led to a reduction in inflammation-related gene expression in the ovaries, and dampened expression of genes that tend to be upregulated in aging

ovaries. Consistently, we observed improved ovarian function and health in the estropausal FMT recipients, supporting a surprising finding whereby old gut microbiota has beneficial effects on ovarian health. Lastly, we identified specific microbial genera and species, through 16S rRNA amplicon sequencing and whole genome shotgun sequencing, respectively, that might drive the observed transcriptomic changes in the ovaries via causal mediation analyses. Overall, our study shows that manipulating the gut microbiota can directly influence ovarian function and health.

Results

Young and estropausal female mice show distinct fecal microbial profiles

To investigate the potential link between changes in the gut microbiome and ovarian aging in mice, we assessed (1) the ovarian health state and (2) microbial profiles of young (YF, 4-months) and naturally aged estropausal (EF, 20-months) C57BL/6JNia female mice[30] (Fig. 1A). To quantify the overall ovarian health state of the mice, we developed a composite "ovarian health index", modeled after the concept of frailty index[31] (Extended Data Fig. 1A). Our goal in constructing this index was to create a standardized, integrative tool that would enable comparative analysis of ovarian function across different datasets. The index combines ovarian follicle counts and serum levels of AMH, FSH, and Inhibin A, using a 3-tier scoring system based on the median values of the young and estropausal groups as reference points. Specifically, values beyond the young median are scored as 3, values between the medians of the young and estropausal groups are scored as 2, and values beyond the estropausal median are scored as 1 (Extended Data Fig. 1A). Given that ovarian follicle count and serum levels of key pituitary and ovarian hormones—AMH, FSH, and Inhibin A—are widely recognized as reliable indicators of ovarian health[32-35], we combined these parameters to form a comprehensive and objective evaluation of ovarian function (Fig.1A-D; see Methods). Additionally, to facilitate accessibility and broader use of the ovarian health index, we developed an R shiny application, allowing the public to analyze their own datasets using this tool (https://alanxu-usc.shinyapps.io/Ovarian_Health_Index_Calculator/).

Consistent with previous reports[30,36], we observed a significant reduction in ovarian follicle counts and serum levels of AMH and Inhibin A, as well as increased FSH levels in the estropausal group (Fig.1B,C and Extended Data Fig. 1B-D). Furthermore, the estropausal group exhibited a significantly lower ovarian health index score compared to the young group (p-value ~0.0117; Fig.1D), validating the subsequent use of our index as a measure of ovarian health and function.

We then collected fecal samples from four independent cohorts of mice and performed 16S rRNA V3-V4 amplicon sequencing to compare the gut microbial profiles of the young and estropausal female mice. 16S rRNA amplicon sequencing allows identification of bacteria at the genus level by amplifying and sequencing variable regions of the 16S rRNA gene (*e.g.* V3-V4 region), which contains unique sequences specific to different species[37]. Quantification and analysis of the sequences from the variable

regions, or amplicon sequence variants (ASVs), have been shown to provide important insights of the microbial compositions and environment[38].

Our analysis focused on both beta diversity, which assesses differences between microbial communities, and alpha diversity, which looks at diversity within a community[39,40]. Beta diversity was evaluated using the Bray-Curtis dissimilarity and Jaccard index (Extended Data Fig. 2A). The analysis of Bray-Curtis dissimilarity and Jaccard index, conducted by cohort, revealed a distinct separation between the young and estropausal female groups (Extended Data Fig. 2A). Moreover, the results of the principal component analysis, applied to center log-ratio (CLR)-transformed and batch-corrected ASV counts, further highlighted clear clustering between the young and estropausal females across 4 independent cohorts of animals (Fig. 1E). Batch correction was performed to account for technical variability across cohorts[41]. Alpha diversity measures the diversity within a single microbial community or ecosystem, focusing on the variety and abundance of ASVs in a specific environment[36]. Importantly, estropausal females exhibited significantly higher scores in both observed features and Shannon entropy compared to the young female group (Fig. 1F). Our results suggest that the estropausal females have a higher biodiversity and increased species richness and evenness. This pattern of increased alpha diversity with age in female mice aligns with findings from previous studies[42]. However, in humans, alpha diversity has been shown variable trends with age, with both increases and decreases reported in different studies[43,44]. Additionally, a recent study reported elevated alpha diversity indices in PCOS model mice[45].

We next asked which specific microbial genera changed in abundance between young and estropausal female mice recurrently across our 4 independent cohorts (Fig. 1G and Extended Data Fig. 2B, 3). Our analysis identified three genera that were more abundant (“UP in EF”) and six that were less abundant (“DOWN in EF”) in the microbiota of estropausal females (Fig. 1G and Extended Data Fig. 2B, 3; absolute effect size > 1, adjusted p-value < 0.05). Most of the differentially abundant genera belonged to the *Lachnospiraceae* family, offering a potential lead for future research on their impact on ovarian health. Previous studies have reported a relative decrease in abundance of microbial species from the *Lachnospiraceae* family with age in humans[46,47]. Further studies will be required to elucidate the molecular mechanisms through which these genera affect ovarian function and health. Additionally, we conducted a predictive analysis of functional consequences of these changes in microbial abundances

using PICRUSt2[48] (Fig. 1H). This analysis suggested an increase in metabolic pathways such as ketogluconate metabolism and the superpathway of glycerol degradation to 1,3-propanediol, while pathways including the superpathway of fatty acid biosynthesis initiation and phospholipases were predicted to decrease in the estropausal group (Fig. 1H). These predicted metabolic changes, including an increase in ketoglutarate and alterations in lipid metabolism, have been previously associated with ovarian cancers, underscoring the potential relevance of our findings to understanding ovarian health[49,50]. Our results collectively underscore the pronounced differences in the fecal microbial profiles between young and estropausal females.

Chemically-induced premature ovarian failure model mice show distinct fecal microbial profiles

The 4-VinylCyclohexene Diepoxide (VCD)-injected mouse model is a follicle-deplete, ovary-intact animal model that is known to recapitulate many key aspects of human ovarian aging[51,52]. VCD accelerates atresia by causing selective loss of primary and primordial follicles in the ovary, while leaving the rest of the ovarian structure intact for residual hormone production[51,52]. We assessed the ovarian health index and fecal microbial profiles of vehicle- and VCD-exposed mice (CTL and VCD, respectively; Extended Data Fig. 4A). Briefly, 4-month-old C57BL/6NTac female and male mice were subjected to daily intraperitoneal injections of either vehicle (safflower oil) or VCD (at a dosage of 160 mg/kg/day) for 15 consecutive days. Then, the mice were maintained for an additional 100 days to ensure the complete development of phenotypes associated with VCD exposure[53] (Extended Data Fig. 4A). To determine whether the observed effects on microbial profiles in females were a direct consequence of VCD-induced ovarian dysfunction rather than off-target effects of VCD administration, we also generated and analyzed data from male mice.

For female mice, ovarian follicle depletion and alterations in crucial ovarian hormone levels (*i.e.* AMH, FSH, and Inhibin A) were confirmed through ovarian histology analysis and serum hormone concentration measurements, respectively (Extended Data Fig. 4B-E). In line with these findings, the VCD-treated group exhibited a markedly lower ovarian health index (p-value ~0.0104; Extended Data Fig. 4F), consistent with overall depleted ovarian function.

Subsequently, we conducted 16S rRNA V3-V4 amplicon sequencing on vehicle- and VCD-treated animals. Analysis through principal component analysis of CLR-transformed ASV counts, along with Bray-Curtis dissimilarity and Jaccard index, demonstrated a distinct separation between the vehicle-treated (CTL) and VCD-exposed groups (Extended Data Fig. 5A-B). Alpha diversity indices, on the other hand, revealed no significant differences between these two groups (Extended Data Fig. 5C). These findings suggest that the overall diversity within the group's communities may appear similar, but they may be different in the species present, their relative abundances and the functions the species perform. Notably, beta diversity analysis of microbial profiles in male mice showed no notable distinctions between vehicle- and VCD-treated groups (Extended Data Fig. 5A, B). Additionally, there were no differences in alpha diversity between these groups (Extended Data Fig. 5D). These findings indicate that the observed effects on microbial profiles in females are causally induced by ovarian dysfunction and not off-target effects of VCD administration.

Our analysis revealed differentially abundant genera from CTL vs. VCD groups (Extended Data Fig. 5E and 6; absolute effect size > 1, adjusted p-value < 0.05). We detected several genera from the *Lachnospiraceae* family, yet none of the unique ASV IDs corresponded with those identified as differentially abundant in the estropausal female mice. Thus, further research to accurately identify the species significant to ovarian aging and health will be important. Then, we utilized PICRUSt2 to predict functional abundance between the CTL and VCD groups (Extended Data Fig. 5F). Notably, we detected down-regulation of the phospholipases pathway in the VCD group, a finding consistent with observations in the estropausal female group (Fig. 1H and Extended Data Fig. 5F). Our findings suggest that physiological ovarian aging and chemically-induced ovarian failure lead to substantially different outcomes on the gut microbiota.

Young and old male mice show distinct fecal microbial profiles

Next, as an important comparison point, we also characterized the fecal microbial profiles of young (4-months) and naturally aged old (20-months) C57BL/JNia male mice (Extended Data Fig. 7A). This comparative study among female and male aging mice, as well as the VCD-exposed mice, aimed to identify differences in microbial profiles attributable to general aging and those specific to ovarian aging.

We collected fecal samples from three independent cohorts of mice and performed 16S rRNA V3-V4 amplicon sequencing to compare the gut microbial profiles of the young and old male mice. Analysis using principal component analysis of CLR-transformed ASV counts, coupled with Bray-Curtis dissimilarity and Jaccard index, showed a distinct divergence between the young and old male groups (Extended Data Fig. 7B-C). However, this separation was less pronounced compared to what was observed in the female cohorts (Fig. 1E). Alpha diversity indices indicated no significant disparities between the two age groups of males (Extended Data Fig. 7D). Similarly, a previous study examining microbial profiles in male mice aged 3-4 months and 19-20 months found comparable alpha diversity index values between the two age groups[54]. Through differential abundance and functional abundance prediction analyses, we identified several genera and functional terms that varied significantly between young and old male mice (Extended Data Fig. 7E-F and 8). Importantly, we observed a few consistent functional terms across female and male aging cohorts. In particular, the L-lysine biosynthesis I pathway was found to be up-regulated, while the pyridoxal 5-phosphate biosynthesis I pathway and the superpathway of pyridoxal 5-phosphate biosynthesis were down-regulated with age in both sexes (Fig. 1H and Extended Data Fig. 7F). These results suggest that these pathways may play roles in the general aging processes, rather than being uniquely related to ovarian aging. Further research will be necessary to elucidate the influence of these functional pathways on the aging process.

Gut microbiota manipulation can induce changes in the ovarian transcriptome

To investigate the potential effects of gut microbiota on ovarian health, we conducted FMT experiments to directly assess how alterations in the gut microbiota after estropause may influence ovarian function. Specifically, young adult female mice (4-months) were subjected to treatment with anti-biotics/anti-mycotic (Ab/Am) treatment to eliminate their initial microbial environment, and then received fecal microbiota grafts from either young (FMT-YF) or estropausal (FMT-EF) female mice (Fig. 2A). Subsequently, the ovaries were harvested for bulk RNA-seq analysis (Fig. 2A). Based on previous research that has shown adverse effects of gut microbiota from donors with ovarian dysfunction, such as PCOS[25], our initial hypothesis was that transplanting fecal matter from estropausal mice could potentially induce estropause-like conditions in the recipient mice.

Multi-dimensional scaling (MDS) analysis of the ovarian RNA-seq dataset revealed a clear separation between the FMT-YF and FMT-EF groups (Fig. 2B). Additionally, we detected 2,131 differentially expressed genes between the FMT-YF and FMT-EF groups (FDR < 5%; Extended Data Fig. 9A). Then, we investigated the pathways that were distinctively regulated between the FMT-YF and FMT-EF groups. Our gene set enrichment analysis (GSEA)[55] results highlighted that pathways related to immune regulation were significantly down-regulated in the FMT-EF groups (Fig. 2C-E; highlighted in red). To evaluate whether these changes were the results of substantial changes in immune cells infiltration in the tissue, we leveraged a publicly available ovarian single-cell RNA-seq dataset[56] to conduct deconvolution analysis, thus allowing us to deduce alterations in immune cell proportions within our dataset. Using two distinct tools, CSCDRNA[57] and Granulator[58], we determined that the proportions of immune cells did not significantly differ between the FMT-YF and FMT-EF groups (Extended Data Fig. 9B), consistent with the notion that the transcriptional changes that we observed may reflect cell autonomous changes in gene expression profiles. In addition, our GSEA results revealed terms associated with chromatin structure and dynamics, including kinetochore, chromatin silencing complex, chromosome, centromeric region, and spindle pole (Fig. 2E). These findings suggest that transcriptional changes in the ovaries may reflect alterations in chromatin organization and chromosome dynamics, processes critical for maintaining oocyte quality[59,60]. Together, these results indicate that pathways associated with both immune regulation and chromatin dynamics distinguish the FMT-YF and FMT-EF groups.

To identify transcription factors potentially driving the transcriptomic alterations observed between the FMT-YF and FMT-EF groups, we utilized Gene Transcription Regulation Database (GTRD)[61] with the GSEA paradigm. While our analysis did not identify any transcription factors meeting the usual stringent criteria of FDR < 5%, we found two transcription factors showing trends of up-regulation and eight displaying down-regulation trends from the FMT-EF group, with an adjusted FDR < 10% threshold (Fig. 2F). Then, we identified publicly available ChIP-seq datasets for the trending transcription factors via the Cistrome Data Browser[62,63], using corresponding *bona fide* peaks to determine potential enrichment by GSEA. Our analysis showed significant negative enrichment scores of Ncoa1 and Usp7-regulated genes within the FMT-EF group (p-value ~0.0138 and ~1e-04, respectively; Extended Data Fig. 9C). Moreover,

we noted that the expression levels of *Ncoa1* and *Usp7* remained consistent across FMT-YF and FMT-EF groups (Extended Data Fig. 9D), suggesting potential post-transcriptional or post-translational regulation. While research on the roles of Ncoa1 and Usp7 in ovarian function is sparse, one study highlighted that Ncoa1 function is important in egg production traits in Shaobo hens[64]. Additionally, an inhibitor of Usp7, P5091, was found to inhibit the proliferation of ovarian cancer cells in another study[65]. Together with our findings, this suggests that Ncoa1 and Usp7 represent potential transcriptional regulators of ovarian function.

Heterochronic FMT may have rejuvenating effects on the ovarian transcriptome of the recipients

Cumulative studies have indicated that aging leads to a pro-inflammatory shift in the ovarian microenvironment, adversely affecting ovarian function and oocyte quality[66,67]. Based on our GSEA results which indicated down-regulation of inflammatory pathways in the ovaries of the FMT-EF group, we next asked whether changes in the ovarian transcriptome upon FMT-EF could represent a more general trend of transcriptional rejuvenation. For this purpose, we analyzed two publicly available bulk RNA-seq datasets profiling ovaries from young (2-3-months) and aged/estropausal (12-months) wild-type female mice[68,69] to identify gene sets that are either up- or down-regulated with ovarian aging (Fig. 3A). To evaluate whether the genes identified from publicly available RNA-seq datasets on ovarian aging ("UP with ovarian aging" and "DOWN with ovarian aging") were significantly regulated in response to FMT-EF, we conducted GSEA using significant age-regulated genes as input gene sets. Surprisingly (and contrary to expectations based on previously reported observation at the somatic level for heterochronic FMT), our findings revealed a significant negative enrichment score for genes that were up-regulated in the context of ovarian aging (p-value ~0.0046; Fig. 3B), suggesting that the ovarian transcriptome of the heterochronic FMT recipients (*i.e.* FMT-EF group) displays transcriptional profiles resembling those of younger females.

As an orthogonal line of evidence, we next asked whether indicators of cellular senescence (as measured by the highly curated senescent marker gene set, SenMayo[70]) were significantly impacted by FMT-EF. Importantly, our results showed a significant negative enrichment score for the SenMayo gene

set in the FMT-EF group, consistent with an overall "rejuvenation" trend for the ovarian transcriptome of FMT-EF mice (p-value ~0.0382; Fig. 3C).

A recently published study highlighted the role of Nicotinamide Adenine Dinucleotide (NAD+) metabolism in ovarian aging, showing that increased NADase CD38 expression accelerated ovarian aging [69]. CD38 deletion or pharmacological inhibition preserved fertility and follicle reserves in aged mice [69]. Building on these findings, we examined the expression of *Cd38* as well as inflammation markers discussed in the study, including *Cdkn1a* and *Il1a* (Fig. 3D). In our analysis, we observed reduced *Cd38* expression in the FMT-EF group compared to the FMT-YF group, along with decreased expression of the inflammation markers (Fig. 3D). These findings suggest the potential involvement of the CD38-NAD pathway in the observed phenotypes of the FMT-EF group.

FMT-EF mice show improved ovarian health

Since we observed large ovarian transcriptome remodeling in the FMT-EF group consistent with a less inflammatory, more youthful ovarian state, we next assessed the ovarian health state of the FMT-YF *vs.* FMT-EF groups to determine whether FMT-EF led to enhanced ovarian function (Fig. 4). We evaluated ovarian health function using a 2-pronged approach (Fig. 4A): (i) calculating the ovarian health index, and (ii) evaluating effective fertility using litter size and time to first pregnancy after mating[71] (Fig. 4).

Consistent with our prediction from the ovarian transcriptomes, the FMT-EF mice exhibited significantly higher scores on the composite ovarian health index than FMT-YF mice (p-value ~0.0255; Fig. 4B, Extended Data Fig. 10A-D), supporting an enhanced ovarian health phenotype. The ovarian health index incorporates multiple parameters, including serum levels of AMH, FSH, and Inhibin A, as well as ovarian follicle counts (Extended Data Fig. 1A). Notably, for the FMT cohorts, FSH levels were measured using two different assay kits during the study due to an update implemented by the core facility conducting the assays. To ensure consistency and comparability of data across cohorts, we applied a correction (see Methods). This adjustment ensured that FSH levels accurately reflected ovarian health and were comparable between cohorts (Extended Data Fig. 10D). Next, we evaluated the result of ovarian function – fertility – through measures of litter size and reproductive success rate. Specifically, there was a suggestive trend for increased litter size in FMT-EF mice (p-value ~0.1726; Fig. 4C). In

addition, FMT-EF mice remained nulliparous for a shorter amount of time after pairing with a young health male (p-value ~0.002; Fig. 4D), also suggestive of improved fertility. To determine whether the inclusion of 0 pup count data influenced our findings, we re-analyzed the latency data after excluding animals with 0 pup counts. Importantly, the latency data remained statistically significant (p-value ~0.0159 without 0 pup counts vs. p-value ~0.002 with all data). Together, our findings are consistent with improved/rejuvenated ovarian function after FMT-EF.

Importantly, no significant differences were observed in body weight between FMT-YF and FMT-EF groups after Ab/Am treatment (Extended Data Fig. 10E and Extended Data Table 1). Additionally, staging of the estrous cycle on the day of sample collection revealed no significant differences between the groups (Extended Data Table 2).

FMT-YF and FMT-EF mice show distinct microbial profiles

Importantly, we next verified that fecal transplants from young or estropausal female mice led to distinct microbial profiles in the recipient mice. For this purpose, we conducted and analyzed 16S rRNA V3-V4 amplicon sequencing on the gut microbiota of FMT-YF and FMT-EF mice (Extended Data Fig. 11).

Principal component analysis of CLR-transformed ASV counts, complemented by Bray-Curtis dissimilarity and Jaccard index, showed a clear segregation between the FMT-YF and FMT-EF groups (Extended Data Fig. 11B). While no significant differences were noted across four alpha diversity indices (Extended Data Fig. 11C), we identified several microbial genera with significant differential abundance between the FMT-YF and FMT-EF groups (absolute effect size > 1, adjusted p-value < 0.05; Extended Data Fig. 11D and 12). Notably, two genera that showed increased abundance in the FMT-EF recipient group were also elevated in the donor estropausal females (*Bacteria;Firmicutes;Clostridia;Clostridiales;Ruminococcaceae* and *Bacteria;Firmicutes;Clostridia; Clostridiales;Lachnospiraceae;Coprococcus 2;uncultured organism ;* Extended Data Fig. 11E). These results indicate that transplanting microbiota from young or estropausal female mice led to changes in the microbial landscape of the recipient mice. Other studies have also reported the selective enrichment of specific microbial species from donor microbiota in recipient subjects[22,72]. These observations may be

attributable to variations in the intestinal microenvironments, which allow the proliferation of certain species.

Subsequently, we used PICRUSt2 to predict functional abundance differences between the FMT-YF and FMT-EF groups (Extended Data Fig. 11F). We identified significant functional groups only with up-regulated functional terms in the FMT-EF group, with no significant down-regulated terms. Notably, there was a significant presence of terms related to the menaquinol biosynthesis pathway, including those involved in 1,4-dihydroxy-6-naphthoate biosynthesis II, 1,4-dihydroxy-6-naphthoate biosynthesis I, and the superpathway of menaquinol-8 biosynthesis II (Extended Data Fig. 11F). Menaquinols, the active hydroquinone forms of vitamin K, also known as menaquinones (MKs), facilitate the carboxylation of vitamin K-dependent proteins, which are crucial for biological processes such as blood clotting, bone health, and heart health[73].

To pinpoint specific microbial species that may contribute to the observed changing in the ovarian health state, we performed whole genome shotgun (WGS) metagenomics on the FMT cohort (Fig. 5A). Consistent with the 16S amplicon sequencing results, PCA analysis of CLR-transformed data and beta diversity analysis revealed distinct clustering between the FMT-YF and FMT-EF groups (Fig. 5B-C). Similarly, no significant differences were observed in alpha diversity indices, reinforcing the similarity in overall microbial diversity between the groups (Fig. 5D). WGS analysis identified 168 differentially abundant microbial species (FDR < 5%; Fig. 5E-F and Extended Data Fig. 13), further confirming distinct microbial compositions in the FMT-YF and FMT-EF groups. Intriguingly, microbial species previously reported to be differentially enriched in the fecal microbiota of PCOS patients, such as *Bacteroides xylanisolvens*, *Bacteroides thetaiotaomicron*, *Parabacteroides distasonis*, and *Bacteroides stercoris*[25], were significantly depleted in the FMT-EF group (Extended Data Table 3).

Functional abundance analysis using HUMAnN3[74] revealed up-regulation of pathways related to menaquinol biosynthesis, including PWY-7371: 1,4-dihydroxy-6-naphthoate biosynthesis II, consistent with predictions from the 16S amplicon analysis (Fig. 5G and Extended Data Fig. 11F). Intriguingly, we detected terms associated with the NAD biosynthesis pathway, such as PWY–7761: NAD salvage pathway II (PNC IV cycle) and PYRIDNUCSYN–PWY: NAD de novo biosynthesis I (from

aspartate)lunclassified, which aligns with our ovarian RNA-seq data showing altered expression of *Cd38* in the FMT-EF ovaries (Fig. 3D, 5G).

Given the stability of menaquinones and their primary synthesis by gut microbiota, we further evaluated their levels in stool samples (MK6-MK13) to explore potential systemic effects post-absorption, as they contribute significantly to the host's vitamin K status. However, no significant differences in MKs concentrations in the stool samples of FMT-YF and FMT-EF animals were observed (Extended Data Fig. 14A,B), although this may be the result of high animal-to-animal variability and/or the high vitamin K content of the standard mouse chow at the USC vivarium dietary (see Discussion).

FMT-YF and FMT-EF mice show distinct serum metabolomic profiles

It is well established that gut microbiota-derived molecules can enter the bloodstream and influence health[75]. Additionally, metabolite levels in plasma have been shown to be affected by aging[76]. To assess whether shifts in the gut microbial profiles of the FMT animals induced changes in circulating metabolites, we performed untargeted metabolomics on serum samples from two independent experimental cohorts (Fig. 6A). First, we performed PCA of the identified metabolites to detect unbiased separation between the FMT-YF and FMT-EF groups. Although non-linear batch effects were present and could not be fully corrected, a clear separation was still evident within each batch (Fig. 6B). Subsequent LDA analysis further showed the distinct metabolomic profiles of the two groups (Fig. 6C). Finally, we extracted metabolites that changed consistently across both cohorts and selected the top 15 based on the LDA loadings (Fig. 6D).

Among the metabolites identified, 3,4-dihydroxyphenylpropionic acid (3,4-DHPPA) and lactamide were significantly decreased in FMT-EF animals at FDR < 0.1 (Fig. 6D, E). 3,4-DHPPA, a microbial metabolite derived from polyphenol metabolism, has been linked to lipid metabolism and broader metabolic regulation[77]. Given the critical role of lipid metabolism in hormonal balance and ovarian function, its reduction in FMT-EF animals may reflect metabolic adaptations that contribute to improved ovarian health. Additionally, while the direct role of lactamide in ovarian function is unclear, microbial-derived lactic acid and its derivatives have been implicated in gut microbiota-driven regulation of reproductive health[78]. For instance, lactic acid bacteria have been shown to influence sex hormone-related gut

microbiota composition, leading to beneficial effects on ovarian physiology in preclinical models[78]. The observed decrease in lactamide levels may indicate broader microbiome-mediated metabolic changes that support ovarian health.

In addition to these significant metabolic changes, palmitoylcarnitine, a key metabolite involved in fatty acid β-oxidation and mitochondrial energy production[79], was elevated in FMT-EF animals according to LDA loadings. This suggests enhanced mitochondrial efficiency and metabolic flexibility, which are essential for oocyte and follicular health[80]. Furthermore, palmitoylcarnitine has been implicated in immune modulation[81], and its increased levels may indicate a metabolic shift supporting both energy homeostasis and an anti-inflammatory ovarian environment. This aligns with our bulk RNA-seq analysis, which revealed a downregulation of inflammatory pathways in the ovaries of FMT-EF animals (Fig. 2C-E).

Conversely, LDA loadings for β-estradiol suggested that serum levels are decreased in FMT-EF mice. Based on the improved ovarian function observed in FMT-EF mice, this may reflect a more physiologically regulated hormonal environment, rather than a pathological decline. Estradiol plays a critical role in ovarian function, lipid metabolism, and mitochondrial activity[82], and its levels may be influenced by gut microbiota-driven metabolic pathways[27]. The gut microbiome is known to modulate steroid hormone metabolism[27], and FMT from EF donors may have contributed to a systemic reprogramming of lipid and hormonal pathways that promote ovarian resilience.

Together, these findings suggest that FMT from estropausal donors induces distinct metabolic shifts that may contribute to the observed improvements in ovarian health. Further studies will be needed to determine the functional impact of these metabolites on ovarian physiology and their potential role in reproductive aging.

Causal mediation analyses reveal microbial species potentially influencing ovarian transcriptome

Lastly, we performed causal mediation analyses to characterize microbial species that may directly influence the ovarian transcriptome remodeling that we observed between FMT-YF and FMT-EF mice (Fig. 7A). From the features exhibiting significant abundance variations between the groups, we identified four microbial species (*Bacteroides zhangwenhongii, Shigella flexneri, Bacteroides stercoris*, and *Bacteroides graminisolvens*) with a significant mediation effect on ovarian transcriptome changes

(Fig. 7B). Interestingly, *Bacteroides stercoris* was previously highlighted as a key contributor to the distinct fecal microbiota profiles between healthy individuals and those with PCOS[25]. Further investigation into the functional roles of these identified species in modulating ovarian function will be essential in future studies. Similarly, we identified four ASV IDs (850e0d58c1aa35238538564a8010e0ff, e4f32cdc3407edb8423447421078fdae, 55ebdcf041fb6b8b4632993423011372, and d4840c45eb37593108d020fb6a63f8e2) with a significant mediation effect on ovarian transcriptome changes (Extended Data Fig. 16).

To further explore the relationship between gut microbiota and ovarian health, we performed Spearman correlation analysis using WGS metagenomics data and serum hormone quantification data (Fig. 7C). This analysis revealed significant correlations between multiple microbial species and hormone levels, including *Shigella flexneri, Parabacteroides merdae,* and *Porphyromonas sp. oral taxon 275,* suggesting these species as potential candidates influencing ovarian function. These findings provide a strong foundation for future studies aimed at experimentally validating the roles of these microbial species in modulating ovarian function and hormone levels.

Discussion

In this study, we examined the fecal microbial profiles of three distinct groups: (1) young and naturally aged estropausal female mice, (2) mice with chemically-induced premature ovarian failure and their control counterparts, and (3) young and naturally aged male mice. Through our comparative analysis, we identified and differentiated between functional pathways that may be unique to ovarian aging (*i.e.* phospholipases pathway) and those specific to general aging (*i.e.* L-lysine biosynthesis I, pyridoxal 5-phosphate biosynthesis I, and superpathway of pyridoxal 5-phosphate biosynthesis). Furthermore, through fecal microbiota transplantation assays, we discovered that alterations in the gut microbiota can significantly impact the ovarian landscape, affecting both fertility and the health state of the ovaries. We also identified specific microbial species as potential mediators of the observed effects on ovarian function. The vitamin K2 and CD38-NAD pathways emerged as potential mechanisms to explore for investigating the underlying causes of the observed phenotypes in our FMT experiments (Fig. 7D). Future

investigations focusing on these species hold significant promise for crafting novel therapeutic strategies aimed at mitigating or potentially reversing ovarian aging.

Ovarian RNA-seq data of the FMT recipients supports causal influence of the gut microbiota on ovarian function

Our analysis of ovarian RNA-seq data from the FMT recipients (FMT-YF vs. FMT-EF) revealed significant changes in the ovarian transcriptome following alterations in the gut microbiota. While existing research underscores the broad effects of the gut microbiome on host health, evidence detailing its direct effects on the transcriptome of various tissues remains sparse. For instance, earlier research demonstrated that mice raised in a germ-free environment exhibit a markedly distinct liver transcriptome compared to their conventionally raised counterparts[26]. To the best of our understanding, the direct influence of gut microbiota on the ovarian transcriptome has not yet been documented. Our analysis not only uncovered significant variations in the ovarian transcriptome among FMT recipient mice (*i.e.* reduced inflammatory pathway in the FMT-EF group), but we also noted the transmission of phenotypic alterations (*i.e.* improved fertility and ovarian health). Collectively, these results offer substantial evidence of gut microbiota's direct role in influencing ovarian function and health. Furthermore, the microbial species and genera, and functional pathways we identified serve as valuable assets for future research aimed at investigating potential therapeutic strategies.

Unexpected advantageous effects of grafting estropausal female fecal microbiota may be due to compensatory mechanisms

Based on previous research that has shown detrimental effects of gut microbiota from donors with ovarian dysfunction, such as PCOS[25], we initially hypothesized that transplanting fecal microbiota from estropausal mice might induce estropause-like phenotypes in the recipient mice. Contrary to our expectations, however, we observed an ovarian transcriptome in the recipients that resembled that of young ovaries, alongside improvements in ovarian health and fertility following the transplantation of microbiota from estropausal females. The unexpected advantageous effects observed could be attributed to a compensatory mechanism. For instance, FSH, required for follicle maturation and ovulation, is found

in elevated levels in post-menopausal women and estropausal mice[2,83,84]. After reproductive senescence, the ovaries no longer produce estrogen or mature eggs, so the pituitary gland compensates by producing more FSH in an attempt to stimulate the now non-responsive ovaries[30]. Similarly, it is conceivable that the gut microbiota in reproductively senescent female mice could be enriched with beneficial microbes and/or metabolites that support ovarian health, perhaps as a compensatory response. Cumulative studies have highlighted the role of gut microbiota in compensatory processes. For instance, one study demonstrated that gut microbiota can influence the levels of peptides that regulate energy balance in the hypothalamus, serving as a mechanism to decrease body fat[85]. Furthermore, an increase in microbes that produce metabolites critical for the nervous system's function—such as serotonin, acetylcholine, histamine, and dopamine—was observed in patients with mild cognitive impairment[86]. Therefore, when young adult female mice received fecal microbiota transplants from estropausal females, it is possible that the enriched gut microbial environment contributed to the manifestation of younger or more reproductively active phenotypes in recipient mice.

Potential involvement of MKs in ovarian health and aging

Although our analysis of functional abundance from both WGS and 16S rRNA amplicon sequencing datasets predicted potential shifts in the biosynthesis pathway of MKs in the FMT mice, we observed no significant differences in the stool concentrations of MKs between the FMT-YF and FMT-EF groups. This lack of observable difference might be attributed to the vitamin K content of the standard chow used by the USC vivarium during our experiments (LabDiet, PicoLab Rodent Diet 20). Specifically, the high vitamin K dietary content could have saturated the system, thus masking subtle variations in MK production by the gut microbiome. Such nuances are typically more pronounced under conditions of a low vitamin K diet[87]. Published studies have shown that vitamin K status influences MK production because gut bacteria require vitamin K substrates to synthesize MKs[87]. In our study, the presence of vitamin K3 (menadione) in the diet, which is converted into MK4 in the body, likely contributed to the high basal MK levels observed in the fecal matter of the recipient mice. While there have been limited studies, MKs have demonstrated potential benefits for ovarian health in specific contexts, such as certain ovarian cancers and in patients with PCOS[88,89]. Additionally, some studies have underscored the anti-inflammatory

properties of MKs[90]. Given our observations of decreased inflammatory function and enhanced ovarian function in the FMT-EF mice, coupled with the documented benefits of MKs, MKs may be therapeutic candidates for improving ovarian health and function. However, further research into the direct effects of MKs on ovarian function will be necessary.

Sex-differences in aging-associated gut microbial profiles

In our comparative study, while we detected certain similarities in the microbial profiles of both females and males with aging, our analysis primarily revealed notable differences between the sexes. Specifically, while aging was associated with significant changes in alpha diversity in female mice, such changes were not observed in males. Moreover, our analyses of differential abundance of microbial genera and predictions of functional abundance revealed substantial differences in the gut microbial profiles and their functions between females and males as they age. Indeed, extensive research has established that aging manifests differently in females and males, a phenomenon known as sex dimorphism in aging[91]. Particularly, the susceptibility to diseases associated with aging, including Alzheimer's disease and obesity, varies significantly between the sexes[92-94]. Furthermore, the disparity in lifespan between females and males is consistently observed across various species[95,96]. In agreement with our findings in this study, sex differences in the gut microbiome associated with aging have previously been documented[97,98]. While the limited number of existing studies suggest a possible influence of sex hormones on the observed sex differences in the gut microbial profiles[99-101], these findings do not negate the potential effects of non-hormonal factors, such as those related to sex chromosomes, on the differences noted between sexes. Given the significant distinctions between sexes highlighted in this study and their varied impacts, it is imperative to consider sex as a contributing factor in future gut microbiome research, not only to deepen our understanding but also to address the specific differences effectively.

The potential role of the CD38-NAD pathway in mediating ovarian rejuvenation in the FMT-EF mice

CD38, a primary NADase in mammalian tissues, plays a pivotal role in regulating NAD+ levels[102]. Emerging evidence implicates the CD38-NAD axis in aging, with increased CD38 expression contributing

549 to age-related declines in NAD+ levels, impairing mitochondrial function and cellular metabolism[103,104]. In
550 the context of ovarian aging, studies have shown that CD38 overexpression accelerates follicular
551 depletion and diminishes ovarian function, whereas CD38 inhibition preserves follicle reserves and fertility
552 in aged mice[69].

553 In this study, we observed reduced *Cd38* expression in the ovaries of the FMT-EF group,
554 alongside downregulation of inflammatory markers such as *Cdkn1a* and *Il1a* (Fig. 3D). Functional
555 pathway predictions from the metagenomics data further supported these findings, revealing enrichment
556 of pathways related to NAD biosynthesis in the FMT-EF group (Fig. 5G). Specifically, pathways such as
557 NAD salvage pathway II (PNC IV cycle) and NAD de novo biosynthesis I (from aspartate) were
558 upregulated (Fig. 5G). These results suggest that the gut microbiota established through estropausal
559 fecal microbiota transplantation may suppress CD38 activity, influencing ovarian NAD metabolism and
560 creating a more favorable ovarian environment. This aligns with previous research linking CD38-mediated
561 NAD+ depletion to inflammation and cellular senescence, processes that are detrimental to ovarian
562 function[105,106].

563 Together, these findings indicate that modulation of the CD38-NAD pathway by gut microbiota
564 may alleviate ovarian inflammation and promote a more youthful transcriptomic profile, contributing to the
565 enhanced ovarian health observed in FMT-EF mice.

566

567 **Limitations of the study**

568 One potential caveat in our chemically induced ovarian failure model is that VCD, while
569 selectively depleting ovarian follicles, is a systemically administered agent and could potentially affect
570 other biological systems. However, studies have shown that VCD's effects are confined to ovarian tissue,
571 and its impact on other organ systems have not been reported[107,108]. To further assess off-target effects,
572 we conducted control experiments in male mice injected with VCD or vehicle, and no significant
573 differences in gut microbial beta diversity indices (Bray-Curtis dissimilarity and Jaccard index) were
574 observed. These findings suggest that the observed microbial changes in female mice are primarily due
575 to ovarian dysfunction rather than direct effects of VCD, though we acknowledge the potential for non-
576 specific effects. Additionally, it is possible that the improved fertility outcomes in the FMT-EF group,

compared to the FMT-YF group, may reflect differences in how aged and young donor microbiota recolonize the gut following antibiotics treatment. For example, the aged microbiota might better adapt to recolonization, reducing the likelihood of artificially poor fertility outcomes in the recipients. Nonetheless, the changes in the microbiota induced by FMT resulted in significant changes in ovarian health, as evidenced by differences in ovarian transcriptomic profiles, fertility outcomes, and overall ovarian health indices in the FMT-YF and FMT-EF groups. Finally, another limitation of the study involves the use of PICRUSt2, which predicts functional abundances based on marker gene sequences. While PICRUSt2 provides insights into potential functional pathways affected by changes in the microbiota, it is a predictive tool and does not directly measure functional abundances. Future studies will require additional functional assays to validate these predictions.

In summary, we performed a comparative analysis of microbial profiles among aging female, aging male and a chemically-induced menopause model mice to characterize microbial genera that are unique to general aging vs. ovarian aging. Our work highlights potential microbial species and genera, and functional pathways that may play key roles in modulating ovarian function.

Acknowledgements

We thank Dr. Victor Ansere and Dr. Juan Bravo for feedback on our manuscript. We also thank Dr. Dario Valenzano for his insightful comments and guidance on microbiome data analysis.

This work was supported by the GCRLE-2020 post-doctoral fellowship from the Global Consortium for Reproductive Longevity and Equality at the Buck Institute, made possible by the Bia-Echo Foundation to M.K., USC Provost's Undergraduate Research Fellowship to J.W., National Institute on Aging (NIA) T32 AG052374 predoctoral fellowship and Diana Jacobs Kalman/AFAR Scholarships for Research in the Biology of Aging to R.J.L., and Pew Biomedical Scholar award #00034120 from the Pew Charitable Trust to B.A.B. Ovarian histological analysis was performed by the Translational Pathology Core at the USC Norris Comprehensive Cancer Center (supported by NCI P30 CA014089). Serum hormone quantification was performed by the University of Virginia Center for Research in Reproduction Ligand Assay and Analysis Core (supported by the Eunice Kennedy Shriver NICHD/NIH Grant R24HD102061). Computational analyses were performed using the Center for Advanced Research Computing (CARC) resources at the University of Southern California (USC). Stool vitamin K concentrations were supported by the USDA Agricultural Research Service under Cooperative Agreement No. 58-1950-7-707. Any opinions, findings, conclusions, or recommendations expressed in this publication are those of the authors and do not necessarily reflect the views of the USDA. We thank Whitaker Cohn, the Assistant Director of the USC Mann Multi-Omics Mass Spectrometry Core, for running the metabolomics samples on their instruments.

Author contributions

M.K. and B.A.B. designed the study. M.K. performed live animal experiments. M.K. and R.L.J. dissected mouse tissues. M.K., J.W. and Y.K analyzed ovarian histology data. A.X. generated R shiny application. M.L., X.F. and S.L.B quantified stool MK concentrations. S.E.P, M.K. and P.A.M performed and analyzed metabolomics data. M.K. and J.W. performed computational analyses. M.K. and B.A.B. wrote the manuscript with input from all authors. All authors edited and commented on the manuscript.

Declaration of interests

620 The authors declare no competing interests.

Methods

Mouse husbandry

All animals were treated and housed in accordance with the Guide for Care and Use of Laboratory Animals. All experimental procedures were approved by the USC's Institutional Animal Care and Use Committee (IACUC) and are in accordance with institutional and national guidelines. Samples were derived from animals on approved IACUC protocol number 20770 and 21212.

For the "aging cohort," female and male C57BL/6JNia mice (4- and 20-month-old animals) were obtained from the National Institute on Aging (NIA) colony at Charles River Laboratories. For the "VCD cohort" and "fecal microbiota transplantation (FMT) cohort", female and male C57BL/6NTac mice (3.5-month-old animals) were ordered from Taconic Biosciences. All animals were acclimated at the specific-pathogen-free animal facility at USC for 2 weeks before any processing. All animals were fed PicoLab Rodent Diet 20 (LabDiet, 5053). The facility is on a 12-h light/dark cycle and animal housing rooms are maintained at 72 °F and 30 % humidity. All animals were euthanized between 8–11 am, by CO_2 asphyxiation followed by cervical dislocation.

For the "VCD cohort," animals were subjected to daily intraperitoneal injections of either vehicle (safflower oil) or VCD (at a dosage of 160 mg/kg/day) for 15 consecutive days. All injections were performed between 8:00 AM and 10:00 AM to minimize variability due to circadian effects. Lethality was observed in male VCD-injected mice (4 out of 10 males in the experimental group within 16 days of the start of injections). Intriguingly all lethality cases occurred in males that had to be single-housed prior to injections due to fighting and wounds. Effects may have been aggravated due to lack of social interactions and/or temperature regulation.

Ovarian follicle counts

Ovaries were fixed in Bouin's solution (Sigma, HT10132) for 24 hrs at room temperature and transferred to 70 % ethanol for storage. Paraffin embedding, tissue sectioning and staining with hematoxylin and eosin (H&E) were performed by the USC Norris Comprehensive Cancer Center Translational Pathology Core Facility. H&E staining slides were imaged on the Keyence BZ-X All-in-One

649 Fluorescence Microscope platform. Three sections per ovary were used to count the number of primordial,
650 primary, secondary, and antral follicles and corpus luteum by three blinded observers. Median counts
651 across the 3 observers were used for data analysis. Statistical significance between groups was
652 assessed using the non-parametric Wilcoxon rank-sum test.
653
654 **Quantification of serum AMH, FSH and Inhibin A concentrations**
655 After euthanasia, blood was collected directly from the heart. Blood was allowed to clot at room
656 temperature for 1 hour, and serum was separated using MiniCollect® Serum Tube (Greiner, 450472),
657 then stored at -80 °C until further processing. Quantification of serum AMH (Rat and Mouse Anti-Müllerian
658 hormone (AMH) ELISA kit, Ansh Labs, AL-113), FSH (Millipore Pituitary Panel Multiplex kit, RPT86K and
659 Ultra-Sensitive Mouse & Rat FSH, UVA Ligand Core, in-house[109]), and Inhibin A (Inhibin A ELISA kit, Ansh
660 Labs, AL-161) levels were performed by the University of Virginia Center for Research in Reproduction
661 Ligand Assay and Analysis Core. Standard normalized values were provided by the core. Statistical
662 significance between groups was assessed using the non-parametric Wilcoxon rank-sum test.
663 For FSH quantification, two different kits were used during the course of the study, necessitating
664 correction of the dataset generated by the ultra-sensitive kit. To ensure consistency, we generated data
665 using both kits with the same serum samples and devised a polynomial model to fit the relationship
666 between the two datasets ($R^2 = 0.90$). The trained polynomial model was then applied to correct the data
667 generated by the Ultra-Sensitive Mouse & Rat FSH assay. This correction process was specifically
668 applied to the data for the FMT cohort. The raw data used to train the model has been uploaded to Github
669 (https://github.com/BenayounLaboratory/Ovarian_Aging_Microbiome).
670
671 **Ovarian health index calculation**
672 The ovarian health index was calculated by integrating two key components: (1) ovarian hormone
673 levels (AMH, FSH, and Inhibin A) and (2) follicle counts (combined counts of primordial, primary,
674 secondary, antral follicles, and corpus luteum). A 3-tier scoring system was used for each parameter.
675 Values beyond the young medians were assigned a score of 3, values between the young and
676 estropausal medians were assigned a score of 2, and values beyond the estropausal medians were

assigned a score of 1. The average hormone score (calculated from the AMH, FSH, and Inhibin A scores) was then combined with the follicle score in a 1:1 ratio to generate the overall ovarian health index. This combined score was scaled to a 0-100 range for ease of interpretation.

Statistical significance between groups was assessed using the Wilcoxon rank-sum test. Scripts used to calculate the ovarian health index are available on the Benayoun lab GitHub at https://github.com/BenayounLaboratory/Ovarian_Aging_Microbiome.

DNA extraction for 16S rRNA amplicon and shotgun metagenomics analyses

Fecal matter for 16S rRNA V3-V4 amplicon and shotgun metagenomics analyses were collected aseptically post-euthanasia. Samples were immediately snap frozen in sterile tubes and stored at -80 °C. DNA extraction was performed using QIAamp Fast DNA Stool Mini Kit (QIAGEN, 51604), following the manufacturer's protocol.

V3-V4 region targeted amplification and sequencing were performed by Novogene Inc. Amplification primers used were CCTAYGGGRBGCASCAG (FWD_341F) and GGACTACNVGGGTWTCTAAT (REV_806R). Amplicon libraries were sequenced on the Illumina NovaSeq 6000 machine. Shotgun metagenomics library preparation and sequencing were performed by Novogene Inc. on the Illumina NovaSeq X machine. De-multiplexed FASTQ files were provided by Novogene Inc. for data analysis.

16S rRNA V3-V4 amplicon sequencing data analysis

Data pre-processing, quality control and denoising

Data pre-processing, quality control and denoising were performed within the QIIME2[110] (v. 2023.7) platform. Each cohort was analyzed independently for memory and computing efficiency. FASTQ files were imported to QIIME2 and denoised using DADA2[111]. Forward and reverse reads were truncated at 226 bp and 224 bp, respectively, to obtain reads with quality scores above 25 and to ensure coverage of the V3-V4 region (–p-trunc-len-f 226 –p-trunc-len-r 224).

Batch correction and principal component analysis of amplicon sequence variants

Previous studies have shown that effectiveness of batch correction tools are dataset-dependent[41]. For batch correction, a previously described benchmarking pipeline[41] was used to select the most effective batch correction tool for our dataset. removeBatchEffect function from limma[112] (v. 3.50.1), Combat from sva[113] (v. 3.42.0) and FAbatch from bapred[114] (v. 1.1) were benchmarked. Denoised feature tables were imported to R using qiime2R[115] package (v. 0.99.6). Then, features with low counts (less than 0.01% of all the counts) were removed and filtered counts were centered log ratio (CLR)-transformed. Based on principal component analysis results (method described below) and variance calculations, FAbatch-corrected values were chosen for downstream analyses.

Principal component analysis of amplicon sequence variants

For principal component analysis (PCA), pca function from mixOmics[116] (v. 6.18.1) was used in R. For female and male aging cohorts, FAbatch-corrected values were used for PCA. For VCD and FMT cohorts, CLR-transformed values were used for PCA.

Beta diversity and alpha diversity analyses

For beta and alpha diversity analyses, phylogenetic trees were generated using the 'qiime phylogeny align-to-tree-mafft-fasttree' command. Rooted phylogenetic trees were used to run the 'qiime diversity core-metrics-phylogenetic' command for beta and alpha diversity analyses. Diversity analysis results were imported to R using qiime2R[115] package (v. 0.99.6) for further plot generation and significance tests. Bray-Curtis dissimilarity and Jaccard index principal coordinate analysis results were used to generate beta diversity plots using ggplot2 (v. 3.4.2). To ensure comparability across different cohorts, we normalized alpha diversity metrics within each cohort by dividing the values of each sample by the median value of the corresponding metric (e.g., observed features, Shannon entropy) within that cohort (e.g., CTL vs. VCD, FMT-YF vs. FMT-EF). This normalization allowed for combined cohort analysis. The statistical significance of differences in alpha diversity between groups was determined using the Wilcoxon rank-sum test.

Differential abundance analysis of microbial genera

Differential abundance analysis of microbial genera was performed using the ALDEx2[117] plugin within the QIIME2[110] platform. Taxonomic classifier was generated using the SILVA[118] (132 release) reference. Reference reads were extracted for CCTAYGGGRBGCASCAG (FWD_341F) and GGACTACNVGGGTWTCTAAT (REV_806R) primer set and a classifier was trained using the 'qiime feature-classifier extract-reads' and 'qiime feature-classifier fit-classifier-naive-bayes' commands, respectively. Differential abundance analysis results and taxonomic classifier were imported to R using qiime2R[115] for comparative analysis and plot generation. For female and male aging cohorts, differential abundance analysis results for each cohort for each sex was combined based on the directionality of the differential abundance measures, identifying features that consistently exhibited either an increase or decrease across all cohorts for each sex. Using Fisher's method and Benjamini-Hochberg (BH) correction method, p-values for each feature's differential abundance were combined and corrected, respectively. Additionally, the mean of effect size across cohorts for each feature was used for analysis. For combined female and aging cohorts, as well as VCD and FMT cohorts, features with an adjusted p-value < 0.05 and an absolute effect size > 1 were identified as significantly different in abundance.

Functional abundance prediction analysis

Functional abundance prediction analysis was performed via the PICRUSt2[48] plugin within the QIIME2[110] platform using default parameters. PICRUSt2 results were imported to R using qiime2R. For differential abundance and statistical significance analyses, ALDEx2[117] was used (500 Monte Carlo samples, Wilcoxon test for statistical testing, effect size calculation enabled, and the interquartile log ratio (iqlr) for denominator calculation). To combine independent cohorts for female and male aging cohorts, Fisher's method and Benjamini-Hochberg multiple testing correction were used to combine and correct the p-values. Also, the mean values of effect sizes were calculated for each feature. Adjusted p-value less than 0.05 and absolute effect size greater than 1 were used as criteria to filter functional pathways that were significantly different in abundance.

Fecal microbiota transplantation

For fecal microbiota transplantation (FMT), animals underwent a 10-day course of antibiotics/antimycotic (Ab/Am) treatment before transplantation. The regimen included ampicillin in drinking water at 1 g/L (Sandoz, 00781), and oral gavage of amphotericin-B (Sigma, A9528) at 1 mg/kg/day, metronidazole (MFR VIONA PHARMACEUTICALS, 096988) at 100 mg/kg/day, vancomycin (Alvogen, Vet-Rx-MW 090160) at 50 mg/kg/day, and neomycin (MFR VETONE, 510570) at 100 mg/kg/day. Starting on the third day after the end of the Ab/Am treatment, FMT was performed biweekly for three weeks via oral gavage. Donor stool samples from more than 30 young or estropausal female mice were pooled and prepared by suspending in saline (20 mg/ml), followed by vortexing and centrifugation to obtain the supernatant. Each recipient animal received 100 μl of the fecal suspension. Two independent cohorts were enrolled in the study, each using independently prepared pools of FMT materials. Sample collection for subsequent processing and analysis occurred three days after the final FMT session.

Ovarian RNA-seq sample preparation

Ovaries were harvested and immediately snap-frozen in sterile tubes, and then stored at -80 °C. For RNA extraction, 600 μl of Trizol reagent (Ambion, 15596018) was added to the ovaries in Lysing Matrix D tubes (MP, 6913500) and tissues were homogenized with a BeadBug 6 microtube homogenizer (Benchmark Scientific, D1036) at 3,500 rpm for 30 seconds for 3 cycles in the cold room. Total RNA was purified using the Direct-Zol RNA Miniprep (Zymo Research, R2052), following the manufacturer's instructions. Integrity and quality of the purified total RNA were assessed on the 4200 TapeStation system (Agilent, G2991A) using High Sensitivity RNA ScreenTapes (Agilent, 5067–5579) to determine the RNA Integrity Number (RIN). Subsequently, mRNA-seq libraries were prepared and sequenced by Novogene Inc. to obtain PE150 sequencing reads on the NovaSeq X Plus platform.

FMT cohort ovarian RNA-seq data analysis

Data quality control and pre-processing

Paired-end 150-bp reads were hard-trimmed to remove the first 6 bases and keep up to 100bp using Fastx Trimmer[119] (v. 0.0.14) and processed using Trim Galore[120] using default parameters (v. 0.6.6).

Trimmed reads were mapped to the mm39 genome reference using STAR[121] (v. 2.7.9a). Read counts were assigned to genes from the mm39 genome reference using subread[122] (v. 2.0.3). After assigning read counts to genes, downstream processing was performed in R (v. 4.1.2). Low count genes (genes with less than 1 count in at least 6 out of 14 RNA-seq libraries) were removed to improve memory and speed efficiency of DESeq2[123], as recommended by the developers. We used surrogate variable analysis to estimate and correct for unwanted experimental noise. R package sva[113] (v. 3.42.0) was used to estimate surrogate variables and the removeBatchEffect function from limma[112] (v. 3.50.1) was used to regress out the effects of surrogate variables and RNA integrity differences (RNA integrity number scores) from raw read counts. To remove extreme values within the read counts, Winsorize function from DescTools[124] (v. 0.99.50) was used to adjust the values above the 99.9th percentile to the values at the 99.9th percentile. DESeq2[123] package (v. 1.34.0) was used for downstream analyses of the RNA-seq data. Genes with FDR < 5% were considered statistically significant. For the multidimensional scaling (MDS) analysis, we calculated the distance between samples using the inverse of Spearman's rank correlation coefficient (1-Rho) as the distance metric. These distances were then input into the cmdscale function in R to compute the MDS coordinates.

Gene ontology analysis of RNA-seq dataset

We used the GSEA[55] approach through the phenoTest package. GO term annotations (ENS.GO.BP, ENS.GO.MF, ENS.GO.CC and GTRD gene sets) were sourced from ENSEMBL (Ensembl 108) and Molecular Signature Database[125]. The t-statistic from DESeq2[123] was used to rank genes for functional enrichment analysis. For readability, only the top ten most-significant pathways with negative NES and top ten most-significant pathways with positive NES are shown in figures if more than that passed the FDR < 5% significance threshold for GO terms and FDR < 10% for GTRD transcription factor targets (see main text for explanation).

Deconvolution analysis of immune cell type proportion

To estimate any differences in the immune cell proportions between FMT-YF and FMT-EF groups of the FMT cohort, single-cell RNA-seq reference-based deconvolution analyses were performed, using

CSCDRNA[126] and Granulator[127]. We downloaded the cell type annotated Seurat object of a publicly available murine ovarian single-cell RNA-seq dataset (Open Science Framework dataset ID 924fz)[56]. In the CSCDRNA analysis, the min.p parameter was set to 0.3 following the authors' recommendation[126], to efficiently exclude the 30% least significant portion of marker genes for each cell type. This threshold was chosen to increase efficiency and reduce noise. For Granulator, the qprogwc method[128] was used with default parameters to estimate the immune cell proportions within the ovarian bulk RNA-seq dataset. Cell proportions were tested for significance using a Wilcoxon test rank-sum test.

Pre-processing and filtering candidate transcription factor-bound genes

For potential transcription factors identified from GSEA[55] analysis against GTRD[61] transcription factor targets, peak information was obtained for Cistrome.org. Peak annotation was performed using HOMER[129] (v. 4.11.1). Genes with peaks annotated in TSS-promoter of protein coding genes were considered direct target genes. Obtained gene lists were used to perform GSEA through the phenoTest (v. 1.42.0) package.

Pre-processing of public ovarian aging datasets

To evaluate the correlation between ovarian aging and FMT gene expression profiles of the ovaries, we pre-processed and analyzed two publicly available ovarian aging datasets (2-3-month-old vs. 12-month-old female mice; BioProject dataset PRJNA100222 and GSA dataset CRA003645)[68,69]. For each dataset, reads were pre-processed and aligned to the mm39 genome reference using the same methods as for the FMT cohort ovarian RNA-seq dataset. Low count genes (genes with less than 1 count in at least 4 out of 7 RNA-seq libraries) were removed. sva[113] (v. 3.42.0) was used to estimate surrogate variables and the removeBatchEffect function from limma[112] (v. 3.50.1) was used to regress out the effects of surrogate variables from raw read counts. DESeq2[123] package (v. 1.34.0) was used for downstream analyses of the RNA-seq data. p-values for common genes between the two datasets were combined and corrected using Fisher's method and BH correction method, respectively. FDR < 1e-5 was used to catalog gene sets that are robustly up- or down-regulated with aging. Obtained gene lists were used to perform GSEA through the phenoTest package.

844

845 **Fertility assay**

846 Fertility assay was performed as previously described[71]. FMT female mice were paired with 4-
847 month-old males at a 1:1 ratio 3 days after the last day of FMT administration until the birth of the first
848 litter. The number of pups in the first litter and the latency, defined as the duration between the pairing
849 date and the birth date of the first litter, were recorded and analyzed. Statistical difference in latency in the
850 1st litter after pairing was evaluated using a log-rank test. For pairs that did not produce pups within the
851 60-day timeframe, the latency was recorded as 60 days.

852

853 **Whole genome shotgun metagenomics analysis**

854 Data quality control and pre-processing

855 Paired-end 150-bp reads were pre-processed to remove sequencing adapters and low-quality
856 reads using Trimmomatic (v. 0.39)[130]. Trimmed reads were then mapped to the mouse reference genome
857 (mm10) using Bowtie2 (v. 2.4.4)[131] to remove host DNA contamination. Unmapped reads from paired-end
858 files were extracted using the --un-conc-gz option in Bowtie2 and used for subsequent analyses. Quality-
859 controlled and host-depleted reads were then processed for taxonomic classification and functional
860 profiling.

861

862 Taxonomic classification, abundance estimation and functional profiling

863 Kraken2 (v. 2.1.2)[132] was used for taxonomic classification of unmapped reads. Reads were
864 classified against a pre-built standard Kraken2 database containing bacterial, archaeal, and viral
865 sequences. Classification outputs were summarized using Bracken (v. 2.7)[133] to refine species- and
866 genus-level abundance estimates. Bracken was configured with a read length of 150 bp and default
867 settings for abundance profiling. Functional profiling was conducted using HUMAnN3 (v. 3.0)[74]. Reads
868 were processed in paired-end mode. Pathway and gene family tables were further merged and
869 normalized using human_join_tables and human_renorm_table functions.

870

871 Alpha and beta diversity and differential abundance analysis

Raw taxonomic abundance tables from Bracken (v. 2.7)[133] were loaded in R and filtered to remove low-abundance and low-prevalence features. Features with total counts <20, relative abundance <0.01%, or prevalence in fewer than 10% of samples were excluded. Samples with high host DNA alignment rates (i.e., MHK271) were also removed. Centered log-ratio (CLR) transformation of filtered relative abundances was performed. Shannon entropy was calculated using the mia[134] (v. 1.12.0) R package. CLR-transformed relative abundance data were analyzed using mixOmics[116] (v. 6.28.0) and Bray-Curtis and Jaccard distance matrices were calculated using vegan (v. 2.6-8). Differential abundance of species was assessed using ALDEx2[117] (v. 1.36.0). Features with adjusted p-values of <0.05 were deemed significant.

Functional pathway analysis

Relative abundance data for microbial pathways from HUMAnN3[74] (v. 3.9) was loaded in R and low-abundance pathways with total abundance below 0.001 across all samples were removed. Differential abundance of microbial pathways between groups was analyzed using ANCOMBC2[135] (v. 2.0.0). Significant pathways with Q-values below 0.1 were identified, and log2-fold change values were used to assess the direction and magnitude of differential abundance.

Stool menaquinone concentration quantification

Frozen stool samples were shipped to the Vitamin K Laboratory at the Tufts University Human Nutrition Research Center on Aging (HNRCA), where stool menaquinones concentrations were measured using the LC/MS, as detailed elsewhere[136].

Serum untargeted metabolomics

Sample processing

Serum samples were stored at -80°C until they were thawed on ice for analysis. Metabolites were extracted by adding 80 μL of ice-cold methanol to 20 μL of serum, followed by incubation on ice with vortexing every 5 minutes. The samples were then centrifuged at 21,300 × g for 10 minutes at 4°C.

Liquid Chromatography-Tandem Mass Spectrometry (LC-MS/MS)

Untargeted metabolomics was performed at the USC Alfred E. Mann Multi-Omics Mass Spectrometry Core. A volume of 10 μL from each sample was injected onto a SeQuant ZIC-pHILIC Column (5 μm, 2.1 mm × 150 mm; Millapore Sigma) using a Vanquish Flex UHPLC System (Thermo Fisher Scientific). Chromatography was conducted at a flow rate of 100 μL/min with an optimized gradient of solvent A (water/20 mM ammonium carbonate, pH 9.8) and solvent B (acetonitrile) as follows: 0 min/97% B, 1 min/97% B, 28 min/75% B, 39 min/50% B, 44 min/20% B, 45 min/20% B, 45 min/97% B, 60 min/97% B. The chromatography system was coupled to a heated electrospray ionization (HESI) source and a hybrid quadrupole-Orbitrap mass spectrometer (Q Exactive, Thermo Fisher Scientific). Mass spectra were acquired in Full MS/data-dependent MS2 mode, alternating between positive and negative ion polarities.

Source parameters were set as follows: a source voltage of 3.5 kV, source temperature of 275°C, sheath gas of 45, auxiliary gas of 10, sweep gas of 2, and capillary temperature of 320°C. Full scans were performed across an m/z range of 70 - 1050 with the following settings: an automated gain control (AGC) target of 5 × 10□, a maximum injection time of 100 ms, and a resolution of 70,000 at m/z 200. Up to five consecutive MS/MS scans were acquired per full scan with the following parameters: quadrupole isolation of charge states 1–7, isolation window of 0.6 m/z, normalized collision energies of 20, 30, and 40, dynamic exclusion of 30 s, AGC target of 1 × 10□, maximum injection time of 100 ms, and resolution of 17,500 at m/z 200.

Data analysis

Raw data were processed using Compound Discoverer (Version 3.3 SP3, Thermo Fisher Scientific) for metabolite identification, retention time alignment, and unknown compound detection across all samples. Metabolites were identified by matching exact masses (delta ppm of >10 or <-10) and fragmentation spectra to the mzCloud database (ddMS2; 'mzCloud Best Match' > 50). For quality control, only ions with a peak rating > 4 in at least six samples within a group were retained. VSN normalized filtered metabolic matrix via normalizeVSN function of limma[112] (v. 3.50.1) was used for PCA analysis. The filtered metabolic matrix was then scaled, and Linear Discriminant Analysis (LDA) was performed via the

MASS (v. 7.3-60.2) R package. Metabolites with a consistent direction of $\log_2$ fold change ($\log_2$FC) between two batches were subsequently retained for abundance analysis.

Causal mediation analysis

Causal mediation analysis to identify specific features and amplicon sequence variants (ASVs) from WGS and 16S rRNA amplicon sequencing datasets from the FMT cohort acting as mediators between the treatment (FMT-YF vs. FMT-EF) and outcome (changes in the ovarian transcriptome profiles) was performed using mediation package[137] (v. 4.5.0) in R. Feature table, taxonomic reference and differential abundance analysis results generated from QIIME2[110] were imported to R using qiime2R[115]. ASVs identified as significant in differential abundance analyses were tested. CLR-transformed ASV counts were used for the mediation analyses. For the outcome variable, the first dimension from the multidimensional scaling (MDS) analysis of the FMT ovarian mRNAseq dataset was used. Linear models were constructed for both the mediator and the outcome, incorporating the treatment as an independent variable in each. The mediate function from the mediation package was then employed to estimate the Average Causal Mediation Effects (ACME), Average Direct Effects (ADE), and Total Effects.

Quantification and statistical analysis

All statistical analysis was performed using the R software, version 4.2.4. For all boxplots, the data is shown with the median, the 25th and 75th percentile of the data, and the whiskers represent 1.5 $*$ the inter-quartile range (IQR). Individual datapoints are always overlayed for transparency and rigor. Specific statistical tests used, the number of biological replicates and how many animals they are indicated in the corresponding figure legends and associated method section.

Data availability

The raw FASTQ files have been deposited to the Sequence Read Archive under accession PRJNA1076509. Raw microscopy pictures of ovarian hematoxylin and eosin staining are available on Figshare (Figshare DOIs: 10.6084/m9.figshare.25749588, 10.6084/m9.figshare.25749594, 10.6084/m9.figshare.25749591, 10.6084/m9.figshare.28462274). Processed serum metabolomics data

can be found in Extended Data Table 4. Raw data can be found on Metabolomics Workbench, project ST003750. All R code was run using R 4.1.2. Any additional information required to reanalyze the data reported in this work paper is available from the corresponding author upon request.

Code availability

All scripts used to analyze the datasets are available on the Benayoun lab GitHub at https://github.com/BenayounLaboratory/Ovarian_Aging_Microbiome.

962 **Figure legends**

963

964 **Fig 1. Characterization of ovarian health state and fecal microbial profiles of young and**
965 **estropausal female mice.** (A) Schematic diagram of the experimental setup of female aging cohorts.
966 Resources from Flaticon.com were used. (B) Boxplot of combined follicle count of young and estropausal
967 mice. (C) Boxplot of serum concentrations of AMH. (D) Boxplot of ovarian health index of young and
968 estropausal mice. (E) Principal component analysis result of CLR-transformed and batch-corrected ASV
969 counts from young and estropausal female mice. Animals from four independent cohorts (C1-C4), n=19-
970 20 per group (variation due to animal death prior to experiment; n=20 for young females; n=19 for
971 estropausal females). (F) Boxplots of Observed features and Shannon entropy indices of young and
972 estropausal female mice. Medians from young females for each cohort were used to normalize indices
973 per cohort. (G) Differential abundance analysis results of microbial genera of young vs. estropausal
974 female mice using ALDEx2. (H) Functional abundance prediction analysis of young vs. estropausal
975 female mice using PICRUSt2. Significance in nonparametric two-sided Wilcoxon rank-sum tests are
976 reported for (B) and (D). YF: Young female; EF: Estropausal female. C: Cohort.

977

978 **Fig 2. Bulk RNA-seq analysis of ovaries from young and estropausal female mice fecal microbiota**
979 **transplantation recipient mice.** (A) Schematic diagram of the experimental setup of fecal microbiota
980 transplantation (FMT) cohort. Fecal microbiota from either young (4 months old) or estropausal (20
981 months old) female mice were transplanted into young (4 months old) female recipient mice. FMT
982 recipient groups are referred to as FMT-YF (receiving young donor microbiota) and FMT-EF (receiving
983 estropausal donor microbiota). (B) Multidimensional scaling (MDS) analysis result of RNA expression
984 between young and estropausal female mice FMT recipient mice (FMT-YF and FMT-EF, respectively).
985 (C-F) Top GSEA enriched terms from (C) Gene Ontology Biological Process (GO BP), (D) Gene Ontology
986 Molecular Function (GO MF), (E) Gene Ontology Cellular Component (GO CC) and (F) Gene
987 Transcription Regulation Database (GTRD – TF targets). Only up to top ten most-upregulated and top ten
988 most-downregulated gene sets are plotted for readability.

989

Fig 3. Analysis of public ovarian aging bulk RNA-seq datasets. (A) Schematic diagram of the analysis setup of public ovarian aging bulk RNA-seq datasets, CRA003645 and PRJNA1002222, from young (2-3-months) and estropausal (12-months) female mice. (B-C) GSEA enrichment score plots of (B) genes that are up-regulated with ovarian aging ("UP with ovarian aging", left panel) and down-regulated with ovarian aging ("DOWN with ovarian aging, right panel), and (C) SenMayo gene set. In both (B) and (C), the black vertical lines indicate the positions of the genes from the gene set within the ranked list of genes. The curve represents the running enrichment score (ES), with the peak indicating the point of maximum enrichment for the gene set. The color scale at the bottom of the plot reflects the ranking metric, where red represents upregulated genes and blue represents downregulated genes. The p-value shown is calculated based on GSEA and adjusted for multiple testing using the Benjamini-Hochberg method. DGE: Differential gene expression. (D) Boxplots of DESeq2 normalized $\log_2$ counts of *Cd38*, *Cdkn1a* and *Il1a*.

Fig 4. Evaluation of fertility and ovarian health state of fecal microbiota transplantation recipient mice. (A) Schematic diagram of the experimental setup. (B) Boxplot of ovarian health index of FMT-YF and FMT-EF mice. Ovarian health index was calculated for two independent cohorts (n=5 or 7 per group and 10 or 14 per cohort). (C) Boxplot of pup counts of first litters of young and estropausal female mice fecal microbiota transplantation recipient mice (FMT-YF and FMT-EF, respectively). Pup counts were measured from two independent cohorts (n=8 or 10 per group and 16 or 20 per cohort). (D) Reproductive success rate analysis result shown as percentages of nulliparous between FMT-YF and FMT-EF. Significance in nonparametric two-sided Wilcoxon rank-sum tests are reported for (B) and (C), and logrank test for (D).

Fig 5. Characterization of fecal microbial profiles of fecal microbiota transplantation recipient mice. (A) Schematic diagram of the experimental setup. (B) Principal component analysis result of CLR-transformed and batch-corrected counts from young and estropausal female mice fecal microbiota transplantation recipient mice (FMT-YF and FMT-EF, respectively). (C) Principal coordinate analysis results of Bray-Curtis dissimilarity (left panel) and Jaccard (right panel) indices. (D) Boxplots of Observed features and Shannon entropy indices of FMT-YF and FMT-EF mice. (E) Volcano plot of differential

abundance analysis results of microbial species of FMT-YF vs. FMT-EF mice using ALDEx2. (F) Bubble plot of top 10 up- and down-regulated microbial species in FMT-EF. (G) Functional abundance analysis of FMT-YF vs. FMT-EF mice using HUMAnN3 (Q-value < 0.1). Significance in nonparametric two-sided Wilcoxon rank-sum tests are reported for (D).

Fig 6. Characterization of serum metabolic profiles of fecal microbiota transplantation recipient mice. (A) Schematic diagram of the experimental setup. (B) PCA plots of identified serum metabolites from two independent FMT cohorts. (C) LDA2 projection scatter plot displaying LDA1 scores for the FMT-YF and FMT-EF groups. (D) Top 15 metabolites contributing to LDA-based separation, ranked by their positive and negative contributions to the LDA axis. (E) Boxplots of 3,4-dihydroxyphenylpropionic acid (3,4-DHPPA) and lactamide serum levels between FMT-YF and FMT-EF groups. Significance in nonparametric two-sided Wilcoxon rank-sum tests are reported for (E).

Fig 7. Causal mediation analysis of microbial species and ovarian transcriptome changes in fecal microbiota transplantation recipient mice. (A) Graphical representation of causal mediation analysis. (B) Causal mediation analysis results of whole genome shotgun metagenomics counts that showed significant mediation effects on changes in the ovarian transcriptome in fecal microbiota transplantation recipient mice. Nonparametric bootstrap confidence intervals with the percentile method are reported. (C) Heatmap of Spearman correlation analysis between CLR-transformed WGS count data and serum hormone quantification data. #: p-value < 0.1; *: p-value < 0.05. (D) Summary diagram. The estropausal female fecal microbiota exhibits increased levels of commensal microbes and metabolites through compensatory mechanisms. As a result, fecal transplantation of estropausal microbiota enhances ovarian health measures. Potential mechanisms, including NAD and vitamin K synthesis pathways, should be further examined. Generic Diagramming Platform (GDP) was used to generate the summary diagram[138]. ACME: Average Causal Mediated Effect; ADE: Average Direct Effect.

Extended Data Fig. legend

Extended Data Fig. 1. Characterization of ovarian health state of young and estropausal female mice. (A) Schematic diagram of ovarian health index calculation. (B) Representative images of ovarian hematoxylin-eosin stained sections. Scale bar: 50 μm. (C) Boxplots of ovarian follicle counts per section. The schematic diagrams of the follicles were created using the Generic Diagramming Platform (GDP)[138]. (D) Boxplots of serum concentrations of FSH and Inhibin A. Significance in nonparametric two-sided Wilcoxon rank-sum tests are reported for (C) and (D). YF: Young female; EF: Estropausal female.

Extended Data Fig. 2. Characterization of fecal microbial profiles of young and estropausal female mice. (A) Principal coordinate analysis results of Bray-Curtis dissimilarity (top panel) and Jaccard (bottom panel) indices. (B) Boxplots of base abundance of differentially abundant microbial genera. YF: Young female; EF: Estropausal female.

Extended Data Fig. 3. Characterization of fecal microbial profiles of young and estropausal female mice. Boxplots of base abundance of differentially abundant microbial genera. YF: Young female; EF: Estropausal female.

Extended Data Fig. 4. Characterization of ovarian health state of VCD cohort mice. (A) Schematic diagram of the experimental setup of VCD cohort. (B) Representative images of ovarian hematoxylin-eosin stained sections. Scale bar: 50 μm. (C-F) Boxplots of (C) ovarian follicle counts per section, (D) combined follicle counts, (E) ovarian health index, and (E) serum concentrations of AMH, FSH and Inhibin A of control and VCD-injected mice. The schematic diagrams of the follicles were created using the Generic Diagramming Platform (GDP)[138]. Significance in nonparametric two-sided Wilcoxon rank-sum tests are reported for (C-F).

Extended Data Fig. 5. Characterization of fecal microbial profiles of VCD cohort mice. (A) Principal component analysis result of CLR-transformed and batch-corrected ASV counts from control and VCD-

injected mice. (B) Principal coordinate analysis results of Bray-Curtis dissimilarity (top panel) and Jaccard (bottom panel) indices. (C, D) Boxplots of normalized observed features and Shannon entropy indices of (C) females, and (D) males. Median from control-injected mice was used to normalize indices. (E) Differential abundance analysis results of microbial genera of control vs. VCD-injected female mice using ALDEx2. (F) Functional abundance prediction analysis of control vs. VCD-injected female mice using PICRUSt2. Significance in nonparametric two-sided Wilcoxon rank-sum tests are reported for (C,D).

Extended Data Fig. 6. Differential abundance analysis of 16S amplicon sequencing data of VCD cohort female mice. Boxplots of base abundance of differentially abundant microbial genera between control and VCD-injected female mice.

Extended Data Fig. 7. Characterization of fecal microbial profiles of young and old male mice. (A) Schematic diagram of the experimental setup of male aging cohorts. (B) Principal component analysis result of CLR-transformed and batch-corrected ASV counts from young and old male mice. Animals from three independent cohorts, n=14 per group (variation due to animal death or abnormal health issues prior to experiment). (C) Principal coordinate analysis results of Bray-Curtis dissimilarity (top panel) and Jaccard (bottom panel) indices. (D) Boxplots of observed features and Shannon entropy indices of young and old male mice. Medians from young males for each cohort were used to normalize indices per cohort. (E) Differential abundance analysis results of microbial genera of young and old male mice using ALDEx2. (F) Functional abundance prediction analysis of young vs. old male mice using PICRUSt2. Significance in nonparametric two-sided Wilcoxon rank-sum tests are reported for (D). YM: Young male; OM: Old male.

Extended Data Fig. 8. Differential abundance analysis of 16S amplicon sequencing data of young and old male mice. Boxplots of base abundance of differentially abundant microbial genera between young and old male mice.

Extended Data Fig. 9. Bulk RNA-seq analysis of ovaries from young and estropausal female mice fecal microbiota transplantation recipient mice. (A) Heat map of significant (FDR < 5%) genes

differentially expressed in FMT-YF vs. FMT-EF mice. (B) Dot plots of immune cell proportions in percentages between young and estropausal fecal microbiota transplantation recipient mice (FMT-YF and FMT-EF, respectively) predicted by deconvolution analyses using CSCDRNA (left panel) and Granulator (right panel). (C) GSEA enrichment score plots Ncoa1-peak (left panel) and Usp7-peak (right panel) genes. (D) Bar plots of normalized $\log_2$ counts of *Ncoa1* and *Usp7* expression.

Extended Data Fig. 10. Characterization of ovarian health state of FMT cohort mice. (A) Representative images of ovarian hematoxylin-eosin stained sections. Scale bar: 50 μm. (B-E) Boxplots of (B) combined ovarian follicle counts, (C) ovarian follicle counts per section, (D) serum concentrations of AMH, FSH (Multiplex assay), FSH (Ultra-sensitive assay), FSH combined and INHBA, and (E) weight percentage difference between day 0 and 16 of FMT regimen. The schematic diagrams of the follicles were created using the Generic Diagramming Platform (GDP)[138].

Extended Data Fig. 11. Characterization of fecal microbial profiles of FMT cohort mice. (A) Principal component analysis result of CLR-transformed and batch-corrected counts from young and estropausal female mice fecal microbiota transplantation recipient mice (FMT-YF and FMT-EF, respectively). (B) Principal coordinate analysis results of Bray-Curtis dissimilarity (left panel) and Jaccard (right panel) indices. (C) Boxplots of observed features and Shannon entropy indices of FMT-YF and FMT-EF mice. (D) Differential abundance analysis results of microbial species of FMT-YF vs. FMT-EF mice using ALDEx2. (E) Venn diagram of overlapping microbial genera between genera that increase in abundance with female aging ("UP in EF") and increase in abundance in FMT-EF recipient mice ("UP in FMT-EF"). (F) Functional abundance prediction analysis of FMT-YF vs. FMT-EF mice using PICRUSt2. Significance in nonparametric two-sided Wilcoxon rank-sum tests are reported for (C). YF: Young female; EF: Estropausal female.

Extended Data Fig. 12. Differential abundance analysis of 16S amplicon sequencing data of FMT cohort mice. Boxplots of base abundance of differentially abundant microbial genera between FMT-YF and FMT-EF mice.

Extended Data Fig. 13. Differential abundance analysis of WGS data of FMT cohort mice. Boxplots of base abundance of differentially abundant microbial species between FMT-YF and FMT-EF mice.

Extended Data Fig. 14. Stool vitamin K quantification of FMT cohort mice. (A) Stool concentrations of combined vitamin K (MK6-MK13) of FMT-YF and FMT-EF. (B) Fold change in stool concentrations of vitamin K (MK6-MK13) of FMT-YF and FMT-EF.

Extended Data Fig. 15. Serum untargeted metabolomics analysis of FMT cohort mice. Boxplots of metabolite abundances of top 15 metabolites contributing to LDA separation between FMT-YF and FMT-EF.

Extended Data Fig. 16. Causal mediation analysis of microbial species and ovarian transcriptome changes in fecal microbiota transplantation recipient mice. (A) Graphical representation of causal mediation analysis. (B) Causal mediation analysis results of 16S amplicon ASVs that showed significant mediation effects on changes in the ovarian transcriptome in fecal microbiota transplantation recipient mice. Nonparametric bootstrap confidence intervals with the percentile method are reported. ACME: Average Causal Mediated Effect; ADE: Average Direct Effect.

Extended Data Table

Extended Data Table 1. Weight measurements of FMT cohort.

Extended Data Table 2. Estrous cycle staging data of FMT cohort.

Extended Data Table 3. ALDEx2 differential abundance analysis result of metagenomics data of FMT cohort.

Extended Data Table 4. MS2-filtered metabolite abundance matrix.

References

1. Davis, S. R. *et al.* Menopause. *Nat Rev Dis Primers* **1**, 15004, doi:10.1038/nrdp.2015.4 (2015).
2. Broekmans, F. J., Soules, M. R. & Fauser, B. C. Ovarian aging: mechanisms and clinical consequences. *Endocr Rev* **30**, 465-493, doi:10.1210/er.2009-0006 (2009).
3. Faddy, M. J. & Gosden, R. G. A model conforming the decline in follicle numbers to the age of menopause in women. *Hum Reprod* **11**, 1484-1486, doi:10.1093/oxfordjournals.humrep.a019422 (1996).
4. Fu, C. *et al.* Association of reproductive factors with dementia: A systematic review and dose-response meta-analyses of observational studies. *EClinicalMedicine* **43**, 101236, doi:10.1016/j.eclinm.2021.101236 (2022).
5. Shuster, L. T., Rhodes, D. J., Gostout, B. S., Grossardt, B. R. & Rocca, W. A. Premature menopause or early menopause: long-term health consequences. *Maturitas* **65**, 161-166, doi:10.1016/j.maturitas.2009.08.003 (2010).
6. Muka, T. *et al.* Association of Age at Onset of Menopause and Time Since Onset of Menopause With Cardiovascular Outcomes, Intermediate Vascular Traits, and All-Cause Mortality: A Systematic Review and Meta-analysis. *JAMA Cardiol* **1**, 767-776, doi:10.1001/jamacardio.2016.2415 (2016).
7. Ossewaarde, M. E. *et al.* Age at menopause, cause-specific mortality and total life expectancy. *Epidemiology* **16**, 556-562, doi:10.1097/01.ede.0000165392.35273.d4 (2005).
8. Hong, J. S. *et al.* Age at menopause and cause-specific mortality in South Korean women: Kangwha Cohort Study. *Maturitas* **56**, 411-419, doi:10.1016/j.maturitas.2006.11.004 (2007).
9. Knobil, E. The neuroendocrine control of the menstrual cycle. *Recent Prog Horm Res* **36**, 53-88, doi:10.1016/b978-0-12-571136-4.50008-5 (1980).
10. Santoro, N., Roeca, C., Peters, B. A. & Neal-Perry, G. The Menopause Transition: Signs, Symptoms, and Management Options. *J Clin Endocrinol Metab* **106**, 1-15, doi:10.1210/clinem/dgaa764 (2021).
11. Randolph, J. F., Jr. *et al.* Change in follicle-stimulating hormone and estradiol across the menopausal transition: effect of age at the final menstrual period. *J Clin Endocrinol Metab* **96**, 746-754, doi:10.1210/jc.2010-1746 (2011).
12. Kelsey, T. W., Wright, P., Nelson, S. M., Anderson, R. A. & Wallace, W. H. A validated model of serum anti-mullerian hormone from conception to menopause. *PLoS One* **6**, e22024, doi:10.1371/journal.pone.0022024 (2011).
13. Weiss, G., Skurnick, J. H., Goldsmith, L. T., Santoro, N. F. & Park, S. J. Menopause and hypothalamic-pituitary sensitivity to estrogen. *JAMA* **292**, 2991-2996, doi:10.1001/jama.292.24.2991 (2004).
14. Xiong, J. *et al.* FSH blockade improves cognition in mice with Alzheimer's disease. *Nature* **603**, 470-476, doi:10.1038/s41586-022-04463-0 (2022).
15. Mao, L., Wang, L., Bennett, S., Xu, J. & Zou, J. Effects of follicle-stimulating hormone on fat metabolism and cognitive impairment in women during menopause. *Front Physiol* **13**, 1043237, doi:10.3389/fphys.2022.1043237 (2022).

16 Xiong, J. *et al.* FSH and ApoE4 contribute to Alzheimer's disease-like pathogenesis via C/EBPbeta/delta-secretase in female mice. *Nat Commun* **14**, 6577, doi:10.1038/s41467-023-42282-7 (2023).

17 Luckey, T. D. Introduction to intestinal microecology. *Am J Clin Nutr* **25**, 1292-1294, doi:10.1093/ajcn/25.12.1292 (1972).

18 Savage, D. C. Microbial ecology of the gastrointestinal tract. *Annu Rev Microbiol* **31**, 107-133, doi:10.1146/annurev.mi.31.100177.000543 (1977).

19 Sender, R., Fuchs, S. & Milo, R. Are We Really Vastly Outnumbered? Revisiting the Ratio of Bacterial to Host Cells in Humans. *Cell* **164**, 337-340, doi:10.1016/j.cell.2016.01.013 (2016).

20 Biagi, E. *et al.* Ageing and gut microbes: perspectives for health maintenance and longevity. *Pharmacol Res* **69**, 11-20, doi:10.1016/j.phrs.2012.10.005 (2013).

21 Zapata, H. J. & Quagliarello, V. J. The microbiota and microbiome in aging: potential implications in health and age-related diseases. *J Am Geriatr Soc* **63**, 776-781, doi:10.1111/jgs.13310 (2015).

22 Parker, A. *et al.* Fecal microbiota transfer between young and aged mice reverses hallmarks of the aging gut, eye, and brain. *Microbiome* **10**, 68, doi:10.1186/s40168-022-01243-w (2022).

23 Kundu, P. *et al.* Neurogenesis and prolongevity signaling in young germ-free mice transplanted with the gut microbiota of old mice. *Sci Transl Med* **11**, doi:10.1126/scitranslmed.aau4760 (2019).

24 Wu, J. *et al.* Association between premature ovarian insufficiency and gut microbiota. *BMC Pregnancy Childbirth* **21**, 418, doi:10.1186/s12884-021-03855-w (2021).

25 Qi, X. *et al.* Gut microbiota-bile acid-interleukin-22 axis orchestrates polycystic ovary syndrome. *Nat Med* **25**, 1225-1233, doi:10.1038/s41591-019-0509-0 (2019).

26 Weger, B. D. *et al.* The Mouse Microbiome Is Required for Sex-Specific Diurnal Rhythms of Gene Expression and Metabolism. *Cell Metab* **29**, 362-382 e368, doi:10.1016/j.cmet.2018.09.023 (2019).

27 Lombardi, P., Goldin, B., Boutin, E. & Gorbach, S. L. Metabolism of androgens and estrogens by human fecal microorganisms. *J Steroid Biochem* **9**, 795-801, doi:10.1016/0022-4731(78)90203-0 (1978).

28 Adlercreutz, H., Martin, F., Jarvenpaa, P. & Fotsis, T. Steroid absorption and enterohepatic recycling. *Contraception* **20**, 201-223, doi:10.1016/0010-7824(79)90094-5 (1979).

29 Eriksson, H. & Gustafsson, J. A. Steroids in germfree and conventional rats. Distribution and excretion of labelled pregnenolone and corticosterone in male and female rats. *Eur J Biochem* **15**, 132-139, doi:10.1111/j.1432-1033.1970.tb00987.x (1970).

30 Finch, C. E. The menopause and aging, a comparative perspective. *J Steroid Biochem Mol Biol* **142**, 132-141, doi:10.1016/j.jsbmb.2013.03.010 (2014).

31 Whitehead, J. C. *et al.* A clinical frailty index in aging mice: comparisons with frailty index data in humans. *J Gerontol A Biol Sci Med Sci* **69**, 621-632, doi:10.1093/gerona/glt136 (2014).

32 Wallace, W. H. & Kelsey, T. W. Human ovarian reserve from conception to the menopause. *PLoS One* **5**, e8772, doi:10.1371/journal.pone.0008772 (2010).

33 Hirshfield, A. N. Development of follicles in the mammalian ovary. *Int Rev Cytol* **124**, 43-101, doi:10.1016/s0074-7696(08)61524-7 (1991).

34 Tehrani, F. R., Mansournia, M. A., Solaymani-Dodaran, M. & Azizi, F. Age-specific serum anti-Mullerian hormone levels: estimates from a large population-based sample. *Climacteric* **17**, 591-597, doi:10.3109/13697137.2014.912262 (2014).

35 Broer, S. L., Broekmans, F. J., Laven, J. S. & Fauser, B. C. Anti-Mullerian hormone: ovarian reserve testing and its potential clinical implications. *Hum Reprod Update* **20**, 688-701, doi:10.1093/humupd/dmu020 (2014).

36 Felicio, L. S., Nelson, J. F. & Finch, C. E. Prolongation and cessation of estrous cycles in aging C57BL/6J mice are differentially regulated events. *Biol Reprod* **34**, 849-858, doi:10.1095/biolreprod34.5.849 (1986).

37 Johnson, J. S. *et al.* Evaluation of 16S rRNA gene sequencing for species and strain-level microbiome analysis. *Nat Commun* **10**, 5029, doi:10.1038/s41467-019-13036-1 (2019).

38 Gupta, S. *et al.* Amplicon sequencing provides more accurate microbiome information in healthy children compared to culturing. *Commun Biol* **2**, 291, doi:10.1038/s42003-019-0540-1 (2019).

39 Knight, R. *et al.* Best practices for analysing microbiomes. *Nat Rev Microbiol* **16**, 410-422, doi:10.1038/s41579-018-0029-9 (2018).

40 Willis, A. D. Rarefaction, Alpha Diversity, and Statistics. *Front Microbiol* **10**, 2407, doi:10.3389/fmicb.2019.02407 (2019).

41 Wang, Y. & LeCao, K. A. Managing batch effects in microbiome data. *Brief Bioinform* **21**, 1954-1970, doi:10.1093/bib/bbz105 (2020).

42 Gamez-Macias, P. E. *et al.* Intestinal Permeability, Gut Inflammation, and Gut Immune System Response Are Linked to Aging-Related Changes in Gut Microbiota Composition: A Study in Female Mice. *J Gerontol A Biol Sci Med Sci* **79**, doi:10.1093/gerona/glae045 (2024).

43 de la Cuesta-Zuluaga, J. *et al.* Age- and Sex-Dependent Patterns of Gut Microbial Diversity in Human Adults. *mSystems* **4**, doi:10.1128/mSystems.00261-19 (2019).

44 Ghosh, T. S., Shanahan, F. & O'Toole, P. W. Toward an improved definition of a healthy microbiome for healthy aging. *Nat Aging* **2**, 1054-1069, doi:10.1038/s43587-022-00306-9 (2022).

45 Luo, M. *et al.* E. coli Nissle 1917 ameliorates mitochondrial injury of granulosa cells in polycystic ovary syndrome through promoting gut immune factor IL-22 via gut microbiota and microbial metabolism. *Front Immunol* **14**, 1137089, doi:10.3389/fimmu.2023.1137089 (2023).

46 Biagi, E. *et al.* Gut Microbiota and Extreme Longevity. *Curr Biol* **26**, 1480-1485, doi:10.1016/j.cub.2016.04.016 (2016).

47 Wang, N. *et al.* Enriched taxa were found among the gut microbiota of centenarians in East China. *PLoS One* **14**, e0222763, doi:10.1371/journal.pone.0222763 (2019).

48 Douglas, G. M. *et al.* PICRUSt2 for prediction of metagenome functions. *Nat Biotechnol* **38**, 685-688, doi:10.1038/s41587-020-0548-6 (2020).

49 Murali, R. *et al.* Deregulated Metabolic Pathways in Ovarian Cancer: Cause and Consequence. *Metabolites* **13**, doi:10.3390/metabo13040560 (2023).

50 Ji, Z. *et al.* Deregulation of Lipid Metabolism: The Critical Factors in Ovarian Cancer. *Front Oncol* **10**, 593017, doi:10.3389/fonc.2020.593017 (2020).
51 Borman, S. M., Christian, P. J., Sipes, I. G. & Hoyer, P. B. Ovotoxicity in female Fischer rats and B6 mice induced by low-dose exposure to three polycyclic aromatic hydrocarbons: comparison through calculation of an ovotoxic index. *Toxicol Appl Pharmacol* **167**, 191-198, doi:10.1006/taap.2000.9006 (2000).
52 Van Kempen, T. A., Milner, T. A. & Waters, E. M. Accelerated ovarian failure: a novel, chemically induced animal model of menopause. *Brain Res* **1379**, 176-187, doi:10.1016/j.brainres.2010.12.064 (2011).
53 Mayer, L. P., Devine, P. J., Dyer, C. A. & Hoyer, P. B. The follicle-deplete mouse ovary produces androgen. *Biol Reprod* **71**, 130-138, doi:10.1095/biolreprod.103.016113 (2004).
54 Boehme, M. *et al.* Microbiota from young mice counteracts selective age-associated behavioral deficits. *Nat Aging* **1**, 666-676, doi:10.1038/s43587-021-00093-9 (2021).
55 Subramanian, A. *et al.* Gene set enrichment analysis: a knowledge-based approach for interpreting genome-wide expression profiles. *Proc Natl Acad Sci U S A* **102**, 15545-15550, doi:10.1073/pnas.0506580102 (2005).
56 Morris, M. E. *et al.* A single-cell atlas of the cycling murine ovary. *Elife* **11**, doi:10.7554/eLife.77239 (2022).
57 Jew, B. *et al.* Accurate estimation of cell composition in bulk expression through robust integration of single-cell information. *Nat Commun* **11**, 1971, doi:10.1038/s41467-020-15816-6 (2020).
58 Newman, A. M. *et al.* Robust enumeration of cell subsets from tissue expression profiles. *Nat Methods* **12**, 453-457, doi:10.1038/nmeth.3337 (2015).
59 Lovasco, L. A. *et al.* Accelerated ovarian aging in the absence of the transcription regulator TAF4B in mice. *Biol Reprod* **82**, 23-34, doi:10.1095/biolreprod.109.077495 (2010).
60 Baumann, C. *et al.* Acute irradiation induces a senescence-like chromatin structure in mammalian oocytes. *Commun Biol* **6**, 1258, doi:10.1038/s42003-023-05641-0 (2023).
61 Yevshin, I., Sharipov, R., Valeev, T., Kel, A. & Kolpakov, F. GTRD: a database of transcription factor binding sites identified by ChIP-seq experiments. *Nucleic Acids Res* **45**, D61-D67, doi:10.1093/nar/gkw951 (2017).
62 Zheng, R. *et al.* Cistrome Data Browser: expanded datasets and new tools for gene regulatory analysis. *Nucleic Acids Res* **47**, D729-D735, doi:10.1093/nar/gky1094 (2019).
63 Mei, S. *et al.* Cistrome Data Browser: a data portal for ChIP-Seq and chromatin accessibility data in human and mouse. *Nucleic Acids Res* **45**, D658-D662, doi:10.1093/nar/gkw983 (2017).
64 Huang, H. Y. *et al.* Association of polymorphisms for nuclear receptor coactivator 1 gene with egg production traits in the maternal line of Shaobo hens. *Br Poult Sci* **52**, 328-332, doi:10.1080/00071668.2011.577057 (2011).
65 Wang, M. *et al.* The USP7 Inhibitor P5091 Induces Cell Death in Ovarian Cancers with Different P53 Status. *Cell Physiol Biochem* **43**, 1755-1766, doi:10.1159/000484062 (2017).
66 Briley, S. M. *et al.* Reproductive age-associated fibrosis in the stroma of the mammalian ovary. *Reproduction* **152**, 245-260, doi:10.1530/REP-16-0129 (2016).

67 Zhang, Z., Schlamp, F., Huang, L., Clark, H. & Brayboy, L. Inflammaging is associated with shifted macrophage ontogeny and polarization in the aging mouse ovary. *Reproduction* **159**, 325-337, doi:10.1530/REP-19-0330 (2020).

68 Zhou, Z. *et al.* Temporal transcriptomic landscape of postnatal mouse ovaries reveals dynamic gene signatures associated with ovarian aging. *Hum Mol Genet* **30**, 1941-1954, doi:10.1093/hmg/ddab163 (2021).

69 Yang, Q. *et al.* NADase CD38 is a key determinant of ovarian aging. *Nat Aging* **4**, 110-128, doi:10.1038/s43587-023-00532-9 (2024).

70 Saul, D. *et al.* A new gene set identifies senescent cells and predicts senescence-associated pathways across tissues. *Nat Commun* **13**, 4827, doi:10.1038/s41467-022-32552-1 (2022).

71 Mehalko, K. *et al.* Lack of accelerated ovarian aging in a follicle-stimulating hormone receptor haploinsufficiency model. *Transl Med Aging* **7**, 1-8, doi:10.1016/j.tma.2023.01.001 (2023).

72 Wrzosek, L. *et al.* Transplantation of human microbiota into conventional mice durably reshapes the gut microbiota. *Sci Rep* **8**, 6854, doi:10.1038/s41598-018-25300-3 (2018).

73 Gong, X., Gutala, R. & Jaiswal, A. K. Quinone oxidoreductases and vitamin K metabolism. *Vitam Horm* **78**, 85-101, doi:10.1016/S0083-6729(07)00005-2 (2008).

74 Beghini, F. *et al.* Integrating taxonomic, functional, and strain-level profiling of diverse microbial communities with bioBakery 3. *Elife* **10**, doi:10.7554/eLife.65088 (2021).

75 Dekkers, K. F. *et al.* An online atlas of human plasma metabolite signatures of gut microbiome composition. *Nat Commun* **13**, 5370, doi:10.1038/s41467-022-33050-0 (2022).

76 Pilley, S. E. *et al.* A metabolic atlas of mouse aging. *bioRxiv*, 2024.2005.2004.592445, doi:10.1101/2024.05.04.592445 (2024).

77 Marquez Campos, E., Stehle, P. & Simon, M. C. Microbial Metabolites of Flavan-3-Ols and Their Biological Activity. *Nutrients* **11**, doi:10.3390/nu11102260 (2019).

78 He, Y. *et al.* Lactic acid bacteria alleviate polycystic ovarian syndrome by regulating sex hormone related gut microbiota. *Food Funct* **11**, 5192-5204, doi:10.1039/c9fo02554e (2020).

79 Dikalov, S., Panov, A. & Dikalova, A. Critical Role of Mitochondrial Fatty Acid Metabolism in Normal Cell Function and Pathological Conditions. *Int J Mol Sci* **25**, doi:10.3390/ijms25126498 (2024).

80 Wang, Z. H. *et al.* Targeting mitochondria for ovarian aging: new insights into mechanisms and therapeutic potential. *Front Endocrinol (Lausanne)* **15**, 1417007, doi:10.3389/fendo.2024.1417007 (2024).

81 Zhang, I. W. *et al.* Palmitoylcarnitine impairs immunity in decompensated cirrhosis. *JHEP Rep* **6**, 101187, doi:10.1016/j.jhepr.2024.101187 (2024).

82 Xu, X. L. *et al.* Estrogen Biosynthesis and Signal Transduction in Ovarian Disease. *Front Endocrinol (Lausanne)* **13**, 827032, doi:10.3389/fendo.2022.827032 (2022).

83 Stachenfeld, N. S. Hormonal changes during menopause and the impact on fluid regulation. *Reprod Sci* **21**, 555-561, doi:10.1177/1933719113518992 (2014).

84 Liu, T., Bowen, R. L., Wilson, A. C. & Atwood, C. S. Estropause, Sex Hormones and Metal Homeostasis in the Mouse Brain. *Front Neurol* **13**, 841822, doi:10.3389/fneur.2022.841822 (2022).

85 Schele, E. *et al.* The gut microbiota reduces leptin sensitivity and the expression of the obesity-suppressing neuropeptides proglucagon (Gcg) and brain-derived neurotrophic factor (Bdnf) in the central nervous system. *Endocrinology* **154**, 3643-3651, doi:10.1210/en.2012-2151 (2013).

86 Fan, K. C. *et al.* Altered gut microbiota in older adults with mild cognitive impairment: a case-control study. *Front Aging Neurosci* **15**, 1162057, doi:10.3389/fnagi.2023.1162057 (2023).

87 Ellis, J. L. *et al.* Dietary vitamin K is remodeled by gut microbiota and influences community composition. *Gut Microbes* **13**, 1-16, doi:10.1080/19490976.2021.1887721 (2021).

88 Tarkesh, F., Namavar Jahromi, B., Hejazi, N. & Tabatabaee, H. Beneficial health effects of Menaquinone-7 on body composition, glycemic indices, lipid profile, and endocrine markers in polycystic ovary syndrome patients. *Food Sci Nutr* **8**, 5612-5621, doi:10.1002/fsn3.1837 (2020).

89 Sibayama-Imazu, T. *et al.* Induction of apoptosis in PA-1 ovarian cancer cells by vitamin K2 is associated with an increase in the level of TR3/Nur77 and its accumulation in mitochondria and nuclei. *J Cancer Res Clin Oncol* **134**, 803-812, doi:10.1007/s00432-007-0349-z (2008).

90 Harshman, S. G. & Shea, M. K. The Role of Vitamin K in Chronic Aging Diseases: Inflammation, Cardiovascular Disease, and Osteoarthritis. *Curr Nutr Rep* **5**, 90-98, doi:10.1007/s13668-016-0162-x (2016).

91 Sampathkumar, N. K. *et al.* Widespread sex dimorphism in aging and age-related diseases. *Hum Genet* **139**, 333-356, doi:10.1007/s00439-019-02082-w (2020).

92 Podcasy, J. L. & Epperson, C. N. Considering sex and gender in Alzheimer disease and other dementias. *Dialogues Clin Neurosci* **18**, 437-446, doi:10.31887/DCNS.2016.18.4/cepperson (2016).

93 Vina, J. & Lloret, A. Why women have more Alzheimer's disease than men: gender and mitochondrial toxicity of amyloid-beta peptide. *J Alzheimers Dis* **20 Suppl 2**, S527-533, doi:10.3233/JAD-2010-100501 (2010).

94 Varghese, M. *et al.* Female adipose tissue has improved adaptability and metabolic health compared to males in aged obesity. *Aging (Albany NY)* **12**, 1725-1746, doi:10.18632/aging.102709 (2020).

95 Austad, S. N. & Fischer, K. E. Sex Differences in Lifespan. *Cell Metab* **23**, 1022-1033, doi:10.1016/j.cmet.2016.05.019 (2016).

96 Lemaitre, J. F. *et al.* Sex differences in adult lifespan and aging rates of mortality across wild mammals. *Proc Natl Acad Sci U S A* **117**, 8546-8553, doi:10.1073/pnas.1911999117 (2020).

97 Markle, J. G. *et al.* Sex differences in the gut microbiome drive hormone-dependent regulation of autoimmunity. *Science* **339**, 1084-1088, doi:10.1126/science.1233521 (2013).

98 Steegenga, W. T. *et al.* Sexually dimorphic characteristics of the small intestine and colon of prepubescent C57BL/6 mice. *Biol Sex Differ* **5**, 11, doi:10.1186/s13293-014-0011-9 (2014).

99 Org, E. *et al.* Sex differences and hormonal effects on gut microbiota composition in mice. *Gut Microbes* **7**, 313-322, doi:10.1080/19490976.2016.1203502 (2016).

100 Vemuri, R. *et al.* The microgenderome revealed: sex differences in bidirectional interactions between the microbiota, hormones, immunity and disease susceptibility. *Semin Immunopathol* **41**, 265-275, doi:10.1007/s00281-018-0716-7 (2019).

101 Kaliannan, K. *et al.* Estrogen-mediated gut microbiome alterations influence sexual dimorphism in metabolic syndrome in mice. *Microbiome* **6**, 205, doi:10.1186/s40168-018-0587-0 (2018).

102 Hogan, K. A., Chini, C. C. S. & Chini, E. N. The Multi-faceted Ecto-enzyme CD38: Roles in Immunomodulation, Cancer, Aging, and Metabolic Diseases. *Front Immunol* **10**, 1187, doi:10.3389/fimmu.2019.01187 (2019).

103 Camacho-Pereira, J. *et al.* CD38 Dictates Age-Related NAD Decline and Mitochondrial Dysfunction through an SIRT3-Dependent Mechanism. *Cell Metab* **23**, 1127-1139, doi:10.1016/j.cmet.2016.05.006 (2016).

104 Gomes, A. P. *et al.* Declining NAD(+) induces a pseudohypoxic state disrupting nuclear-mitochondrial communication during aging. *Cell* **155**, 1624-1638, doi:10.1016/j.cell.2013.11.037 (2013).

105 Chini, C. C. S. *et al.* CD38 ecto-enzyme in immune cells is induced during aging and regulates NAD(+) and NMN levels. *Nat Metab* **2**, 1284-1304, doi:10.1038/s42255-020-00298-z (2020).

106 Covarrubias, A. J. *et al.* Senescent cells promote tissue NAD(+) decline during ageing via the activation of CD38(+) macrophages. *Nat Metab* **2**, 1265-1283, doi:10.1038/s42255-020-00305-3 (2020).

107 Wright, L. E. *et al.* Comparison of skeletal effects of ovariectomy versus chemically induced ovarian failure in mice. *J Bone Miner Res* **23**, 1296-1303, doi:10.1359/jbmr.080309 (2008).

108 National Toxicology, P. Toxicology and Carcinogenesis Studies of 4-Vinyl-1-cyclohexene Diepoxide (CAS No. 106-87-6) in F344/N Rats and B6C3F1 Mice (Dermal Studies). *Natl Toxicol Program Tech Rep Ser* **362**, 1-249 (1989).

109 Ongaro, L. *et al.* Development of a Highly Sensitive ELISA for Measurement of FSH in Serum, Plasma, and Whole Blood in Mice. *Endocrinology* **162**, doi:10.1210/endocr/bqab014 (2021).

110 Bolyen, E. *et al.* Reproducible, interactive, scalable and extensible microbiome data science using QIIME 2. *Nat Biotechnol* **37**, 852-857, doi:10.1038/s41587-019-0209-9 (2019).

111 Callahan, B. J. *et al.* DADA2: High-resolution sample inference from Illumina amplicon data. *Nat Methods* **13**, 581-583, doi:10.1038/nmeth.3869 (2016).

112 Ritchie, M. E. *et al.* limma powers differential expression analyses for RNA-sequencing and microarray studies. *Nucleic Acids Res* **43**, e47, doi:10.1093/nar/gkv007 (2015).

113 Leek, J. T. & Storey, J. D. Capturing heterogeneity in gene expression studies by surrogate variable analysis. *PLoS Genet* **3**, 1724-1735, doi:10.1371/journal.pgen.0030161 (2007).

114 Hornung, R., Boulesteix, A. L. & Causeur, D. Combining location-and-scale batch effect adjustment with data cleaning by latent factor adjustment. *BMC Bioinformatics* **17**, 27, doi:10.1186/s12859-015-0870-z (2016).
115 Bisanz, J. <https://github.com/jbisanz/qiime2R> (
116 Rohart, F., Gautier, B., Singh, A. & Le Cao, K. A. mixOmics: An R package for 'omics feature selection and multiple data integration. *PLoS Comput Biol* **13**, e1005752, doi:10.1371/journal.pcbi.1005752 (2017).
117 Fernandes, A. D. *et al.* Unifying the analysis of high-throughput sequencing datasets: characterizing RNA-seq, 16S rRNA gene sequencing and selective growth experiments by compositional data analysis. *Microbiome* **2**, 15, doi:10.1186/2049-2618-2-15 (2014).
118 Yilmaz, P. *et al.* The SILVA and "All-species Living Tree Project (LTP)" taxonomic frameworks. *Nucleic Acids Res* **42**, D643-648, doi:10.1093/nar/gkt1209 (2014).
119 Gordon, A. <http://hannonlab.cshl.edu/fastx_toolkit/> (
120 Krueger, F. <https://www.bioinformatics.babraham.ac.uk/projects/trim_galore/> (
121 Dobin, A. *et al.* STAR: ultrafast universal RNA-seq aligner. *Bioinformatics* **29**, 15-21, doi:10.1093/bioinformatics/bts635 (2013).
122 Liao, Y., Smyth, G. K. & Shi, W. featureCounts: an efficient general purpose program for assigning sequence reads to genomic features. *Bioinformatics* **30**, 923-930, doi:10.1093/bioinformatics/btt656 (2014).
123 Love, M. I., Huber, W. & Anders, S. Moderated estimation of fold change and dispersion for RNA-seq data with DESeq2. *Genome Biol* **15**, 550, doi:10.1186/s13059-014-0550-8 (2014).
124 Signorell, A. <https://andrisignorell.github.io/DescTools/> (
125 Liberzon, A. *et al.* The Molecular Signatures Database (MSigDB) hallmark gene set collection. *Cell Syst* **1**, 417-425, doi:10.1016/j.cels.2015.12.004 (2015).
126 Karimnezhad, A. More accurate estimation of cell composition in bulk expression through robust integration of single-cell information. *Bioinform Adv* **2**, vbac049, doi:10.1093/bioadv/vbac049 (2022).
127 Pfister, S., Kuettel, V., Ferrero, E. <https://github.com/Novartis/granulator> (
128 Gong, T. & Szustakowski, J. D. DeconRNASeq: a statistical framework for deconvolution of heterogeneous tissue samples based on mRNA-Seq data. *Bioinformatics* **29**, 1083-1085, doi:10.1093/bioinformatics/btt090 (2013).
129 Heinz, S. *et al.* Simple combinations of lineage-determining transcription factors prime cis-regulatory elements required for macrophage and B cell identities. *Mol Cell* **38**, 576-589, doi:10.1016/j.molcel.2010.05.004 (2010).
130 Bolger, A. M., Lohse, M. & Usadel, B. Trimmomatic: a flexible trimmer for Illumina sequence data. *Bioinformatics* **30**, 2114-2120, doi:10.1093/bioinformatics/btu170 (2014).
131 Langmead, B., Wilks, C., Antonescu, V. & Charles, R. Scaling read aligners to hundreds of threads on general-purpose processors. *Bioinformatics* **35**, 421-432, doi:10.1093/bioinformatics/bty648 (2019).
132 Wood, D. E., Lu, J. & Langmead, B. Improved metagenomic analysis with Kraken 2. *Genome Biol* **20**, 257, doi:10.1186/s13059-019-1891-0 (2019).

133 Lu, J. *et al.* Metagenome analysis using the Kraken software suite. *Nat Protoc* **17**, 2815-2839, doi:10.1038/s41596-022-00738-y (2022).
134 mia: Microbiome analysis (2025).
135 Lin, H. & Peddada, S. D. Multigroup analysis of compositions of microbiomes with covariate adjustments and repeated measures. *Nat Methods* **21**, 83-91, doi:10.1038/s41592-023-02092-7 (2024).
136 Karl, J. P., Fu, X., Dolnikowski, G. G., Saltzman, E. & Booth, S. L. Quantification of phylloquinone and menaquinones in feces, serum, and food by high-performance liquid chromatography-mass spectrometry. *J Chromatogr B Analyt Technol Biomed Life Sci* **963**, 128-133, doi:10.1016/j.jchromb.2014.05.056 (2014).
137 Tingley, D., Yamamoto, T., Hirose, K., Keele, L. & Imai, K. mediation: R Package for Causal Mediation Analysis. *Journal of Statistical Software* **59**, 1 - 38, doi:10.18637/jss.v059.i05 (2014).
138 Jiang, S. *et al.* Generic Diagramming Platform (GDP): a comprehensive database of high-quality biomedical graphics. *Nucleic Acids Res* **53**, D1670-D1676, doi:10.1093/nar/gkae973 (2025).

Figure 1

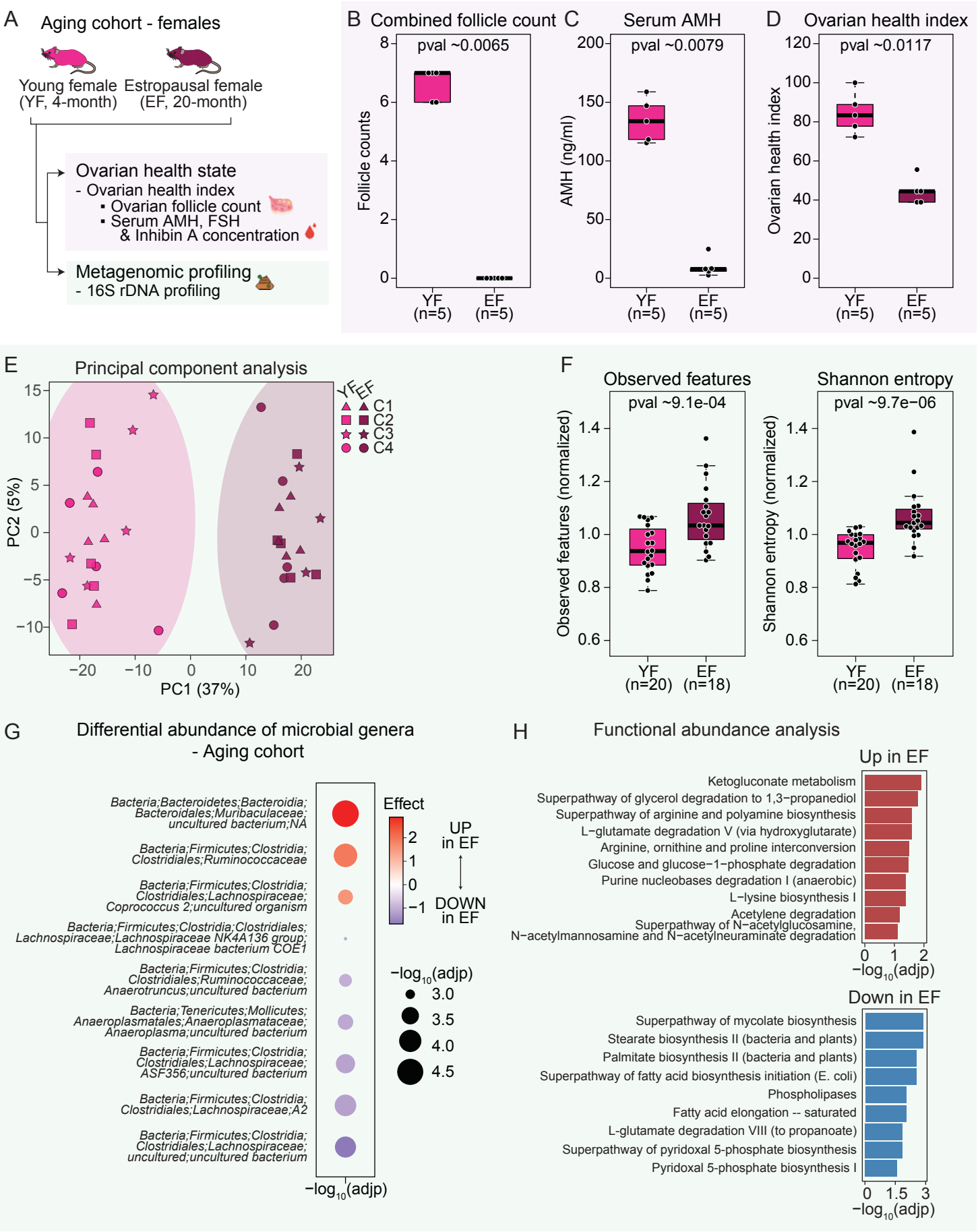

Figure 2

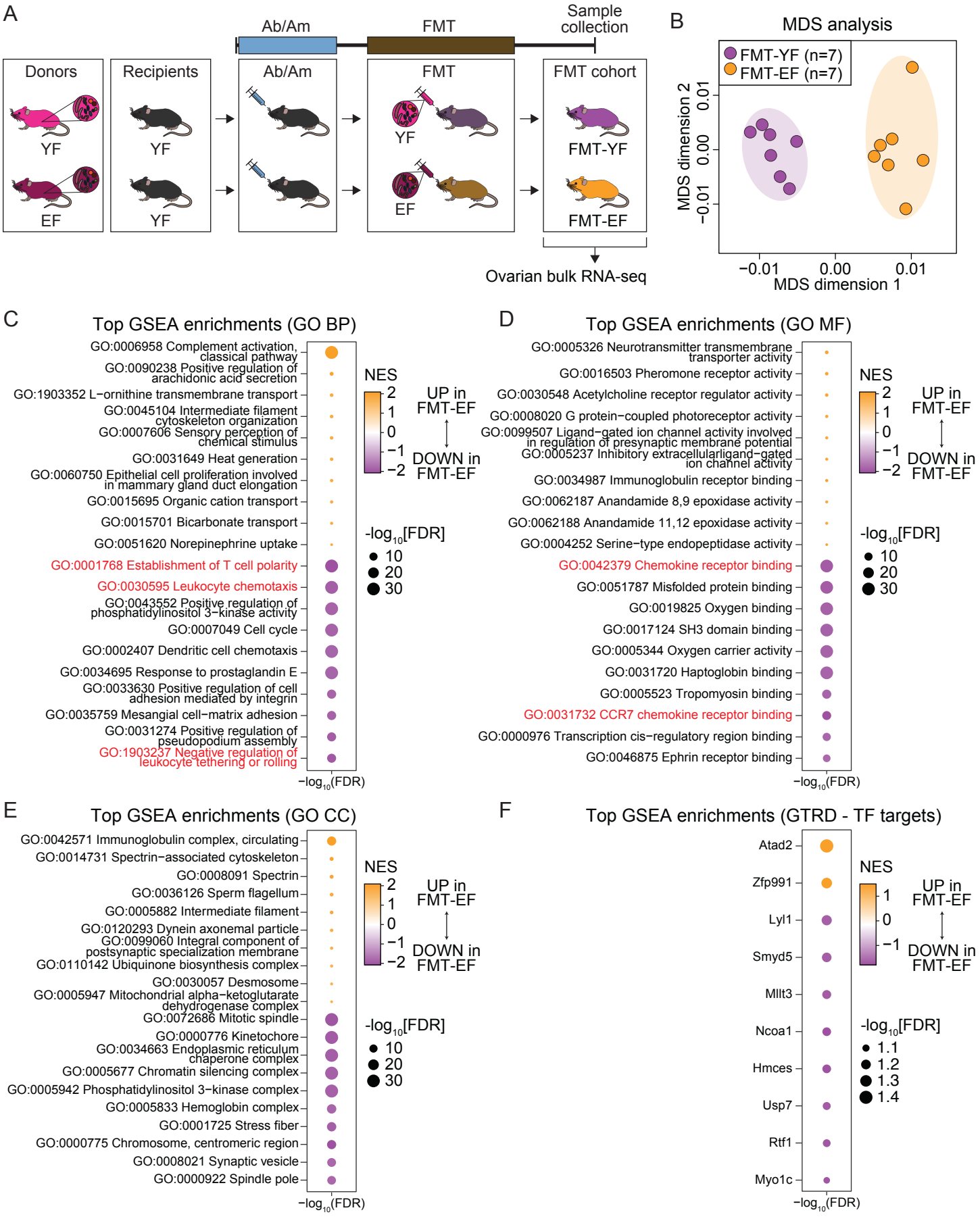

Figure 3

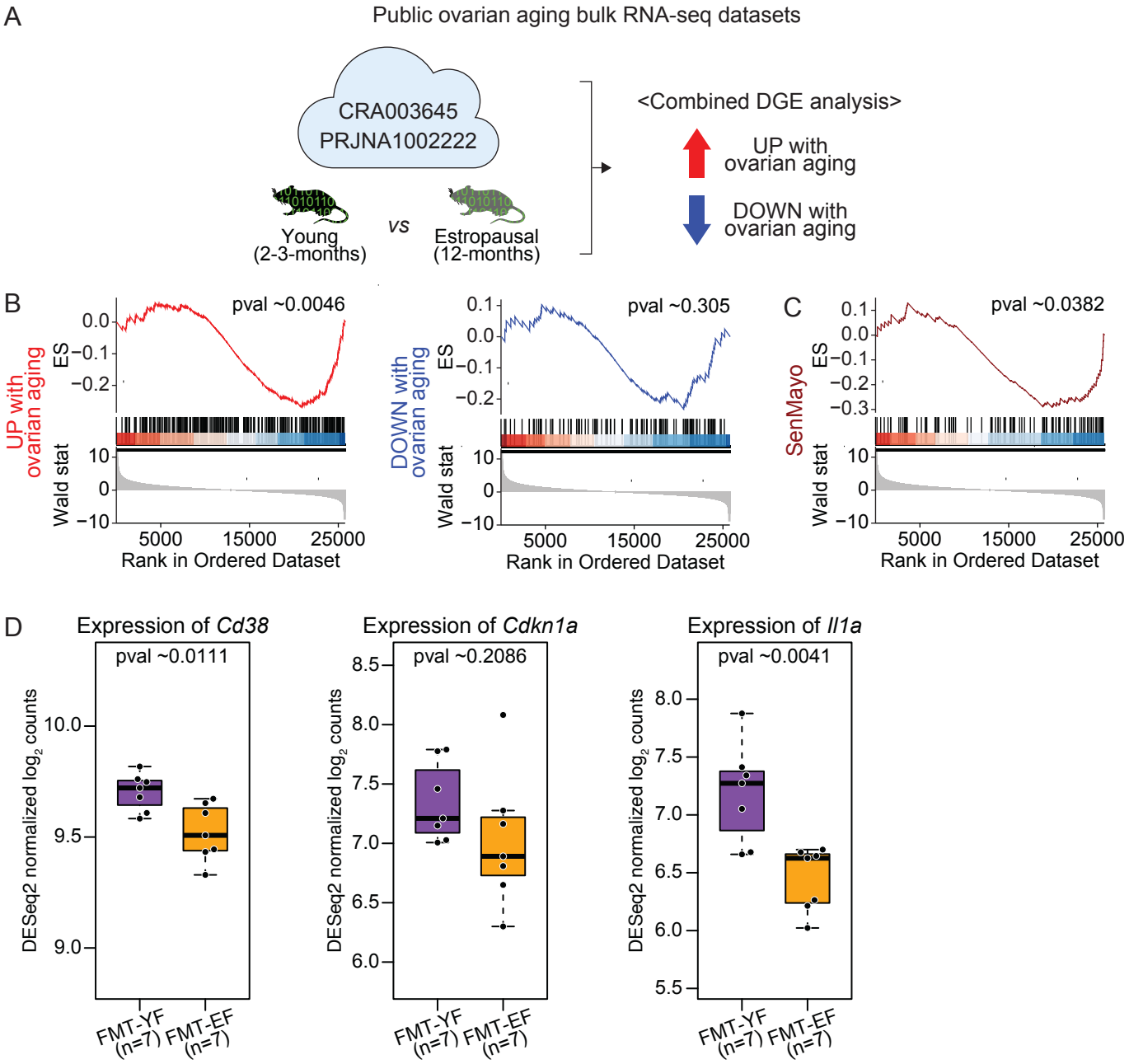

Figure 4

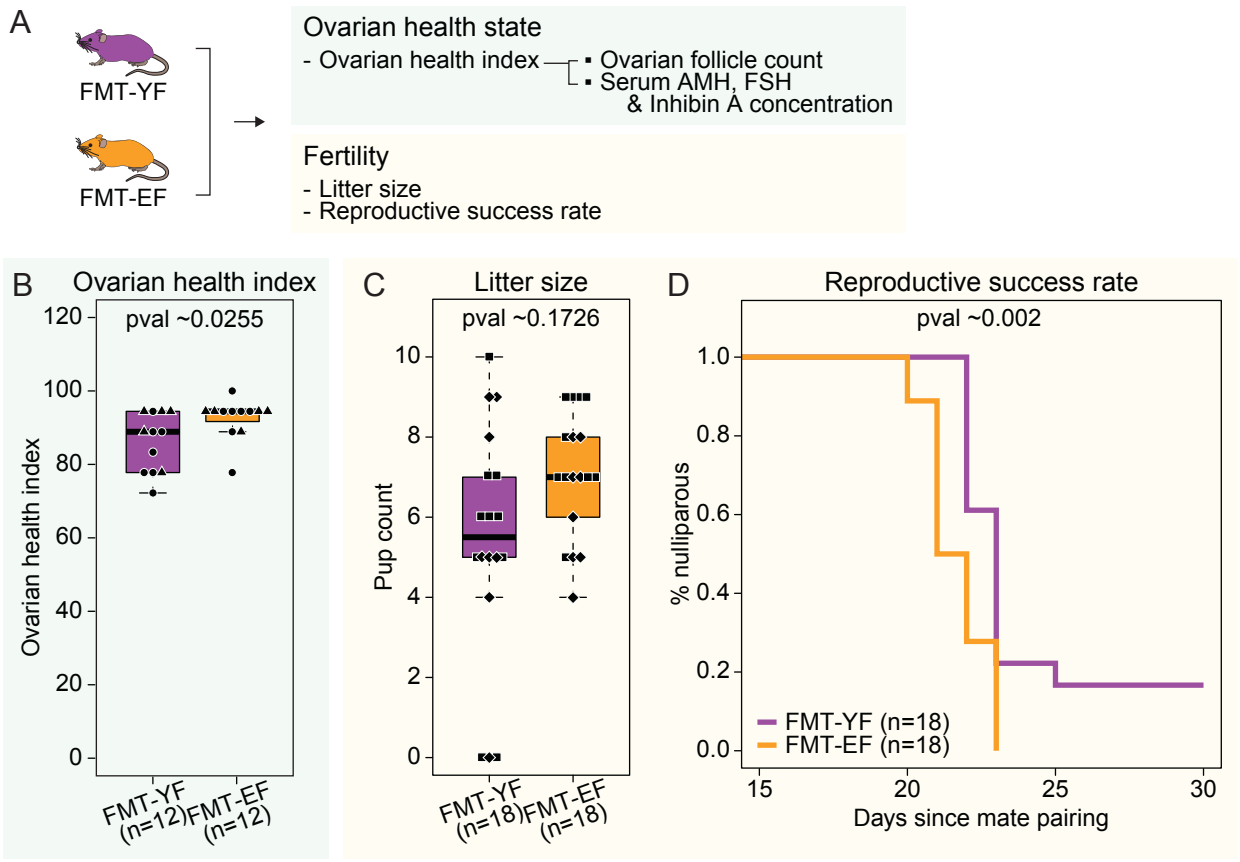

Figure 5

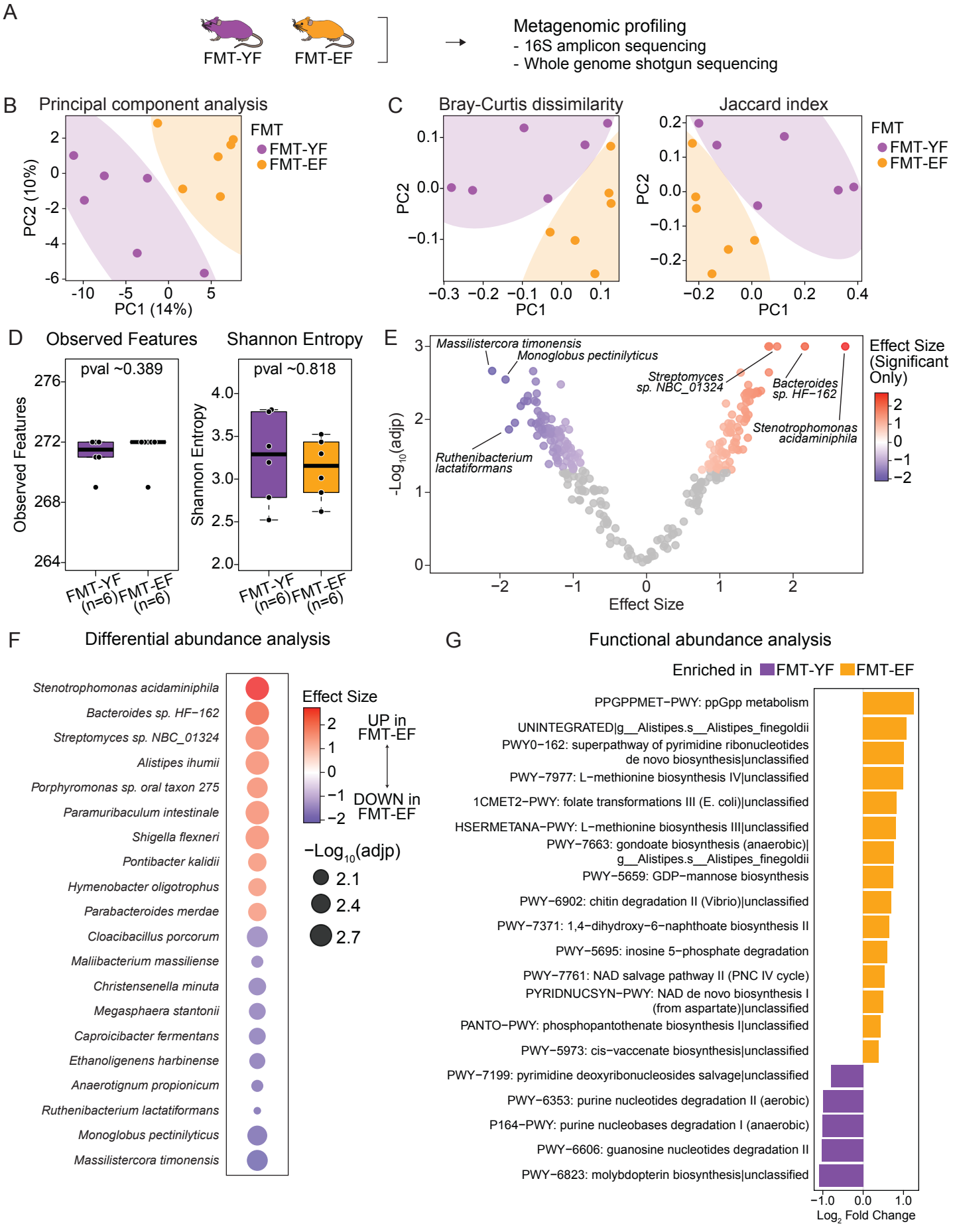

Figure 6

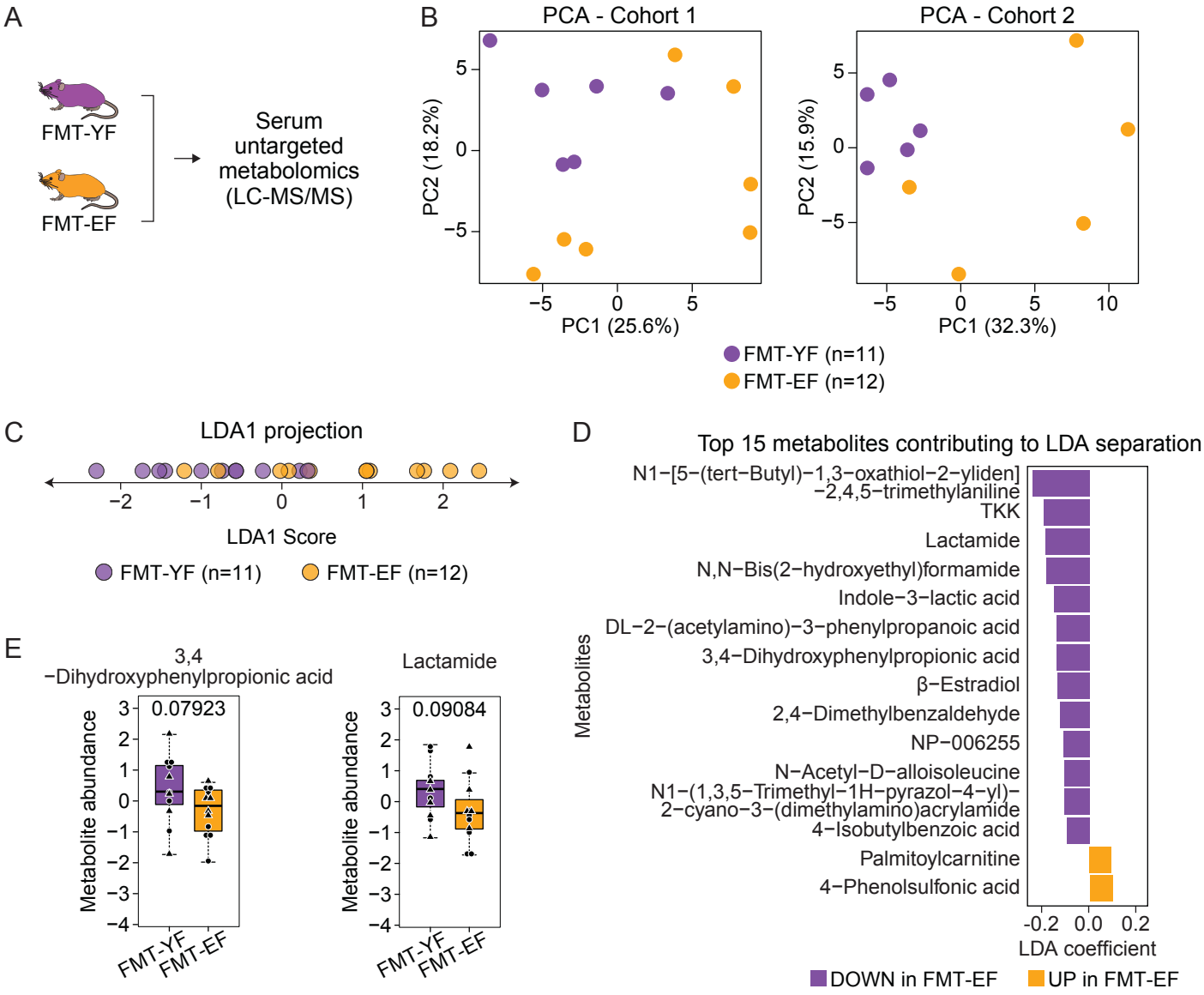

Figure 7

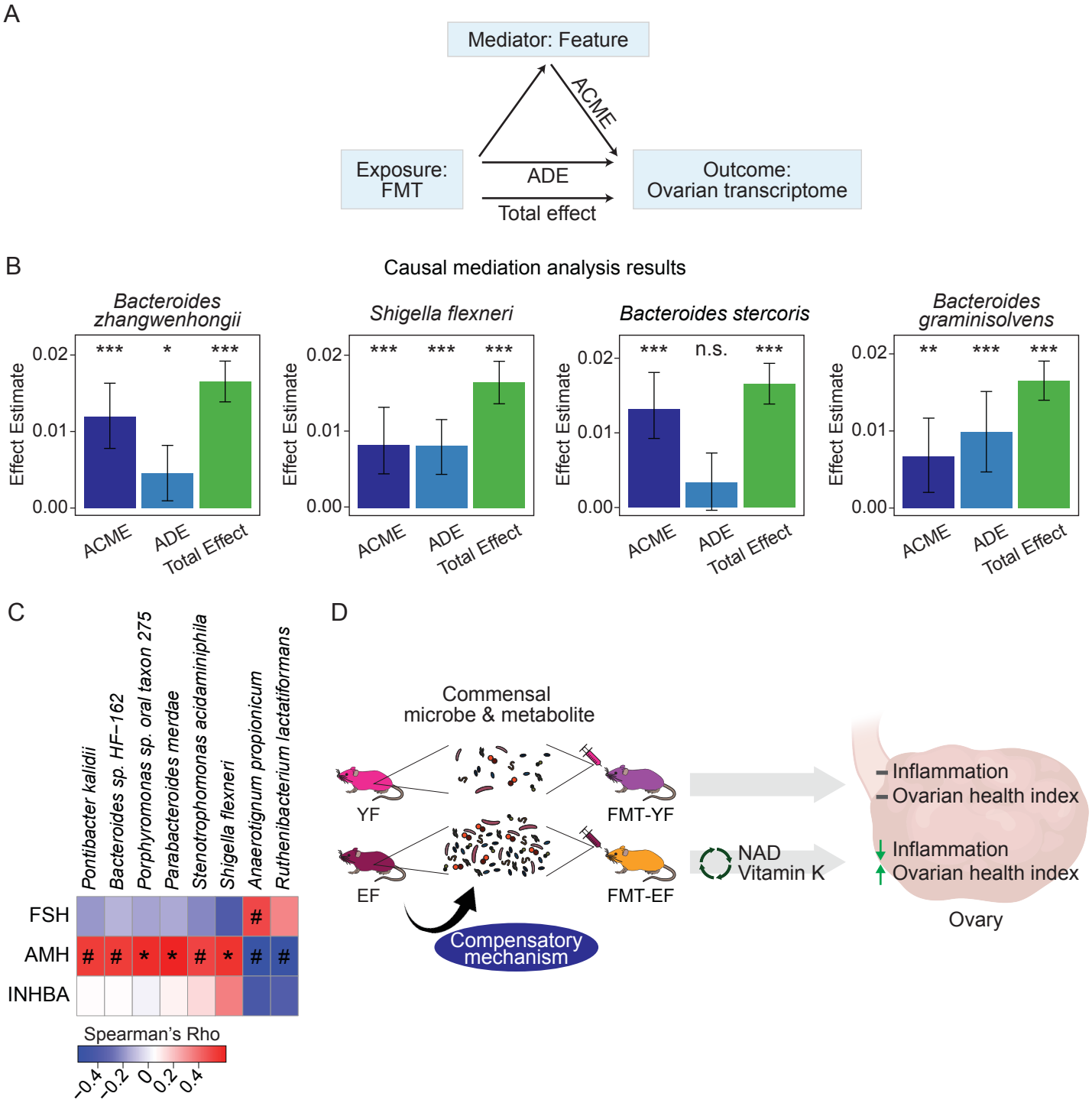

6.4 Clinical response to EPA supplementation in patients with major depressive disorder is associated with higher plasma concentrations of pro-resolving lipid mediators

Stefania Lamon-Fava, MD PhD[a], Minying Liu, MS[a], Boadie W. Dunlop, MD[b], Becky Kinkead, MD[c], Pamela J. Schettler, PhD[b], Jennifer C. Felger, MD[b], Thomas R. Ziegler, MD[d], Maurizio Fava, MD[e], David Mischoulon, MD PhD[e] *, Mark Hyman Rapaport, MD[c] *.

[a]Jean Mayer USDA Human Nutrition Research Center on Aging at Tufts University, Boston, MA; [b] Department of Psychiatry and Behavioral Sciences, Emory University, Atlanta, GA; [c] Huntsman Mental Health Institute, Department of Psychiatry, University of Utah, Salt Lake City, UT; [d] Department of Medicine, Emory University, Atlanta, GA; [e] Department of Psychiatry, Massachusetts General Hospital, Boston, MA.

*Co-senior authors

PMID: 36635595 **PMCID:** PMC10156711 **DOI:** 10.1038/s41386-022-01527-7

Running title: EPA, SPMs and MDD

Corresponding Author:

Stefania Lamon-Fava, MD PhD
Cardiovascular Nutrition Laboratory
Jean Mayer USDA Human Nutrition Research Center on Aging
Tufts University
711 Washington Street
Boston, MA 02111
Email: stefania.lamon-fava@tufts.edu

ABSTRACT

Chronic inflammation has been implicated in the pathophysiology of major depressive disorder (MDD). Activating the resolution of inflammation through ω-3 fatty acid supplementation may prove to be a successful therapeutic strategy for the treatment of MDD.Patients with MDD, body mass index >25 kg/m^2 and plasma high-sensitivity C-reactive protein ≥3 μg/mL (n=61) were enrolled in a 12-week randomized trial consisting of 4 parallel arms: EPA 1, 2, and 4 g/d, and placebo. The supplement contained EPA and DHA in a 3.9:1 ratio. Depression symptoms were assessed using the IDS-C30 scale. Plasma fatty acids and pro-resolving lipid mediators (SPMs) were measured in 42 study completers at baseline and at the end of treatment by liquid chromatography/mass spectrometry. The response rate (≥50% reduction in IDS-30 score) was higher in the 4 g/d EPA arm than placebo (Cohen d = 0.53). In the 4 g/d EPA arm, responders had significantly greater increases in 18-hydroxyeicosapentaenoic acid (18-HEPE) and 13-hydroxydocosahexaenoic acid (13-HDHA) than non-responders ($p < 0.05$). Within the 4 g/d EPA arm, the increase in 18-HEPE was significantly associated with reductions in plasma hs-CRP concentrations ($p < 0.05$) and IDS-C30 scores ($p < 0.01$). In summary, response rates were greater among patients with MDD randomized to EPA 4 g/d supplementation and in those who showed a greater ability to activate the synthesis of 18-HEPE. The inverse association of 18-HEPE with both systemic inflammation and symptoms of depression highlights the activation of the resolution of inflammation as a likely mechanism in the treatment of MDD with ω-3 fatty acid supplementation.

Abbreviations used: DHA, docosahexaenoic acid; DPA, docosapentaenoic acid; EPA, eicosapentaenoic acid; HDHA, hydroxy docosahexaenoic acid; HEPE, hydroxyeicosapentaenoic; HETE, hydroxyeicosatetraenoic acid; hs-CRP, high sensitivity C reactive protein; LT, leukotriene; LX, lipoxin; Mar, maresin; P, protectin; PG, prostaglandin; Rv, resolvin; SPM, specialized pro-resolving lipid mediator; TX, thromboxane.

INTRODUCTION

Chronic low-grade inflammation plays an important role in the pathogenesis of several non-communicable diseases, including those affecting the central nervous system. Symptoms of major depressive disorder (MDD) are frequently observed when the immune system is activated, such as during infections or in inflammatory autoimmune diseases or conditions associated with chronic inflammation.[1-3] Inflammation is characterized by an initial phase of immune cell activation and secretion of pro-inflammatory cytokines, prostaglandins (PG) and leukotrienes (LT), followed by the resolution phase of inflammation.[4, 5] The resolution phase is mediated by specialized pro-resolving lipid mediators (SPMs) derived in large part from conversion of the ω-3 fatty acids eicosapentaenoic acid (EPA, 20:5 ω3), docosapentaenoic acid (DPA, 22:5 ω3) and docosahexaenoic acid (DHA, 22:6 ω3) via cyclooxygenase (COX) and lipoxygenase (LOX) enzymatic pathways.[6] SPMs include resolvins (Rv), protectins (P), and maresins (Mar) that act by binding to specific membrane receptors present on peripheral immune cells, but also on neurons and microglia.[7-9] The resolution phase of inflammation is characterized by efferocytosis of cell debris and apoptotic cells by specialized macrophages and by the counter-regulation of pro-inflammatory mediators to promote homeostasis.[6]

Chronic inflammation is thought to result from an impaired resolution phase.[6] Several studies have shown dysregulation of SPMs in conditions associated with low-grade chronic inflammation, such as obesity and cardiovascular disease.[10, 11] Lower concentrations of SPMs have also been observed in the cerebrospinal fluid and the hippocampus of patients with neurodegenerative diseases compared to controls.[8] However, it is not known whether deficient concentrations of SPM result from lower dietary intakes of the ω-3 fatty acid precursors or from an impaired ability to activate the resolution machinery to produce SPM.

MDD is common among children and adults with obesity,[12] and the rate of depression increases with BMI.[13] Obesity is characterized by low-grade chronic inflammation and is associated with lower SPM concentrations in adipose tissue.[14, 15] In mice, obesity and dietary intake of ω-3 fatty acid intake have opposite effects on MSFD2A2 (major facilitator superfamily domain-containing protein 2), a cell membrane transporter that mediates the translocation of DHA across the blood-brain barrier.[16] Therefore, it has been hypothesized that obesity may lead to reduced availability of ω-3 fatty acids in the brain and lower local SPM synthesis. However, leukocytes from individuals with obesity also display lower activity of 15-LOX, an enzyme involved in the synthesis of several SPMs.[10] We and others have shown that plasma and tissue concentrations of ω-3 fatty acids can be increased via supplementation in a dose-dependent fashion.[17-19] This has the potential to increase the substrate availability for SPM production.[17-19]

Meta-analysis studies of randomized controlled trials examining the potential of ω-3 supplements to improve clinical depression have reported reduced depression severity with formulations containing pure EPA or greater than 60% EPA, but not with supplements containing pure DHA or greater than 60% DHA.[20, 21] EPA supplementation may be an effective therapeutic option for the sub-group of patients with MDD who are overweight or with obesity and have low-grade chronic inflammation.[22] However, the threshold for effective SPM synthesis following ω-3 supplementation is not known. In addition, in the current era of precision medicine, it is important to identify biomarkers that may predict therapeutic response and the mechanism(s) driving the response.

We had previously conducted a randomized, double-blind, placebo-controlled, parallel-arm study in patients with MDD to evaluate the clinical response to three different doses of EPA (1 g/d, 2 g/d, and 4 g/d) and the association between reduction in depression severity following

EPA supplementation and changes in inflammation, as assessed by plasma high sensitivity C reactive protein (hs-CRP) and peripheral blood monocyte mitogen-stimulated tumor necrosis factor α (TNFα) production.[23] The study showed better response rates and lower plasma hs-CRP levels with EPA 4 g/d than placebo. The current study is a secondary analysis of the EPA dose finding study and is aiming at assessing the biosignature of response to EPA supplementation in patients with MDD.

METHODS

Study participants

The study design and participants' characteristics have been previously described.[23] Briefly, eligible individuals were required to have non-psychotic MDD (diagnosed using the Mini International Interview version 7.0.2), a depression severity score ≥ 25 on the Inventory of Depressive Symptomatology – 30 item (IDS-C30), a body mass index (BMI) > 25 kg/m^2, and low-grade chronic inflammation (plasma high-sensitivity C reactive protein, hs-CRP, ≥ 3 μg/mL). Participants were recruited at two sites, Emory University (Atlanta, GA) and Massachusetts General Hospital (Boston, MA). Subjects with a high dietary intake of ω-3 fatty acids, as assessed by dietary history using Food Processor, or taking fish oil supplements were excluded from the study. Sixty-one subjects enrolled into the double-blind study and 45 completed it. Forty-two participants had baseline and week 12 plasma samples obtained for the assessment of SPMs.

Study design

The study had a randomized, double-blind, placebo-controlled, parallel-arm design, consisting of four arms: 1) placebo, 2) EPA 1 g/d, 3) EPA 2 g/d, and 4) EPA 4 g/d.[23] The

supplementation phase lasted 12 weeks. EPA was provided in capsules, each containing approximately 590 mg of EPA and 152 mg DHA in triglyceride form. Matched placebo capsules contained soybean oil (approximately 51% linoleic acid, 25% oleic acid and 6% α-linolenic acid, but no EPA or DHA). Study participants were instructed to take eight capsules each day, four in the morning and four in the evening, with meals. Study subjects were asked to avoid taking non-steroidal anti-inflammatory drugs (NSAIDs) for at least 24 hours before visits. The IDS-C30 scale is a validated clinician-rated measure which has been previously described.[24] Hs-CRP was measured by an immunoturbidometric method using reagents and calibrators from Sekisui. The study protocol was approved by the IRB at both institutions and is registered on ClinicalTrials.gov (NCT02553915). All subjects provided written informed consent.

Fatty acid and SPM analysis

Fasting blood samples were collected in the morning in EDTA tubes at weeks 0 (baseline) and 12, centrifuged at 1000 *g* for 25 min at 4°C, and plasma was immediately stored at -80°C until analysis. All samples were batch-analyzed at the end of the study. For the analysis of plasma fatty acids, samples were hydrolyzed, and the fatty acid concentrations were assessed by ultrahigh-performance liquid chromatography/mass spectrometry as previously described.[17, 25] The concentration of individual fatty acids was validated against standard curves generated for each fatty acid. Fatty acid concentrations were then converted to molar percent of total plasma fatty acids (mol%). The plasma concentration of lipid mediators derived from EPA, DPA, DHA and AA were assessed by liquid chromatography-mass spectrometry as previously described.[17, 26, 27] Briefly, 100 μl of plasma was spiked with 5 ng each of PGE_1-d_4, RvD2-d_5, LTB_4-d_4, and 15S-hydoxyeicosatetraenoic acid-d_8 (15S-HETE-d_8) as internal standards for analyte recovery and quantitation. Lipid metabolites were extracted with C18 extraction columns and then

subjected to LC-MS analysis. Data were collected with Analyst 1.6 software and quantitated using MultiQuant software (AB Sciex). All quantified lipid mediators were identified by comparison with authenticated standards (Cayman Chemicals, Ann Arbor. MI).

Peripheral blood mononuclear cells

Peripheral blood mononuclear cells (PBMC) were isolated from fasting blood collected in sodium citrate Vacutainer Cell Preparation Tubes (Becton Dickinson, NJ). Cells were resuspended in cell culture medium (RPMI-1640, 10% fetal bovine serum, 100 U penicillin, 100 µg streptomycin) and plated in 12-well plates at the density of 2 x 10^6 cell/well. Two wells were treated as control and two wells were treated with 10 ng/ml lipopolysaccharide (LPS). After 5 hours incubation, cells were scraped and cell pellet and cell culture medium were separately collected after centrifugation. Concentrations of interleukin-6 (IL-6) and tumor necrosis factor α (TNF-α) in cell culture media were quantified using V-PLEX immunoassay kits from Meso Scale Diagnostics (MD).

Statistical analyses

Statistical analyses were conducted in R (version 3.5.2). Variables with skewed distribution are presented as median and interquartile range (75 percentile – 25 percentile). Response to treatment was defined as ≥ 50% reduction in IDS-C30 scores at week 12, relative to baseline. Differences between responders and non-responders were assessed by exact Wilcoxon-Mann-Whitney test. Partial Least-Squares Discriminant Analysis (PLS-DA) of the change in plasma lipid mediators was performed on normalized and scales data using MetaboAnalyst 5.0 (https://www.metaboanalyst.ca), a web-based platform for comprehensive analysis of quantitative metabolomic data. Associations between depression scores, inflammation, and fatty

acid and lipid mediator concentrations were assessed by Spearman's rank-order correlation tests. A p value ≤ 0.05 was considered statistically significant.

RESULTS

The results of the primary outcomes of the trial have been reported.[23] The study participants' age, BMI, depression scores and plasma hs-CRP concentrations at baseline in the four treatment arms are shown in **Table 1**. There were no significant differences in baseline characteristics among the four groups. Moreover, baseline plasma concentrations of EPA, DPA, DHA and AA, and of their related lipid mediators, were similar among the four arms (**Supplementary Table**). Response to treatment occurred in 16 of the 35 subjects in the EPA treatment arms [5 of 13 (38%) in EPA 1 g/d, 4 of 11 (36%) in EPA 2 g/d, and 7 of 11 (64%) in EPA 4 g/d arm], and in 4 of the 10 subjects in the placebo arm (40%). At baseline, the amount of plasma EPA, DHA and AA and the concentration of their related lipid mediators were similar between responders and non-responders (**Table 2**).

The changes in plasma EPA, DHA and AA, defined as the difference between week 12 and baseline, were similar in responders and non-responders within each treatment arm (**Supplementary Figure**). A non-significant trend ($p = 0.25$) was observed for EPA, but not DHA, in the 4 g/d arm.

The PLS-DA score plot of the changes in lipid mediators derived from EPA, DHA, and AA in all subjects receiving active EPA supplementation indicated a partial separation of responders and non-responders (**Figure 1**).

Figure 2 shows the change in lipid mediators following treatment in responders and non-responders by treatment arm. The change in plasma 18-HEPE was significantly greater in

responders than non-responders in the 4 g/d arm ($p < 0.01$), but a trend for greater increases in responders than non-responders was also observed for 11-HEPE and 15-HEPE ($p=0.067$) (**Figure 2**). In the 4 g/d EPA arm, the change in plasma DHA-derived 13-HDHA was also significantly greater in responders than non-responders ($p < 0.05$) (**Figure 2**). There was a non-significant trend for a lowering of AA-derived lipid mediators in non-responders, and an increase in 12-HETE and PGE_2 in responders in the EPA 4 g/d arm (**Figure 2**). No significant differences between responders and non-responders were observed in the 1 and 2 g/d arms. When all EPA treatment groups were combined, changes in TXB_2 were significantly higher (median [IQR], 431 [3,600] and -1250 [-2535] pg/mL, respectively; $p=0.04$) and changes in 18-HEPE (594 [1597] and 361 [426] pg/mL; $p=0.067$) and 13-HDHA (311 [402] and 51 [202] pg/mL; $p=0.067$) were higher in responders than non-responders. RvE1 was not detected by our assay at baseline and end of treatment. However, RvE2 was detected at end of treatment in four out of six responders and none of four non-responders, and RvE3 in five of six responders and one of four non-responders.

Within the 4 g/d EPA arm, reductions in hs-CRP were significantly correlated with reductions in IDS-C30 scores ($p < 0.05$) (**Table 3**). Increases in 18-HEPE, 15-HEPE, and 17-HDHA were significantly correlated with reductions in IDS-30 scores. In addition, increases in 18-HEPE and 15-HEPE were significantly correlated with reductions in hs-CRP.

DISCUSSION

EPA supplementation reduced clinical symptoms of depression, defined as achieving ≥ 50% reduction in IDS-C30 scores, in 64% of participants in the 4 g/d arm, relative to 40% in the placebo arm. At baseline, study participants who responded to treatment had plasma concentrations of EPA, DHA, DPA, AA and related lipid mediators similar to non-responders.

However, after supplementation, there was a trend for greater increases in some of the lipid mediators derived from these fatty acids in responders versus non-responders, and differences were significant for 18-HEPE and 13-HDHA in the 4 g/d arm. To our knowledge, this is the first clinical trial demonstrating a differential response to EPA supplementation in patients with MDD, with overall greater ability to synthesize EPA- and DHA-derived lipid mediators in responders than non-responders.

Chronic low-grade inflammation is a characteristic feature of metabolic syndrome, obesity and cardiovascular disease, and has recently emerged as a contributing factor to diseases of the central nervous system, including MDD, Parkinson's disease and Alzheimer's disease.[2, 28] Impairment in the active process of inflammation resolution is thought to play a significant role in chronic inflammation, and several pre-clinical and clinical studies have demonstrated lower levels of SPM production associated with chronic inflammation. Mice on a high-fat diet had higher concentrations of pro-inflammatory lipid mediators and lower concentrations of SPMs in their adipose tissue, compared to control mice.[14, 29] In subjects with obesity, it has been reported that leukocytes had significantly lower levels of DHA-derived SPMs, relative to levels of the classic inflammatory mediators LTB4 and PGs, than subjects without obesity.[10] Lower SPM concentrations have also been observed in subjects with cardiovascular disease.[11] A healthy control group was not included in our study and therefore we do not know if the baseline plasma concentrations of ω-3 fatty acids and lipid mediators in our participants with MDD were lower than those of healthy age- and sex-matched subjects. At baseline, patients with MDD who responded to EPA supplementation had plasma concentrations of EPA and DHA and of their derived lipid mediators similar to non-responders, but responders showed a greater increase in EPA- and DHA-derived lipid mediators following supplementation than non-responders. Since

responders and non-responders achieved overall similar plasma concentrations of EPA, DHA and AA following supplementation, it is unlikely that the availability of precursors for the synthesis of SPMs played a significant role in the response to supplementation.

Other mechanisms such as the activation of enzymatic pathways involved in SPM synthesis may account, at least in part, for the differences in response. Immune cells of subjects with obesity exhibit lower concentrations of 17-HDHA, a 15-LOX metabolite of DHA, but, when these cells were incubated with 17-HDHA, the production of SPMs was rescued.[10] These findings suggest a potential deficit in 15-LOX activity in subjects with obesity which may lead to lower synthesis of precursors and SPMs. In our study, other metabolites derived from other enzymatic pathways were also different between responders and non-responders. Specifically, 18-HEPE was one of the most important lipid mediators differentiating responders and non-responders. 18-HEPE is synthesized by both COX and cytochrome P450. It has been shown that COX-2 activation follows a biphasic pattern during inflammation: the first peak occurs during the early pro-inflammatory phase and is associated with increased PGE_2 secretion and pro-inflammatory cytokine expression, and the second peak coincides with the resolution phase of inflammation and is characterized by increased PGD_2 synthesis, reduction in neutrophil recruitment, and increase in macrophage mobilization from the inflammation site.[30, 31] In our study, TXB_2, which is also synthesized in response to COX-2 activation, was significantly elevated after EPA supplementation in responders. Therefore, it may be hypothesized that the biphasic COX-2 activation is an important player in the resolution phase of inflammation and that both EPA- and AA-derived lipid mediators may be increased during resolution.

The results of our study are somewhat in contrast with those of a study conducted in 16 patients with MDD and supplemented with 1.6 g/d EPA and 0.8 g/d DHA for six weeks, where

responders had higher mol% DHA, but not EPA mol%, in plasma phospholipids than non-responders.[32] It should be noted that in that study none of the responders but most of the non-responders had previously taken antidepressants and therefore the results may have been affected by patient characteristics related to treatment resistance. A meta-analysis of ω-3 fatty acid supplementation studies conducted in patients with MDD found that only supplementation with pure EPA or fish oil mostly containing EPA demonstrated significant therapeutic effect.[21] In contrast, pure DHA or preparations containing mostly DHA did not show significant improvement in depression.[21] The lack of response to DHA supplementation may be due to the different metabolism of EPA and DHA in the brain and the preferential incorporation of DHA into cell membrane phospholipids, with DHA accounting for up to 40% of all fatty acids in some regions of the brain,[33] and EPA mostly subjected to beta-oxidation.[34] However, both EPA and DHA may undergo conversion to SPM in the brain as 15-LOX is expressed by neurons and microglia.[35] In a mouse model of depression, intracranial administration of RvE1-3 or RvD1-2 was associated with reduced symptoms.[36-38] The contribution of EPA- and DHA-derived lipid mediators to clinical response in MDD therefore needs to be further investigated.

Efficacy of EPA supplementation was greater in the 4 g/d arm, consistent with findings from cardiovascular prevention studies[39] and suggests activation of the resolution phase of inflammation as a mechanism of clinical response. In the 4 g/d arm, plasma levels of both RvE2 and RvE3 were detectable in most responders, compare to no or low detection in non-responders. The strong association between changes in 18-HEPE and 15-HEPE, the precursors of RvE1-4, with changes in depression symptoms and plasma hs-CRP concentrations are highly suggestive of a mechanistic role of EPA-derived SPMs on inflammation and subsequent reduction in depression. A significant correlation between the increase in the concentration of selective SPMs

and circulating immune cell characteristics following administration of a high dose of a marine oil and SPM supplement was previously reported in another study.[40]

A strength of this study was the selection of patients with MDD and with chronic inflammation, who are the ideal target for activation of the resolution of inflammation. In addition, we were able to correlate changes in plasma SPMs with hs-CRP, a marker of systemic inflammation, and with clinical symptoms of depression. One limitation of our study was the sample size, with a small number of subjects in each group of responders and non-responders. Our analyses were exploratory. The parent study was limited by a high placebo response rate.[23] In the original report, we remarked that placebo responders had lower baseline IDS-C30 scores than non-responders, a commonly reported finding,[41] while clinical responders had similar mean baseline IDS-C30 scores compared to non-responders. Baseline plasma IL-6 levels in placebo responders versus non-responders also suggested that placebo may be more effective in subjects with MDD and lower baseline inflammation. This may impact the current findings. Our results strongly support a need for larger and definitive trials. We were also unable to report plasma concentrations of E-series and D-series resolvins at baseline and in the placebo arm due to levels below the detection limit of our assay.

Taken together, the results of our study indicate a dose-dependent reduction in depression symptoms following EPA supplementation. Among study participants receiving EPA, those who responded showed a greater ability to activate the synthesis of 18-HEPE. In addition, the increase in 18-HEPE following EPA supplementation in the 4 g/d arm was highly and negatively correlated with both systemic inflammation and symptoms of depression, highlighting the activation of the resolution of inflammation as a likely mechanism in the treatment of MDD.

Author contribution

Stefania Lamon-Fava: Conceptualization, Formal analysis, Investigation, Methodology, Resources, Supervision, Writing - original draft

Minying Liu: Data curation, Formal analysis, Methodology

Boadie Dunlop: Investigation, Writing - reviewing and editing

Becky Kinkead: Investigation, Project administration, Writing - reviewing and editing

Pamela Schettler: Data curation, Formal analysis, Methodology, Writing - reviewing and editing

Jennifer Felger: Investigation, Writing - reviewing and editing.

Thomas R. Ziegler: Conceptualization, Writing - reviewing and editing

Maurizio Fava: Conceptualization, Formal analysis, Funding acquisition, Investigation, Methodology, Writing - reviewing and editing.

David Mischoulon: Conceptualization, Formal analysis, Funding acquisition, Investigation, Methodology, Writing – review and editing

Mark Hyman Rapaport: Conceptualization, Formal analysis, Funding acquisition, Investigation, Methodology, Project administration, Supervision, Writing - reviewing and editing

Funding

This work was supported by the National Institutes of Health grant UG3 AT008857.

Competing interests

Lamon-Fava S., Liu M, Dunlop B, Kinkead B, Schettler P, Felger J, Ziegler TR, Fava M and Rapaport MH report no conflict of interest. Mischoulon D has received research support from Nordic Naturals and consulted for Pharmavite LLC. Nordic Naturals provided the high-EPA fish oil capsules for this study but was not involved in the design of the study, the collection and analysis of data, and in the manuscript writing and decision to publish.

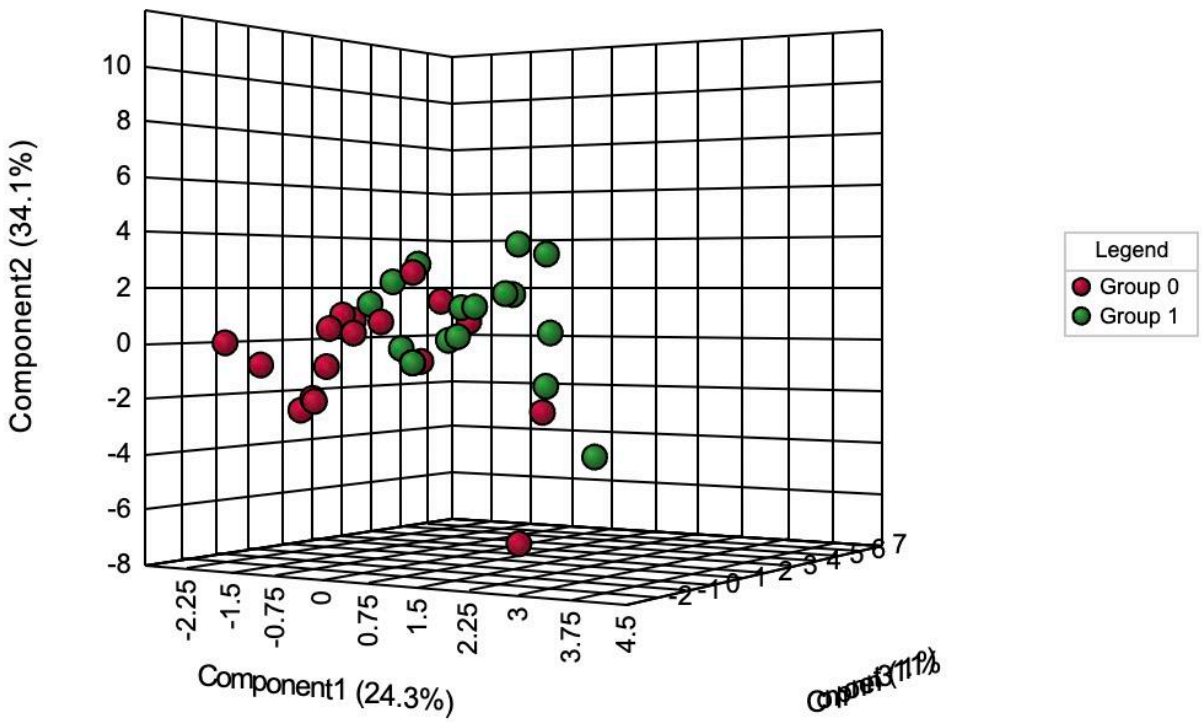

Figure 1. PLS-DA of changes in lipid mediators derived from EPA, DHA and AA in responders and non-responders in the combined treatment arms.

Figure 2. Median changes in lipid mediators in responders (green) and non-responders (red) by treatment group. Top row: EPA-derived lipid mediators; middle row: DHA-derived lipid mediators; and bottom row: AA-derived lipid mediators. * p <0.05, responders versus non-responders in same treatment arm.

REFERENCES

1. Dantzer R, O'Connor JC, Freund GG, Johnson RW and Kelley KW. From inflammation to sickness and depression: when the immune system subjugates the brain. *Nature Reviews Neuroscience*. 2008;9:46-56.
2. Kohler CA, Freitas TH, Maes M, de Andrade NQ, Liu CS, Fernandes BS, Stubbs B, Solmi M, Veronese N, Herrmann N, Raison CL, Miller BJ, Lanctot KL and Carvalho AF. Peripheral cytokine and chemokine alterations in depression: a meta-analysis of 82 studies. *Acta Psychiatr Scand*. 2017;135:373-387.
3. Felger JC, Haroon E, Woolwine BJ, Raison CL and Miller AH. Interferon-alpha-induced inflammation is associated with reduced glucocorticoid negative feedback sensitivity and depression in patients with hepatitis C virus. *Physiology & behavior*. 2016;166:14-21.
4. Serhan CN and Savill J. Resolution of inflammation: the beginning programs the end. *Nature Immunol*. 2005;6:1191-7.
5. Buckley CD, Gilroy DW and Serhan CN. Proresolving lipid mediators and mechanisms in the resolution of acute inflammation. *Immunity*. 2014;40:315-27.
6. Serhan CN and Levy BD. Resolvins in inflammation: emergence of the pro-resolving superfamily of mediators. *J Clin Invest*. 2018;128:2657-2669.
7. Chiurchiu V, Leuti A, Dalli J, Jacobsson A, Battistini L, Maccarrone M and Serhan CN. Proresolving lipid mediators resolvin D1, resolvin D2, and maresin 1 are critical in modulating T cell responses. *Sci Transl Med*. 2016;8:353ra111.
8. Wang X, Zhu M, Hjorth E, Cortes-Toro V, Eyjolfsdottir H, Graff C, Nennesmo I, Palmblad J, Eriksdotter M, Sambamurti K, Fitzgerald JM, Serhan CN, Granholm AC and Schultzberg M. Resolution of inflammation is altered in Alzheimer's disease. *Alzheimers Dement*. 2015;11:40-50 e1-2.
9. Ye ZN, Zhuang Z, Wu LY, Liu JP, Chen Q, Zhang XS, Zhou ML, Zhang ZH, Li W, Wang XL and Hang CH. Expression and cell distribution of leukotriene B4 receptor 1 in the rat brain cortex after experimental subarachnoid hemorrhage. *Brain Res*. 2016;1652:127-134.
10. Lopez-Vicario C, Titos E, Walker ME, Alcaraz-Quiles J, Casulleras M, Duran-Guell M, Flores-Costa R, Perez-Romero N, Forne M, Dalli J and Claria J. Leukocytes from obese individuals exhibit an impaired SPM signature. *FASEB J*. 2019;33:7072-7083.
11. Aday AW and Ridker PM. Targeting Residual Inflammatory Risk: A Shifting Paradigm for Atherosclerotic Disease. *Front Cardiovasc Med*. 2019;6:16.
12. Luppino FS, de Wit LM, Bouvy PF, Stijnen T, Cuijpers P, Penninx BW and Zitman FG. Overweight, obesity, and depression: a systematic review and meta-analysis of longitudinal studies. *Arch Gen Psychiatry*. 2010;67:220-9.
13. Rethorst CD, Bernstein I and Trivedi MH. Inflammation, obesity, and metabolic syndrome in depression: analysis of the 2009-2010 National Health and Nutrition Examination Survey (NHANES). *J Clin Psychiatry*. 2014;75:e1428-32.
14. Neuhofer A, Zeyda M, Mascher D, Itariu BK, Murano I, Leitner L, Hochbrugger EE, Fraisl P, Cinti S, Serhan CN and Stulnig TM. Impaired local production of proresolving lipid mediators in obesity and 17-HDHA as a potential treatment for obesity-associated inflammation. *Diabetes*. 2013;62:1945-56.
15. Claria J, Lopez-Vicario C, Rius B and Titos E. Pro-resolving actions of SPM in adipose tissue biology. *Mol Aspects Med*. 2017;58:83-92.

16. Sandoval KE, Wooten JS, Harris MP, Schaller ML, Umbaugh DS and Witt KA. Mfsd2a and Glut1 Brain Nutrient Transporters Expression Increase with 32-Week Low and High Lard Compared with Fish-Oil Dietary Treatment in C57Bl/6 Mice. *Curr Dev Nutr*. 2018;2:nzy065.
17. Lamon-Fava S, So J, Mischoulon D, Ziegler TR, Dunlop BW, Kinkead B, Schettler PJ, Nierenberg AA, Felger JC, Maddipati KR, Fava M and Rapaport MH. Dose- and time-dependent increase in circulating anti-inflammatory and pro-resolving lipid mediators following eicosapentaenoic acid supplementation in patients with major depressive disorder and chronic inflammation. *Prostaglandins Leukot. Essent. Fat. Acids.* 2021;164:102219.
18. Ostermann AI, West AL, Schoenfeld K, Browning LM, Walker CG, Jebb SA, Calder PC and Schebb NH. Plasma oxylipins respond in a linear dose-response manner with increased intake of EPA and DHA: results from a randomized controlled trial in healthy humans. *Am J Clin Nutr*. 2019;109:1251-1263.
19. Schuchardt JP, Schneider I, Willenberg I, Yang J, Hammock BD, Hahn A and Schebb NH. Increase of EPA-derived hydroxy, epoxy and dihydroxy fatty acid levels in human plasma after a single dose of long-chain omega-3 PUFA. *Prostaglandins Other Lipid Mediat.* 2014;109-111:23-31.
20. Martins JG. EPA but not DHA appears to be responsible for the efficacy of omega-3 long chain polyunsaturated fatty acid supplementation in depression: evidence from a meta-analysis of randomized controlled trials. *J Am Coll Nutr*. 2009;28:525-42.
21. Liao Y, Xie B, Zhang H, He Q, Guo L, Subramaniapillai M, Fan B, Lu C and McLntyer RS. Efficacy of omega-3 PUFAs in depression: A meta-analysis. *Transl Psychiatry*. 2019;9:190.
22. Rapaport MH, Nierenberg AA, Schettler PJ, Kinkead B, Cardoos A, Walker R and Mischoulon D. Inflammation as a predictive biomarker for response to omega-3 fatty acids in major depressive disorder: a proof-of-concept study. *Mol Psychiatry*. 2016;21:71-9.
23. Mischoulon DD, DW;Kinkead, B; Schettler, PJ; Lamon-Fava, S; Rakofsky, JJ; Nieremberg, AA; Fava, M; Rapaport, MH. Omega-3 Fatty Acids for Major Depressive Disorder With High Inflammation: A Randomized Dose-Finding Clinical Trial. *J Clin Psychiatry*. 2022;83:e1-e10.
24. Rush AJ, Gullion CM, Basco MR, Jarrett RB and Trivedi MH. The Inventory of Depressive Symptomatology (IDS): psychometric properties. *Psychol Med*. 1996;26:477-86.
25. Hellmuth C, Weber M, Koletzko B and Peissner W. Nonesterified fatty acid determination for functional lipidomics: comprehensive ultrahigh performance liquid chromatography-tandem mass spectrometry quantitation, qualification, and parameter prediction. *Analytical Chem*. 2012;84:1483-90.
26. Maddipati KR, Romero R, Chaiworapongsa T, Zhou SL, Xu Z, Tarca AL, Kusanovic JP, Munoz H and Honn KV. Eicosanomic profiling reveals dominance of the epoxygenase pathway in human amniotic fluid at term in spontaneous labor. *FASEB J*. 2014;28:4835-46.
27. Markworth JF, Vella L, Lingard BS, Tull DL, Rupasinghe TW, Sinclair AJ, Maddipati KR and Cameron-Smith D. Human inflammatory and resolving lipid mediator responses to resistance exercise and ibuprofen treatment. *Am J Physiol Regul Integr Comp Physiol*. 2013;305:R1281-96.
28. Calsolaro V and Edison P. Neuroinflammation in Alzheimer's disease: Current evidence and future directions. *Alzheimers Dement*. 2016;12:719-32.
29. Li P, Oh DY, Bandyopadhyay G, Lagakos WS, Talukdar S, Osborn O, Johnson A, Chung H, Maris M, Ofrecio JM, Taguchi S, Lu M and Olefsky JM. LTB4 promotes insulin resistance

in obese mice by acting on macrophages, hepatocytes and myocytes. *Nat Med*. 2015;21:239-247.
30. Rajakariar R, Hilliard M, Lawrence T, Trivedi S, Colville-Nash P, Bellingan G, Fitzgerald D, Yaqoob MM and Gilroy DW. Hematopoietic prostaglandin D2 synthase controls the onset and resolution of acute inflammation through PGD2 and 15-deoxyDelta12 14 PGJ2. *PNAS*. 2007;104:20979-84.
31. Gao Y, Zhang H, Luo L, Lin J, Li D, Zheng S, Huang H, Yan S, Yang J, Hao Y, Li H, Gao Smith F and Jin S. Resolvin D1 Improves the Resolution of Inflammation via Activating NF-kappaB p50/p50-Mediated Cyclooxygenase-2 Expression in Acute Respiratory Distress Syndrome. *J Immunol*. 2017.
32. Gananca L, Galfalvy HC, Oquendo MA, Hezghia A, Cooper TB, Mann JJ and Sublette ME. Lipid correlates of antidepressant response to omega-3 polyunsaturated fatty acid supplementation: A pilot study. *Prostaglandins Leukot. Essent. Fat. Acids*. 2017;119:38-44.
33. Lacombe RJS, Chouinard-Watkins R and Bazinet RP. Brain docosahexaenoic acid uptake and metabolism. *Mol Aspects Med*. 2018;64:109-134.
34. Chen CT, Domenichiello AF, Trepanier MO, Liu Z, Masoodi M and Bazinet RP. The low levels of eicosapentaenoic acid in rat brain phospholipids are maintained via multiple redundant mechanisms. *J Lipid Res*. 2013;54:2410-22.
35. Kanzler MA, Van Dyke AM, He Y, Hewett JA and Hewett SJ. Mice lacking L-12/15-lipoxygenase show increased mortality during kindling despite demonstrating resistance to epileptogenesis. *Epilepsia Open*. 2018;3:255-263.
36. Deyama S, Ishikawa Y, Yoshikawa K, Shimoda K, Ide S, Satoh M and Minami M. Resolvin D1 and D2 Reverse Lipopolysaccharide-Induced Depression-Like Behaviors Through the mTORC1 Signaling Pathway. *Int J Neuropsychopharmacol*. 2017;20:575-584.
37. Deyama S, Shimoda K, Ikeda H, Fukuda H, Shuto S and Minami M. Resolvin E3 attenuates lipopolysaccharide-induced depression-like behavior in mice. *J Pharmacol Sci*. 2018;138:86-88.
38. Deyama S, Shimoda K, Suzuki H, Ishikawa Y, Ishimura K, Fukuda H, Hitora-Imamura N, Ide S, Satoh M, Kaneda K, Shuto S and Minami M. Resolvin E1/E2 ameliorate lipopolysaccharide-induced depression-like behaviors via ChemR23. *Psychopharmacology (Berl)*. 2018;235:329-336.
39. Bhatt DL, Steg PG, Miller M, Brinton EA, Jacobson TA, Ketchum SB, Doyle RT, Jr., Juliano RA, Jiao L, Granowitz C, Tardif JC, Ballantyne CM and Investigators R-I. Cardiovascular Risk Reduction with Icosapent Ethyl for Hypertriglyceridemia. *N Engl J Med*. 2019;380:11-22.
40. Souza PR, Marques RM, Gomez EA, Colas RA, De Matteis R, Zak A, Patel M, Collier DJ and Dalli J. Enriched Marine Oil Supplements Increase Peripheral Blood Specialized Pro-Resolving Mediators Concentrations and Reprogram Host Immune Responses: A Randomized Double-Blind Placebo-Controlled Study. *Circulation Res*. 2020;126:75-90.
41. Papakostas GI and Fava M. Does the probability of receiving placebo influence clinical trial outcome? A meta-regression of double-blind, randomized clinical trials in MDD. *Eur Neuropsychopharmacol*. 2009;19:34-40.

Table 1. Baseline characteristics of study participants by treatment group.

	Placebo (n=10)	**EPA 1 g/d (n=13)**	**EPA 2 g/d (n=11)**	**EPA 4g/d (n=11)**
Men/Women (n)	2/8	4/9	3/8	4/7
Age (y)	52±13	41±16	47±15	43±15
BMI (kg/m^2)	38.8 (9.6)	33.0 (6.7)	34.3 (7.7)	35.7 (8.8)
Hs-CRP (μg/mL)	6.9 (4.5)	3.6 (8.3)	4.8 (1.2)	3.9 (4.7)
IDS-C30	36.6±10.5	36.1±7.4	31.4±7.1	31.5±5.0

Data presented as mean±SD or median (IQR)

Table 2. Baseline plasma concentrations of EPA, DPA, DHA, AA and their derived lipid mediators in non-responders versus responders in the combined active treatment arms (EPA 1 g/d, 2 g/d, and 4 g/d).

	Non-responders (n=19)	Responders (n=16)	P value*
EPA			
EPA, mol%	0.42 (0.32)	0.43 (0.36)	0.85
5-HEPE, pg/mL	50 (29)	55 (53)	0.31
11-HEPE, pg/mL	43 (48)	49 (38)	0.70
12-HEPE, pg/mL	806 (2094)	588 (1838)	0.60
15S-HEPE, pg/mL	92 (62)	79 (87)	0.67
18-HEPE, pg/mL	47 (29)	47 (25)	0.88
DPA			
DPA, mol%	0.37 (0.17)	0.34 (0.26)	0.83
RvD5 $_{DPA}$, pg/mL	15 (6)	14 (3)	0.73
DHA			
DHA, mol%	7.42 (4.59)	7.11 (3.40)	0.42
4-HDHA, pg/mL	60 (45)	56 (39)	0.57
7-HDHA, pg/mL	18 (14)	18 (17)	0.93
13-HDHA, pg/mL	145 (251)	165 (248)	0.60
14-HDHA, pg/mL	1810 (4012)	1580 (2254)	0.55
17-HDHA, pg/mL	30 (25)	31 (26)	0.82
RvD1, pg/mL	85 (103)	120 (121)	0.95
AA			
AA, mol%	10.11 (3.68)	10.52 (5.66)	0.80
5-HETE, pg/mL	355 (326)	445 (515)	0.40
11-HETE, pg/mL	1603 (1956)	1234 (2225)	0.67
12-HETE, pg/mL	9622 (13191)	9502 (15867)	0.99
15-HETE, pg/mL	1182 (689)	1306 (1268)	0.53
PGE_2, pg/mL	1139 (1536)	965 (1904)	0.80
TXB_2, pg/mL	2634 (3220)	1528 (4013)	0.72
LTB_4, pg/mL	31 (17)	21 (29)	0.29

Median (IQR); *P value, Wilcoxon rank-sum test.

Table 3. Spearman correlations among changes in variables from baseline to week 12 in the 4 g/d treatment group.

	IDS-C30	Hs-CRP	IL-6 (PBM	TNF (PBM	5-HEPE	11-HEPE	12-HEPE	5-HEPE	18-HEPE	4-HDHA	7-HDHA	14-HDHA	17-HDHA	5-HETE	11-HETE	12-HETE	15-HETE	PGE_2	TXB_2
IDS-C30	1	.61*	.11	.17	-.21	-.57	-.20	-.71*	-.80**	-.27	-.04	-.15	-.77*	-.08	-.17	-.06	.03	-.40	-.34
Hs-CRP		1	-.10	.37	-.30	-.50	-.34	-.68*	-.73*	-.11	-.31	-.15	-.28	.10	.02	.01	-.11	-.12	-.06
IL-6 (PBMC)			1	.21	;18	.09	-.22	.12	-.04	-.26	-.30	-.17	-.13	.07	.04	-.10	.03	.65	.20
TNF (PBMC)				1	-.73*	-.60	-.29	-.64*	-.07	-.48	-.75*	-.05	-.53	-.39	-.15	-.03	-.13	-.41	.58
5-HEPE					1	.89**	.65*	.69*	.32	.89**	.93***	.47	.87**	.78**	.62^	.38	.61*	-.17	-.37
11-HEPE						1	.60	.87**	.55	.79**	.73*	.46	.79**	.67*	.67*	.35	.57	.07	-.07
12-HEPE							1	.40	.52	.65*	.75*	.95***	.89**	.46	.39	.86**	.60	-.41	.05
15-HEPE								1	.57	.51	.54	.23	.51	.37	.29	.11	.18	.00	-.17
18-HEPE									1	.33	.23	.43	.39	-.09	.08	.29	.00	.24	.04
4-HDHA										1	.83**	.54	.83**	.79**	.74*	.40	.68*	-.38	-.20

7-HDHA											1	.56	.92***	.74**	.50	.47	.60	-.39	-.48
14-HDHA												1	.79**	.42	.43	.95***	.66**	.32	.24
17-HDHA													1	.73*	.66*	.72*	.77**	-.24	-.09
5-HETE														1	.85**	.34	.86**	-.17	-.38
11-HETE															1	.40	.91	.14	.08
12-HETE																1	.67	-.23	.34
15-HETE																	1	.00	.05
PGE_2																		1	.62*
TXB_2																			1

*p<0.05, **p<0.01, ***p<0.001

7. APPENDIX C: ABSTRACTS

7.1 An exploratory case-control study on associations of bacterially derived vitamin K forms with the intestinal microbiome and obesity-related osteoarthritis

Minying Liu [1], Gregory Matuszek [1], M. Andrea Azcarate-Peril [2], Richard F Loeser [3], M Kyla Shea [1]
[1] USDA Human Nutrition Research Center on Aging at Tufts University, Boston, MA
[2] Division of Gastroenterology and Hepatology and UNC Microbiome Core, Center for Gastrointestinal Biology and Disease, University of North Carolina School of Medicine, Chapel Hill, North Carolina, USA
[3] Division of Rheumatology, Allergy, and Immunology and the Thurston Arthritis Research Center, University of North Carolina School of Medicine, Chapel Hill, NC

Background: Evidence suggests natural metabolites produced by intestinal microorganisms may have beneficial or harmful effects on osteoarthritis (OA). This could include menaquinones, which are bacterially-synthesized biologically active vitamin K forms abundant in the intestinal microbiome.
Objective: The overall goal of this study was to evaluate the association of intestinally-derived menaquinones with obesity-related OA.
Methods: This case-control study used data and biospecimens derived from a sub-group of Johnston County Osteoarthritis Study participants. Fecal menaquinone concentrations and microbial composition were determined in 52 obese participants with hand and knee OA and 42 age- and sex-matched obese participants without OA. The inter-relationships between the fecal menaquinones were evaluated using principal component analysis. Differences in alpha and beta diversity and microbial composition across menaquinone clusters were evaluated using analysis of variance.
Results: Samples clustered into three groups: cluster 1 characterized by higher fecal menaquinone -8, -9, and -10 concentrations, cluster 2 characterized by lower overall menaquinone concentrations, and cluster 3 characterized by higher menaquinone-12 and -13. Overall, fecal menaquinone clusters did not differ between participants with or without OA ($p=0.707$). Microbial diversity did not differ across the fecal menaquinone clusters (all F-test $p>0.12$). However, the relative abundance of bacterial taxa differed among clusters, with a higher abundance of *Coprococcus*, *Prevotella*, and *Eggerthella* in cluster 2 compared to cluster 1, a higher abundance of *Oscilospira, Dorea* and *Eubacterium,* and *Bacteroides* in cluster 3 compared to cluster 1, and a higher abundance of *Prevotella, Sutterella* and *Dorea* in cluster 3 compared to cluster 2 (all $p<0.001$).

Funding: Tufts University CTSI NIH Clinical and Translational Science Award (UL1TR002544), the US Department of Agriculture (cooperative agreement), the Arthritis Foundation, the National Center for Advancing Translational Sciences (NCATS) (UL1TR002489), and the National Institute of Arthritis and Musculoskeletal and Skin Diseases (P30AR072580). The Johnston County Osteoarthritis Project is funded in part by the Centers for Disease Control and Prevention (U01 DP006266). The UNC Microbiome Core is supported in part by the National Institute of Diabetes and Digestive and Kidney Diseases (P30 DK034987 and P30 DK056350) and the Office of the Director, NIH (P40 OD010995).

Presented at Nutrition 2023 (ASN), Boston, MA

7.2 Alternating the Gut Microbiome through Oral Broad-Spectrum Antibiotics Influenced Colon and Liver Long-Chain Menaquinones in Mice

Minying Liu [1], Christopher J. Hernandez [2], Chongshan Liu [2,3], Erika L. Cyphert [2,3], Jennifer Lee [1], Sarah L. Booth [1], Xueyan Fu [1], M. Kyla Shea [1]
[1] Human Nutrition Research Center on Aging, Tufts University, Boston, MA
[2] Bioengineering and Therapeutic Sciences, University of California, San Francisco, CA
[3] Sibley School of Mechanical and Aerospace Engineering, Cornell University, Ithaca, NY

Objective: Long-chain menaquinones (LCMKs) are vitamin K forms produced by gut bacteria. In young male mice, antibiotic treatment altered LCMK concentrations in cecum and liver. However, the influence of antibiotic treatment on LCMK tissue concentrations in older mice in female is unknown. We sought to determine the response of tissue LCMK concentrations in older male and female mice to oral antibiotic-induced alterations in the gut microbiome.

Method: Four-week-old male and female C57BL/6 mice (n=45/sex, 15/group) were treated with broad-spectrum antibiotics (ampicillin and neomycin) in drinking water from 19-22 months (AND), or 4-22 months (ADD), or not at all. Tissue LCMKs (for the purpose of this study, MK9-12) were quantified by LC-MS and HPLC and were compared by sex and treatment groups using 2-factor ANOVA.

Results: Among the tissues analyzed (liver, kidney, jejunum, and colon), LCMKs were detected in liver and colon. Male mice treated with antibiotics in either ADD or AND had higher colon MK9-12 concentrations (all P values $\leq$0.01). MK10 was the only LCMK identified in liver, and its concentration was lower in female mice that received oral antibiotics (P=0.003). LCMK concentrations in colon and liver did not differ by dosing duration regimens in either males or females (all P values $\geq$0.14). Moreover, female mice exhibited higher liver MK10 concentrations than male mice across treatment groups (P<0.001). No sex differences were observed in colon LCMK content (all P values $\geq$0.33).

Conclusion: Manipulation of the intestinal microbiome through oral antibiotic treatment influenced LCMK content in liver and colon regardless of dosing duration. This study expands our understanding of the contribution of bacterially produced LCMKs to tissue vitamin K concentrations. Future studies are needed to explore potential mechanisms for the transportation of LCMKs from colon to peripheral tissue.

Funding: NIA R01AG067997 and the USDA Agricultural Research Service Cooperative Agreement No. 58-1950-7-707

Presented at Nutrition 2024 (ASN), Chicago, IL

7.3 Dietary Menaquinone-9 Supplementation Does Not Influence Bone Tissue Quality or Bone Mineral Density in Mice

Minying Liu[1], Chongshan Liu[23], Nicolas Cevallos[2], Tristan Silfverskiold[1], Benjamin N Orbach[1], Christopher J Hernandez[2], Xueyan Fu[1], Jennifer Lee[1], Sarah L Booth[1], M Kyla Shea[1]
[1] Human Nutrition Research Center on Aging, Tufts University, Boston, MA
[2] Orthopaedic Surgery, University of California, San Francisco, CA
[3] Sibley School of Mechanical and Aerospace Engineering, Cornell University, Ithaca, NY

Objective: Vitamin K has been implicated in skeletal health because vitamin K-dependent proteins are present in bone. While there are multiple forms of vitamin K, most research has focused on phylloquinone, which is found mainly in plant-based foods, and menaquinone-4 (MK4), which is a metabolite of phylloquinone. However, there are additional forms of vitamin K that are bacterially produced that may influence bone health but have not yet been studied extensively. Herein, we evaluated the effects of menaquinone-9 (MK9), a bacterially produced form of vitamin K on bone tissue quality and bone mineral density (BMD) in young mice.

Method: Four-week-old male (n=32) and female (n=32) C57BL/6 mice were supplemented with 0.06 mg/kg diet or 2.1 mg/kg diet of MK9 for 12 weeks. During week 11, a sub-group of mice (n=7/sex/group) received daily deuterium-labeled MK9 to trace its metabolic fate in bone. Skeletal outcomes, including bone geometry, tissue quality, and total body BMD were assessed. Liver and bone vitamin K concentrations were quantified using mass spectrometry. Difference in outcome measures between groups within sex were analyzed using an independent t-test.

Results: Liver MK4 and MK9 concentrations were significantly higher in mice fed 2.1 mg MK9/kg diet compared to those receiving 0.06 mg MK9/kg diet, regardless of sex (all $p \leq 0.017$). MK4 was the only vitamin K form detected in bone, with 63-67% of skeletal MK4 in mice fed 2.1 mg MK9/kg diet derived from deuterium-labeled MK9. Femoral tissue strength, maximum bending moment, section modulus, and BMD did not differ significantly between diet groups in either sex (all $p \geq 0.083$). Cross-sectional area ($p=0.003$) and moment of inertia ($p=0.001$) were lower in female mice receiving 2.1 mg MK9/kg diet compared to those receiving 0.06 mg MK9/kg diet, but no differences were found in male mice.

Conclusion: Despite dietary MK9 being a dietary precursor to MK4 in bone, dietary MK9 supplementation did not affect bone tissue quality or bone mineral density.

Funding: NIAMS R01AG067997 and US Department of Agriculture Agricultural Research Service Cooperative Agreement No. 58-8050-3-003

Presented at Nutrition 2025 (ASN), Orlando, FL